# Towards Stimuli-Responsive Polymers for Rheological Control


## Waldron, Christopher


A thesis submitted in partial fulfilment of the requirements for the degree of *Doctor of Philosophy in Chemistry*


Department of Chemistry

University of Warwick


2014

# List of Abbreviations

| | |
|---|---|
| 2F-BiB | Bis(2-bromoisobutyrate) |
| AIBN | 2,2'-Azo-bis-isobutyrylnitrile |
| ARGET | Activators regenerated by electron transfer |
| ATRP | Atom transfer radical polymerization |
| AV | Absolute viscosity |
| BA | Butyl acrylate |
| CRP | Controlled radical polymerization |
| CTA | Chain transfer agent |
| d | Doublet |
| DBTDL | Dibutyltin dilaurate |
| DCM | Dichloromethane |
| DMF | Dimethyl formamide |
| DMSO | Dimethyl sulfoxide |
| EBiB | Ethyl-2-bromoisobutyrate |
| FT-IR | Fourier transform- infra red |
| HEA | 2-Hydroxyethyl acrylate |
| ICAR | Initiators for continuous activator generation |
| IPA | Isopropyl alcohol (Propan-2-ol) |
| IV | Intrinsic viscosity |
| KV | Kinematic viscosity |
| LA | Lauryl acrylate |
| LCST | Lower critical solution temperature |
| LRP | Living radical polymerization |
| LS | Light scattering |

| | |
|---|---|
| m | Multiplet |
| MA | Methyl acrylate |
| MALDI-TOF MS | Matrix assisted laser desorption ionization - time of flight mass spectroscopy |
| MeOH | Methanol |
| $Me_6$TREN | *N,N,N ',N ',N ",N* "-Hexamethyl-[tris(aminoethyl)amine] |
| $M_n$ | Number average molecular weight |
| $M_w$ | Weight average molecular weight |
| NiPAM | *N*-isopropyl acrylamide |
| NMP | Nitroxide mediated polymerization |
| NMR | Nuclear magnetic resonance |
| P-(BA) | Poly (butyl acrylate) |
| PDI | Polydispersity index |
| PEG | Poly(ethylene glycol) |
| PMDETA | *N,N,N ',N ',N "*-Pentamethyldiethylaminotriamine |
| ppm | Parts per million |
| PRE | Persistent radical effect |
| q | Quartet |
| RAFT | Reversible addition fragmentation chain transfer |
| RDRP | Reversible deactivation polymerization |
| SARA | Supplemental activators and reducing agents |
| SEC | Size exclusion chromatography |
| SEM | Scanning electron microscopy |
| SET-LRP | Single electron transfer living radical polymerization |
| SSI | Shear stability index |
| t | Triplet |

| | |
|---|---|
| TE | Thickening efficiency |
| TEA | Triethylamine |
| THF | Tetrahydrofuran |
| TR | Treat rate |
| TREN | Tris(2-aminoethyl) amine |
| UPy | 2-ureido-4[1H]Pyrimidinone |
| VI | Viscosity Index |
| VM | Viscosity modifier |
| XPS | X-ray photoelectron spectroscopy |

# Table of Contents

## List of Figures

## List of Tables

# List of Equations

## Acknowledgements

Firstly, I must of course thank Professor Dave Haddleton for giving me the chance to work his group, for all his support, guidance and for giving me the opportunity to travel the world a bit. Remarkably I never even had a passport prior to joining the group! I genuinely cannot thank you enough for this experience, and the opportunities it will bring in the future. I'll always be keeping an eye on how the Baggies are doing from now on.

My thanks also go to Lubrizol, for without their funding, this project would not have been possible. On that note, many thanks to my industrial supervisors; Dr Tim Smith and Dr Paul O'Hora for their guidance and for hosting me during summer 2014. I'm also grateful to Dr Kieran Trickett for assisting with the rheology.

A special thank you to my former colleagues at Unilever, in particular Dr Adam Jarvis for giving me my first taste of polymer chemistry, and for pointing me in the direction of Warwick!

Thank you to Professor Virgil Percec at the University of Pennsylvania for being kind enough to allow me to spend some time in his group in 2013, and to Dr Shampa Samanta for all her help. I've been very fortunate to have had such a rewarding experience working abroad.

There are numerous technical staff who we all take for granted and without whom we would get little done – and so I'd like to extend my thanks to Dr Ivan Prokes (NMR), Dr Ben Douglas (Science City), Phil Aston (Mass Spec) and Dr Marc Walker (XPS) for keeping our precious instrumentation running.

I have had a number of inspirational teachers throughout my life and I would like to thank Mrs McGregor, Mr White (yes, he really was my chemistry teacher), Mr Twist and Mr Thompson for nurturing my interest in science from a young age.

Now on to the Haddleton group members. A huge thanks to Dr Paul Wilson for being such a great postdoc to have around, for all the help and football chat. I look forward to seeing the future Wilson group. Also, thank you to Dr Ronan McHale for pushing me to get that first paper done, I really appreciate it. To all the other group members past and present: Athina (my copper co-conspirator), Ant, George, Kay, Jenny C, Jenny K, Jamie, Chris S, Danielle, Gabit, Kristian, Muxiu, Vasiliki, George P., Fehaid, Chongyu, Sam (x2), George, Olivier, Tum, Glen, Dan, Mat, Stacy, James, Claudia and Raj. Thank you all for making my stay in the group a great one.

Finally I would like to thank Jacquelynne, the most important person in all of this, for moving to Warwick with me, for her love, support, cups of tea and various baked goods that I know the whole group will miss! I couldn't have done this without you and I look forward to getting married next year and starting another adventure. Last but certainly not least, I want to thank my friends (there are too many, you all know who you are!) and my family; Mum and Dad, Sheila and Brian, Nana, Adam, Caroline, Gareth, Jen and all the kids. This is dedicated to all of you.

## Declaration

Experimental work contained in this thesis is original research carried out by the author, unless otherwise stated, in the Department of Chemistry at the University of Warwick, between October 2011 and October 2014. No material contained herein has been submitted for any other degree, or at any other institution.

Results from other authors are referenced in the usual manner throughout the text.

Date:

Christopher Waldron

## Abstract

The aim of this work, sponsored by Lubrizol, was to develop polymers for potential use as novel viscosity modifiers for automotive oils. The broader scope was to build towards the incorporation of stimuli-responsive behaviour (temperature, shear, pH *etc.*), since there is currently no such technology on the market which does so. The Haddleton group has developed expertise in $Cu^{(0)}$-mediated RDRP techniques, and so these were utilized throughout the thesis.

As a starting point, α,ω-functional lipophilic poly(butyl acrylates) were synthesized, which were then functionalized post-polymerization using thio-bromo substitution with a view to inducing associative thickening. During this investigation, a novel biphasic reaction scheme was noted, wherein the polymer was observed to phase separate from the solvent/catalyst mixture. Additionally, some previously unreported ligand effects were found. The incorporation of ureido-pyrimidinone hydrogen bonding motifs to lipophilic poly(acrylates) was also pursued, with the subsequent materials showing interesting rheological characteristics.

The biphasic $Cu^{(0)}$-mediated RDRP system was then used to synthesize poly(lauryl) and (butyl acrylate) star polymers with exceptional degrees of control over the molecular weights and dispersity. These reactions were then successfully scaled up to produce enough materials to undergo some standard industrial tests, to assess their suitability as VMs.

Lastly, a collaborative side-project was also undertaken which moved away from generating oil-soluble polymers to examining the feasibility of grafting poly(NiPAM) brushes from water purification membranes using aqueous 'SET-LRP'. This was shown to be possible, as demonstrated using a range of surface analysis techniques.

# Chapter 1: Introduction

*'May all your molecules be long, and your equations short'*

- *Professor Peter H. Plesch*

## 1.1 Oil Additives

Oil is a critical component of an engine; it is there to keep the various parts moving and to reduce wear at the interfaces of those parts, preventing damage. In addition to its lubricating function, engine oil also acts as a medium for removing contaminants from the engine and serves as a coolant. Any loss of these vital functions can result in engine damage and an expensive trip to the garage. To combat this, motor oils are typically sold containing a 'package' of additives[1-3] designed to provide or enhance the properties of the base fluid and also to improve the durability of the oil itself. These additives normally account for around 20% of the product and include but are not limited to the following outlined in **Table 1.1**.

The oil additive industry is a large and profitable business with in the region of one billion motor vehicles in the world today[4] and, whilst car manufacturers are facing increased legislative requirements[5, 6] to improve fuel efficiency and the 'green' credentials of their vehicles, there is currently excellent scope for new innovations in this area. The purpose of this research project was to develop viscosity modifiers (VMs) and thus the next sub-chapter will discuss these in more detail as well as outline some of the basic principles of viscosity.

| Additive | Purpose | Typical Composition |
|---|---|---|
| **Detergents** | Cleaning and sludge prevention | Metallic sulfonates, phosphonates, phenolates |
| **Antioxidants** | Prevention of oxidative damage to the oil itself | Aromatic amines, phenols |
| **Dispersants** | Prevents coagulation of impurities by suspension | Amides, aromatics |
| **Corrosion Inhibitors** | Rust/corrosion prevention of metallic engine parts | Zinc dithophosphates |
| **Viscosity Modifiers** | Oil thickening | Polyolefins, poly(methacrylates) |
| **Friction Modifiers** | Lowers friction coefficients between moving parts | Molybdenum disulfide |
| **Anti-foam Agents** | Inhibits formation of air bubbles/foams | Polysiloxanes |
| **Pour Point Depressants** | Allows low temperature flow of oil | Poly(phenols), poly(methacrylates) |

***Table 1.1*** *The typical additives found in automotive oils*

## 1.2 An Introduction to Concepts of Viscosity

Viscosity is a quantity used to describe a fluid's resistance to flow, in more general terms it describes how 'thick' or 'thin' a fluid sample is. It was first quantified mathematically by Sir Isaac Newton in his seminal 1687 work[7], where he stated:

"*The resistance, arising from the want of lubricity in the parts of a fluid, is, caeteris paribus, proportional to the velocity with which, the parts of the fluid are separated from each other."*

This resistance arizes from the internal molecular interactions of the molecules in the fluid, in other words, if two moving surfaces are separated by a homogenous fluid layer, the only friction that arises is that of the internal friction of the fluid itself.Fluids can be categorized as being either *Newtonian* or *non-Newtonian.* The former, according to Newton's Law, applies to fluids whose viscosity remains constant irrespective of the force applied to it, for example the viscosity of water will remain the same no matter how fast it is stirred. However, this law does take into consideration changes in temperature or pressure. The second classification, *non-Newtonian,* applies to fluids whose viscosity changes depending on the force being applied or changes in temperature, time and pressure. These can further loosely be sub-categorized as *shear thinning* or *shear thickening*. As the names suggest, the viscosity of shear thickening materials increases with shear, the opposite is true for those which are shear thinning. There are two related measures of fluid viscosity, known as *dynamic* (or absolute) and *kinematic* viscosity. These will be discussed in the following sub-chapters.

### 1.2.1 Absolute (Dynamic) Viscosity

The absolute viscosity (η) can be defined as: "*The tangential force per unit area (F) required to move a horizontal plane with respect to a stationary plane at unit velocity (U) when maintained a unit distance (h) apart by the fluid*." This is described in **Figure 1.1** and given mathematically using Newton's law of viscosity, which can then be rearranged to give η in Poise (**Equation 1.1**). The Poise is a large and impractical number and, as such, values are most often quoted in centipoise (cP) instead.

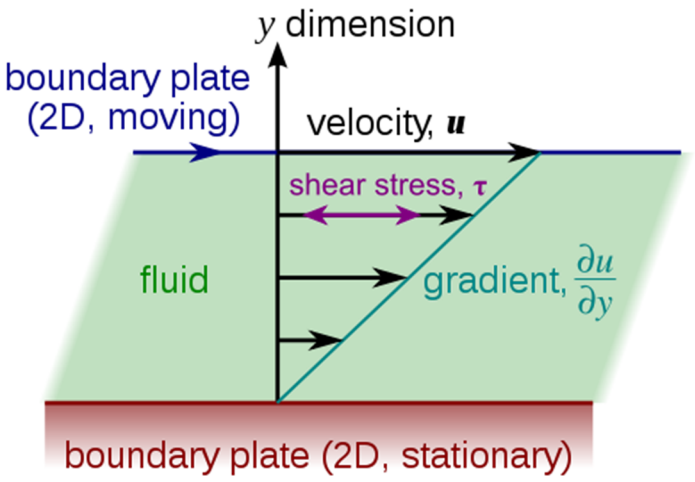


***Figure 1.1*** *Pictorial representation of the laminar shear of fluid between two plates. Reproduced from Wikipedia under a Creative Commons BY-SA 3.0 license*

$$F = \eta A \frac{u}{y}$$

$$\eta = \frac{F/A}{u/y} = \frac{\text{shear stress}}{\text{shear rate}} = \frac{\text{dynes cm}^2}{\text{s}^{-1}} = \text{Poise}$$

***Equation 1.1*** *(Top) Newton's law of viscosity and (Bottom) subsequent rearrangement*

### 1.2.2 Kinematic Viscosity (KM)

The kinematic viscosity describes a fluid's resistance to flow under gravity and is the ratio of a fluids absolute viscosity to its density. It is obtained by dividing the absolute viscosity by its mass density, as given by **Equation 1.2**, and is often measured using a capillary viscometer. The SI unit is the Stoke (St), and, like the Poise, it is often a large number and so is usually divided by 100 to give the value in centistokes (cSt).

$$KV = \frac{\eta}{\rho}$$

***Equation 1.2*** *Expression for the determination Kinematic Viscosity (KV)*

Since density is temperature dependent, it follows that the kinematic viscosity will change depending on the temperature of the system. It is thus important for both the absolute viscosity and density of the fluid to be calculated at the same given temperature. This is an important factor in the context of engine lubrication as any oil will experience a wide range of temperature inside of an engine. Intuitively, the KV of a lubricant will be inversely proportional to its temperature and by using the Walther equation (**Equation 1.3**), a plot can be constructed which can predict the KV between two points (**Figure 1.2**).

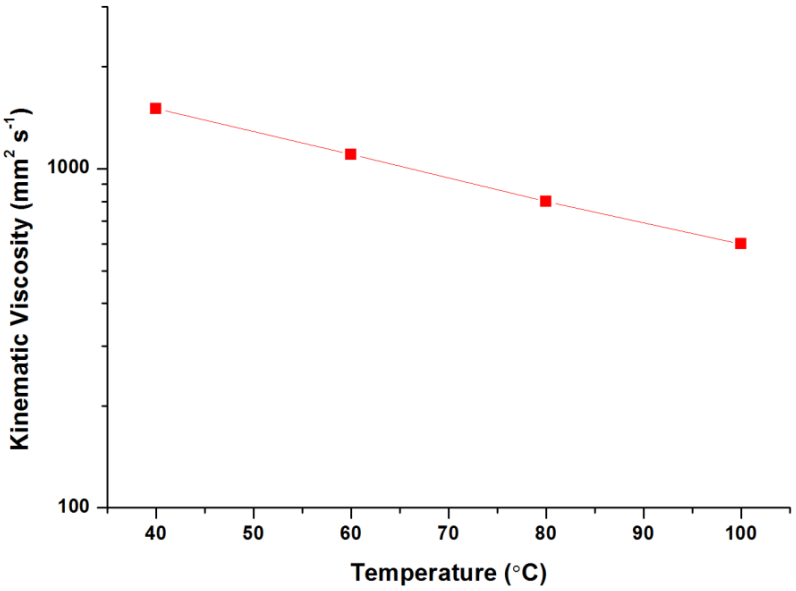


***Figure 1.2*** *Arbitrary log plot of KV vs temperature*

$$Log_{10}\big(Log_{10}(KV + a)\big) = b - cLog_{10}(T)$$

***Equation 1.3*** *Walther's equation for calculating KV where a, b and c are machine based constants and T is the absolute temperature*

Since KV is usually measured with a capillary viscometer, a derivation can be made to **Equation 1.3** where the KV is given by the length of the capillary squared, divided by the time taken for the sample to move that length (**Equation 1.4**).

$$KV = \frac{\eta}{\rho} = \frac{force\ x\ length}{area\ x\ velocity} \Big/ \frac{mass}{volume} = \frac{length^2}{time}$$

***Equation 1.4*** *Derivation of Walther's equation for the calculation of KV using capillary viscometry*

### 1.2.3 Viscosity Index (VI)

The viscosity index (VI) is an arbitrary number used to indicate the temperature dependence of an oil's KV and is an important parameter when selecting a lubricant. It was developed in 1929[8] by researchers at the Standard Oil Development Company and arose due to the need of finding a way of distinguishing oils from different parts of the USA. Texan oils were observed to be more susceptible to shear thinning compared with those from Pennsylvania. On this new scale, oils from Texas were assigned a VI of 0 and the ones from Pennsylvania rated 100. The equation for calculating VI, Equation 1.5, is given below.

$$\boldsymbol{VI = 100\frac{(L-U)}{(L-H)}}$$

***Equation 1.5*** *Calculating VI*

This deceptively simple looking equation requires some further explanation as to what its various parameters are. U is defined as the KV of the sample in question at 40°C, L and H are standard values derived from American Society for Testing and Materials (ASTM) D2270 standards. L is defined as the KV of an imaginary oil at 40°C which has the same KV as the test oil at 100°C and has a VI of 0, similarly, H is also the KV of an imaginary oil at 40°C which has the same KV as the test oil at 100°C but is given a VI of 100. These relationships are further illustrated in **Figure 1.3**.

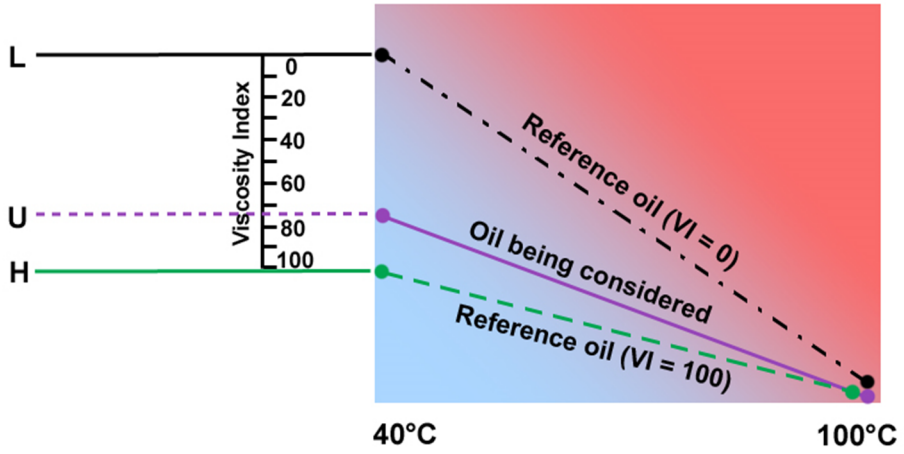


***Figure 1.3*** *Graph quantifying Equation 1.5*

In order to obtain the VI for a given sample, one must measure its KV at 100°C and then obtain the derived values of L and H which are given in the ASTM D2270 tables. For example a KV of 50.0 gives L = 2618 H = 919.6. If it then has a KV of 100 cSt at 40°C, its VI can be calculated using **Equation 1.5**:

$$\mathbf{VI = 100 \times (2618\text{-}100) / (2618\text{-}919.6) = 148.257}$$

An oil that has a smaller change in kinematic viscosity with increasing temperature will have a higher VI than an oil with a greater viscosity change across the same temperature range (**Figure 1.4**). The former would therefore be considered to be the better lubricant as it will maintain its viscosity better at higher temperatures.

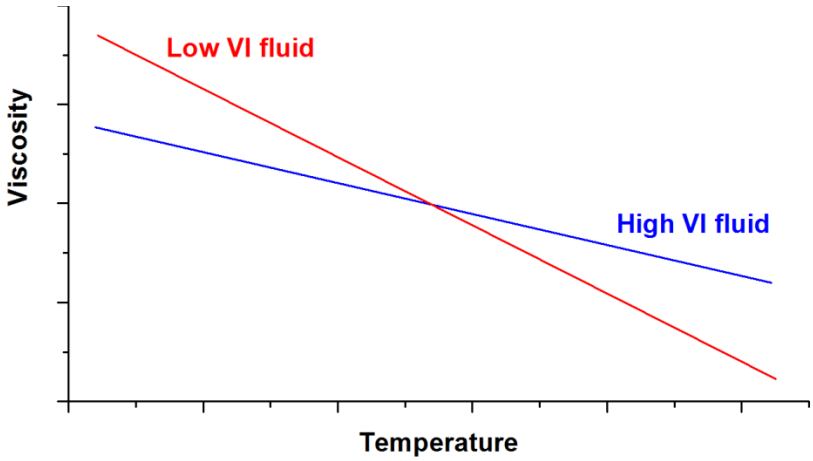


***Figure 1.4*** *A hypothetical comparison between a low VI oil and a high VI oil*

With the development of Viscosity Index Improvement additives (VIIs), **Equation 1.5** became unsuitable as the oils being tested were able to have VI's of over 100. This lead to a new derivation, the Viscosity Index Extension ($VI_E$), which was intended to account for this problem whilst retaining the aspects of the old system (**Equation 1.6**).

$$VI_E = 100 + 140((10n) - 1)$$

$$n = \frac{logH - logU}{logKV_{100}}$$

***Equation 1.6*** *The equation for calculating $VI_E$ where U and H are as described in Equation 1.5*

## 1.3 Viscosity Modifiers (VMs)

Now that the concepts of viscosity have been discussed and, how it is measured, we can now examine viscosity modifiers, the roles that they perform and their modes of action.

As earlier discussed, oil provides several essential functions for the smooth running of an engine and its viscosity is a key component. If the viscosity of the oil is too low, excessive wear will result as well as heat generation due to mechanical friction. Likewise, if the viscosity is too high the oil may not flow, hindering its ability to lubricate, or it can cause too much energy to be used in making the parts move also causing the system to overheat. Oils typically reduce in viscosity with increasing temperature; the ideal lubricant would maintain a constant viscosity across the entire temperature range to which it is exposed. The purpose of a viscosity modifier (VM) is to reduce the extent of the increase in viscosity as the temperature is lowered, or reduce the extent of the decrease in viscosity as the temperature is raised, or ideally both of these. A VM also needs to be able to achieve this in a cost effective manner and be stable with respect to temperature and shear, since they will be exposed to these in an engine.

In 1958, Theodore W. Selby of General Motors published research into the effect of polymeric additives on the rheological properties of mineral oils at different temperatures and shear rates[9]. Upon adding poly(alkyl methacrylates) and poly(isobutylenes) to the base oil, thickening and non-Newtonian characteristics were observed, an effect attributed to '*the difficulty the molecules experience in getting past one another during flow of the fluid mass; the greater the difficulty, the higher the viscosity".* In other words, when large molecules (eg. polymers) are

dissolved in a solvent, the smaller solvent molecules have difficulty moving past them increasing the internal friction of the fluid and also the viscosity. The higher the molecular weight of the additive, the greater this effect is and so polymers are well suited for this purpose.

Polymers are able to act as VMs due to the phenomenon of their hydrodynamic volume, which is dependent on the solvent and temperature. Simply put, the higher the solubility of the polymer, or the higher the temperature, the greater the hydrodynamic volume. At lower temperatures the polymer chains will remain relatively entangled within themselves, which keeps the interactions between the polymer and the oil low and maintaining the viscosity at this temperature. As the temperature increases, so does the hydrodynamic volume due to increased solvation, expansion and untangling of the chains. This assists in the viscosity being maintained at higher temperatures which would normally cause the viscosity to drop in the absence of a VM (**Figure 1.5**).

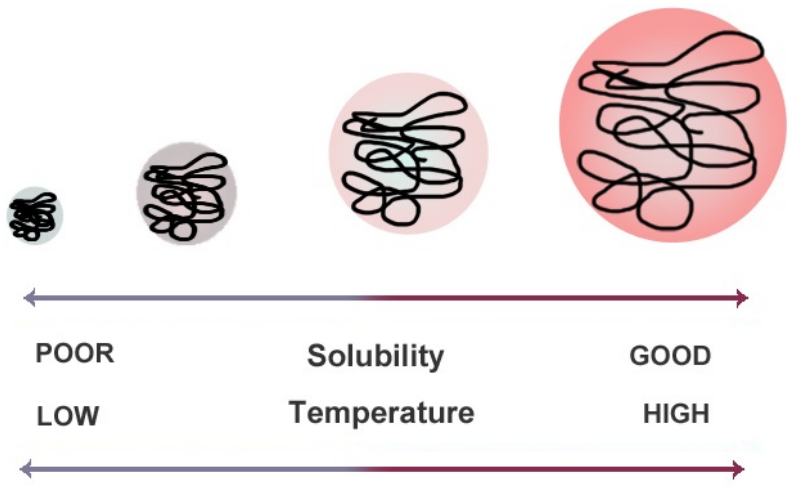


***Figure 1.5*** *The effect of temperature on the solubility and hydrodynamic volume of a polymer*

Ideally, a polymer will have minimal solubility at low temperature otherwise it is not classed as a VM, rather a 'thickener' as per Selby's definition. In such a case, the additive will have a similar effect on the viscosity across the entire temperature range.

### 1.3.1 Shear Stability and Thickening Efficiency

An important property of a VM is its ability to resist damage from the intense shearing forces in an engine/driveline as this will inevitably have a negative impact on their performance[10]. As discussed earlier the performance of a VM is molecular weight dependent, however with increasing molecular weight there is an associated increase in the propensity to be affected by shear[11]. One can counteract this by using additives of a lower molecular weight, however more will be needed in order to provide a similar benefit and so this comes at an increased cost. As such, there is a trade-off between the amount of VM added (known as the Treatment Rate) and the shear stability. The shear stability of a VM is defined by its Shear Stability Index (SSI) and is calculated using **Equation 1.7**. The consequence of this is that a VM with a low SSI number is more stable with respect to shear and *vice versa*.

$$SSI = \frac{m_i - m_f}{m_f - m_0} \times 100$$

***Equation 1.7*** *Equation for the calculation of SSI where $m_i$ = the initial viscosity of the oil containing the VM, $m_f$ = final viscosity of the oil after being sheared and $m_0$ = viscosity of the lubricant without any VM*

A further parameter to quantify is the Thickening Efficiency (TE), which is defined as a VMs ability to thicken an oil with reference to the amount that has been added (the Treatment Rate, TR) and is calculated using **Equation 1.8**.

$$TE = \left( log_{10} \left( \frac{KV_{100}oil + VM}{KV_{100}base\ oil} \right) \right) TR$$

***Equation 1.8*** *Calculation TE, where $KV_{100}$ oil+VM = the KV of the oil and VM blend at 100°C, $KV_{100}$ base oil = the KV of the base oil at 100°C and TR = Treatment Rate*

Using **Equations 1.7** and **1.8**, the TE and SSI of a given VM can be calculated and a comparison made. A generalized scheme is given in **Figure 1.6** and illustrates how increasing molecular weight gives increased TE but at the same time, lowers the SSI. It is obvious that a compromise has to be made between the two factors.

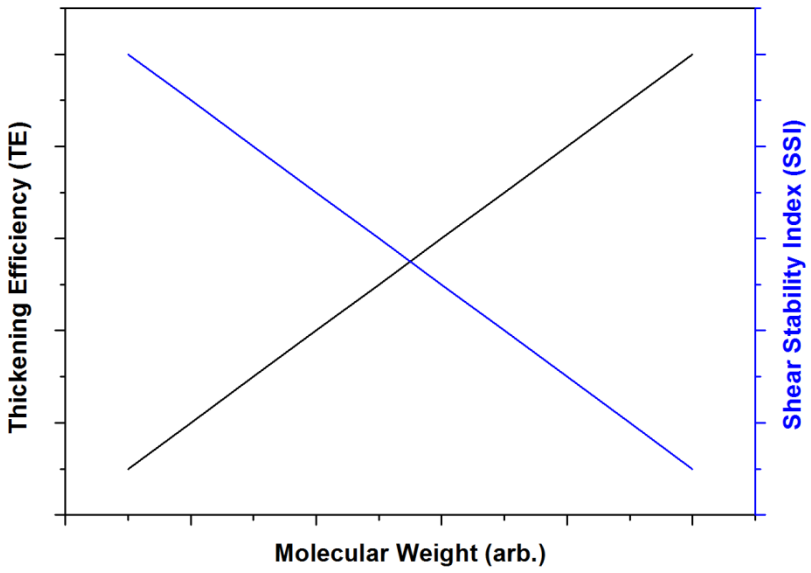


***Figure 1.6*** *An arbitrary illustration of how shear stability and thickening efficiency change with the molecular weight of a VM*

## 1.4 An Introduction to Radical Polymerization

Controlled Radical Polymerization (CRP) is used throughout the experimental work in this thesis and so, in this introductory part, an overview of radical polymerization techniques will be presented, beginning with Free Radical Polymerization (FRP). The theory behind FRP has been studied many for decades and is now a matter of 'textbook' knowledge[12-14].

### 1.4.1 Free Radical Polymerization

**IUPAC Definition[15]**

*"A chain polymerization in which the kinetic-chain carriers are radicals.*

*Note: Usually, the growing chain end bears an unpaired electron"*

The first step in FRP is **Initiation**, where *primary radicals* are formed from the decomposition of an initiator molecule. This most commonly occurs via thermal homolytic cleavage (thermal initiation) or by photolysis (photoinitiation) and generally such initiators are organic peroxides and azo compounds, as illustrated in **Figure 1.7**. Upon generation of these *primary radicals*, they can then react with a monomer unit, M to give *an initiating radical* which is the start of the polymer chain (**Figure 1.8**).

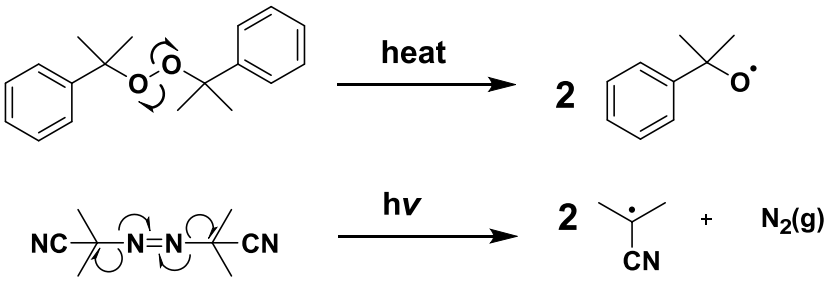


***Figure 1.7*** *The thermal decomposition of dicumyl peroxide and, the photolysis of AIBN to form two primary radicals*

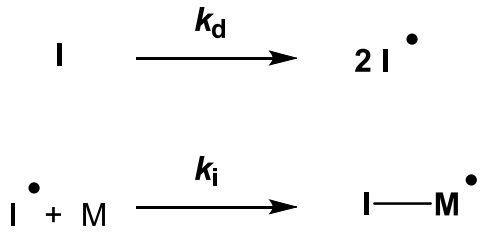


***Figure 1.8*** *The initiation step of a FRP, where I = initator, M = monomer, $k_d$ is the rate constant of initiator decomposition and $k_i$ is the rate consant of initiation*

Practically, the rate of initiating radical formation is much greater than the rate of initiator decomposition and so the latter is taken to be the rate limiting step in the process. Hence, an overall expression for the rate of initiation ($R_i$) can be derived which only takes $k_d$ into consideration (**Equation 1.9**). The term '2 'in the expression accounts for the fact that 2 I• are formed from the decomposition of the initiator molecule.

$$R_i = 2fk_d[I]$$

***Equation 1.9*** *Expression for the rate of initiation*

Term *f* in the equation is known as the Initiator Efficiency, which is the ratio between the total number of radicals formed and the number of radicals which provide a successful initiation event. In practice this number is typically <1 as the high reactivity of the primary radicals leads to a number of undesirable side reactions such as recombining with themselves (**Figure 1.9**), or reacting with the initiator molecules or solvent.

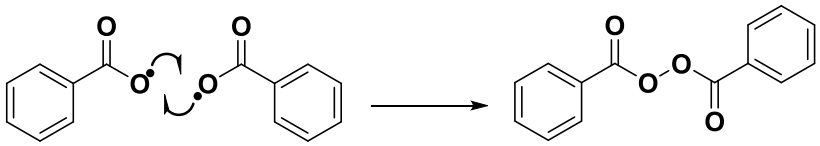


***Figure 1.9*** *The recombination of primary benzoyl radicals*

The second step in a FRP is **Propagation**. The initiating radicals produced in the first step can undergo radical addition to the vinyl bond of a monomer, resulting in a free radical chain which can react with other monomer units in a sequential manner, illustrated in **Figure 1.10** and **1.11**.

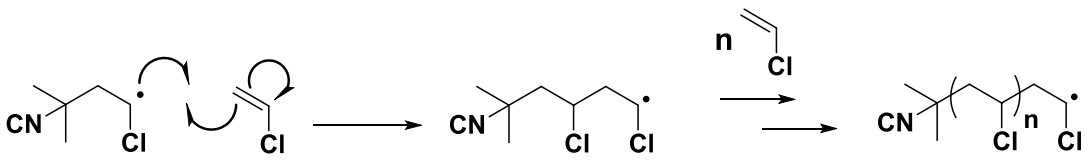


***Figure 1.10*** *The propagation steps for the free radical polymerization of vinyl chloride, initiated by AIBN*

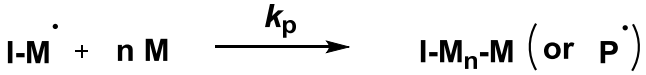


***Figure 1.11*** *Simplified expression for propagation, with rate constant $k_p$*

The overall rate of propagation ($R_p$) is given by the rate of monomer consumption with time and can be expressed in terms of the monomer concentration [M], the concentration of propagating radicals [P·] and the rate constant $k_p$ which is the sum of the rate constants for each monomer addition (**Equation 1.10**).

$$R_p = k_p[M][P\cdot]$$

***Equation 1.10*** *Expression for the rate of propagation*

Propagation will continue until either all of the monomer has been consumed or until some sort of **Termination** event has occurred. Termination occurs when the radical reacts in such a way that it is irreversibly quenched – with no free radical, monomer units cannot add to the chain and thus the growing polymer chain becomes 'dead'.

Similar to the primary radicals, the active polymer chains can terminate due to reacting with the solvent, initiator radicals or other impurities. However the primary method of termination is through the bimolecular termination between two chains, which has two different chemical events; termination by combination and termination by disproportionation which are kinetically identical (**Figure 1.12**).

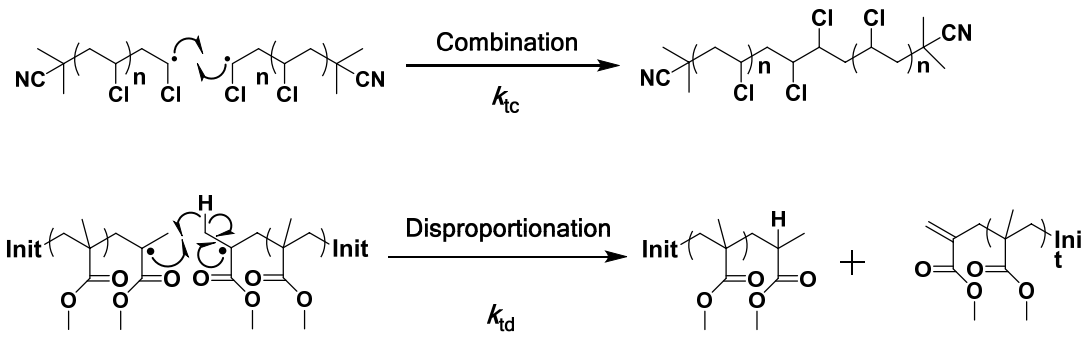


***Figure 1.12*** *The two termination modes: the termination by combination of poly(vinyl chloride) and the termination by disproportionation of poly(methyl methacrylate)*

With termination by combination, two radical chains meet head on and couple to form one single chain which is now 'dead' and is of the molecular weight of the two consisting chains. In the case of disproportionation, a radical abstracts a proton from another chain to produce one chain capped with a double bond and the other with a hydrogen. In this case, the number of polymer chains remains the same.

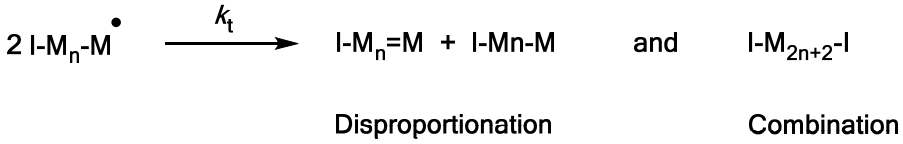


***Figure 1.13*** *Simplified scheme illustrating termination*

The overall rate of termination, $R_t$, can be defined in terms of the rate at which the propagating radicals (P·) are consumed, where $k_t$ equals the sum of the rate constants of combination and disproportionation (**Equation 1.11**).

$$R_t = 2k_t[P\cdot]^2$$

***Equation 1.11*** *Expression for the rate of termination, where $k_t = k_{tc} + k_{td}$*

Another factor to consider with FRP is **Chain Transfer** in which, contrary to the modes of chain termination above, results in the quenching of one radical with the production of a new one which sometimes, but not always results in further propagation itself, ie. this event does not result in the loss of a radical from the system. Chain transfer can occur to the solvent, monomer, initiator and to a second polymer chain which usually results in branching. Chain transfer events generally result in a reduction in the average molecular weight of the product. Due to this, specific Chain Transfer Agents (CTAs) can be added to purposefully induce this lowering of the molecular weight and control the molecular weight of the product. Examples of two chain transfer modes are illustrated in **Figures 1.14** and **1.15**.

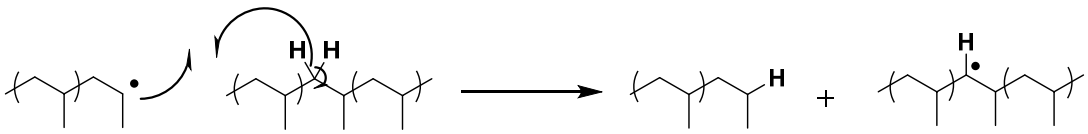


***Figure 1.14*** *Chain transfer of poly(propylene), to a second poly(propylene) molecule*

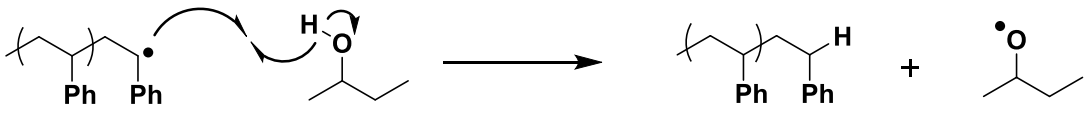


***Figure 1.15*** *Chain transfer of poly(styrene), to solvent (sec-butanol)*

The effectiveness of a CTA is described by its chain transfer constant $C_s$, which is the ratio of the rate constant of chain transfer ($k_{tr}$) to the rate constant of propagation ($k_p$) (**Equation 1.12**).

$$C_s = \frac{k_{tr}}{k_p}$$

***Equation 1.12*** *Expression for the chain transfer constant, $C_s$*

Experimentally, chain transfer constants are most often obtained using the Mayo equation (**Equation 1.13**), where $DP_n$ is the Degree of Dolymerization of the product, $DP_{n0}$ is the Degree of Polymerization for the product obtained in the absence of the chain transfer agent, and [S] and [M] are the respective concentrations of the chain transfer agent and monomer.

$$\frac{1}{DP_n} = \frac{1}{DP_{n0}} + C_s \frac{[S]}{[M]}$$

***Equation 1.13*** *The Mayo Equation*

In order to derive the overall kinetic expression for the polymerization, a number of assumptions must be made to account for the fact that it is practically very difficult to directly measure the number of propagating species in the reaction ($P^{\bullet}$). Using a steady state approximation it is assumed that the rates of initiation and termination are equal ($R_i$=$R_t$) and that the net rate of radical generation is zero, meaning that the radical concentration remains the same throughout the reaction (**Equation 1.14**).

$$R_i = R_t = 2k_t[P\bullet]^2$$

$$[P\bullet] = \left(\frac{R_i}{2k_t}\right)^{1/2}$$

$$R_p = k_p\,[M]\left(\frac{R_i}{2k_t}\right)^{1/2}$$

***Equation 1.14*** *Expression for the rate of a free radical polymerization using the steady state approximation*

Since the rate of initiation is limited by the rate of initiator decomposition (as it is far slower), we can also assume that $R_i = R_d$ and substitute this into the equation to give an expression for the overall rate of polymerization (**Equation 1.15**).

$$R_i = R_d = 2fk_d[I]$$

$$R_p = k_p\,[M]\left(\frac{fk_d[I]}{k_t}\right)^{1/2}$$

***Equation 1.15*** *Expression for the overall rate of a free radical polymerization*

The utility of FRP lies in its simplicity – such reactions can be carried out in solution, bulk, dispersion and emulsion conditions which all have large scale industrial applicability. Indeed, polymers synthesized by FRP are produced on the billion kilogram scale *per annum*, providing us with a number of familiar products such as poly(styrene), poly(propylene) and poly(vinyl chloride).

### 1.4.2 Controlled/Living Radical Polymerization

Despite the robustness of free radical polymerization, it has a major disadvantage in that it has poor control over the molecular weight of the product. It is also difficult to incorporate end group functionality the product or to generate complex structures and morphologies. The desire to overcome this has led to a number of new techniques being developed which allow polymerizations to occur in a 'living' or 'controlled' manner, resulting in polymers with low mass dispersities and chains which remain active even when all of the monomer has been exhausted.

The term 'living' was first coined by Szwarc in 1956[16], with reference to his work on anionic polymerization. A living system has minimal termination or chain transfer events and so if all of the chains are initiated simultaneously (or more usually, at about the same time), they will all grow at similar rates and so should have comparable chain lengths, low overall dispersity and precise control over the polymer architecture. The chain ends also retain their activity, allowing for the synthesis of block copolymers by the addition of a new monomer. However, since termination events inevitably do occur in radical polymerizations, the term 'living' is now discouraged by IUPAC[17] in favour of 'controlled' or 'reversible-deactivation radical polymerization' (RDRP). In the case of RDRP, this control is achieved by establishing an equilibrium between active radical species and dormant chains, several of these techniques (NMP, ATRP, RAFT and SET-LRP) will be discussed later in the chapter.

### 1.4.2.1 The Kinetics of a Living Radical Polymerization

As already mentioned, the fundamental assumptions with a 'living' radical polymerization is that all chains are initiated at t = 0, all chains propagate at the same rate and that there is an absence of chain transfer and termination reactions. As a result, the rate of propagation is simply the rate of monomer consumption with time. This can be expressed in terms of the propagating radical concentration (P•) using **Equation 1.16**, where [P•] is equal to the concentration of the initiator at t = 0 and $k_p$ is the rate constant of propagation.

$$R_p = \frac{-d[M]}{dt} = k_p[P\bullet][M]$$

***Equation 1.16*** *Expression for the overall rate of a 'living' radical polymerization*

A corollary of this is that a plot of $\ln([M]_0/[M]_t)$ against time (**Equation 1.17**) should be linear for a truly 'living' system, due to the initial assumption that the radical concentration, [P•], remains constant due to low or zero termination events. Thus, such a plot can be used as part of a test for the 'livingness' of a radical polymerization and in addition, the value of $k_p$ can be obtained from its gradient. Note that due to the steady state approximation, normal free radical polymerisation also leads to linear first order kinetics so this test also applies with the linear evolution of $M_n$ with conversion.

$$\frac{-d[M]}{dt} = k_p[P\bullet][M]$$

$$\frac{1}{[M]}d[M] = -k_p[P\bullet]dt$$

$$\frac{1}{[M]}d[M] = -k_p[P\bullet]\int_{t_0}^{t_t} dt = -k_p[P\bullet]t$$

$$\int_{[M]_0}^{[M]_t} \frac{1}{[M]}d[M] = ln[M]_0^t = -k_p[P\bullet]t$$

$$ln[M]_t - ln[M]_0 = -k_p[P\bullet]t$$

$$ln\frac{[M]_t}{[M]_0} = -k_p[P\bullet]t$$

$$\boxed{ln\frac{[M]_0}{[M]_t} = k_p[P\bullet]t}$$

***Equation 1.17*** *The rearranged and integrated form of Equation 1.15, where $[M]_0$ is the monomer concentration at t=0 and $[M]_t$ is the monomer concentration at a given time in the polymerization*

With some of the basic concepts regarding living radical polymerization now considered, some of the contemporary LRP techniques in use will be discussed in the following sub-chapters.

### 1.4.2.2 Nitroxide Mediated Polymerization (NMP)

NMP utilizes a nitroxide free-radical in order to establish an equilibrium between itself and an alkoxyamine consisting of an initiating or propagating radical reversibly bound to the nitroxide. The use of nitroxides was first reported by Rizzardo and co-workers in the patent literature[18]. It was then further developed by Georges et. al.[19] where they reported the synthesis of narrow molecular weight styrenic resins using 2,2,6,6-tetramethylpiperidynyl-N-oxy (TEMPO), now considered the classic 'first generation' NMP agent. However the high temperatures (>120°C) needed to cleave the alkoxyamine lead to the development of new nitroxides which could mediate the polymerization at lower temperature and also allow acrylic and diene monomers to be used, as well as styrene[20, 21].

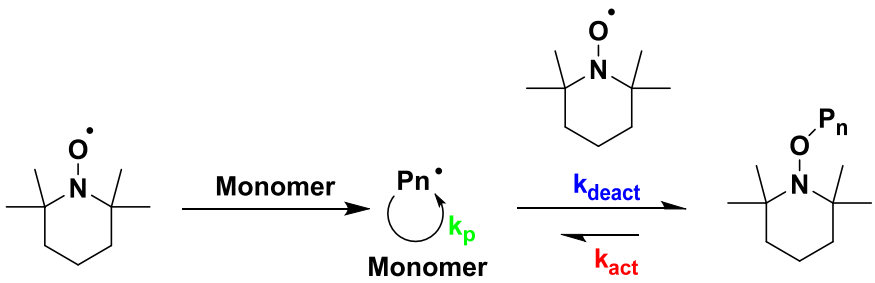


***Figure 1.16*** *The mechanism of NMP using TEMPO*

### 1.4.2.3 Atom Transfer Radical Polymerization (ATRP)

ATRP was discovered independently by Sawamoto[22] and Matyjaszewski[23] in 1995 and represents something of a paradigm shift in the field of polymer synthesis. In this system, a redox-active metal halide/ligand complex (most commonly $M^{I}$) abstracts a halogen from an alkyl halide initiator to generate an $M^{II}$ complex ($k_{act}$) and an initiator radical which can then react with monomer ($k_p$) to start a propagating chain. This chain can then be deactivated by the $M^{II}$ complex transferring the abstracted halogen back to from a $P_n$-X dormant chain 'capping' it and reforming the initial $M^{I}$ species ($k_{deact}$) which can then re-initiate and so on. This equilibrium heavily favours the side of the dormant chains and so the radical concentration in kept low, thus limiting termination reactions and providing control over the polymerization. Furthermore, the retention of the terminal halide groups on the polymer allows for continuous re-initiation thus making this a pseudo-living system. In general, ATRP is restricted to monomers which contain an electron withdrawing substituent adjecent to the vinyl group which is able to stabilize the resulting radical; these include (meth)acrylates, styrenes and (meth)acrylamides.

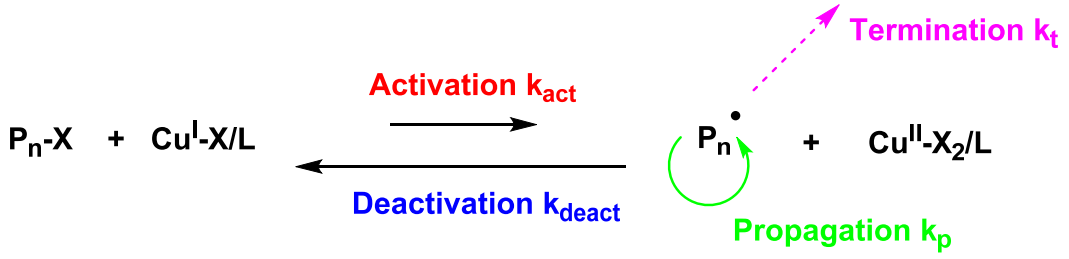


***Figure 1.17*** *The ATRP mechanism as reported by Matyjaszewski et. al.*

The initial work by Sawamoto et. al. utilized a ruthenium $^{(II)}$ based catalyst whereas Matyjaszewki's system uses copper $^{(I)}$ catalysts. The latter now enjoys near-ubiquity in the literature, however despite this, a number of other transition metal catalysts

have been investigated including palladium[24, 25], nickel[26-28], iron[28-30], molybdenum[31, 32] and osmium[33]. Typical ATRP initiators are alkyl halides, usually bromides, with α-halo esters being the most common as these mimic the dormant chain end of the resulting polymer. Examples of these include ethyl 2-bromoisobutyrate (EBiB) and methyl 2-bromopropionate (MBP), however aromatic halides such as tosyl chloride have also been used[34]. The ligands utilized are almost always bi- or multi-dentate nitrogen ligands such as TREN, Bipy, PMDETA and pyridine imines[35, 36]. Some drawbacks of ATRP are that a relatively high reaction temperature is often needed (~80°C), it is sensitive to air and stoichiometric amounts of the catalyst are required, meaning that the product itself can contain high quantities of metal which may be undesirable, unless removed *via* some post-polymerization process. Efforts to reduce the catalyst loading has led to the ARGET[37] and ICAR[38] ATRP concepts being developed as well as a more recent electrochemically mediated ATRP[39].

#### 1.4.2.4 Reversible Addition Fragmentation Chain Transfer Polymerization (RAFT)

A second successful CRP process developed was RAFT, first reported in 1998 by Rizzardo and co-workers[40] and, like ATRP, represented a step-change in the field. In this system a thiocarbonyl thio species is utilized as a chain transfer agent to bring the polymerization under control and the accepted mechanism is outlined below. The first step in the polymerization is the generation of an initiator-derived primary radical which is usually obtained via a 'traditional' thermal initiator such as AIBN. These radicals then initiate a polymer chain which can add to the CTA to give a radical intermediate. Fragmentation can then occur to produce R· which can re-initiate (chain transfer), or the original propagating radical can be released.

Control over the polymerization is obtained via the dynamic exchange of active chain ends (chain equilibration) whilst keeping the majority of chains 'capped' with the CTA, making them dormant.

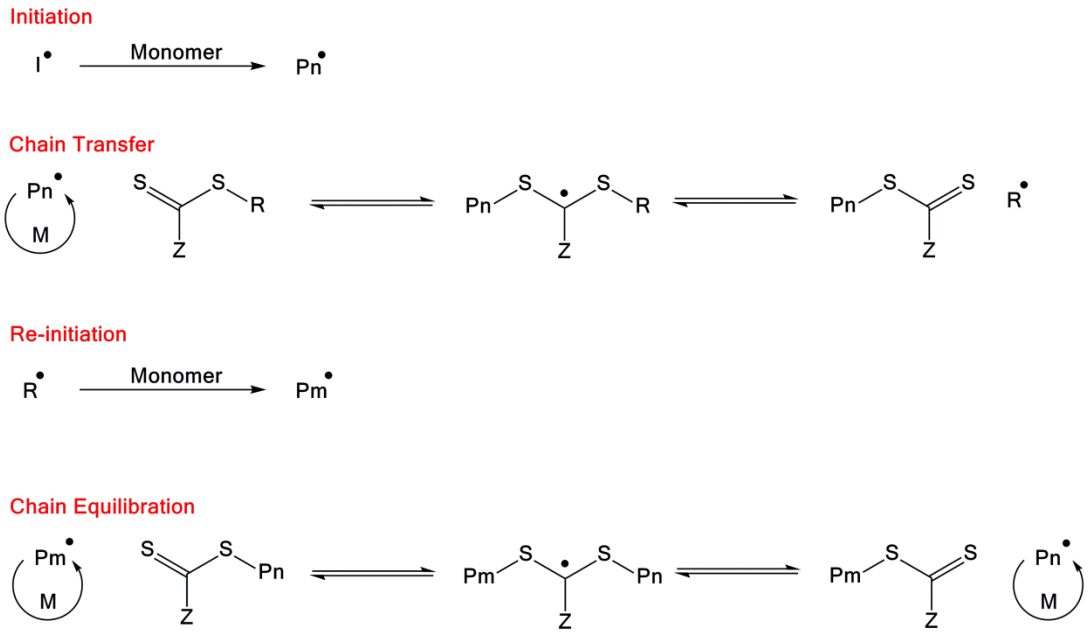


***Figure 1.18*** *The RAFT mechanism as reported by Rizzardo et. al.(reference 40)*

The usefulness of the RAFT process lies in the fact that it can be applied to most monomers which are able to undergo traditional FRP, such as (meth)acrylates, (meth)acrylamides, styrenes[41], vinyl esters[42, 43] and vinyl amides[44, 45]. Poly (vinyl acetate) and poly(*N*-vinyl pyrrolidone) (NVP) in particular have proven a challenge to synthesize using other CRP methods[46, 47] and so RAFT has allowed for the controlled polymerization of some of these more difficult monomers. The drawback is that typically one has to tailor the CTA to the desired monomer (often by altering the *Z* group) which requires extra synthetic steps, in addition since most of the polymer chains will be capped with the CTA this often imparts a yellow or pink colour to the which may be undesirable depending on the intended use.

### 1.4.2.5 Single Electron Transfer Living Radical Polymerization (SET-LRP)

Building on earlier work investigating routes to the LRP of vinyl chloride[48, 49], SET-LRP was first reported by Percec and co-workers in 2006[50]. In this work, the '*ultrafast*' synthesis of acrylates, methacrylates, and vinyl chloride at ambient temperature was achieved to remarkably high molecular weights with exceptional control ($M_n$ >1x10$^6$, $Đ_M$=1.1). Furthermore, a new reaction mechanism was reported (**Figure 1.19**).

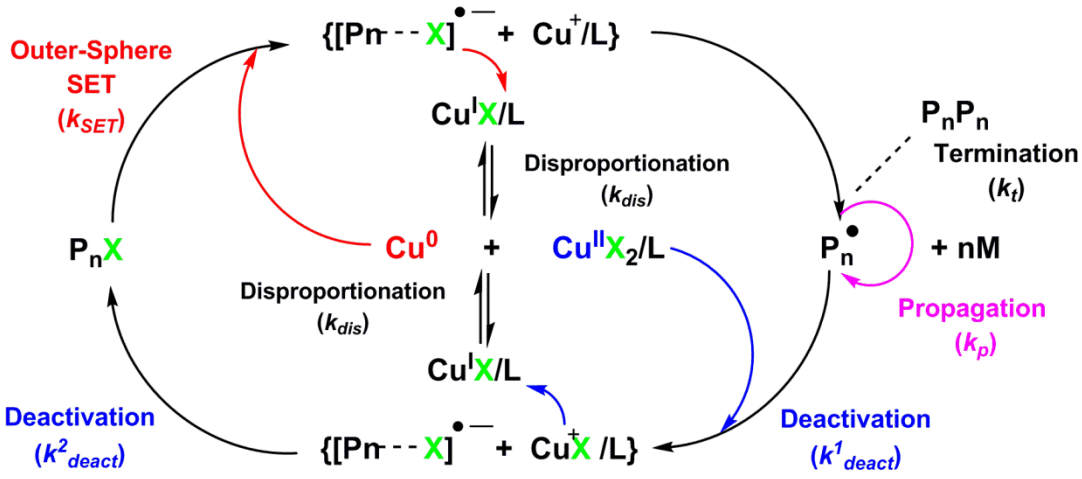


***Figure 1.19*** *The SET-LRP proposed mechanism*

SET-LRP is conceptually similar to ATRP in that it relies on the establishment of an equilibrium between active and dormant chains, with the active chains being reversibly 'capped' via halide transfer using a copper/ligand complex. The key difference is that the activator is zero-valent copper rather than a Cu$^I$ halide. In the proposed mechanism, Cu$^0$ abstracts the halogen from an alkyl halide initiator via an OSET[51, 52] process, undergoing a one electron reduction and producing a radical

anion intermediate which rapidly decomposes to give Pn$^{\bullet}$ plus $Cu^{I}X/L$. Percec then states that the $Cu^{I}X/L$ undergoes instantaneous and complete disproportionation to form $Cu^{0}$ and $Cu^{II}X_2/L$. This 'nascent' $Cu^{0}$ can then activate again and the $Cu^{II}$ complex can deactivate the now propagating polymer chain, regenerating $Cu^{I}$ which then undergoes disproportionation and so on. The key step in the proposed mechanism is the 'spontaneous' disproportionation of the in situ generated $Cu^{I}X/L$, as it is this process which maintains the levels of $Cu^{0}$ and $Cu^{II}X_2/L$ required for the polymerization to occur in a controlled manner. As such, the choice of solvent and ligand [53, 54 55, 56] is an important consideration as both can affect the position of equilibrium for the disproportionation of $Cu^{I}$. The typical ligands used are *N*- ligands such as $Me_6$TREN, TREN, PMDETA and HMTETA, with $Me_6$TREN being the most popular in the literature. These are able to stabilize $Cu^{II}$ which moves the position of $K_{dis}$ towards the right, thus favouring disproportionation. Conversely, pyridine imine ligands and BIPY, which stabilise $Cu^{I}$ *via* transfer of electron density from the metal into a π* oribal, are not able to facilitate disproportionation at ambient temperature.

Since its inception, SET-LRP has found wide use as a synthetic tool, in addition to the extensive work carried out with regards to the mechanism (discussed later). This technique has been used to synthesize, *inter alia,* complex multiblock co-polymers with sequence control[57-60], star polymers[57, 61], hydrophobic polymers[61-68], and nanoparticles, conjugates and glycopolymers[69-72] for therapeutic applications. Additionally, SET-LRP from surfaces[73-76] and using flow reactors[77-80] has been reported as well as the exploration of an optimized system for conducting the process in water[81-83]. The most recent developments involve the use of a novel photocatalytic system[80, 84-87].

### 1.4.2.6 SET-LRP vs SARA-ATRP: The Mechanistic Debate

Since the inception of SET-LRP in 2006, there has been a vigorous and ongoing debate[88, 89] in the academic forum regarding the true mechanistic nature of $Cu^{(0)}$-mediated RDRP, with respect to ATRP. The main proponents of this argument are Percec, who sides with SET-LRP and Matyjaszewski, who believes the actual mechanism to be Supplemental Activators and Reducing Agents (SARA)-ATRP. Both systems broadly utilize the same components (ie. $Cu^{(0)}$, acrylate monomers, alkyl halide initiators, polar solvents, amine ligands) and yet the proposed mechanisms differ in several fundamental aspects. The range of publications regarding this debate is vast and it is beyond the scope of this introduction to cover all of the various arguments in detail, however an overview of some of the salient points will be given below.

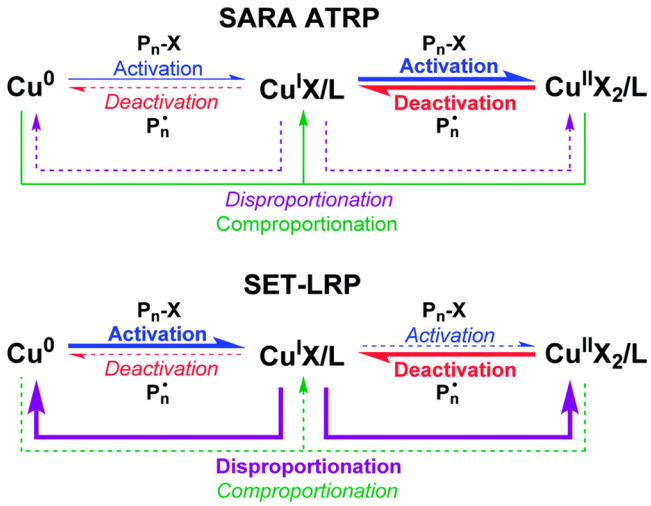


***Figure 1.20*** *(Above) the SARA ATRP mechanism and (below) the SET-LRP mechanism, reproduced from reference 88*

The most fundamental difference regards the role of the $Cu^{(0)}$ in the system (wire, powder, 'nacent' or otherwise). Percec proposes that the $Cu^{(0)}$ is the predominant activating species and that no discernible activation *via* $Cu^{(I)}$ takes places owing to their 'instantaneous' disproportionation under the conditions which promote this (polar solvent, $Cu^{(II)}$ stabilising ligands). This activation step is postulated to occur via an Outer Sphere Electron Transfer (OSET) step, forming a radical anion intermediate which rapidly decomposes into $Cu^{(I)}L/X$. This is supported by various experimental and computational studies[52, 90, 91]. Contrary to Percec's work, Matyjaszewski argues that the $Cu^{(0)}$ is merely a supplemental activator and reducing agent (SARA), and that the $Cu^{(I)}$ species formed *in situ* are the main activator. This has been determined experimentally by comparing the activation rate coefficients of alkyl halides by both $Cu^{(0)}$ and $Cu^{(I)}$[92, 93]. These model studies concluded that the rate of activation by $Cu^{(0)}$ is ~$1x10^4$ times slower than that by $Cu^{(I)}$ in DMSO and, to illustrate this, it was calculated that to match the activity of 1 μM $Cu^{(I)}/Me_6TREN$ complex, one would require 2 km of 0.25mm diameter $Cu^{(0)}$ wire. Thus from a simple kinetic standpoint, $Cu^{(I)}$ is the dominant activator and the polymerization occurs through the ATRP mechanism. Additional experiments also showed that the $Cu^{(0)}$ can also serve as a reducing agent, generating $Cu^{(I)}$ via comproportionation. Electrochemical and computational[94, 95] studies also suggest that the activation step also occurs via an Inner Sphere Electron Transfer (ISET), as opposed to the OSET mechanism proposed by Percec, due to the apparently lower bond dissociation enthalpies calculated for this process.

Another related point of debate is over the disproportionation process and whether the $Cu^{(I)}$ formed via $Cu^{(0)}$ activation disproportionates or, instead, primarily activates alkyl halides. As discussed earlier, the rapid disproportionation of $Cu^{(I)}$ to form highly active 'nacent' $Cu^{(0)}$ is critical to the proposed mechanism of SET-LRP and so experiments were conducted by the Percec group in order to demonstrate that

$Cu^{(I)}$ is inactive during the polymerization. In one such experiment (**Figure 1.21**), the reaction mixture was carefully decanted into another vessel to separate it from the $Cu^{(0)}$ present[96]. Since the decanted mixture still contains any soluble $Cu^{(I)}$ species, if it were an activator under these conditions then it would be expected that the reaction would still proceed to some extent. However, it was found that the reaction completely ceased, leading the authors to conclude that $Cu^{(0)}$ must be the main activator and that disproportionation dominates.

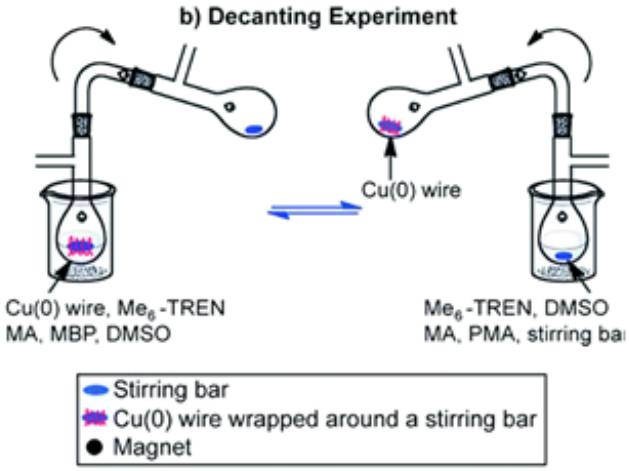


***Figure 1.21*** *Decantation experiment reproduced from reference 96*

This conclusion was challenged by Matyjaszewski who states that since ATRP is subject to the persistent radical effect (PRE), the ppm levels of $Cu^{(I)}$ and $Cu^{(II)}$ present in the solution are unable to sustain the reaction due to rapid termination causing the $Cu^{(I)}$ to be irreversibly converted to $Cu^{(II)}$. This is contrary to previous work by Percec in which SET-LRP reactions were reported to have '100%' end group fidelity, showing that the bimolecular termination required for the PRE does not occur and that the $Cu^{(II)}Br_2$ produced is solely due to the rapid disproportionation of $Cu^{(I)}$. Thus, $Cu^{(I)}$ cannot be an activator in this system. Once

again this was disputed by Matyjaszewski as he argues that a complete retention of end group fidelity must violate the principle of halogen conservation[97].

Matyjaszewski further investigated the nature of the disproportionation/comproportionation equilibria in order to challenge the concept of 'instantaneous' disproportionation required for the SET-LRP mechanism[98-100]. In the DMSO polymerization system it was reported that with a significant ligand concentration, comproportionation is by far the dominant process, since the position of equilibrium is dependent on the ligand concentration. At equilibrium it was calculated that $Cu^{(I)}$ accounted for 99.95% of the soluble species in the system but this is perhaps obfuscatory since the $[Cu^{(II)}]$:[L] ratios employed ([1]:[6]) are atypical of those used in a standard 'SET-LRP' reaction. Indeed the authors also state that when the concentration of ligand is reduced, the extent of disproportionation is much higher and is the dominant process.

It is difficult to draw definite conclusions with regards to which mechanism is correct. Evidently, this is a highly-complex system and indeed it might be that the true mechanism is a hybrid of these concepts. For the purposes of this thesis, the specific reaction mechanism is perhaps irrelevant as the products formed are the same regardless; indeed the utility of $Cu^{(0)}$-mediated RDRP is not under debate, as evidenced by the wealth of non-mechanistic, synthetic works published.

| Process | In SARA ATRP | In SET-LRP |
|---|---|---|
| **Activation by $Cu^{I}$** | Major activation pathway of alkyl halides | Does not occur due to instantaneous loss of $Cu^{I}$ by disproportionation |
| **Activation by $Cu^{0}$** | Supplemental activation pathway of alkyl halides, compensating for termination | Exclusive activation pathway of alkyl halides |
| **Activation mechanism** | Inner sphere electron transfer (ISET) | Outer sphere electron transfer (OSET) |
| **Deactivation by $Cu^{II}$** | Major deactivation pathway of alkyl radicals | Major deactivation pathway of alkyl radicals |
| **Deactivation by $Cu^{I}$** | Negligible | Negligible |
| **Disproportionation of $Cu^{I}$** | Minimal contribution, since $Cu^{I}$ participates primarily in alkyl halide activation | Instantaneous, leading to the (re)generation of the $Cu^{0}$ activator and $Cu^{II}$ deactivator |
| **Comproportionation between $Cu^{II}$ and $Cu^{0}$** | Occurs under certain conditions to compensate for termination | Does not occur |
| **Radical termination** | Minimal extent of termination build up of $Cu^{II}Br_2$ species is directly correlated with loss of end-group functionality | Proceeds in the absence of termination, giving ultrafast polymerization and ultrahigh molecular weight. (Complete preservation of chain end functionality at 100% monomer conversion) |

***Table 1.2*** *Comparison of the various processes between SET-LRP and SARA-ATRP, reproduced from reference 88*

## 1.5 References


1. http://www.bobistheoilguy.com/, Accessed 2014.
2. T. V. Liston, *Lubric. Eng.*, 1992, 48, 389-397.
3. A. B. Ewa and D. L. Gordon, in *Lubricant Additives*, CRC Press, 2009, pp. 457-491.
4. *Ward's AutoWorld*, 2011.
5. EU Regulation No 443/2009, 2009.
6. US NHTSA 20117-2025 CAFE Regulation, 2011.
7. I. Newton, *Philosophiæ Naturalis Principia Mathematica*, 1687, Book 2.
8. E. W. Dean, Davies E. G. W., *Chem. Metall. Eng.*, 1929, 36, 618-619.
9. T. W. Selby, *ASLE Transactions*, 1958, 1, 68-76.
10. I. I. Kudish, R. G. Airapetyan and M. J. Covitch, *Tribol. Trans.*, 2003, 46, 1-10.
11. J. A. Odell and A. Keller, *J. Polym. Sci. B Polym. Phys.*, 1986, 24, 1889-1916.
12. G. Odian, in *Principles of Polymerization*, John Wiley & Sons, Inc., 2004.
13. G. Moad and D. H. Solomon, in *The Chemistry of Radical Polymerization*, Elsevier, 2006.
14. K. Matyjaszewski and T. P. Davis, in *Handbook of Radical Polymerization*, John Wiley & Sons, Inc., 2003.
15. IUPAC, *Glossary of basic terms in polymer science (IUPAC Recommendations), Pure Appl. Chem.* , 1996, 68, 2287–2311.
16. M. Szwarc, *Nature*, 1956, 178, 1168-1169.
17. D. Jenkins Aubrey, G. Jones Richard and G. Moad, in *Pure Appl. Chem.*, 2009, vol. 82, p. 483.
18. D. H. Solomon, E. Rizzardo and P. Cacioli, US Patent US4581429 A, 1986.

19. M. K. Georges, R. P. N. Veregin, P. M. Kazmaier and G. K. Hamer, *Macromolecules*, 1993, 26, 2987-2988.

20. D. Benoit, V. Chaplinski, R. Braslau and C. J. Hawker, *J. Am. Chem. Soc.*, 1999, 121, 3904-3920.

21. M. Lansalot, B. Charleux, J. P. Vairon, R. Pirri and P. Tordo, *ACS, Polym. Preprints,* , 1999, 40, 317-318.

22. M. Kato, M. Kamigaito, M. Sawamoto and T. Higashimura, *Macromolecules*, 1995, 28, 1721-1723.

23. J.-S. Wang and K. Matyjaszewski, *J. Am. Chem. Soc.*, 1995, 117, 5614-5615.

24. M. Sunjuk, A. S. Abu-Surrah, K. A. Abu Safieh, A. K. Qaroush and F. a. M. Al-Qaisi, *Arab. J. Chem.*, 2013.

25. P. Lecomte, I. Drapier, P. Dubois, P. Teyssié and R. Jérôme, *Macromolecules*, 1997, 30, 7631-7633.

26. E. Duquesne, J. Habimana, P. Degée and P. Dubois, *Macromolecules*, 2005, 38, 9999-10006.

27. E. Duquesne, P. Degee, J. Habimana and P. Dubois, *Chem. Commun.* 2004, 640-641.

28. R. K. O'Reilly, M. P. Shaver and V. C. Gibson, *Inorg. Chim. Acta*, 2006, 359, 4417-4420.

29. S.-i. Nakanishi, M. Kawamura, H. Kai, R.-H. Jin, Y. Sunada and H. Nagashima, *Chem. Eur. J.*, 2014, 20, 5802-5814.

30. H. Zhang and U. S. Schubert, *J. Macromol. Chem. Phys.*, 2004, 42, 4882-4894.

31. E. Le Grognec, J. Claverie and R. Poli, *J. Am. Chem. Soc.*, 2001, 123, 9513-9524.

32. F. Stoffelbach, R. Poli and P. Richard, *J. Organomet. Chem.*, 2002, 663, 269-276.

33. W. A. Braunecker, Y. Itami and K. Matyjaszewski, *Macromolecules*, 2005, 38, 9402-9404.

34. P. A. Gurr, M. F. Mills, G. G. Qiao and D. H. Solomon, *Polymer*, 2005, 46, 2097-2104.

35. D. M. Haddleton, M. C. Crossman, B. H. Dana, D. J. Duncalf, A. M. Heming, D. Kukulj and A. J. Shooter, *Macromolecules*, 1999, 32, 2110-2119.

36. D. M. Haddleton, C. B. Jasieczek, M. J. Hannon and A. J. Shooter, *Macromolecules*, 1997, 30, 2190-2193.

37. W. Jakubowski, K. Min and K. Matyjaszewski, *Macromolecules*, 2005, 39, 39-45.

38. K. Matyjaszewski, W. Jakubowski, K. Min, W. Tang, J. Huang, W. A. Braunecker and N. V. Tsarevsky, *Proc. Natl. Acad. Sci.*, 2006, 103, 15309-15314.

39. A. J. D. Magenau, N. C. Strandwitz, A. Gennaro and K. Matyjaszewski, *Science*, 2011, 332, 81-84.

40. J. Chiefari, Y. Chong, F. Ercole, J. Krstina, J. Jeffery, T. P. Le, R. T. Mayadunne, G. F. Meijs, C. L. Moad and G. Moad, *Macromolecules*, 1998, 31, 5559-5562.

41. A. Goto, K. Sato, Y. Tsujii, T. Fukuda, G. Moad, E. Rizzardo and S. H. Thang, *Macromolecules*, 2001, 34, 402-408.

42. M. H. Stenzel, L. Cummins, G. E. Roberts, T. P. Davis, P. Vana and C. Barner-Kowollik, *Macromol. Chem. Physic.*, 2003, 204, 1160-1168.

43. F. Zhao, A. Mahdavian, M. Teimouri, E. Daniels, A. Klein and M. El-Aasser, *Colloid Polym. Sci.*, 2012, 290, 1247-1255.

44. V. Mishra and R. Kumar, *J. Appl. Polym. Sci.*, 2012, 124, 4475-4485.

45. A. Guinaudeau, S. Mazieres, D. J. Wilson and M. Destarac, *Polym. Chem.*, 2012, 3, 81-84.

46. C. Granel, R. Jérôme, P. Teyssié, C. B. Jasieczek, A. J. Shooter, D. M. Haddleton, J. J. Hastings, D. Gigmes, S. Grimaldi, P. Tordo, D. Greszta and K. Matyjaszewski, *Macromolecules*, 1998, 31, 7133-7141.

47. X. Lu, S. Gong, L. Meng, C. Li, S. Yang and L. Zhang, *Polymer*, 2007, 48, 2835-2842.

48. A. D. Asandei and V. Percec, *J. Polym. Sci. A Polym. Chem.*, 2001, 39, 3392-3418.

49. V. Percec, A. V. Popov, E. Ramirez-Castillo, M. Monteiro, B. Barboiu, O. Weichold, A. D. Asandei and C. M. Mitchell, *J. Am. Chem. Soc.*, 2002, 124, 4940-4941.

50. V. Percec, T. Guliashvili, J. S. Ladislaw, A. Wistrand, A. Stjerndahl, M. J. Sienkowska, M. J. Monteiro and S. Sahoo, *J. Am. Chem. Soc.*, 2006, 128, 14156-14165.

51. B. M. Rosen and V. Percec, *J. Polym. Sci. A Polym. Chem.*, 2008, 46, 5663-5697.

52. T. Guliashvili and V. Percec, *J. Polym. Sci. A Polym. Chem.*, 2007, 45, 1607-1618.

53. G. Lligadas, B. M. Rosen, M. J. Monteiro and V. Percec, *Macromolecules*, 2008, 41, 8360-8364.

54. G. Lligadas and V. Percec, *J. Polym. Sci. A Polym. Chem.*, 2008, 46, 6880-6895.

55. G. Wilkinson and A. Cotton, *Advanced Inorganic Chemistry*, John Wiley & Sons, Inc., 1970.

56. B. M. Rosen, X. Jiang, C. J. Wilson, N. H. Nguyen, M. J. Monteiro and V. Percec, *J. Polym. Sci. A Polym. Chem.*, 2009, 47, 5606-5628.

57. C. Boyer, A. Derveaux, P. B. Zetterlund and M. R. Whittaker, *Polym. Chem.*, 2012, 3, 117-123.

58. C. Boyer, A. H. Soeriyadi, P. B. Zetterlund and M. R. Whittaker, *Macromolecules*, 2011, 44, 8028-8033.

59. A. Anastasaki, C. Waldron, P. Wilson, C. Boyer, P. B. Zetterlund, M. R. Whittaker and D. Haddleton, *ACS Macro Lett.*, 2013, 2, 896-900.

60. Q. Zhang, A. Anastasaki, G.-Z. Li, A. J. Haddleton, P. Wilson and D. M. Haddleton, *Polym. Chem.*, 2014, 5, 3876-3883.

61. C. Waldron, A. Anastasaki, R. McHale, P. Wilson, Z. Li, T. Smith and D. M. Haddleton, *Polym. Chem.*, 2014, 5, 892-898.

62. A. Anastasaki, C. Waldron, V. Nikolaou, P. Wilson, R. McHale, T. Smith and D. M. Haddleton, *Polym. Chem.*, 2013, 4, 4113-4119.

63. C. Boyer, A. Atme, C. Waldron, A. Anastasaki, P. Wilson, P. B. Zetterlund, D. Haddleton and M. R. Whittaker, *Polym. Chem.*, 2013, 4, 106-112.

64. S. R. Samanta, A. Anastasaki, C. Waldron, D. M. Haddleton and V. Percec, *Polym. Chem.* 2013, 4, 5555-5562.

65. S. R. Samanta, A. Anastasaki, C. Waldron, D. M. Haddleton and V. Percec, *Polym. Chem.*, 2013, 4, 5563-5569.

66. S. R. Samanta, R. Cai and V. Percec, *Polym. Chem.*, 2014.

67. S. R. Samanta, M. E. Levere and V. Percec, *Polym. Chem.*, 2013, 4, 3212-3224.

68. S. R. Samanta and V. Percec, *Polym. Chem.*, 2014, 5, 169-174.

69. Q. Zhang, J. Collins, A. Anastasaki, R. Wallis, D. A. Mitchell, C. R. Becer and D. M. Haddleton, *Angew. Chem., Int. Ed.*, 2013, 52, 4435-4439.

70. Q. Zhang, P. Wilson, A. Anastasaki, R. McHale and D. M. Haddleton, *ACS Macro Lett.*, 2014, 3, 491-495.

71. M. W. Jones, M. I. Gibson, G. Mantovani and D. M. Haddleton, *Polym. Chem.*, 2011, 2, 572-574.

72. K. Bebis, M. W. Jones, D. M. Haddleton and M. I. Gibson, *Polym. Chem.*, 2011, 2, 975-982.

73. S. Ding, J. A. Floyd and K. B. Walters, *J. Polym. Sci. A Polym. Chem.*, 2009, 47, 6552-6560.

74. J. O. Zoppe, R. A. Venditti and O. J. Rojas, *J. Colloid Interf. Sci.*, 2012, 369, 202-209.

75. J. O. Zoppe, Y. Habibi, O. J. Rojas, R. A. Venditti, L.-S. Johansson, K. Efimenko, M. Österberg and J. Laine, *Biomacromolecules*, 2010, 11, 2683-2691.

76. Z. Hao, D. Wang, H. Chen, J. Sun and Y. Xu, *J. Agr. Food Chem.*, 2014, 62, 1765-1770.

77. N. Chan, M. F. Cunningham and R. A. Hutchinson, *Polym. Chem.*, 2012, 3, 486-497.

78. N. Chan, M. F. Cunningham and R. A. Hutchinson, *J. Polym. Sci. A Polym. Chem.*, 2013, 51, 3081-3096.

79. J. A. Burns, C. Houben, A. Anastasaki, C. Waldron, A. A. Lapkin and D. M. Haddleton, *Polym. Chem.*, 2013, 4, 4809-4813.

80. B. Wenn, M. Conradi, A. D. Carreiras, D. M. Haddleton and T. Junkers, *Polym. Chem.*, 2014, 5, 3053-3060.

81. Q. Zhang, P. Wilson, Z. Li, R. McHale, J. Godfrey, A. Anastasaki, C. Waldron and D. M. Haddleton, *J. Am. Chem. Soc.*, 2013, 135, 7355-7363.

82. C. Waldron, Q. Zhang, Z. Li, V. Nikolaou, G. Nurumbetov, J. Godfrey, R. McHale, G. Yilmaz, R. K. Randev, M. Girault, K. McEwan, D. M. Haddleton, M. Droesbeke, A. J. Haddleton, P. Wilson, A. Simula, J. Collins, D. J. Lloyd, J. A. Burns, C. Summers, C. Houben, A. Anastasaki, M. Li, C. R. Becer, J. K. Kiviaho and N. Risangud, *Polym. Chem.*, 2014, 5, 57-61.

83. Q. Zhang, Z. Li, P. Wilson and D. M. Haddleton, *Chem. Commun.*, 2013, 49, 6608-6610.

84. A. Anastasaki, V. Nikolaou, G. S. Pappas, Q. Zhang, C. Wan, P. Wilson, T. P. Davis, M. R. Whittaker and D. M. Haddleton, *Chem. Sci.*, 2014.

85. A. Anastasaki, V. Nikolaou, A. Simula, J. Godfrey, M. Li, G. Nurumbetov, P. Wilson and D. M. Haddleton, *Macromolecules*, 2014, 47, 3852-3859.

86. A. Anastasaki, V. Nikolaou, Q. Zhang, J. Burns, S. R. Samanta, C. Waldron, A. J. Haddleton, R. McHale, D. Fox, V. Percec, P. Wilson and D. M. Haddleton, *J. Am. Chem. Soc.*, 2013, 136, 1141-1149.

87. Y.-M. Chuang, A. Ethirajan and T. Junkers, *ACS Macro Lett.*, 2014, 3, 732-737.

88. D. Konkolewicz, Y. Wang, P. Krys, M. Zhong, A. A. Isse, A. Gennaro and K. Matyjaszewski, *Polym. Chem.*, 2014, 5, 4396-4417.

89. D. Konkolewicz, Y. Wang, M. Zhong, P. Krys, A. A. Isse, A. Gennaro and K. Matyjaszewski, *Macromolecules*, 2013, 46, 8749-8772.

90. B. M. Rosen and V. Percec, *J. Polym. Sci. A Polym. Chem.*, 2007, 45, 4950-4964.

91. N. H. Nguyen, B. M. Rosen and V. Percec, *J. Polym. Sci. A Polym. Chem.*, 2011, 49, 1235-1247.

92. D. Konkolewicz, P. Krys, J. R. Góis, P. V. Mendonça, M. Zhong, Y. Wang, A. Gennaro, A. A. Isse, M. Fantin and K. Matyjaszewski, *Macromolecules*, 2014, 47, 560-570.

93. C.-H. Peng, M. Zhong, Y. Wang, Y. Kwak, Y. Zhang, W. Zhu, M. Tonge, J. Buback, S. Park, P. Krys, D. Konkolewicz, A. Gennaro and K. Matyjaszewski, *Macromolecules*, 2013, 46, 3803-3815.

94. C. Y. Lin, M. L. Coote, A. Gennaro and K. Matyjaszewski, *J. Am. Chem. Soc.*, 2008, 130, 12762-12774.

95. A. A. Isse, A. Gennaro, C. Y. Lin, J. L. Hodgson, M. L. Coote and T. Guliashvili, *J. Am. Chem. Soc.*, 2011, 133, 6254-6264.

96. M. E. Levere, N. H. Nguyen, H.-J. Sun and V. Percec, *Polym. Chem.*, 2013, 4, 686-694.

97. Y. Wang, M. Zhong, Y. Zhang, A. J. D. Magenau and K. Matyjaszewski, *Macromolecules*, 2012, 45, 8929-8932.

98. Y. Wang, M. Zhong, W. Zhu, C.-H. Peng, Y. Zhang, D. Konkolewicz, N. Bortolamei, A. A. Isse, A. Gennaro and K. Matyjaszewski, *Macromolecules*, 2013, 46, 3793-3802.

99. M. Zhong, Y. Wang, P. Krys, D. Konkolewicz and K. Matyjaszewski, *Macromolecules*, 2013, 46, 3816-3827.

100. D. Konkolewicz, P. Krys and K. Matyjaszewski, *Acc. Chem. Res.*, 2014.

# Chapter 2: Copper$^{(0)}$-Mediated RDRP in a Self-Generating Biphasic System

In this chapter, the synthesis of α,ω-functional lipophilic poly(acrylates) using Cu$^{(0)}$-mediated CRP is reported. During the initial synthesis of poly(butyl acrylates), phase separation of the resultant polymer was observed during the polymerization. Subsequent investigation of this phenomenon revealed that despite the apparent separation of the polymer phase from the catalytic species, the reaction was able to proceed in a controlled, living manner as evidenced by successful iterative chain extensions. Details regarding the reactivity of the ligand were also revealed by during this study. The telechelic poly(n-butyl acrylates) were then functionalized by thioetherification of their terminal bromides, which proceeded in an orthogonal manner to yield lipophilic polymers furnished with α,ω-polar end groups. Methods to polymerize even more hydrophobic monomers using this method was also investigated and the remarkable robustness of the system demonstrated by successful kilogram-scale reactions.

## 2.1 Introduction

As briefly discussed in the introduction, viscosity modifiers are able to act by increasing the internal friction of the fluid they are dissolved in. More specifically, this mechanism can be described by the Hydrodynamic Volume Exclusion process (HDV) which simply states that a given solute (ie, a polymer) will occupy a certain volume within the solution which excludes the possibility of some other substance occupying that same volume. Thus when more solute is added, less volume is available in the solution, leading to increased viscosity[1, 2]. Such materials are described as *non-associative* thickeners; that is to say that the thickening mechanism proceeds in the absence of intermolecular associations. These constitute the majority of VM's for non-aqueous applications on the market[3]. The other class of thickener is *associative*[4], which in addition to the thickening provided by structuring the continuous phase through HDV, also involves the association of the polymer chains through secondary interactions to create networks which builds the viscosity further. Such associations can be, for example, *via* hydrogen bonding, the formation of hydrophilic/hydrophobic domains (eg. block co-polymers) and through the attractive forces between charged species (e.g. ionomers[5, 6]). Associative thickeners enjoy near-ubiquity in aqueous formulations (personal care products, paints)[7] but are mostly restricted to the academic and patent literature for non-aqueous/automotive applications. Ionomers dominate this particular area of research[8-15] with a focus on delivering shear-thickening behaviour.

One such notable example came from researchers at ExxonMobil who in the late 1980s discovered that sodium-sulfonated poly(styrenes) were able to provide shear-thickening in toluene and xylene[13, 14, 16, 17]. Shear-thickening in non-polar solvents has also been observed for α,ω-lithium sulfonato poly(styrene)[15] and α,ω-

lithium carboxylato poly(butadiene)[12] ionomers. These shear-thickening properties would be highly desirable for automotive applications; however the high quantities of sulfur and the metal counter-ions in the polymer backbone bring with them the risk of engine contamination and so these materials are unsuitable for use.

## 2.2 Initial Synthesis of Telechelic Poly(butyl acrylates)

The initial aim of the project was to synthesize telechelic lipophilic acrylates, which will be oil soluble, and to then functionalize them at both ends with polar/hydrophilic groups. These end-groups may then associate in solution, leading to an increase in viscosity due to the increased effective molecular weight of the polymer.

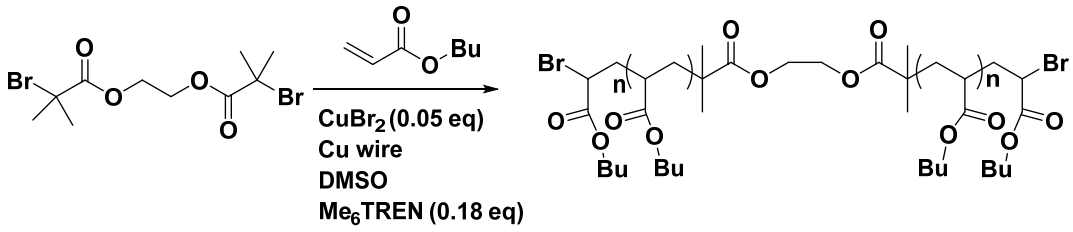


***Figure 2.1*** *Proposed synthetic route to telechelic poly(n-butyl acrylates)*

To this end, $Cu^{(0)}$-mediated CRP was chosen as the polymerization method. The advantages of this technique have been outlined in the introduction but of particular interest in this case is that the use of a bifunctional alkyl halide initiator allows for the synthesis of telechelic polymers with a reactive handle at both the α- and ω-ends which can then be utilized for post-polymerization functionalization. The initial step was to synthesize a bifunctional initiator (2F-BiB), which was achieved by reacting ethylene glycol with two molar equivalents of α-bromoisobutyryl bromide to ensure the esterification of both alcohol groups – an important consideration as any mono-functional product could act as a chain stopper for any resultant association of the polymer chains, post-functionalization. Confirmation of the desired product was confirmed by $^1$H NMR (**Figure 2.2**).

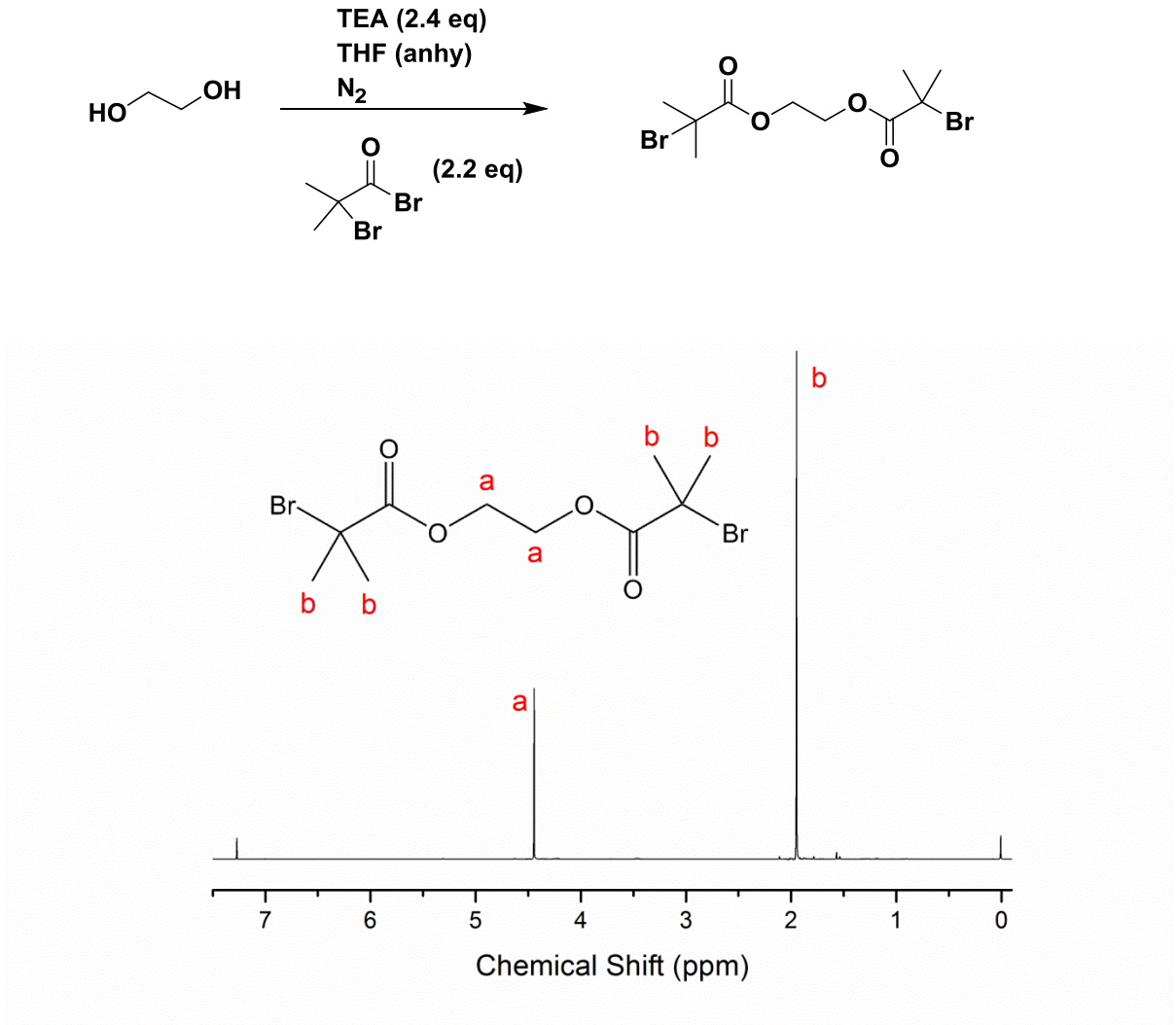


***Figure 2.2*** *Reaction scheme and $^{1}H$ NMR (400MHz in $CDCl_3$) spectra for the synthesis of 2F-BiB bifunctional initiator*

Butyl acrylate was selected as the monomer due to its hydrophobicity and was polymerized using the bifunctional initiator ethylene bis(2-bromoisobutyrate) (2F-BiB) in the presence of $Cu^{(II)}Br_2$, $Me_6TREN$ and Cu(0) wire in DMSO at 25°C (monomer : solvent = 50:50 v/v, [M]:[-Br]:[$Cu^{(II)}$]:[L] = 35:1:0.05:0.18). A molecular weight of 4500 g $mol^{-1}$ was targeted both for ease of characterization and also to prevent the effective molecular weight of any functionalized, associated polymers being too high. The reaction was allowed to proceed overnight, reaching >99%

conversion determined by $^{1}$H NMR, yielding a polymer with $M_n$ = 4200 g mol$^{-1}$ and $Đ_M$ = 1.10.Furthermore, an interesting phenomenon was observed; upon switching off the stirrer the reaction mixture formed two layers – a clear, viscous upper layer and a lower layer with green colouration.

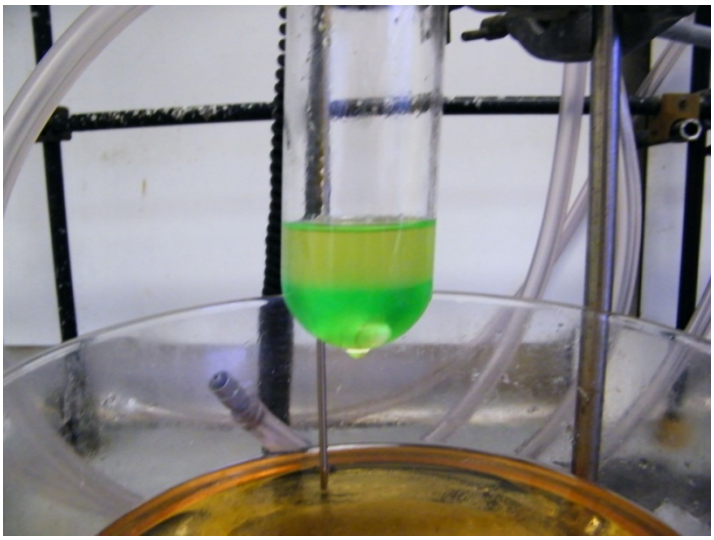

***Figure 2.3*** *Schlenk tube, post-reaction for the $Cu^{(0)}$-mediated radical polymerization of n-butyl acrylate using 2F-BiB bifunctional initiator via $Cu^{(0)}$-mediated RDRP in DMSO at ambient temperature, [M]:[-Br]:[$Cu^{(II)}$]:[L] = 35:1:0.05:0.18. The bi-phasic reaction mixture can be seen*

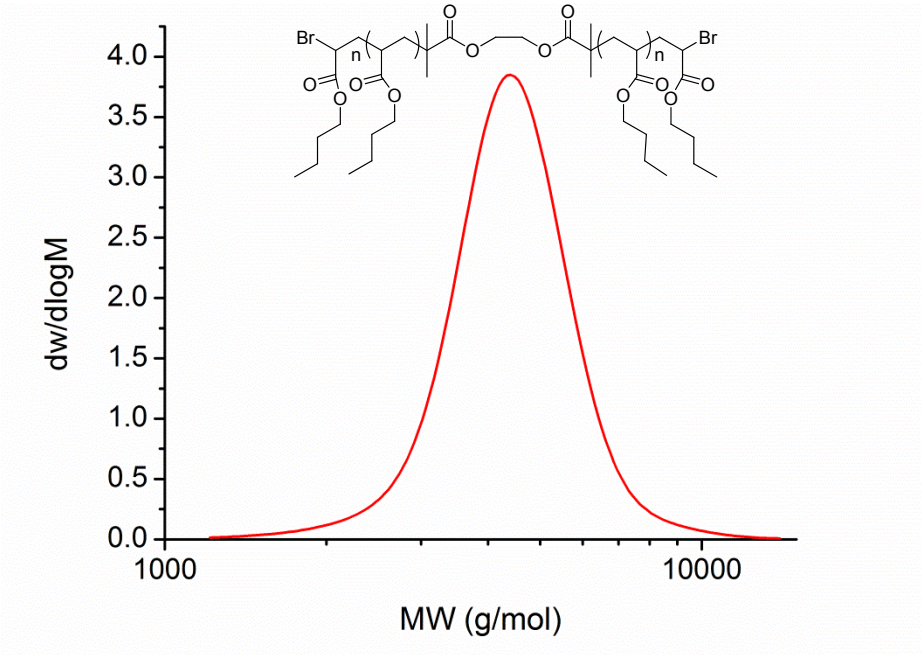


***Figure 2.4*** *SEC chromatogram for the polymerization of n-butyl acrylate using 2F-BiB bifunctional initiator via $Cu^{(0)}$-mediated RDRP in DMSO at ambient temperature, [M]:[-Br]:[$Cu^{(II)}$]:[L] = 35:1:0.05:0.18. $M_n$ = 4200 g $mol^{-1}$, $Đ_M$ = 1.10*

### 2.2.1 MALDI-TOF Analysis

MALDI-TOF MS analysis of this polymer shows two major distributions, unlike the monomodal distribution seen using SEC. The main distribution corresponds to the desired bifunctional polymer, the end group fidelity of which is confirmed by both the *m/z* values which are in close agreement with theoretical values and the isotopic pattern which indicates the presence of two bromide terminal groups (**Figure 2.5**).

The second, lower molecular weight distribution is that of polymer which has been terminated at one end via loss of a bromide but continued to grow from the other; this again is elucidated by the agreement with theoretical mass values and splitting patterns. This effect is attributed to chain transfer to ligand in the early stages of the reaction, where the ligand can react with the initiator at a comparable rate to the monomer.

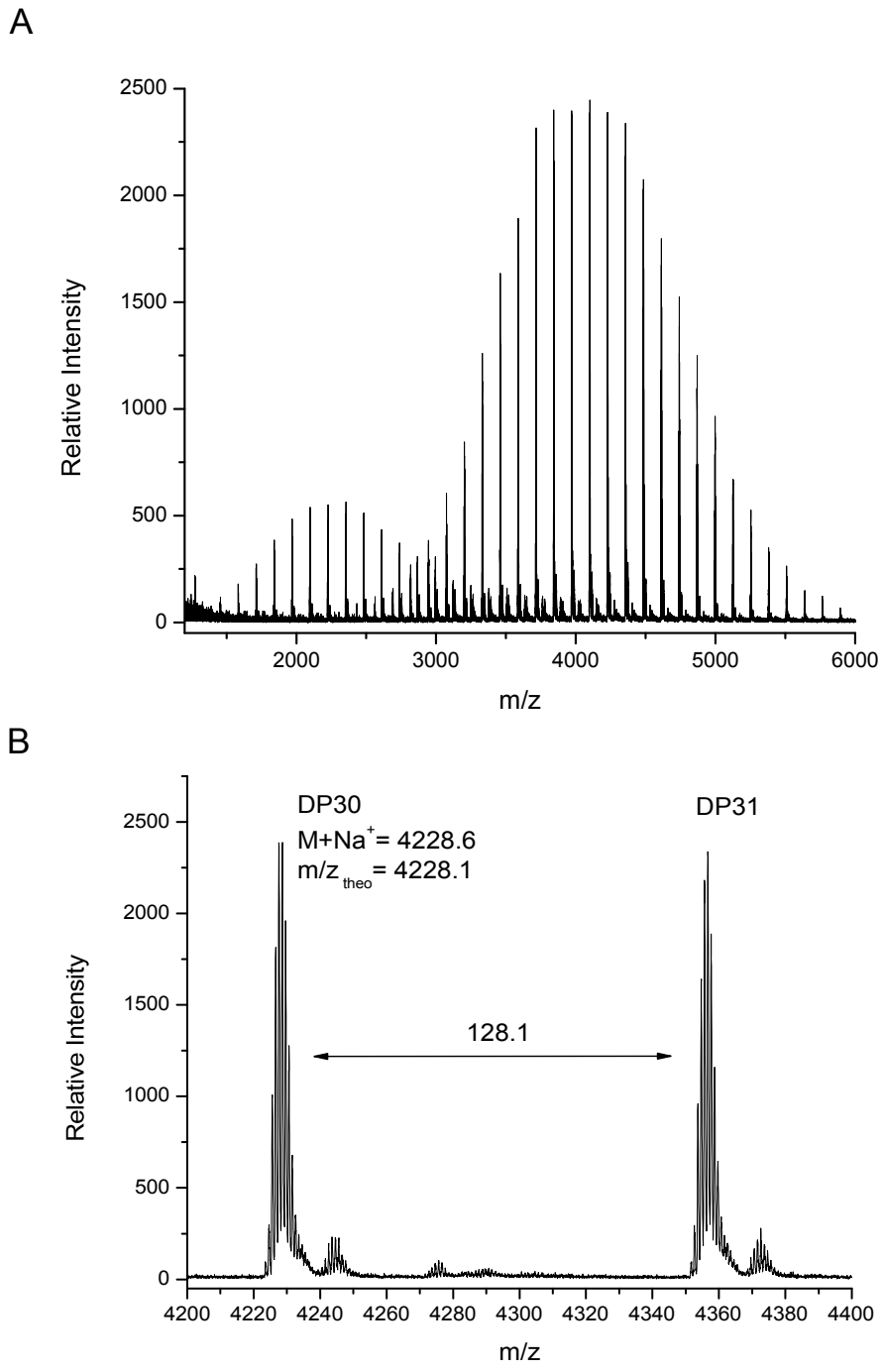


***Figure 2.5*** *(A) MALDI-TOF MS spectra for the polymerization of n-butyl acrylate using 2F-BiB bifunctional initiator via $Cu^{(0)}$-mediated RDRP in DMSO at ambient temperature, [M]:[-Br]:[$Cu^{(II)}$]:[L] = 35:1:0.05:0.18, at >99% conversion (B) expansion from 4200-4400 m/z*

### 2.2.2 Reaction Kinetics

To test the 'livingness' of this biphasic system, a kinetic experiment was carried out using the same reaction conditions as described previously. Targeting a molecular weight of 4500 g $mol^{-1}$, the reaction was monitored over time and the samples submitted for $^{1}H$ NMR and SEC analysis. A linear plot of $M_n$ vs. conversion (%) was obtained, which is indicative of a living polymerization.

A plot of $\ln[M_0]/[M_t]$ vs. time shows two linear domains: the first appears to show slow reaction ($k^{app}_{p} = 0.003$ $min^{-1}$) before a dramatic increase in the apparent rate at around 60 minutes with $k^{app}_{p} = 0.047$ $min^{-1}$. This change in rate coincides with the phase separation of the polymer from the reaction mixture (**Figure 2.3**), with the $M_n$ at this point being between 1 and 2 kg $mol^{-1}$. This observation of phase separation accompanied by a dramatic increase in the reaction rate was also noted by our collaborators at the University of New South Wales (UNSW)[18]. The kinetic plots are given in **Figure 2.6**.

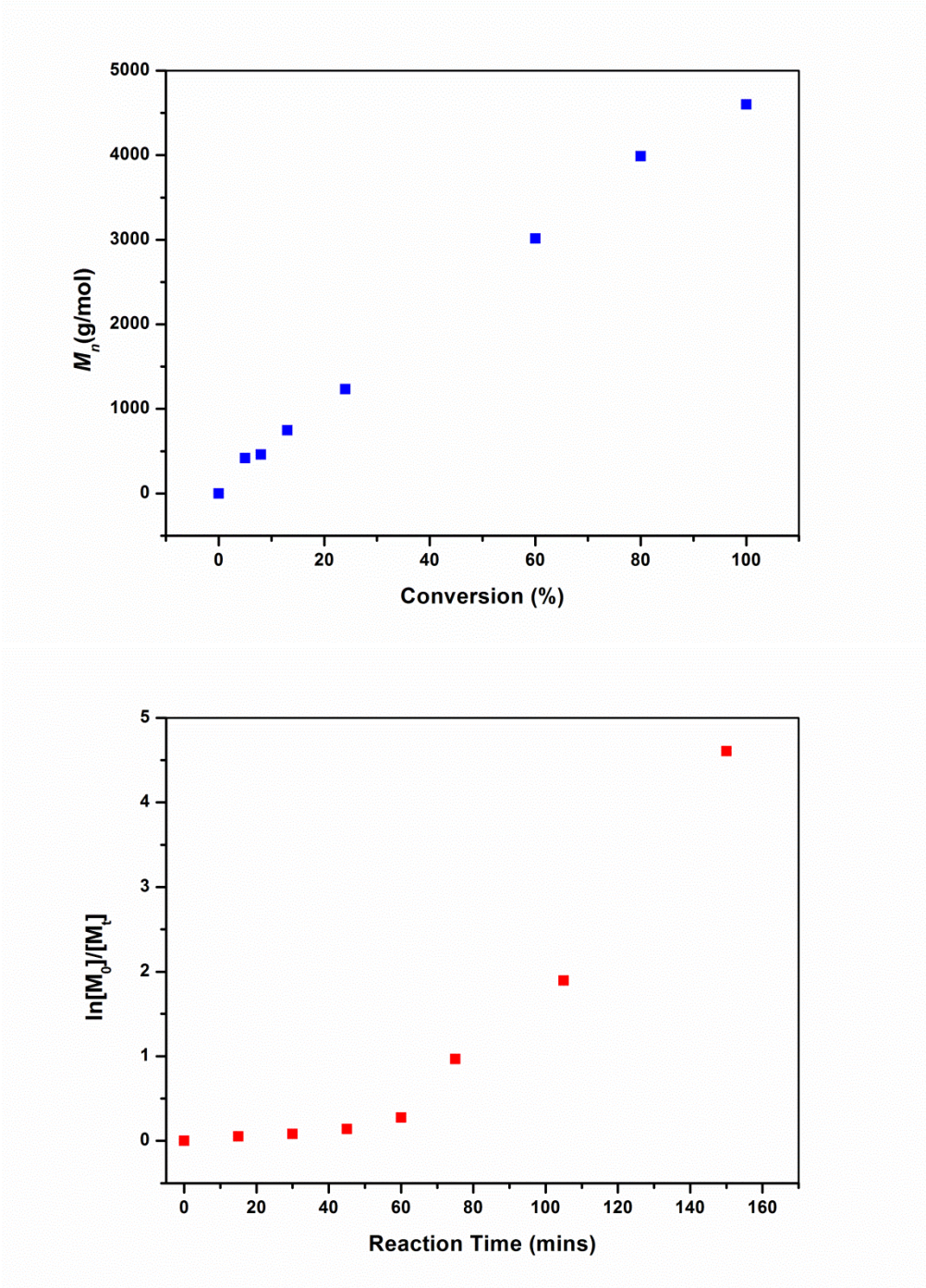


***Figure 2.6*** *Kinetic data for the polymerization of n-butyl acrylate using 2F-BiB bifunctional initiator via $Cu^{(0)}$-mediated RDRP in DMSO at ambient temperature, [M]:[-Br]:[$Cu^{(II)}$]:[L] = 35:1:0.05:0.18. Shown above is a plot of ln[$M_0$]/[$M_t$] vs. time and below is a plot of $M_n$ vs. conversion (%)*

### 2.2.3 Analysis of Layers

Intuitively, one might assume that the upper viscous phase is polymer which has precipitated from the highly polar DMSO solvent due to its hydrophobicity. Furthermore, it may also be deduced that the intense green colouration of the bottom layer indicates that this is where a significant amount of the copper species (Cu/L) is present. To investigate this further each layer was sampled and analysed using $^{1}$H NMR spectroscopy, SEC, elemental analysis, and MALDI-TOF MS.

Both layers were tested after the reaction had reached complete conversion (>99%). The $^{1}$H NMR spectrum of the top layer reveals the presence of n-butyl acrylate polymer, solvent (~20 wt%) and no monomeric peaks. For the bottom layer, only solvent peaks are observed (**Figure 2.7**). Upon repeating the reaction, the layers were sampled after 1.5 hours (**Figure 2.8**) reaction time (at approximately 50% conversion) giving similar results; the top layer contains polymer, solvent and monomer and the bottom layer only monomer and solvent with no polymer. SEC analysis of both layers also confirms that the top contains polymer and the bottom layer is polymer free. These findings are a strong indication that the initial assumption is correct and that the polymer phase separates from the reaction mixture giving an upper polymer phase and a lower phase containing only solvent/monomer/Cu species.

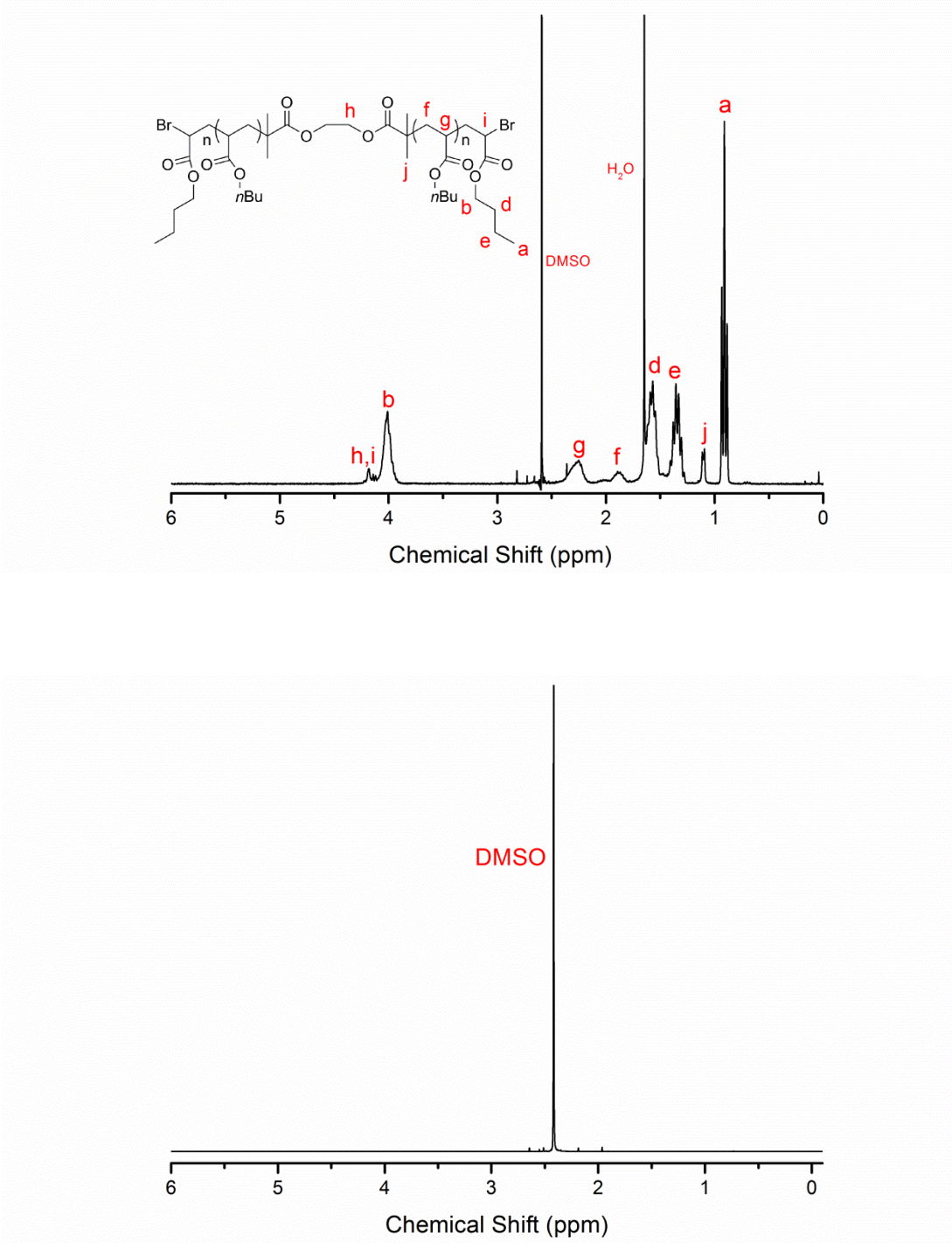


***Figure 2.7*** *$^{1}$H NMR spectra for the polymerization of n-butyl acrylate using 2F-Bib bifunctional initiator via $Cu^{(0)}$-mediated RDRP in DMSO at ambient temperature, [M]:[-Br]:[$Cu^{(II)}$]:[L] = 35:1:0.05:0.18 at >99% conversion. A) Upper 'polymer' phase B) lower phase*

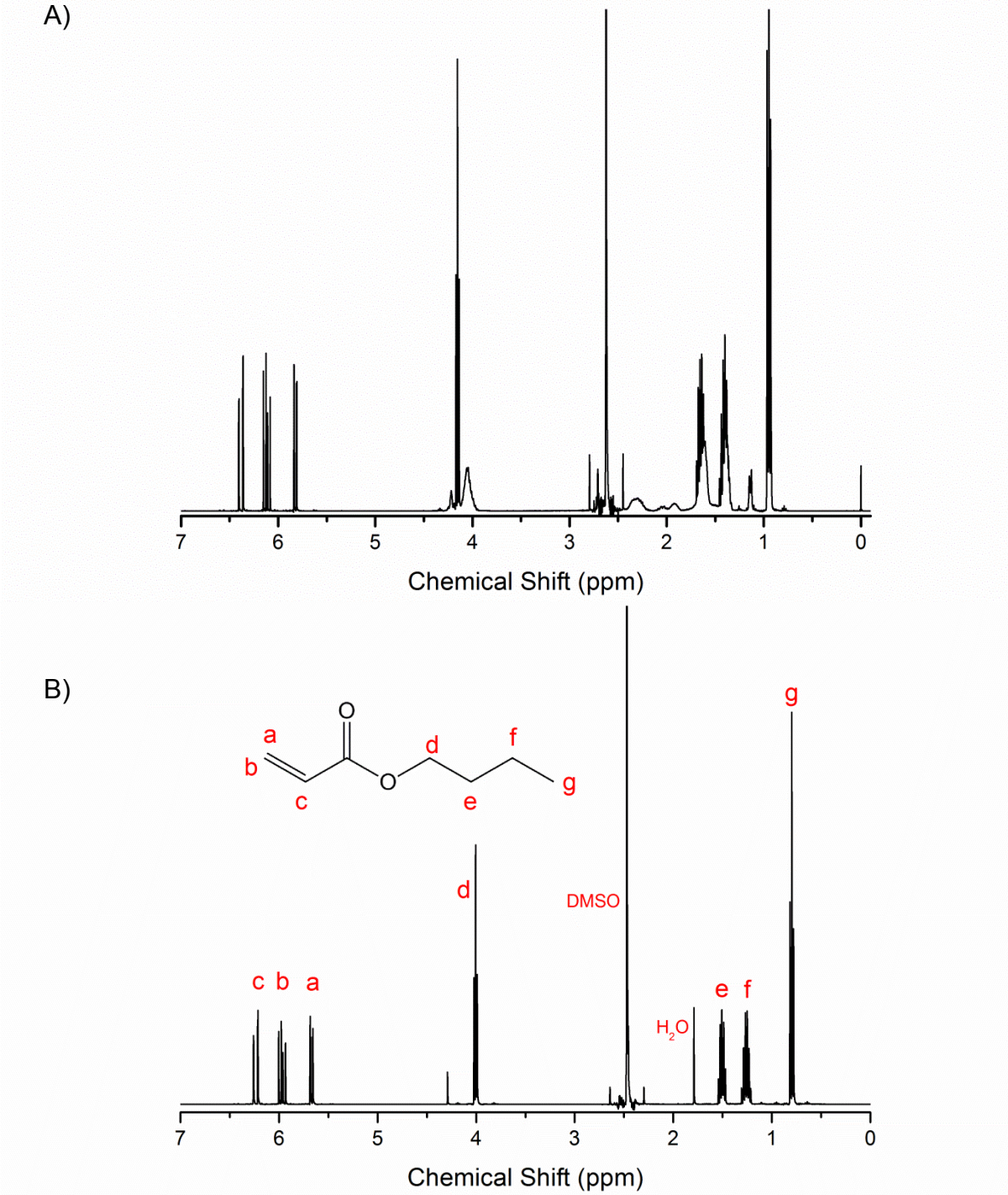


***Figure 2.8*** *$^{1}$H NMR spectra for the polymerization of n-butyl acrylate using 2F-Bib bifunctional initiator via $Cu^{(0)}$-mediated RDRP in DMSO at ambient temperature, [M]:[-Br]:[$Cu^{(II)}$]:[L] = 35:1:0.05:0.18 at 1.5 hours reaction time. A) Upper 'polymer' phase B) lower phase*

To obtain a quantitative measure as to the levels of Cu species in the polymer phase, (X-Ray Photoelectron Spectroscopy (XPS) and Inductively Coupled Plasma Mass Spectroscopy (ICP-MS) analysis was carried out at UNSW on a sample of crude poly(*n*-butyl acrylate) taken directly from the upper layer of the reaction mixture. No Cu was detected via XPS, indicating that there are no Cu species in this layer or that the levels were below the detection threshold of the instrument (0.05 atom%) (**Figure 2.9**, **Table 2.1**). The amounts of Cu detected by ICP-MS were in the order of 0.016 wt%, a very low value when compared to polymers synthesized using typical ATRP which have copper levels of around 1wt-%/1000 ppm prior to purification[19, 20]. These results suggest that the phase separation results in a near total separation of the polymer from the catalyst, as initially indicted by the lack of colouration in the upper phase and strong green colour in the lower phase.

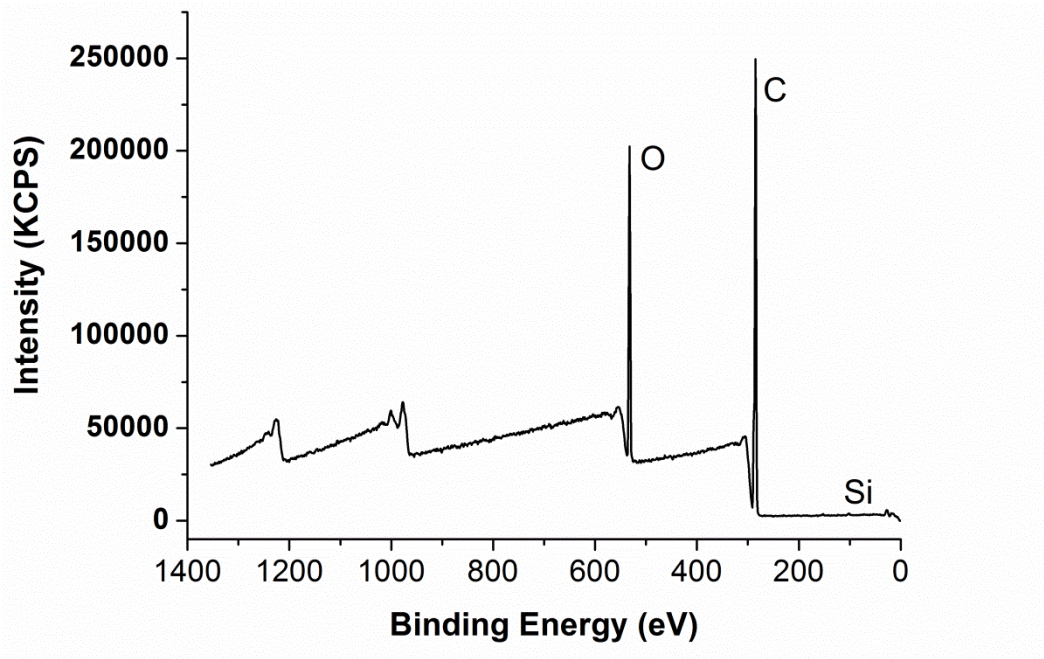


***Figure 2.9*** *Wide XPS spectrum of crude poly(n-butyl acrylate) (upper layer) obtained via $Cu^{(0)}$-mediated RDRP in DMSO*

| Type | Binding Energy (eV) | Atom-% |
|---|---|---|
| **C 1s** | | 68.68 |
| **O 1s** | 282-2.89 | 20.05 |
| **Si 2p** | 105.6 | 0.27 |
| **Cu 3s** | 124-125 | Non-detectable |
| **Cu 2p1/2** | 932-933 | Non-detectable |
| **Cu 2p3/2** | 934-935 | Non-detectable |

***Table 2.1*** *Elemental analysis derived from XPS of crude poly(n-butyl acrylate) (upper layer) obtained via $Cu^{(0)}$-mediated RDRP in DMSO*

### 2.2.4 Polymerization of Other Monomers

The polymerization was repeated but with isomers of *n*-butyl acrylate (*iso*- and *tert*-) (**Table 2.2, Figure 2.10**). Phase separation is also observed and the polymerizations proceeded with good control, however a small increase in the dispersity can be observed. We have attributed this effect simply due to the increase in steric bulk from *n*- to *iso*- to *tert*. Additionally in the case of poly(*t*-butyl acrylate), the increased $T_g$ causes it to form a more 'solid' mass upon phase separation, hindering its ability to react efficiently.

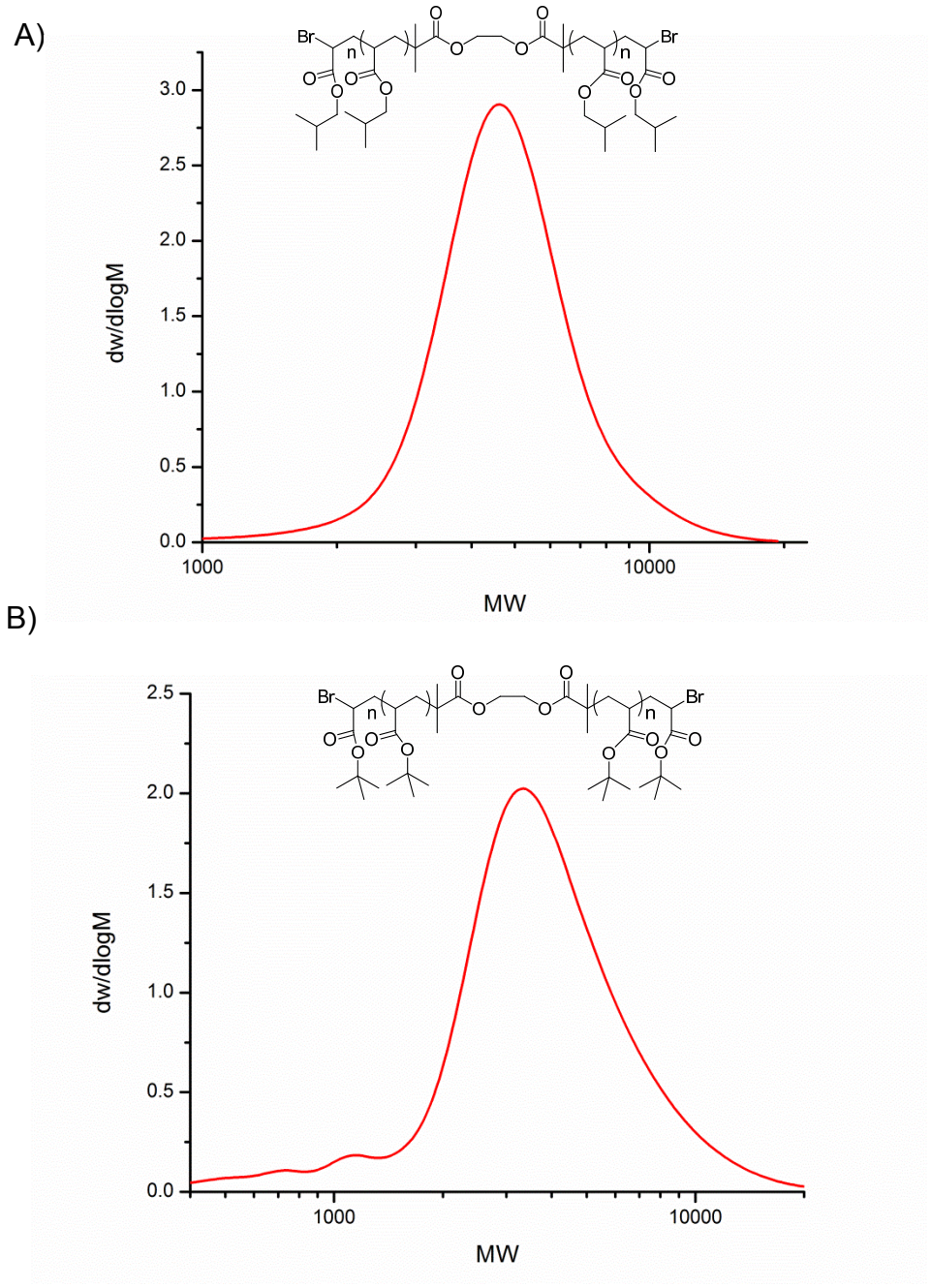


***Figure 2.10*** *SEC chromatograms for the polymerization of isobutyl acrylate (top) and tertiary butyl acrylate (bottom) via* $Cu^{(0)}$*-mediated RDRP in DMSO at ambient temperature,* $[M]:[\text{-Br}]:[Cu^{(II)}]:[L] = 35:1:0.05:0.18$

Finally, the effects of some more hydrophobic acrylates (lauryl and 2-ethyl hexyl acrylate) were examined (**Table 2.2**, **Figure 2.11**). As these monomers are insoluble in DMSO at ambient temperature, the reaction mixture was in two phases at the start of the polymerization. Polymerization was achieved as indicated by a high monomer conversion (>90%), however the large molecular weights and high mass dispersity achieved indicate that control of the reaction has been lost. Thus it is important for the monomers to be soluble in the polar solvent whilst the polymer becomes insoluble.

| Monomer | Target $M_n$ (g mol$^{-1}$) | $M_n$ (SEC) | $Đ_M$ |
|---|---|---|---|
| ***n*-butyl acrylate** | 4480 | 4 200 | 1.10 |
| ***iso*-butyl acrylate** | 4480 | 4 300 | 1.16 |
| ***tert*-butyl acrylate** | 4480 | 2 900 | 1.42 |
| **lauryl acrylate** | 4480 | 22 300 | 2.23 |
| **2-ethylhexyl acrylate** | 4480 | 4 500 | 5.75 |

***Table 2.2*** *Summary of the polymerization data for the synthesis of hydrophobic poly(acrylates) using $Cu^{(0)}$-mediated RDRP in DMSO*

A)

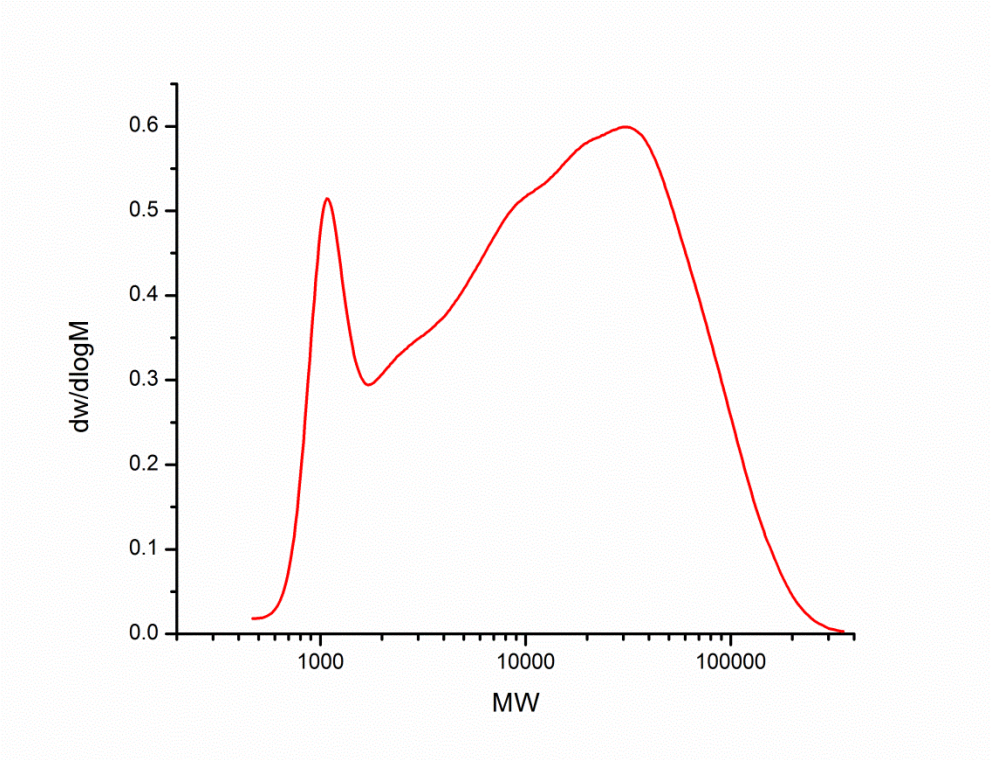


B)

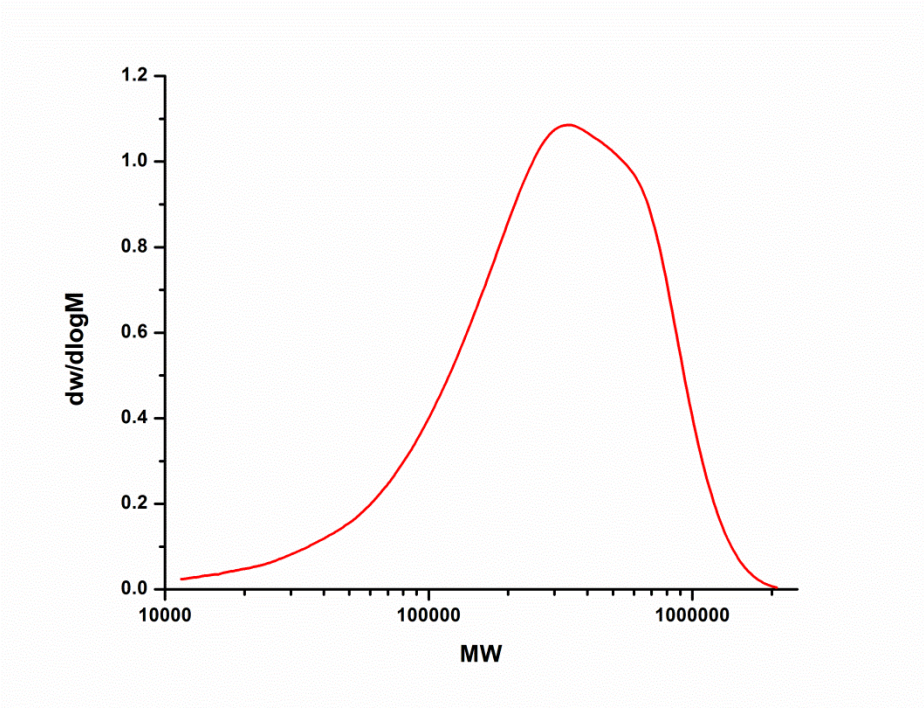


***Figure 2.11*** *SEC chromatograms for the polymerization of 2-ethyl hexyl acrylate (A) and lauryl acrylate (B) via $Cu^{(0)}$-mediated RDRP in DMSO at ambient temperature, [M]:[-Br]:[$Cu^{(II)}$]:[L] = 35:1:0.05:0.18. SEC data is given in Table 2.2*

## 2.3 Investigation into the Effect of Ligand Concentration

As mentioned previously, MALDI-TOF analysis of telechelic poly(*n*-BA) synthesized showed the presence of two distinct species; the desired bifunctional polymer with α-ω bromo functionality and a second in which there has been the loss of –Br from one end resulting in 'dead' polymer.

Other studies in our group[21] demonstrated that free ligand can cause chain-breaking events during $Cu^{(0)}$-mediated RDRP polymerizations, namely via chain transfer to ligand and quaternization of the ligand onto the ω-end of the polymer, resulting in a loss of –Br. Based on these findings it was felt that the observed termination found for these telechelic polymers may also be caused by reactions with the ligand and so experiments to assess the effect of differing ligand concentration were carried out. *n*-butyl acrylate was polymerized in DMSO at room temperature using the telechelic 2F-BiB initiator in the presence of $Cu^{(0)}$ wire, $Cu^{(II)}Br_2$ (0.05eq) and $Me_6$TREN of varying concentration (0.12, 0.18 and 0.36eq), targeting a DP of 35 ($M_n$ = 4,800).

| Experiment | [M]:[I]:[$Cu^{(II)}$]:[L] | Conversion (%) | $M_n$ (theo) | $M_n$ (SEC) | $Đ_M$ |
|---|---|---|---|---|---|
| **1** | 35:1:0.05:0.12 | >99 | 4800 | 4900 | 1.13 |
| **2** | 35:1:0.05:0.18 | >99 | 4800 | 4300 | 1.16 |
| **3** | 35:1:0.05:0.36 | >99 | 4800 | 5500 | 1.15 |

***Table 2.3*** *Summary of the polymerization data for the synthesis of hydrophobic poly(acrylates) using $Cu^{(0)}$-mediated RDRP in DMSO with varying ligand concentration. [L] = $Me_6$TREN*

In all cases, near quantitative conversion is obtained with good agreement between theoretical and experimental molecular weights and low mass dispersities, all of which are indicative of a well-controlled polymerization. Analysis of the SEC chromatograms reveal monomodal distributions with minimal tailing at either the low or high molecular weight ends, again evidence of a controlled reaction **(Figure 2.12**).

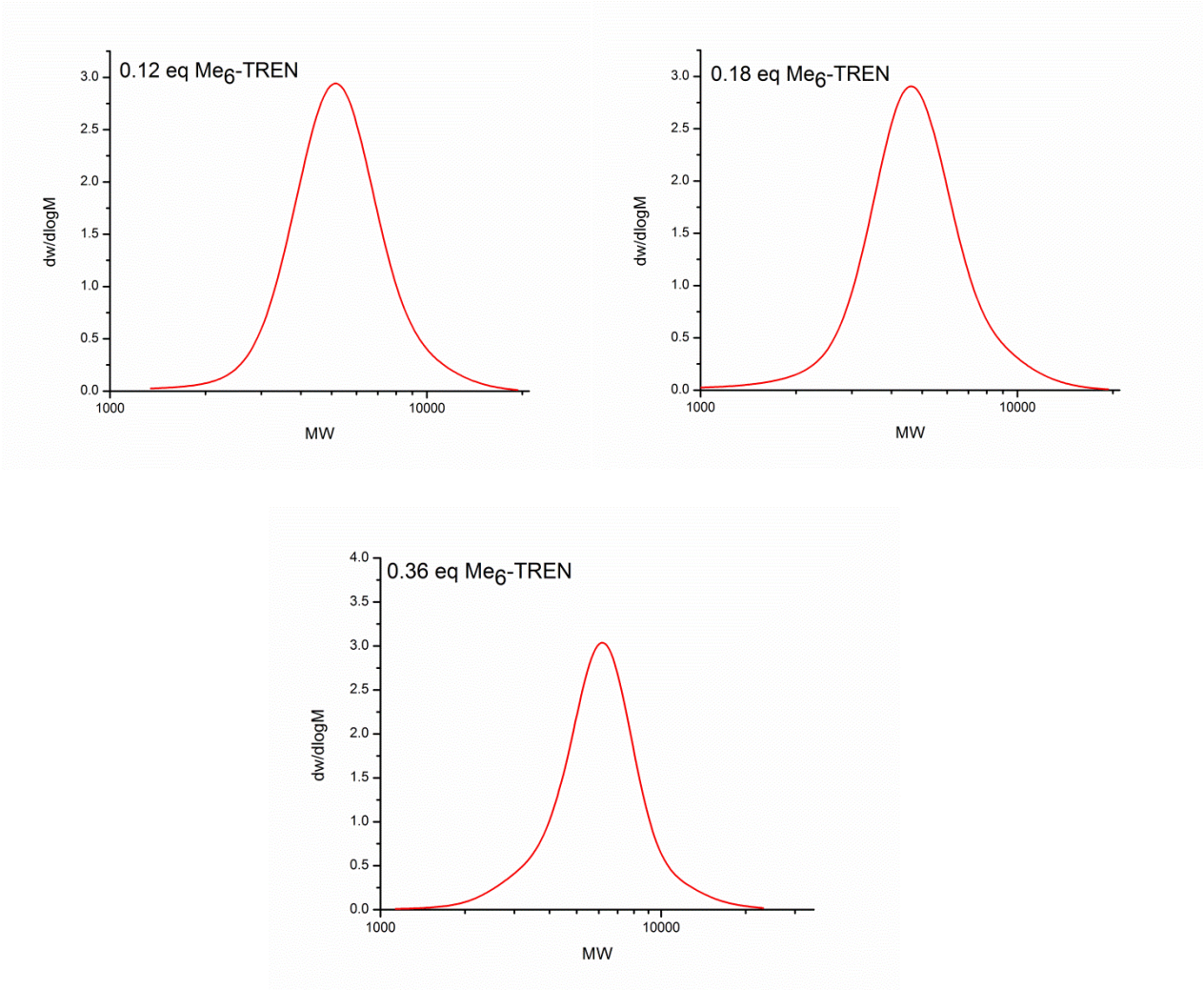


***Figure 2.12*** *SEC chromatograms for the polymerization of n-butyl acrylate using $Cu^{(0)}$-mediated RDRP in DMSO at room temperature, with varying ligand levels. [M]:[I]:[$Cu^{(II)}$]:[L] = 35:1:0.05:0.12, 35:1:0.05:0.18 and 35:1:0.05:0.36*

However, as per the previous analysis using MALDI-TOF MS, it can be seen that the initial data does not tell the full story of what is occurring during the reaction (**Figures 2.13-2.15**). Again, two distributions are present, the 'major' one being the desired bifunctional polymer and the 'minor' in which one –Br has been lost from one end. Furthermore, it can be seen that the 'minor' undesired distribution dramatically increases with ligand concentration and is effectively supressed when the level of ligand is reduced to 0.12 eq. This supports the hypothesis of free ligand causing termination, in line with the other results obtained in our group[21].

This is an as yet unseen effect of the ligand in such reactions and would not have been detected were it not for this extra level of characterization and is perhaps surprising given the number of radical polymerization papers in the literature (both ATRP and $Cu^{(0)}$-mediated RDRP) utilising $Me_6$TREN as the ligand. Importantly, it now allows for the optimization of the conditions for future reactions with 0.12eq being chosen as a good compromise between the suppression of ligand-induced termination reactions and acceptable reaction rate.

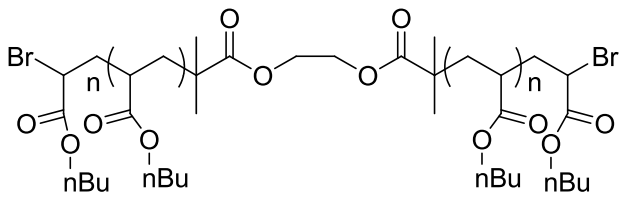


A)

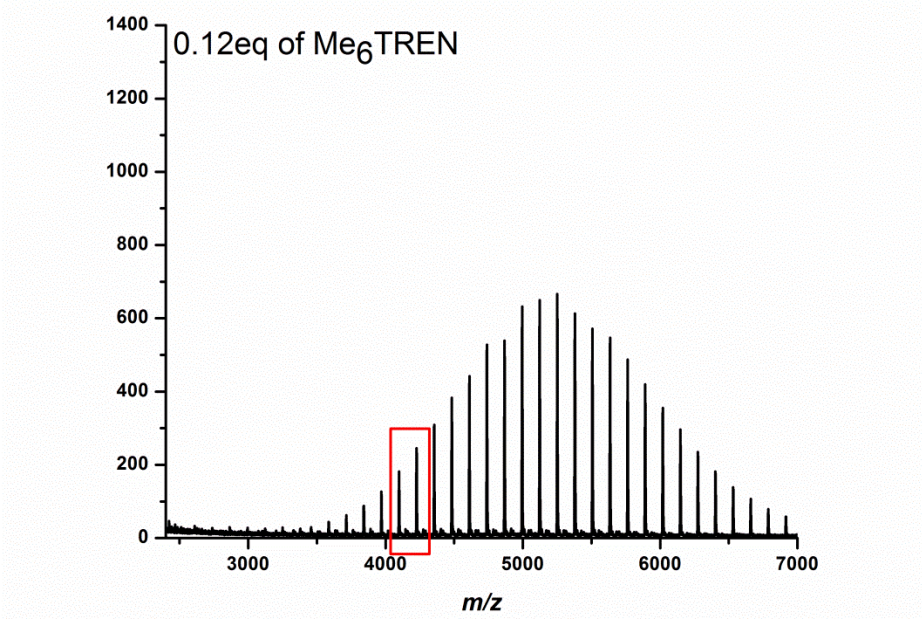


B)

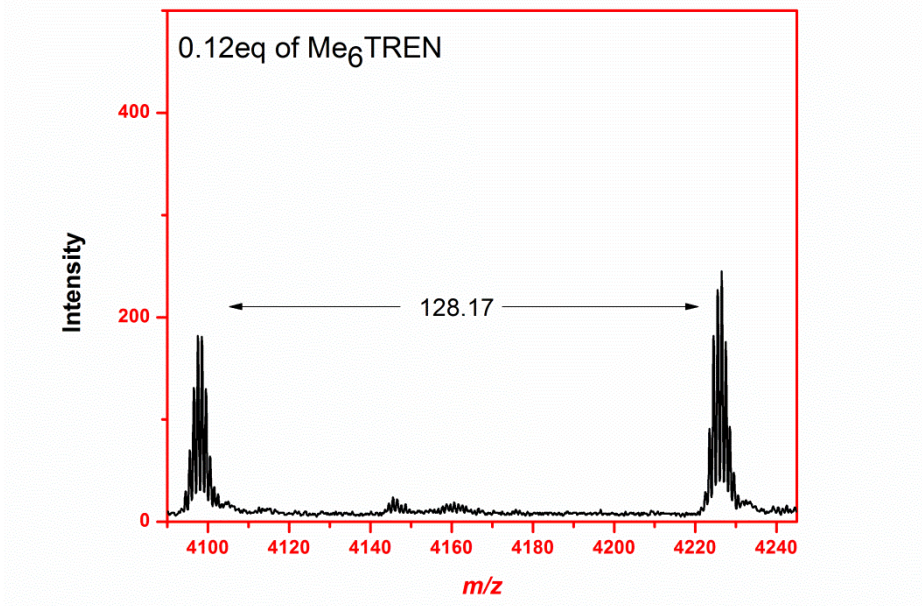


***Figure 2.13*** *(A) MALDI-TOF MS spectrum of poly(n-BA) and (B) expansion obtained via* $Cu^{(0)}$*-mediated RDRP in DMSO at room temperature [M]:[I]:*$[Cu^{(II)}]$*:[L] = 35:1:0.05:0.12*

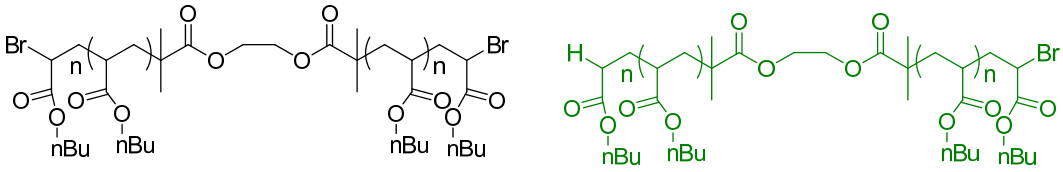


A)

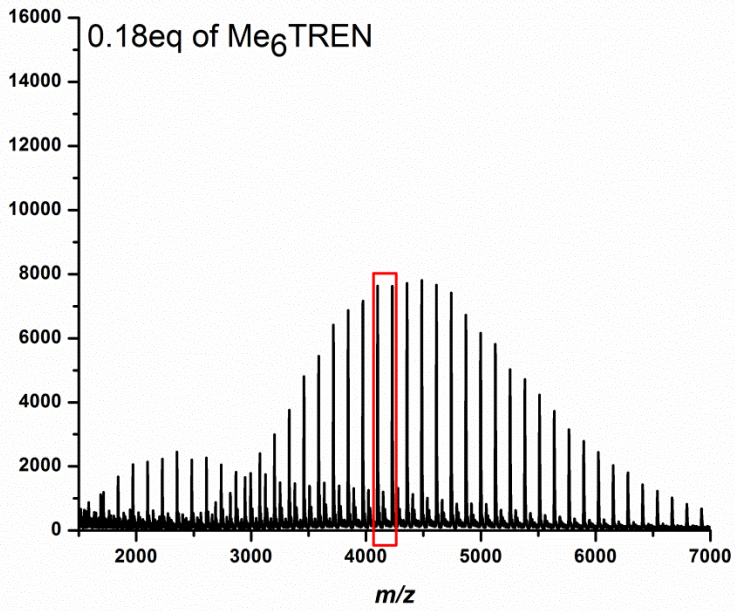


B)

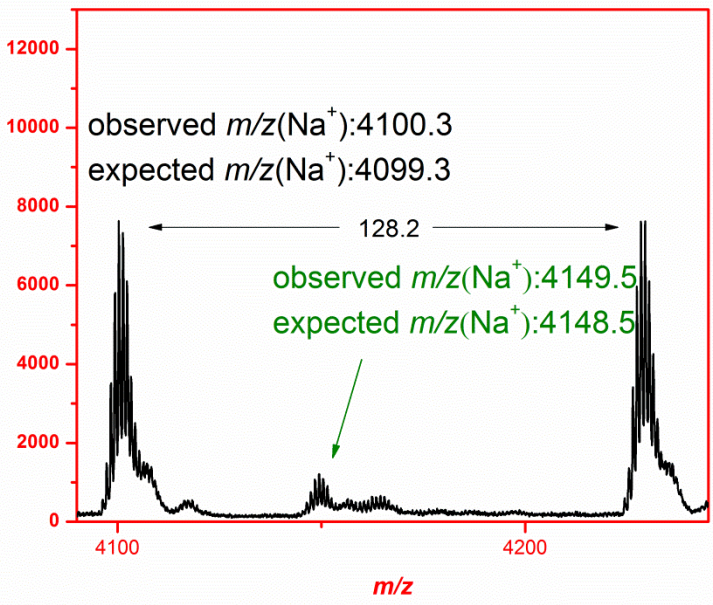


***Figure 2.14*** *(A) MALDI-TOF MS spectrum of poly(n-BA) and (B) expansion obtained via* $Cu^{(0)}$*-mediated RDRP in DMSO at room temperature [M]:[I]:*$[Cu^{(II)}]$*:[L] = 35:1:0.05:0.18*

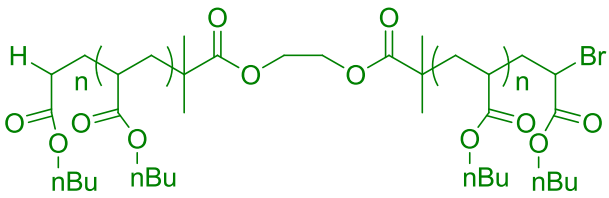


A)

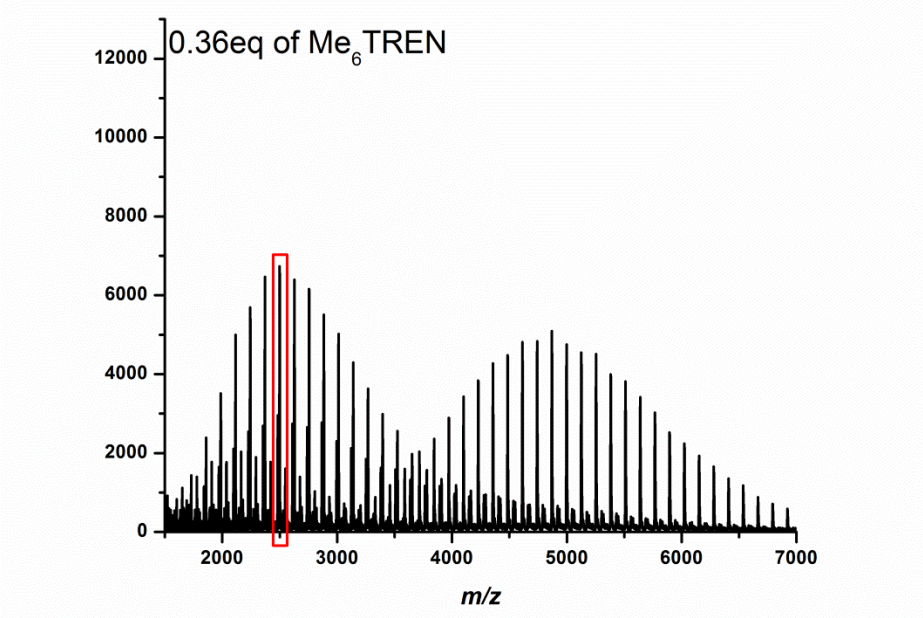


B)

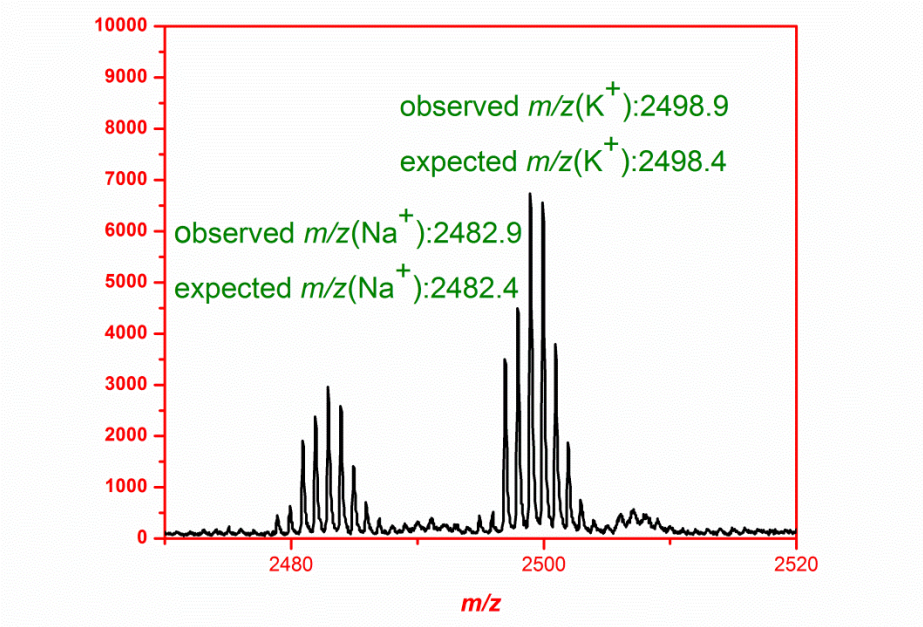


***Figure 2.15*** *MALDI-TOF MS spectrum of poly(n-BA) and expansion obtained via $Cu^{(0)}$-mediated RDRP in DMSO at room temperature [M]:[I]:[$Cu^{(II)}$]:[L] = 35:1:0.05:0.36*

## 2.4 Higher Molecular Weight/Chain Extension Experiments

Thus far, only low molecular weight polymers have been targeted which raises the question at to the effect of molecular weight on this biphasic system (ie. does the polymer simply precipitate out at a certain molecular weight and then cease to propagate?). This was investigated by targeting a higher molecular weight (10,000 $gmol^{-1}$) using the now optimized polymerization conditions ([-Br]:[$Me_6$TREN]:[$Cu^{(II)}Br_2$] = 1: 0.12: 0.05 in DMSO) and a monofunctional poly(butyl acrylate) with $M_n$ = 11,000 g $mol^{-1}$ and $Đ_M$ = 1.09 was obtained at 98% conversion. This result shows that higher molecular weights can indeed be targeted and achieved with a high degree of control, which is again surprising given the heterogeneous nature of the reaction.

Since this is a living polymerization and that higher molecular weights can be produced, this raises the possibility of chain extending the polymer via monomer addition at full conversion. Doing so would further test the biphasic system and also see if there is an upper molecular weight limit to this reaction scheme. To the previously synthesized poly(*n*-BA) reaction mixture ($M_n$ = 11 kg $mol^{-1}$) a further aliquot of degassed monomer was added to target a molecular weight increase of 10 kg $mol^{-1}$. Upon reaching complete conversion the same amount of monomer was again added and this cycle repeated four times in total. The results of these chain extension experiments are outlined in **Table 2.3** and **Figure 2.16** below.

| Number of Blocks | Theoretical $M_n$ (g mol$^{-1}$) | Experimental $M_n$ (SEC, g mol$^{-1}$) | Conversion (%) | $Đ_M$ |
|---|---|---|---|---|
| **1** | 10,000 | 11,000 | 98 | 1.1 |
| **2** | 20,000 | 19,000 | 98 | 1.09 |
| **3** | 30,000 | 27,000 | 94 | 1.1 |
| **4** | 40,000 | 38,000 | 94 | 1.09 |
| **5** | 50,000 | 53,000 | 90 | 1.07 |

***Table 2.4*** *One-pot iterative chain extensions of telechelic poly(n-butyl acrylate) synthesized using $Cu^{(0)}$-mediated RDRP in DMSO. [I]:[$Me_6$TREN]:[$Cu^{(II)}Br_2$] = 1: 0.12: 0.05. Kinetic and SEC data are given in Figure 2.16*

These results demonstrate the ability to carry out chain extensions in an iterative manner without the loss of the control associated with a living polymerization. In all cases near-quantitative conversion is achieved with each monomer addition and the obtained molecular weights closely match with that of theory. The SEC chromatograms show minimal tailing, indicating clean re-initiation and the narrow dispersities indicate that there is little/no loss of control when carrying out chain extensions in this biphasic system. In addition, it is apparent that relatively high molecular weights can be targeted, despite the phase separation observed.

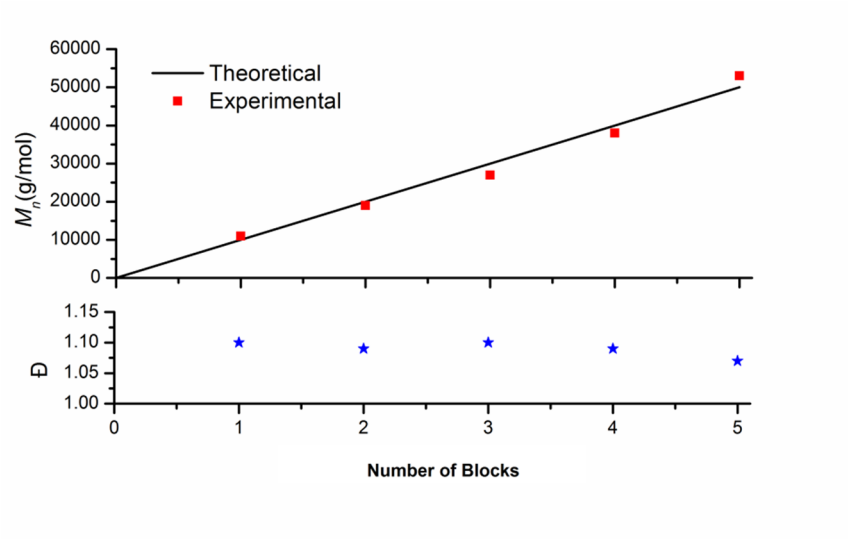


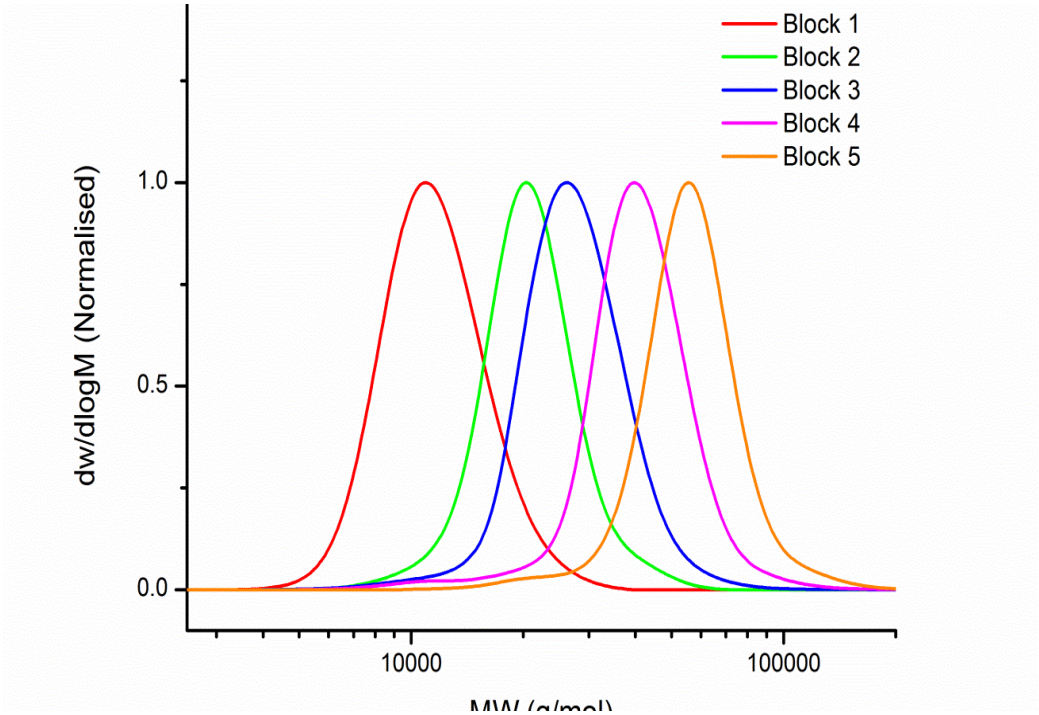


***Figure 2.16*** *Number average molecular weights, dispersities and SEC chromatograms for the iterative chain extensions of telechelic poly(n-BA) in DMSO at ambient temperature. Conversions are displayed in Table 3. [I]:[$Me_6$TREN]:[$Cu^{(II)}Br_2$] = 1: 0.12: 0.05*

## 2.5 Functionalization of telechelic poly(*n*-butyl acrylates) Using Thio-Bromo Substitution

The excellent end group fidelity of the previously synthesized poly(*n*-butyl acrylates) allow for the terminal bromides to be exploited in order to introduce functionality. This can be achieved via nucleophillic substitution of the bromide groups with a thiol to generate a thioether (**Figure 2.17**). This thio-halogen substitution is often referred to as a 'click' reaction[22-25] as it proceeds at room temperature with high efficiency, fast rate, use benign catalysts, and can be carried out in the presence of oxygen/water.

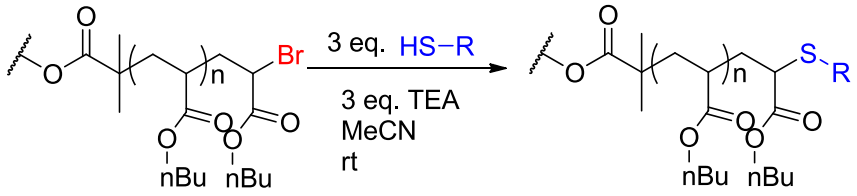


***Figure 2.17*** *Functionalization of polymers via thioetherifaction of terminal bromide atoms*

Telechelic poly(*n*-BA) ($M_n$ = 4 kg mol$^{-1}$) was reacted with a slight excess (3eq) of thiogylcerol in the presence of triethylamine (TEA) with MeCN as the solvent. MALDI-TOF MS was used as the principle characterization technique for this study due to its previously reported utility for the quantatative mass analysis of polymers[26-30] Reaction monitoring by MALDI-TOF MS (**Figure 2.18**) reveals dissapearance of the starting material and the appearance of a new species with *m/z* values concomitant with the complete substitution of both α-ω terminal bromides with thioglycerol. The product was then isolated by precipitating the reaction mixture into cold methanol.

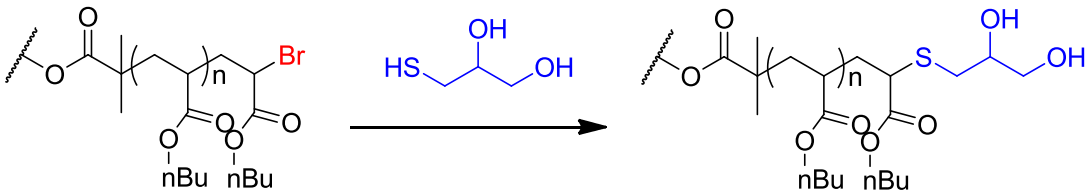


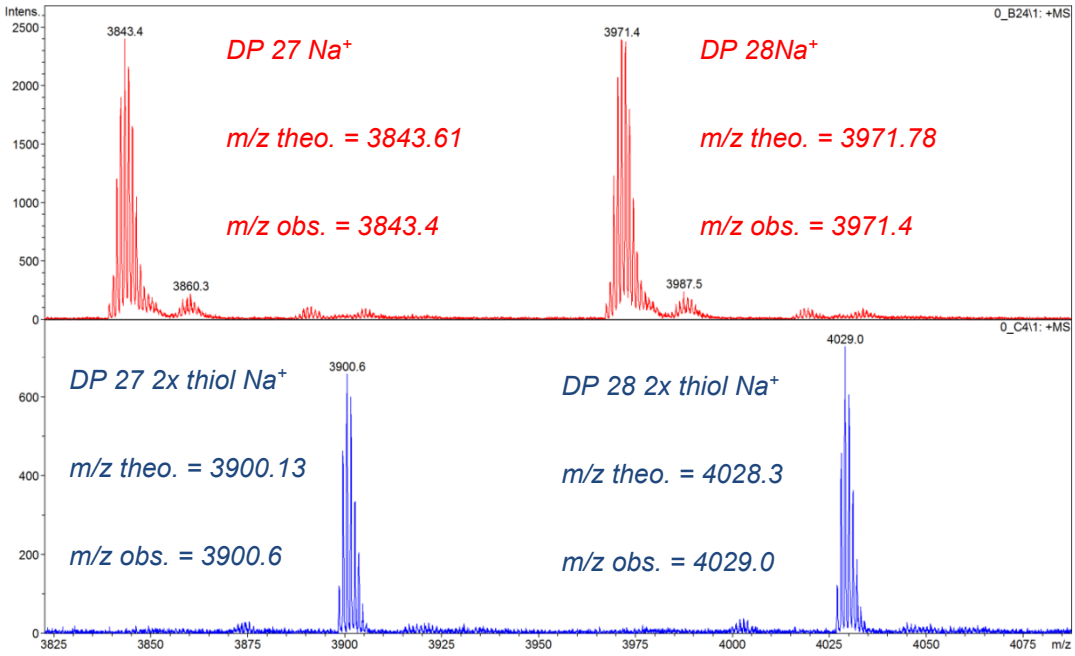


***Figure 2.18*** *Expanded MALDI-TOF MS spectra for the reaction of telechelic poly(n-butyl acrylate),* $M_n$ *= 4.1 kg mol*$^{-1}$ *with thioglycerol. The red spectrum is that of the starting material and the blue is the reaction mixture after three hours*

Using the same reaction conditions, the experiments were then repeated using 2-mercaptoethanol and thioacetic acid. In both cases quantatitive substitution of the terminal bromides with two thiol groups was again observed using MALDI-TOF MS (**Figures 2.19** and **2.20** respectively). A reaction using sodium methanethiosulfonate was also attempted (**Figure 2.21**), which does not require the use of a base. With this, all of the starting material was consumed to give ~90% bisubstitued product with the remaining 10% being monosubstituted.

A final thiol, thioglycolic acid was then investigated. This reaction was largely unsuccessful, compared with the previous reactions attempted it can be seen that a large amount of the starting polymer remains, with a small mixture of mono and disubstituted products formed (**Figure 2.22**). This failure can be attributed to the fact that since the thiol is an acid, it can be neutralized by the basic TEA catalyst to form the corresponding triethylammonium salt and precipitate out of solution.

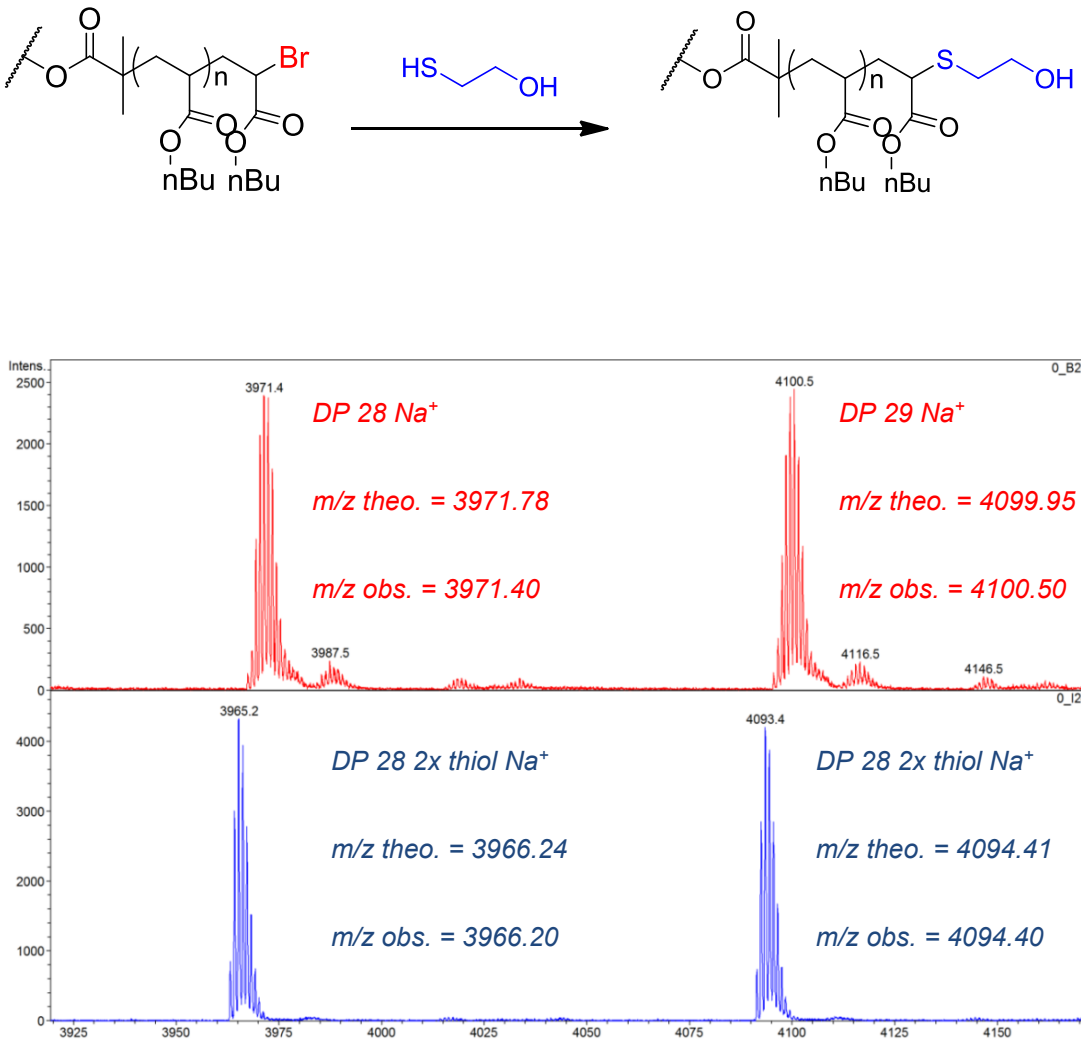


***Figure 2.19*** *Expanded MALDI-TOF MS spectra for the reaction of telechelic poly(n-butyl acrylate), $M_n$ = 4.1 kg mol$^{-1}$ with mercaptoethanol. The red spectrum is that of the starting material and the blue is the reaction mixture after three hours*

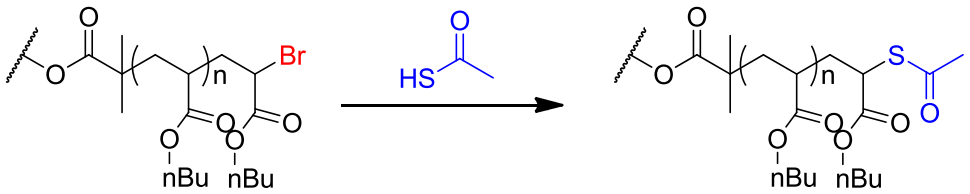


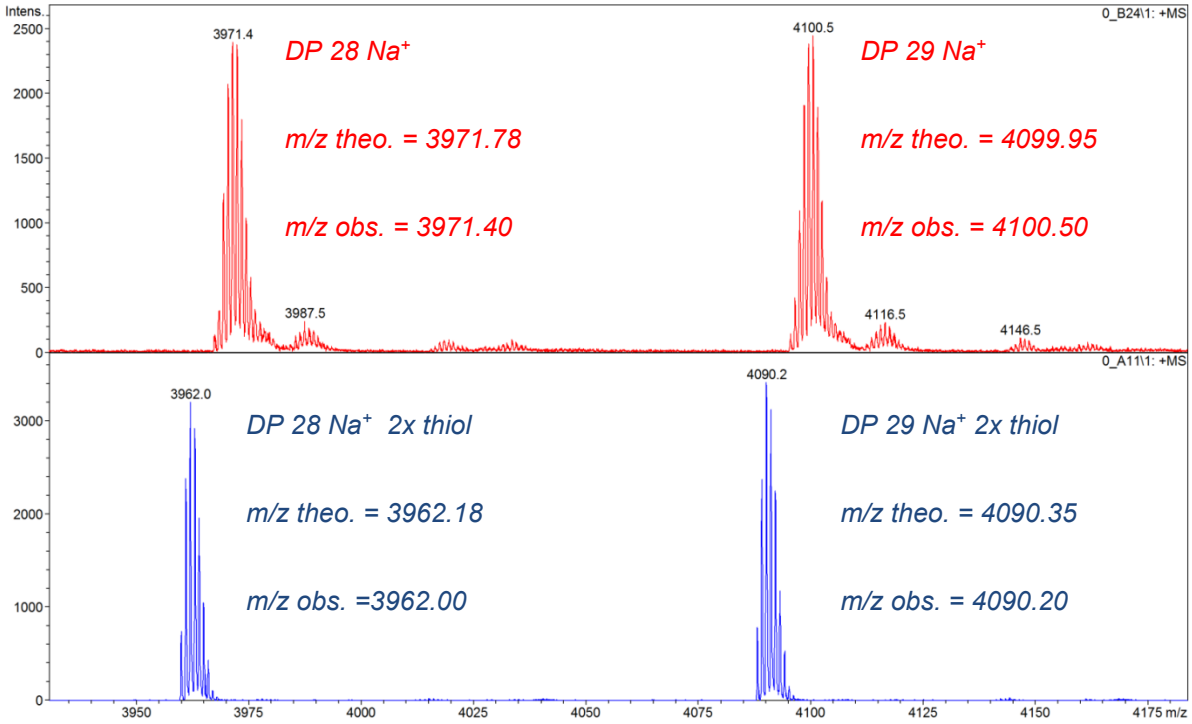


***Figure 2.20*** *Expanded MALDI-TOF MS spectra for the reaction of telechelic poly(n-butyl acrylate), 4.1 kg mol$^{-1}$ with thioacetic acid. The red spectrum is that of the starting material and the blue is the reaction mixture after three hours*

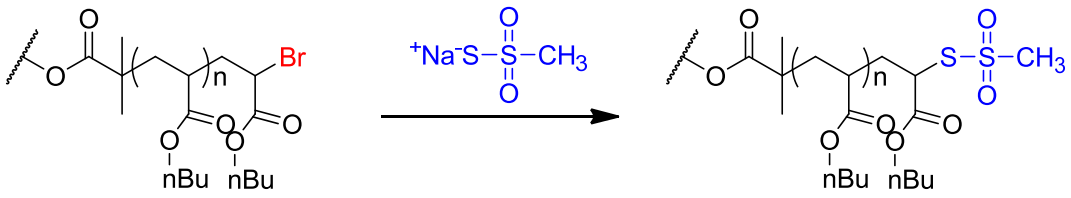


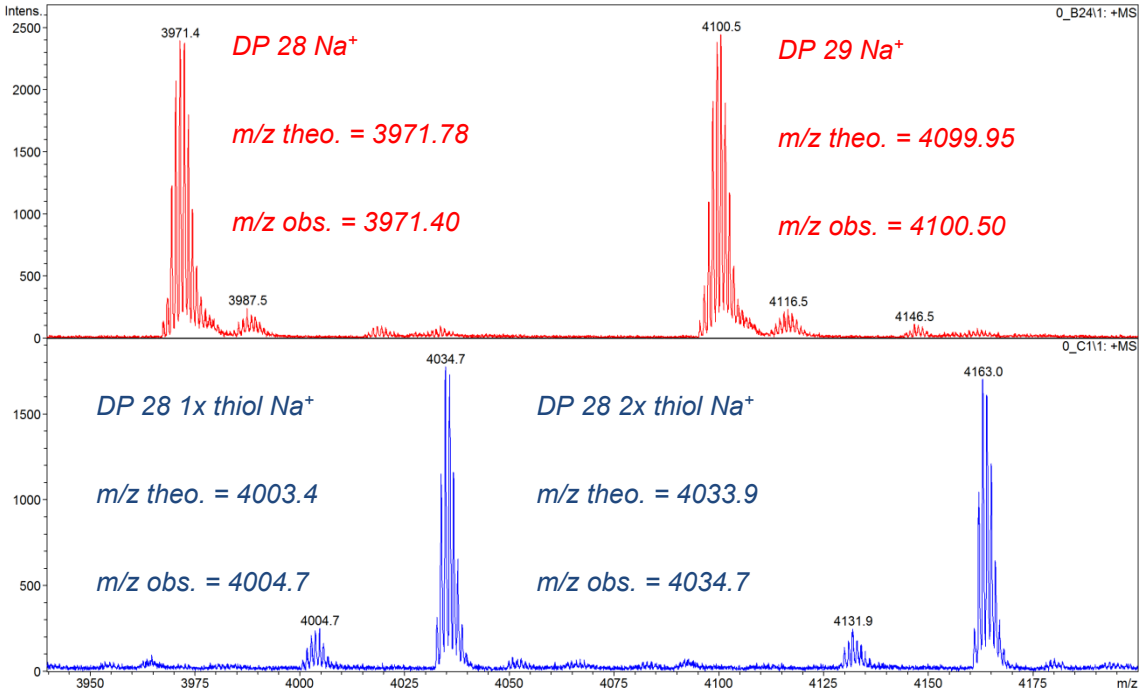


***Figure 2.21*** *Expanded MALDI-TOF MS spectra for the reaction of telechelic poly(n-butyl acrylate), 4.1 kg mol$^{-1}$ with sodium methanethiosulfonate. The red spectrum is that of the starting material and the blue is the reaction mixture after three hours*

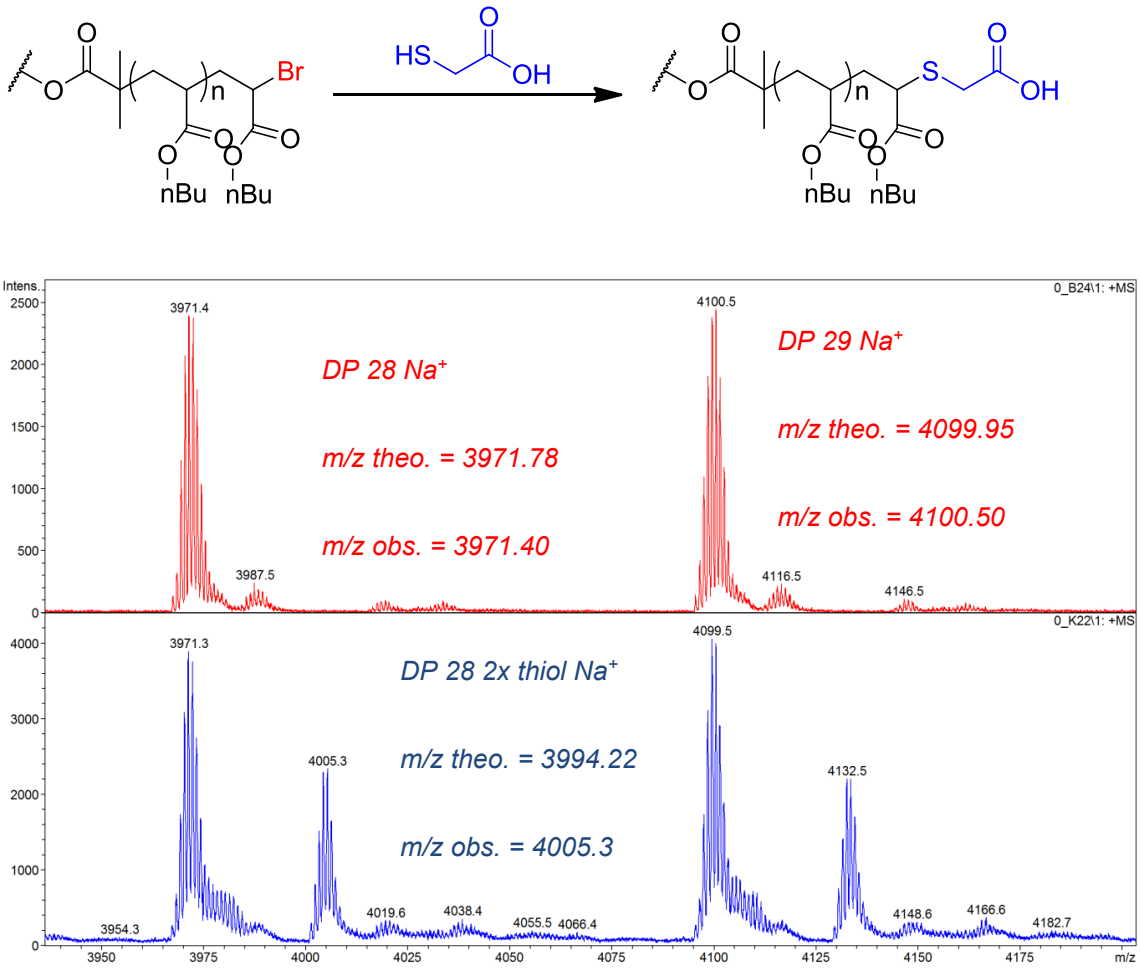


***Figure 2.22*** *Expanded MALDI-TOF MS spectra for the reaction of telechelic poly(n-butyl acrylate), 4.1 kg mol$^{-1}$ with thioglycolic acid. The red spectrum is that of the starting material and the blue is the reaction mixture after three hours*

## 2.6 Using mixed solvent systems to polymerize lipophilic monomers via $Cu^{(0)}$-mediated RDRP

A previously discussed limitation with the methodology used so far is the inability to carry out the controlled polymerization of long-chain acrylate monomers in DMSO. Such monomers (lauryl and 2-ethyl hexyl acrylate) were found to be insoluble and although polymerization with complete conversion was obtained, the reactions were highly uncontrolled and resulted in large mass dispersities. For the purposes of having oil-soluble materials, being able to polymerize lipophilic monomers would be advantageous and so a study was conducted into the use of mixed solvent systems to facilitate this whilst also retaining the advantages of the biphasic system.

Such a solvent system would need to both solubilize the monomer but not the polymer and also confer the polarity needed for $Cu^{(0)}$-mediated RDRP. Mixtures of toluene with DMSO and methanol were used in addition to isopropyl alcohol which, despite being highly polar, was able to dissolve these monomers. Using the 2F-BiB bifunctional initiator and the optimized reaction conditions ([-Br]:[$Cu^{(II)}$]:[L] = 1:0.05:0.12), lauryl acrylate was polymerized targeting a molecular weight of 3000 g $mol^{-1}$. In all cases, complete conversion was obtained with the SEC data (Table 3) indicating a well-controlled polymerization ($Đ_M$ = 1.06 – 1.16). Furthermore, as with the previous poly(butyl acrylates) phase separation of the polymer was observed, although in IPA the polymer phase was at the bottom with the solvent on top.

| Solvent | $M_n$ (g mol$^{-1}$) | $M_w$ (g mol$^{-1}$) | $Đ_M$ | Conversion (%) |
|---|---|---|---|---|
| **4:1 Toluene/DMSO** | 3300 | 3900 | 1.16 | >99 |
| **Isopropyl Alcohol (IPA)** | 3200 | 3400 | 1.06 | >99 |
| **4:1 Toluene/Methanol** | 2900 | 3100 | 1.06 | >99 |

***Table 2.4*** *Summary of SEC and conversion data for the polymerization of telechelic poly(lauryl acrylate) using $Cu^{(0)}$-mediated RDRP in various solvents, ([-Br]:[$Cu^{(II)}$]:[L] = 1:0.05:0.12)*

The mass dispersities obtained in IPA and the toluene/methanol mixture were significantly lower than that of the toluene/DMSO mixture and MALDI-TOF MS analysis of each polymer showed no clear difference between them, indicating that each solvent system produces essentially the same product. For the purposes of selecting a 'best' solvent, IPA has several advantages over the others; it is a cheap common industrial solvent (produced on the million tonne scale), has a boiling point low enough for it to be removed under vacuum at room temperature, and relative to toluene, low toxicity.

## 2.7 Large Scale Feasibility of Biphasic $Cu^{(0)}$-mediated RDRP

Given the industrial nature of this project, it was important to at least have some appreciation for any large scale applicability of the techniques used. As such, during a visit to Lubrizol's research labs, some attempts were made to take the polymerization method used in this chapter from the gram, up to the kilogram scale. This was facilitated by the recent purchase of some Radley 'Reactor Ready' 5 litre reactors fitted with overhead stirrers, ideal for this application.

The synthesis of poly(*n*-butyl acrylates) using a monofunctional initiator (EBiB) in the presence of $CuBr_2$, $Me_6TREN$ ([I] : [L] : $[Cu^{(II)}]$ = [1]:[0.12]:[0.05]) and $Cu^{(0)}$ wire was attempted. Molecular weights of 10 and 20 kg $mol^{-1}$ were targeted and the reactions conducted in DMSO (50:50 solvent:monomer by volume) with a total volume of 4 litres. In keeping with the industrial nature, all of the reagents were either purchased from Sigma-Aldrich or obtained directly from Lubrizol's manufacturing plant and were used as received. Copper wire (~1 m) was wrapped around a stirrer paddle before adding all of the reagents aside from the ligand, before degassing the mixture using a nitrogen sparge tube for one hour. The ligand was then added and the polymerization allowed to proceed overnight. In both cases, conversions of ~90% were obtained, with reasonably good agreement between the target and experimental molecular weights obtained (**Table 2.5**).

| Target $M_n$ (g mol$^{-1}$) | $M_n$ (g mol$^{-1}$) | $M_w$ (g mol$^{-1}$) | $Đ_M$ |
|---|---|---|---|
| **10 000** | 11 200 | 12900 | 1.15 |
| **20 000** | 21 000 | 26200 | 1.25 |

***Table 2.5*** *Summary of SEC data for the large-scale polymerization of (n-butyl acrylate) using $Cu^{(0)}$-mediated RDRP ([-Br]:[$Cu^{(II)}$]:[L] = 1:0.05:0.12)*

The dispersities obtained are higher in comparison to those obtained for the smaller scale reactions, however they still indicate a controlled polymerization. There are a number of factors which may cause this, such as the purity of the reagents, the stirring rate, the amount of copper wire or the degas time. There will be a general need to optimize the conditions in future, nevertheless these reactions were intended as a feasibility study and so it is pleasing that we were able to scale up the procedures with such apparent success. Photographs of the reactor set-up are given in **Figures 2.23** and **2.24**, which show the reaction a t = 0 and after being left overnight.


***Figure 2.23*** *Four litre scale polymerization of (n-butyl acrylate) using $Cu^{(0)}$-mediated RDRP ([-Br]:[$Cu^{(II)}$]:[L] = 1:0.05:0.12), t = 0*


***Figure 2.24*** *Four litre scale polymerization of (n-butyl acrylate) using $Cu^{(0)}$-mediated RDRP ([-Br]:[$Cu^{(II)}$]:[L] = 1:0.05:0.12) t = 2 h, after cessation of stirring*

## 2.8 Conclusions

Telechelic butyl and lauryl acrylate polymers have successfully been synthesized and in the process, a new biphasic reaction mechanism has been reported and investigated. When polymerizing in DMSO, the polymer phase separates resulting in near-total separation of the polymer from the copper catalyst *in situ* as, evidenced by elemental analysis. This occurs with no loss of control and the polymers can then subsequently be chain extended within this biphasic system and different molecular weights can be targeted. The isomers of BA can also be polymerized; however monomers that are insoluble in DMSO such as lauryl acrylate fail to react in a controlled manner. Conducting these polymerizations in mixed solvent systems or IPA offers a route to polymerizing these highly lipophilic monomers in an analogous fashion to BA, whilst retaining the biphasic system.

The telechelic poly(butyl acrylates) made have also been successfully functionalized via thioetherification of the bromide end groups to produce di-end functionalized polymers. This chemistry is very efficient with >99% conversion obtained for a number of thiols at room temperature in a matter of hours. MALDI-TOF MS was also proven to be a powerful tool for monitoring these reactions as purification of the product is not required and $^{1}$H NMR analysis can be difficult due to peak overlap/broadening.

Finally, some kilogram scale $Cu^{(0)}$-mediated RDRP was attempted which showed that we were able to successfully scale up the polymerization of *n*-BA around 400-fold, giving some indication as to the possible industrial applicability of the technique.

## 2.9 Experimental Procedures:

### 2.9.1 Materials

Ethyl 2-bromoisobutyrate (EBiB, Aldrich, 98 %), copper $^{(II)}$ bromide ($Cu_2Br$, Sigma-Aldrich, 99 %), tetrahydrofuran (THF, Sigma, 99 %) and dimethyl sulfoxide (DMSO, Fluka, AR) were all used as received. Copper wire (diameter = 0.25 mm) was activated by washing in concentrated sulfuric acid for 10 min. Monomers, such as *n*-butyl acrylate (nBA, Aldrich, 99%), lauryl acrylate, *iso*-butyl acrylate, *tert*-butyl acrylate and 2-ethylhexyl acrylate were de-inhibited by percolating over a column of basic alumina.

### 2.9.2 Analytical Techniques

$^1$H NMR spectra were recorded using a Bruker AC400 (400 MHz) spectrometer employing $CDCl_3$ as solvent unless otherwise stated. Monomer conversions were determined via $^1$H NMR spectroscopy, comparing the signal areas from the vinyl protons (δ ~ 6.50-6.00 ppm) 3H/mol to the signal area of $OCH_2$ signal (at ~4.0 ppm). Chemical shifts are cited as parts per million (ppm) and the following abbreviations are used to abbreviate multiplicities; s = singlet, d = doublet, t = triplet, q = quartet, m = multiplet.

All MALDI-TOF MS experiments were carried out on a Bruker UltraFLEX II TOF/TOF-MS instrument equipped with a 337 nm nitrogen laser, ion acceleration voltage of 25 kv and pulse extraction delay time of 90 ns. The instrument was

operated in reflectron mode unless otherwise stated and with each spectra being the summation of typically 1000 laser shots in order to maximise the signal to noise ratio. Sample preparation: Each polymer (0.5 mg/mL) was prepared in THF with sodium iodide (1 mg/mL) and saturated 2,5 dihydroxybenzoic acid (DCTB) matrix in a 1:0.1:1 ratio (sample:salt:matrix). 0.5μL of the mixture was then spotted onto the target plate and analysed.

Gel Permeation Chromatography (SEC) was conducted on an Agilent 390-LC system in $CHCl_3$ at ambient temperature, equipped with refractive index and viscometry detectors, 2 × PLgel 5 μm mixed-D columns (300 × 7.5 mm), 1 × PLgel 5 μm guard column (50 × 7.5 mm) and autosampler. The mobile phase was $CHCl_3$ with 2% triethylamine in order to prevent samples sticking to the columns. A calibration curve was generated with commercial linear poly-methyl acrylate standards ranging from 500 to $10^6$ g $mol^{-1}$.

XPS was conducted using a Kratos Axis ULTRA XPS equipped with a 165 mm hemispherical analyzer. The incident radiation was monochromatic A1 X-rays (1486.6 eV) at 225 W (15 kV, 15 ma). Survey (wide) scans were taken at an analyzer pass energy of 160 eV and multiplex (narrow) higher resolution scans at 20 eV. Survey scans were carried out over 1200 eV binding energy with 1.0 eV steps and a dwell time of 100 ms. Poly(n-butyl acrylate) samples were placed on silica plate and analysed by XPS.

ICP-MS was carried out using a PerkinElmer quadrupole Nexion ICPMS. The instrument was been previously calibrated using copper standard solution in water. Sample preparation: un-purified poly(n-butyl acrylate) (10 mg) obtained by $Cu^{(0)}$-mediated RDRP in DMSO was dissolved in THF (0.200 mL) and then the solution was added drop wise to a hydrochloric acid solution (9.8 mL, 0.1 M of HCl). The

solution was mixed for 14 hours before analysis by ICP-MS to determine copper concentration. Each sample was analysed four times, and the average of the four values was calculated.

## 2.9.3 Synthetic Procedures

### 2.9.3.1 A Typical Cu(0)-meditated RDRP of Telechelic *n*-Butyl Acrylate

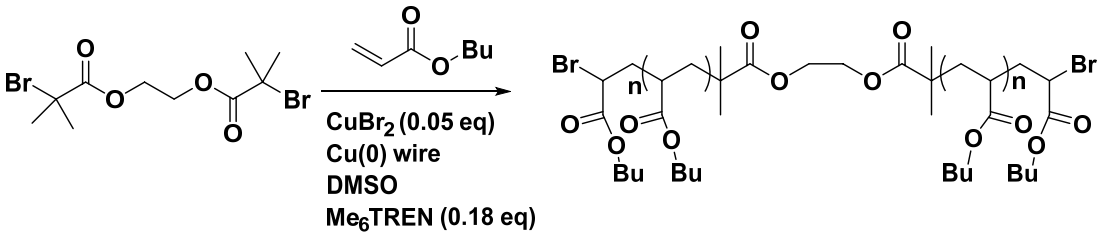


*n*-butyl acrylate (BA, 5 mL, 35 mmol, 20 eq), DMSO (5 mL), Ethylene bis(2-bromoisobutyrate) (2F-BiB) (0.3g, 0.88 mmol, 1.00 eq C-Br), $CuBr_2$ (9.8 mg, 0.044 mmol, 0.05 eq) and pre-activated copper wire (5 cm) wrapped around magnetic stir bar were added to a Schlenk tube. A rubber septum was then fitted and the reaction mixture degassed via nitrogen bubbling for 10 minutes. Degassed $Me_6TREN$ (0.048 mL, 0.16 mmol, 0.18 eq) was then added via an airtight syringe and the reaction left to polymerize overnight at 25°C.

Samples of the reaction mixture and polymer were removed for $^1H$ NMR, SEC and MALDI-TOF MS analysis. The samples for $^1H$ NMR was simply diluted with CDCl3,

while the samples for SEC were diluted with $CHCl_3$ then passed over an alumina column to remove metal salts.

### 2.9.3.2 Synthesis of Bifunctional Initiator; Ethylene bis(2-bromoisobutyrate) (2F-BiB)

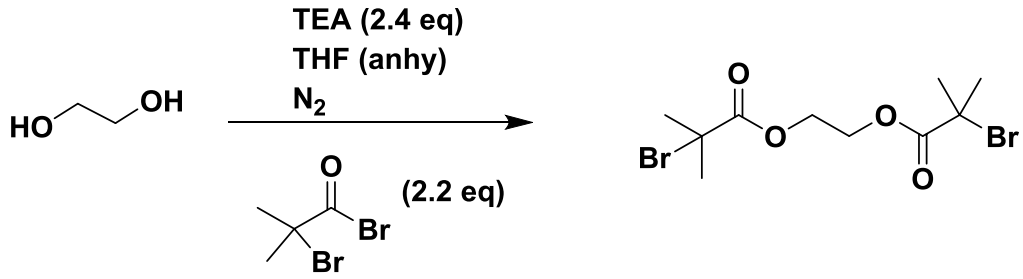


Ethylene glycol (1.80 mL, 32.4 mmol) and an excess of triethylamine (9.90 mL, 71.3 mmol) were added to a 500 mL round bottom flask with a stirrer bar and was flushed with nitrogen for 15 minutes on an ice bath. Anhydrous THF (150 mL) was added to the flask via an airtight syringe, and allowed to cool to 0°C. Under a nitrogen atmosphere, 2-bromoisobutyryl bromide (8.40 mL, 68.1 mmol) was added slowly via a dropping funnel. Care was taken in order to minimize the exotherm generated by the reaction. The solution was then left to stir overnight at ambient temperature. The reaction mixture was filtered in order to remove the triethylammonium bromide salt formed, and the solution concentrated by rotary evaporation. The resulting yellow/brown solution was then stirred with 0.10 M aqueous sodium carbonate to hydrolyze any remaining 2-bromoisobutyryl bromide. The crude product was then extracted with dichloromethane (3x50 mL) using a separating funnel and the combined dichloromethane extracts dried with anhydrous

magnesium sulfate then filtered. The solvent was removed via rotary evaporation yielding yellow crystals upon cooling. The product was purified using flash column chromatography using 3:1 ethyl acetate:hexane to give white crystals (8.2 g, 70.3 %). The product may also be purified by repeated recrystallization from hot methanol.

$^{1}$H NMR (400 MHz, $CDCl_3$): δ (ppm) 4.44 (t, 4H, OC***H***$_2$C***H***$_2$O), 1.94 (s, 12H, C(C***H***$_3$)$_2$).

$^{13}$C NMR (100 MHz, $CDCl_3$): δ (ppm) 63.32, 55.44 and 30.85.

Further details, along with interactive NMR spectra can be found on ChemSpider Synthetic Pages DOI: 10.1039/SP693

### 2.9.3.3 Synthesis of N,N,N',N'',N''-Hexamethyl-[tris(aminoethyl)amine] ($Me_6$TREN)

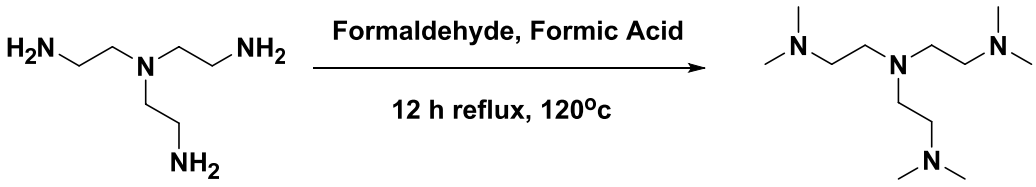


Tris-(2-aminoethyl)amine (50.00 mL, 0.33 mol) was added dropwise over a period of 1 hour to a mixture of formic acid (320 mL, 8.15 mol) and formaldehyde (270.9 mL, 3.64 mol) with vigorous stirring and using a large ice bath to cool the reaction mixture. The reaction was refluxed for 12 hours at 120°C. After leaving to cool, the volatile fractions were removed *in vacuo*, and a saturated sodium hydroxide solution was used to adjust the mixture to approximately pH 10. The oil layer was

extracted into chloroform and dried with magnesium sulfate (~20 g). The solvent was then removed *in vacuo* to yield a yellow oil. The oil was distilled under reduced pressure to give a colourless liquid and stored under nitrogen and in the fridge (55g). $^{1}$H NMR ($CDCl_3$, 400 MHz), δ (ppm): 2.55 and 2.32 (t, 12 H, $(CH_3)_2NC\boldsymbol{H}_2C\boldsymbol{H}_2NR$), 2.17 (s, 18 H, $(C\boldsymbol{H}_3)_2NR$).

$^{13}$C NMR ($CDCl_3$, 100 MHz), δ (ppm): 57.5, 53.1, 45.9. FT-IR: v (ppm) 1035, 1124. ESI-MS (*m/z*): [M+] 231.25 (*230.25 Th*eo.)

Further details, along with interactive NMR/IR spectra can be found on ChemSpider Synthetic Pages DOI: 10.1039/SP694

### 2.9.3.4 Functionalization of Poly(*n*-butyl acrylate) Using Thio-Bromo Click

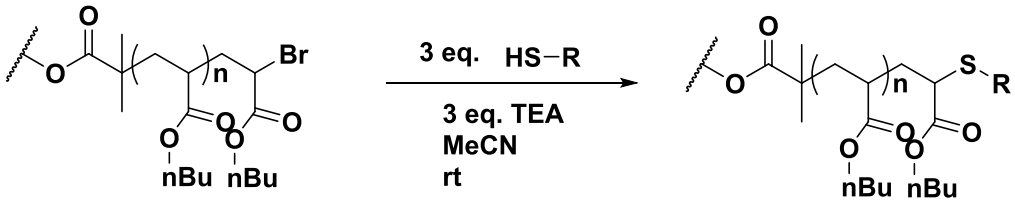


Telechelic poly(*n*-BA), synthesized according to Procedure 2.7.3.1 (1g) and thiol (3eq) were charged into a reaction vessel, along with 3 mL MeCN and a stirrer bar. TEA (3eq) was added and the mixture left to react overnight. Samples were drawn for analysis before the reaction mixture was concentrated *in vacuo*. The mixture was then precipitated into ice cold methanol and the product dried in an oven under reduced pressure.

## 2.10 References


1. R. Mai, A. Pekarovicova and P. Fleming, *Proceedings of the 58th TAGA Annual Technical Conference*, 2006.
2. M. F. Molaire, *NIP & Digital Fabrication Conference*, 2007, 2007, 653-656.
3. R. M. Mortier, M. F. Fox and S. T. Orszulik, *Chemistry and Technology of Lubricants*, Springer, 2010.
4. G. Fonnum, J. Bakke and F. Hansen, *Colloid and Polymer Science*, 1993, 271, 380-389.
5. M. R. Tant, K. A. Mauritz and G. L. Wilkes, *Ionomers: synthesis, structure, properties and applications*, Springer, 1997.
6. A. Eisenberg and K.-S. Kim, *Introduction to Ionomers*, 1998.
7. M. A. Winnik and A. Yekta, *Current opinion in colloid & interface science*, 1997, 2, 424-436.
8. D. G. Peiffer, R. D. Lundberg and I. Duvdevani, *Polymer*, 1986, 27, 1453-1462.
9. R. Lundberg and H. Makowski, *J. Polym. Sci., B Polym. Chem.*, 1980, 18, 1821-1836.
10. R. Lundberg and R. Phillips, *J. Polym. Sci., B Polym. Chem.*, 1982, 20, 1143-1154.
11. R. D. Lundberg, *Journal of Applied Polymer Science*, 1982, 27, 4623-4635.
12. C. Maus, R. Fayt, R. Jérôme and P. Teyssié, *Polymer*, 1995, 36, 2083-2088.
13. T. Witten, *Journal de Physique*, 1988, 49, 1055-1063.
14. T. A. Witten and M. H. Cohen, *Macromolecules*, 1985, 18, 1915-1918.
15. C. Chassenieux, J.-F. Tassin, J.-F. Gohy and R. Jérôme, *Macromolecules*, 2000, 33, 1796-1800.

16. B. Gabrys, J. S. Higgins, C. W. Lantman, W. J. MacKnight, A. M. Pedley, D. G. Peiffer and A. R. Rennie, *Macromolecules*, 1989, 22, 3746-3751.

17. A. M. Pedley, J. S. Higgins, D. G. Peiffer, A. R. Rennie and E. Staples, *Polym. Commun.* 1989, 30, 162-165.

18. C. Boyer, A. Atme, C. Waldron, A. Anastasaki, P. Wilson, P. B. Zetterlund, D. Haddleton and M. R. Whittaker, *Polym. Chem.* 2013, 4, 106-112.

19. H. Tang, N. Arulsamy, M. Radosz, Y. Shen, N. V. Tsarevsky, W. A. Braunecker, W. Tang and K. Matyjaszewski, *J. Am. Chem. Soc.*, 2006, 128, 16277-16285.

20. K. Matyjaszewski, W. Jakubowski, K. Min, W. Tang, J. Huang, W. A. Braunecker and N. V. Tsarevsky, *Proc. Natl. Acad. Sci.*, 2006, 103, 15309-15314.

21. A. Anastasaki, C. Waldron, P. Wilson, R. McHale and D. M. Haddleton, *Polym. Chem.*, 2013, 4, 2672-2675.

22. B. M. Rosen, G. Lligadas, C. Hahn and V. Percec, *J. Polym. Sci., A Polym. Chem.*, 2009, 47, 3940-3948.

23. A. B. Lowe and M. A. Harvison, *Aust. J. Chem.*, 2010, 63, 1251-1266.

24. J. Xu, L. Tao, C. Boyer, A. B. Lowe and T. P. Davis, *Macromolecules*, 2009, 43, 20-24.

25. C. E. Hoyle, A. B. Lowe and C. N. Bowman, *Chem. Soc. Rev.*, 2010, 39, 1355-1387.

26. W. Yan, J. A. Gardella Jr and T. D. Wood, *J. Am. Soc. Mass Spectrom.*, 2002, 13, 914-920.

27. H. Chen, M. He, J. Pei and H. He, *Anal. Chem.*, 2003, 75, 6531-6535.

28. H. Räder and W. Schrepp, *Acta Polym.*, 1998, 49, 272-293.

29. R. Adden, W. Niedner, R. Müller and P. Mischnick, *Anal. Chem.*, 2006, 78, 1146-1157.

30. P. Lloyd, K. Duddaby, J. Varney, E. Scrivener, P. Derrick and D. Haddleton, *Eur. J. Mass Spectrom.*, 1995, 1, 293-300.

# Chapter 3: Synthesis and Characterization of Core-first Acrylate Stars Using $Cu^{(0)}$-Mediated RDRP

In Chapter 2, the synthesis of telechelic functional acrylates via $Cu^{(0)}$-mediated RDRP was described. Herein, the $Cu^{(0)}$-mediated RDRP of lipophilic monomers (*n*-butyl and lauryl acrylate) from multi-functional alkyl halide initiators is discussed. A range of highly defined lipophilic poly(acrylate) stars were prepared to relatively high molecular weights ($M_{n,target}$ > 100 000 g $mol^{-1}$ in some cases) and high monomer conversions (≥99%) with excellent control retained over molecular weight distributions (dispersity values as low as 1.03). Phase separation of star polymers from the reaction media during polymerization is seen to occur which is advantageous in reducing star–star coupling in certain cases, without limiting the attainment of near quantitative conversions. A comparison was made between heterogeneous and homogeneous polymerization protocols to illustrate this finding.

The polymerization methods were used to produce poly(lauryl acrylate) stars bearing different numbers of arms, which was also conducted on a scale large enough to provide sufficient material to undergo rheological testing. The tests showed that the star polymers synthesized were able to function as VMs, however no dependence on the number of arms was observed.

## 3.1 Introduction

Star polymers attract considerable interest in macromolecular science due to their novel architectures and interesting properties in both solution and bulk phases and potential for high degrees of functionality relative to their linear counterparts[1-7]. Such polymers have found a wide variety of uses ranging from drug delivery[3-9] to magnetic resonance imaging[10, 11] and catalysis[12-16]. Lipophilic star polymers are particularly attractive from an industrial standpoint, with investigations into their application as rheological modifiers[17, 18].

Star polymers are normally targeted using two distinct synthetic approaches, namely arm-first[19-23] and core-first methods[24-27]. In the arm-first approach, linear mono-functional polymer chains are pre-formed and subsequently directly coupled to a multi-functional molecular core. Whilst this technique has its merits and in particular in limiting the possibility of star-star coupling reactions, a significant drawback involves a molecular weight dependent arm-coupling efficiency whereby increasing molecular weight and/or steric bulk of the arms leads to difficulties in attaining full functionalization at the core. Not only does this yield stars with disparate numbers of arms, coupling inefficiencies can also lead to significant linear polymeric impurities. A corollary of the arm first approach involves chain extending linear polymers in the presence of a molecular cross-linker to create the core *in situ*.[22, 28-30]. While this approach may not appear to promise the same level of molecular definition across all stars, it often serves to limit linear impurities in the final product[29].

The second, core-first approach involves multi-functional initiator molecules which allow several polymer chains to be grown concurrently from a central locus in a

one-pot system. Notably, in the absence of significant chain transfer events during polymerization, this approach should yield negligible linear contaminants. However, an on-going drawback of this core-first approach, especially when combined with radical polymerization techniques, has been a tendency for significant bimolecular termination events between growing stars, particularly at high molecular weights and high conversions. [26] As star polymers inherently contain multiple propagation sites relative to the mono/bi-functionality of their linear analogues, any individual star is statistically much more likely to undergo a radical-radical coupling interaction with a second star prior to performing all requisite propagation steps. This current contribution seeks to exploit recent advances in controlled/living radical polymerization technology to significantly reduce, even eliminate, such termination events in the core-first approach.

Numerous controlled/living polymerization techniques have been exploited in the pursuit of ever-improved molecular control in star polymer synthesis. These techniques include living ionic polymerizations[31, 32] and ring opening metathesis polymerizations (ROMP)[16,33] as well as several controlled/living radical polymerization approaches such as reversible addition fragmentation chain transfer (RAFT[29, 33-36]), atom-transfer radical polymerization (ATRP[26,30,38-41]) and nitroxide mediated polymerization (NMP[20,42-44]).

Recently single electron transfer living radical polymerization (SET-LRP) has also been explored as a tool for star polymer synthesis. Paillet et al. [37] utilized a combination of SET-LRP and NMP in the preparation of n-butyl acrylate (nBA) containing star branch polymers in a core-first approach. Ding et al. [38] and Whittaker et al.[39] have separately reported core-first approaches to relatively low molecular weight poly(methyl acrylate; MA) stars via SET-LRP. Whittaker showed excellent end-group fidelities allowing access to low dispersity block copolymer

stars, however, no associated quantification of the degree of star-star coupling was discussed. Whittaker et al. later developed the chemistry further using an iterative chain extension procedure to access multi-block copolymer stars in one-pot systems containing a variety of acrylate monomers[40].

### 3.1.2 Star Polymers As Rheological Modifiers

Star polymer based rheological additives can already be found in commercial engine oil products; indeed it was Lubrizol who first brought these to the market in 2008 with their Asteric™ product which is based on poly(methylmethacrylate) arm-first stars synthesized using RAFT[41] (this was also one of, if not the first, full scale commercial uses of the RAFT methodology).

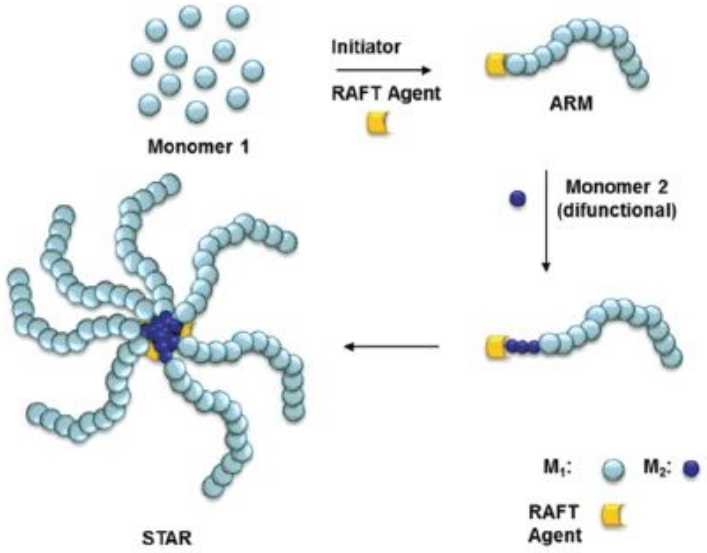


Figure 4. Manufacture of star polymer using RAFT technology

***Figure 3.1*** *The Lubriozol Asteric star polymer VM, synthesized via RAFT polymerization*

One of the major advantages of using star, as opposed to linear polymers is their increased shear stability, which is an important consideration given the large shearing forces in an engine/drivetrain. If a shearing force is applied to a polymer in solution, it's structure will deform and if the shearing force is strong enough, scission can occur. Experimentally this has been observed to occur at the middle of a linear polymer which is the point at which it is under the most stress. In such an instance, the molecular weight will be halved and since the thickening is dependent on the molecular weight of the VM, there will be a large drop in the VI.

Star polymers typically do not shear at their core, rather breakage occurs at the arms. If an arm is cleaved through some chemical or mechanical process, the resultant drop in molecular weight and accompanying loss of VI is much less when compared to a linear polymer of the same molecular weight (**Figure 3.2**). It also follows that the higher the number of arms, the less pronounced the effect on VI will be if any of them are lost.

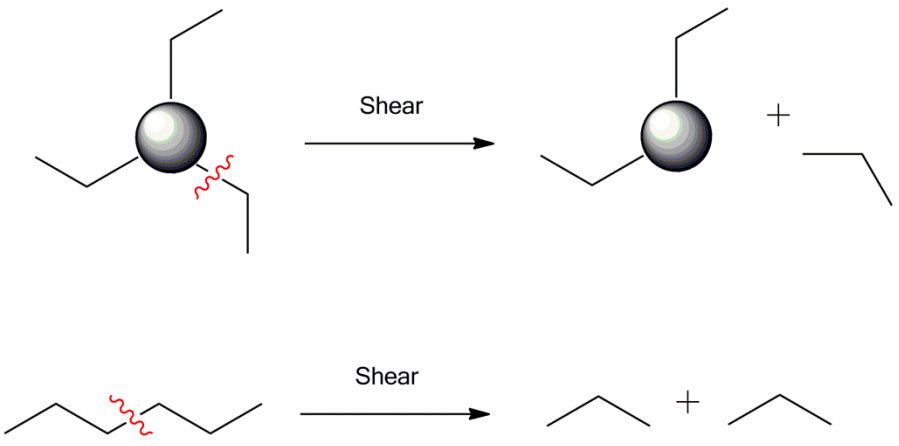


***Figure 3.2*** *Comparing the molecular weight loss when shearing a 3-arm star versus its linear equivalent. Loss of an arm results in a one third reduction in the molecular weight, whereas cleaving the linear polymer in the middle halves its molecular weight*

Previous work carried out in our group[42], also in collaboration with Lubrizol showed that in addition to the increased shear stability, star poly(acrylates) also showed markedly increased VI, absolute viscosities and reduced viscosities at low temperature versus the linear analogues making them an interesting target for further study. Furthermore it is also known that (meth)acrylate polymer VMs bearing a long alkyl chain provide more desirable properties when compared with hydrocarbon based ones (such as poly(ethylene/propylene). With this in mind, long chain ($C_4$-$C_{12}$) acrylic monomers were chosen for the synthesis of star polymers using the $Cu^{(0)}$-mediated RDRP methodology discussed in Chapter 2, and their suitability as viscosity modifiers evaluated.

## 3.2 Synthesis of Poly(butyl acrylate) 8-arm Stars

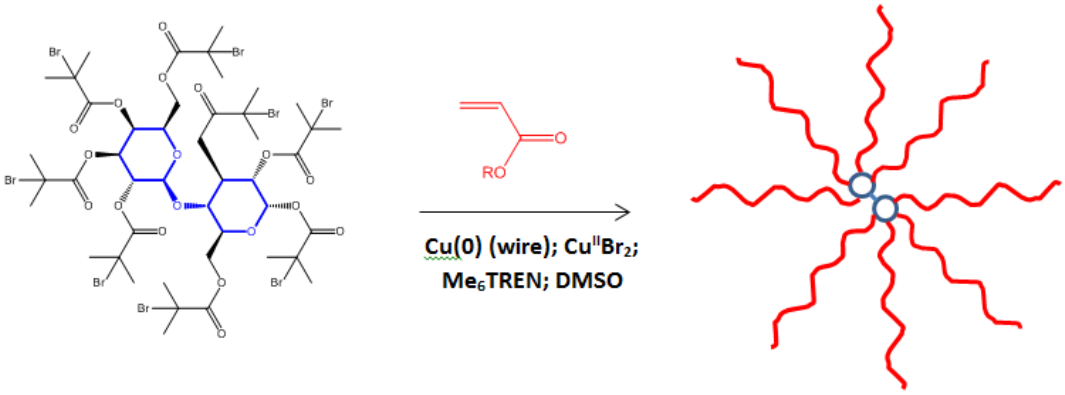


***Figure 3.3*** *General scheme for poly(acrylate) star polymer synthesis from octa-functional lactose initiator via Cu$^{(0)}$-mediated RDRP*

As a starting point to the study an *octa*-functional lactose based initiator (*octa*-*O*-bromoisobutyryl lactose) was prepared as described in the literature[43] and used to synthesize poly(*n*-BA) star polymers. Polymerizations were conducted in DMSO at ambient temperature with $Me_6$TREN as the ligand in the presence of Cu(0) wire and $Cu^{(II)}Br_2$ ([-Br]:[$Me_6$TREN]:[$Cu^{(II)}Br_2$] = 1: 0.18: 0.05) and were left to react overnight. In the first instance a theoretical $M_n$ of 20 kg $mol^{-1}$ was targeted.

As observed previously in the linear polymerization of *n*-BA in DMSO, phase separation of poly(*n*-BA) star polymers occurred early in the polymerization on reaching molecular weight of approximately 2000 g $mol^{-1}$. Crucially, polymer powders did not precipitate fully from solution but rather a monomer/solvent swollen upper polymer phase and a monomer/solvent/catalyst rich lower phase were observed. While phase separation occurred relatively early in the polymerization, the absence of full scale precipitation of polymers, allowed polymerization to continue in the monomer/solvent swollen polymer phase to reach near quantitative

conversions. The first reaction yielded a polymer of $M_n$ = 18 800 g mol$^{-1}$, $Đ_M$ = 1.09 at 90% conversion, determined via SEC and $^1$H NMR respectively (**Figure 3.4**).

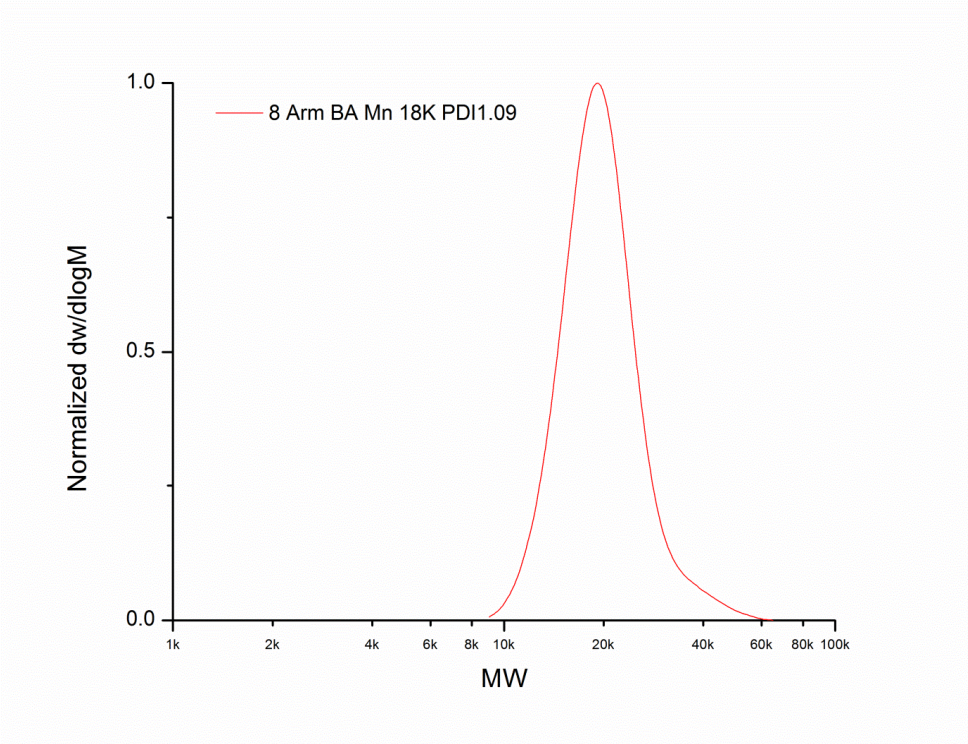


***Figure 3.4*** *SEC chromatogram of star polymer obtained by the Cu$^{(0)}$-mediated RDRP of butyl acrylate in DMSO. Target $M_n$ = 20 kg mol$^{-1}$, conversion = 90%*

Characterization data, **Table 3.1**, illustrate the synthesis of high molecular weight poly(*n*-BA) star polymers with dispersities centred around 1.1 to high monomer conversions (85 - 99%). The low mass dispersity values and mono-modal SEC chromatograms (**Figure 3.5**) suggest a significantly reduced degree of star-star coupling when compared to similar star polymerizations to high molecular weights and conversions.

While there is some deviation of measured molecular weights from theoretical values, it is well understood that star polymers adopt significantly different hydrodynamic volumes relative to the linear standards used here for calibration. As observed in previous research[44], it is apparent from the data that this effect becomes more pronounced as the molecular weight of the stars increase. During this investigation analysis was attempted using a universal calibration with SEC, however, it was found that the low molecular weights and extremely narrow dispersities of the samples resulted in them being unsuitable for Mark–Houwink analysis at this point. The SEC chromatograms showing the viscosity detector data are presented for qualitative comparison (**Figure 3.7b**) as any star-star coupling would be more apparent using such a detector.

| Experiment | DP (target, per star) | $M_n$ (theory) (g mol$^{-1}$) | Conversion (%) | $M_n$ (SEC) (g mol$^{-1}$) | $Đ_M$ |
|---|---|---|---|---|---|
| A | 45 | 7300 | 85 | 7900 | 1.07 |
| B | 97 | 14000 | 88 | 13500 | 1.10 |
| C | 160 | 22000 | 90 | 18800 | 1.09 |
| D | 238 | 32000 | 85 | 26300 | 1.09 |
| E | 378 | 50000 | 91 | 35000 | 1.06 |
| F | 1002 | 130000 | >99 | 72500 | 1.15 |

***Table 3.1*** *Cu-mediated star polymerization of n-BA from octa-functional initiator in DMSO. ([-Br]:[$Me_6$TREN]:[$Cu^{(II)}Br_2$] = 1: 0.18: 0.05)*

Overall, the preliminary data in **Table 3.1** suggest the phase separation event is benign, and does not lead to any apparent loss of polymerization control to high conversions. As suggested in the introduction, it is possible that the observed degree of control may, at least in part, be a direct consequence of the star polymers phase separating from the reaction medium, thus rendering them less likely to partake in star-star coupling reactions. It is conceivable that polymeric stars present in a viscous monomer-swollen polymer phase are less likely to interact with surrounding stars due to reduced mobility in this phase. Additionally, the physical separation of the polymer phase from the Cu(0) catalyst may also result in a lower radical concentration, giving greater control over the polymerization.

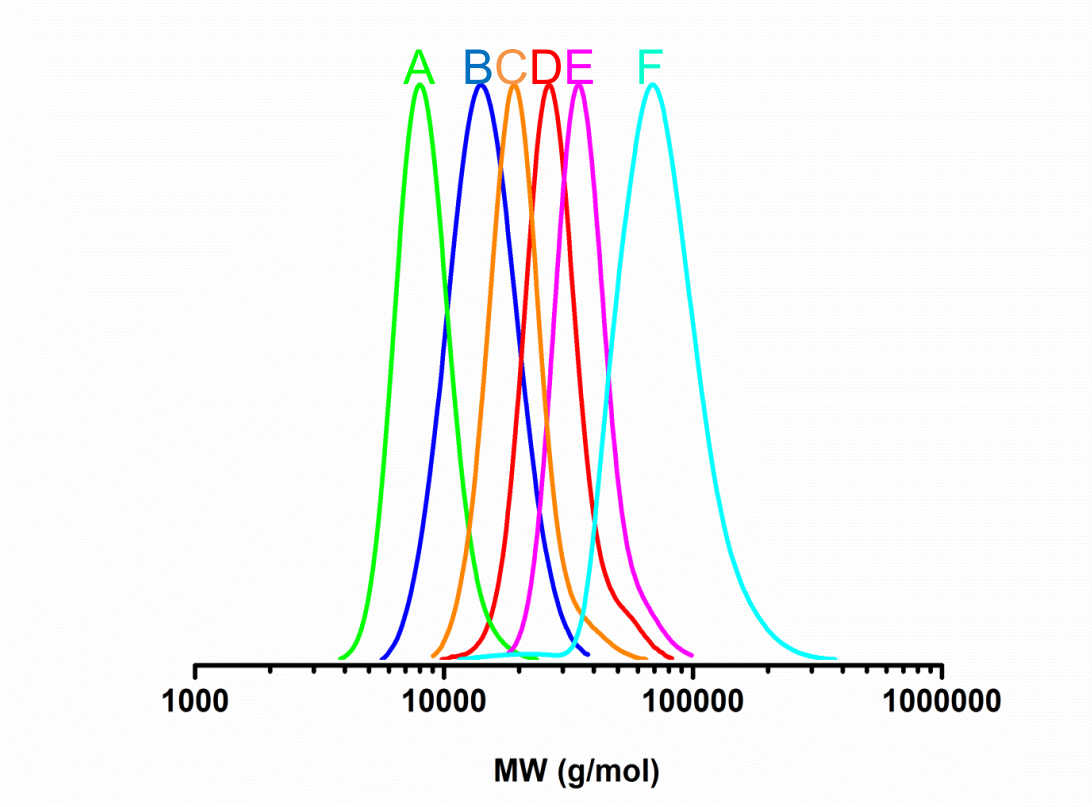


***Figure 3.5*** *Molecular weight distributions for poly(n-BA) star experiments A-F in Table 3.1*

### 3.2.1 Synthesis of poly(butyl acrylate) 8-arm stars – Kinetics

In order to further assess the degree of control of these polymerization a kinetic experiment (target $M_n$ = 10,000 g mol$^{-1}$) was carried out using the same reaction conditions as used previously. Samples of the reaction mixture were regularly taken and analysed in order to determine the conversion, molecular weight and mass dispersity at each given time interval. This allowed for kinetic plots to obtained, along with plots of conversion, $M_n$ and dispersity vs. time. Examination of the data reveals quite rapid polymerization, with 85% conversion obtained after one hour. The linear evolution of molecular weight with conversion, low mass dispersities and linear increase of $\ln[M_0]/[M_t]$ versus time are indicative of a pseudo-living polymerization.

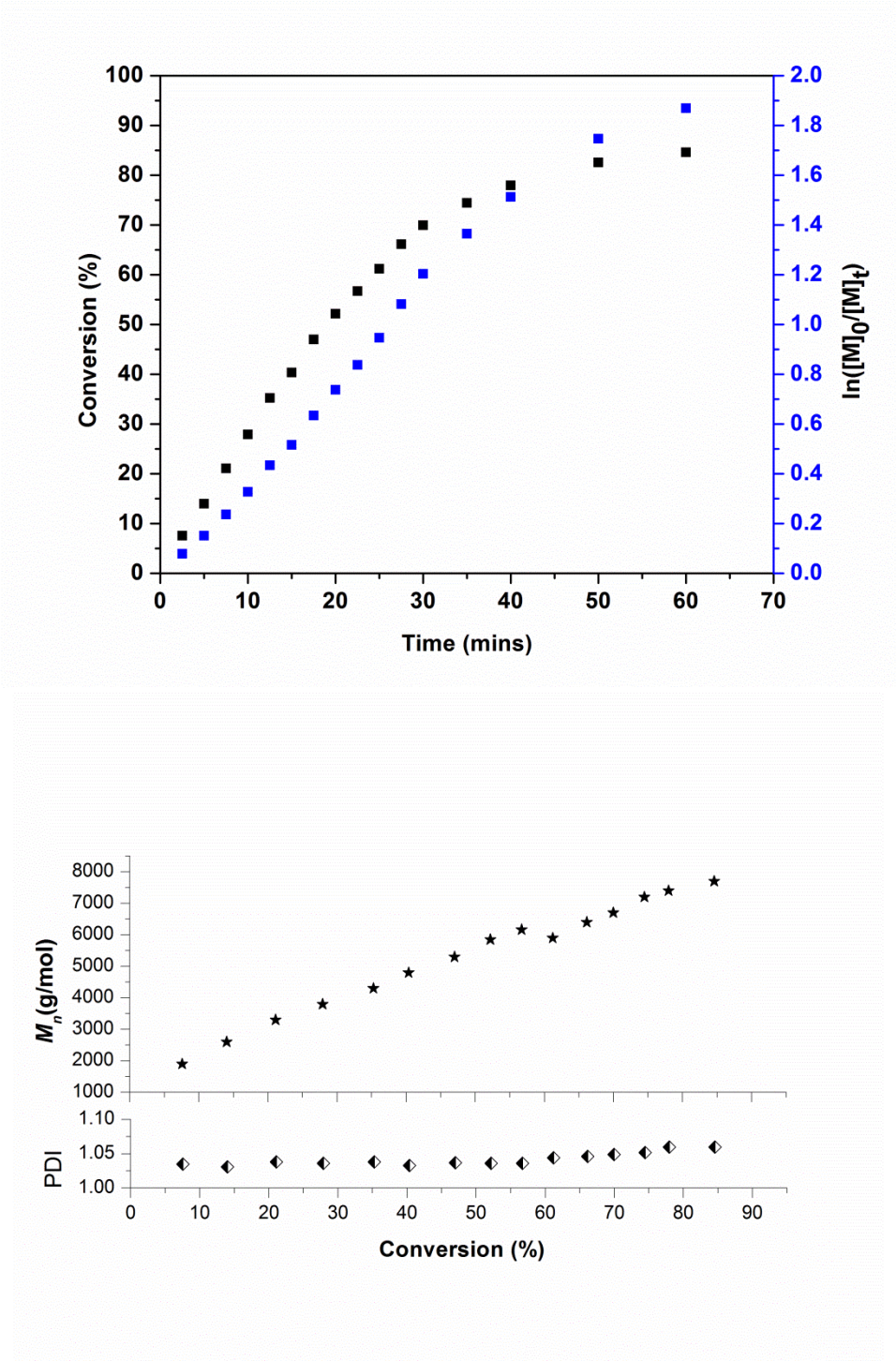


***Figure 3.6*** *Kinetic data (top) and $M_n$ and dispersity plotted as a function of conversion (bottom) for the $Cu^{(0)}$-mediated RDRP of n-BA in DMSO from octa-functional lactose initiator (see Figure 3.7 for SEC chromatograms). ([-Br]:[$Me_6$TREN]:[$Cu^{(II)}Br_2$] = 1: 0.18: 0.05)*

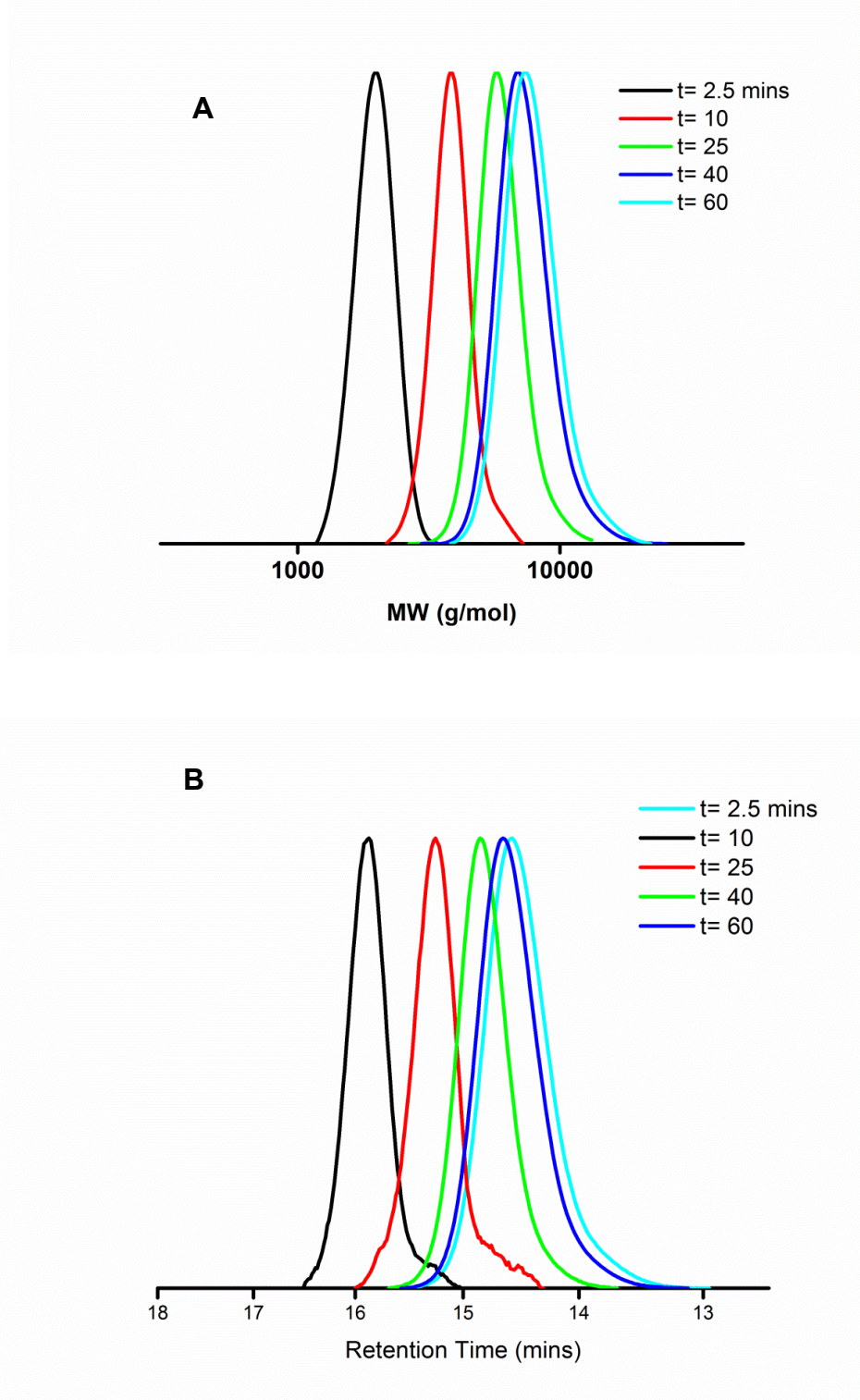


***Figure 3.7*** *SEC Chromatograms from two different detectors for the kinetic experiment, showing evolution of molecular weight with time. A) Refractive Index detector, B) Viscometry detector*

## 3.3 Investigating the Role of Phase Separation

To elucidate any role of phase separation in limiting star-star coupling, two experimental approaches were devised: i) a less hydrophilic acrylate (methyl acrylate; MA) was polymerized under the precise conditions used for poly(*n*-BA) star polymer synthesis and ii) a less polar solvent (IPA) was used for the *n*-BA polymerization. Crucially, both approaches allow for retention of the star polymers in solution throughout polymerization, thus providing a robust comparison of the heterogeneous and homogeneous systems. MA was chosen in the former approach as poly(MA) is fully soluble in DMSO and MA monomer exhibits similar reactivity to *n*-BA in $Cu^{(0)}$-mediated RDRP in solution.[45] IPA was chosen in the former approach as a compromise between a solvent of lesser polarity than DMSO to retain the poly(*n*-BA) stars in solution, whilst retaining sufficient polarity in the reaction medium such that the disproportionation reaction of Cu(I) is favoured (as deemed essential in the SET-LRP mechanism). Poly(MA) star polymers were prepared in DMSO using the same initiator and $Cu^{(0)}$-mediated RDRP conditions as described above. A comparison between similar DP and similar MW poly(MA) and poly(*n*-BA) star polymers is made in **Figures 3.8a 3.8b** respectively and **Table 3.2**.

| Monomer | Solvent | Phase Separation? | DP (target) (per star) | $M_n$ (theory) g mol$^{-1}$ | Conversion (%) | $M_n$ (SEC) g mol$^{-1}$ | $Đ_M$ |
|---|---|---|---|---|---|---|---|
| **MA** | DMSO | No | 157 | 15 000 | 93 | 12 100 | 1.05 |
| **BA** | DMSO | Yes | 183 | 25 000 | 88 | 21 400 | 1.03 |
| **MA** | DMSO | No | 237 | 22 000 | 90 | 19 500 | 1.06 |
| **BA** | IPA | No | 183 | 25 000 | 84 | 20 000 | 1.07 |

***Table 3.2*** *Investigating the role of phase separation*

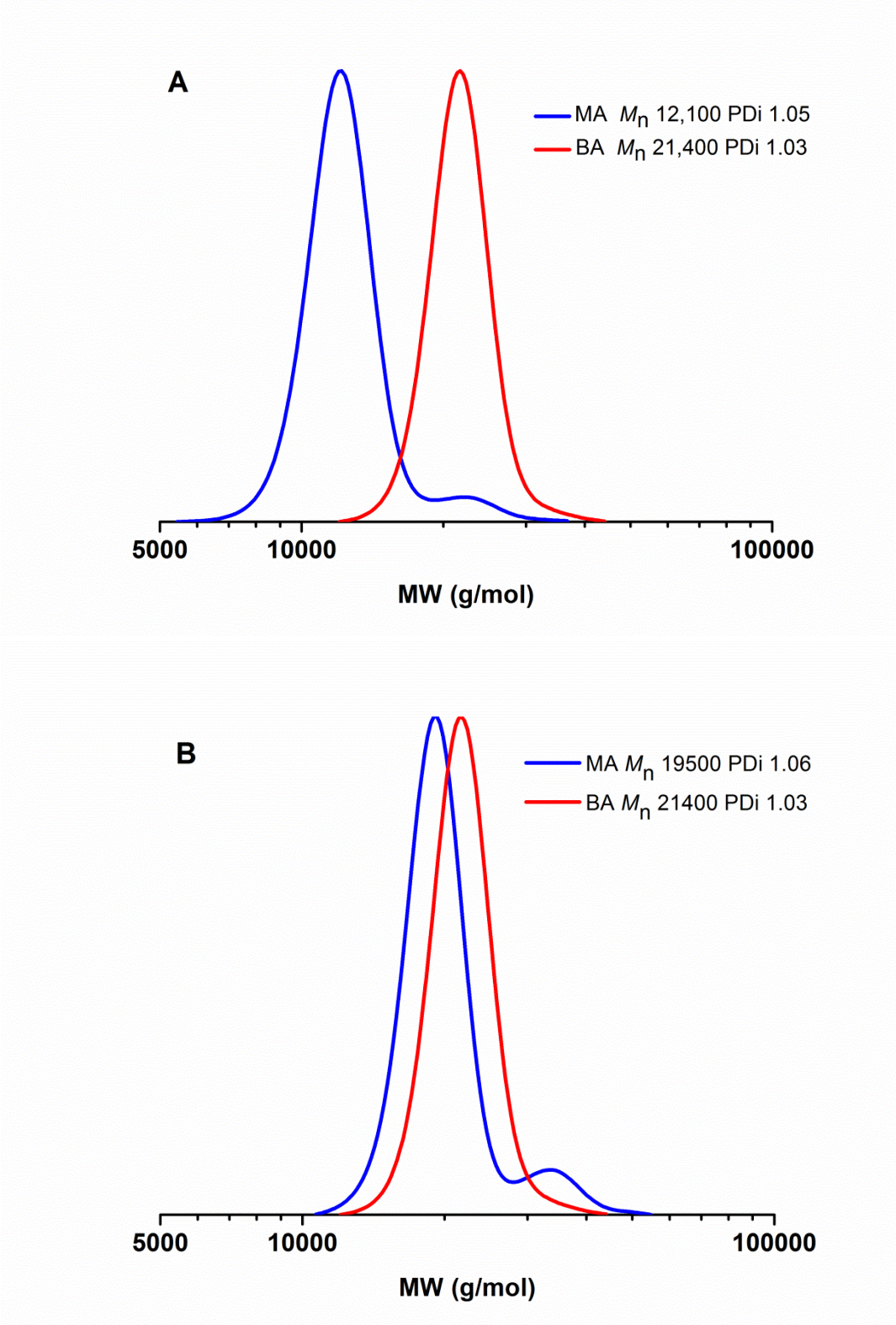


***Figure 3.8*** *SEC comparison of similar DP (A) and similar MW (B) poly(MA) and poly(BA) stars prepared via $Cu^{(0)}$-mediated RDRP in DMSO. ([-Br]:[$Me_6$TREN]:[$Cu^{(II)}Br_2$] = 1: 0.18: 0.05)*

Despite the low $Đ_M$ attained in both instances, examination of the SEC chromatograms reveals an obvious high molecular weight shoulder in the poly(MA) stars which is not apparent in the poly(*n*-BA) SEC chromatogram included as a comparison. Overall, one can conclude from this assessment that phase separation is likely to play a role in reducing star-star coupling.

In the second comparative approach, a poly(*n*-BA) star polymer was prepared in a wholly homogeneous IPA reaction medium and is compared to a similar molecular weight poly(*n*-BA) star polymer prepared in DMSO, **Figure 3.8**. While high conversions (>8%) and low $Đ_M$ values (<1.10) were attained in both cases, the SEC chromatogram comparison again reveal a significant difference between the heterogeneous and homogeneous regimes.

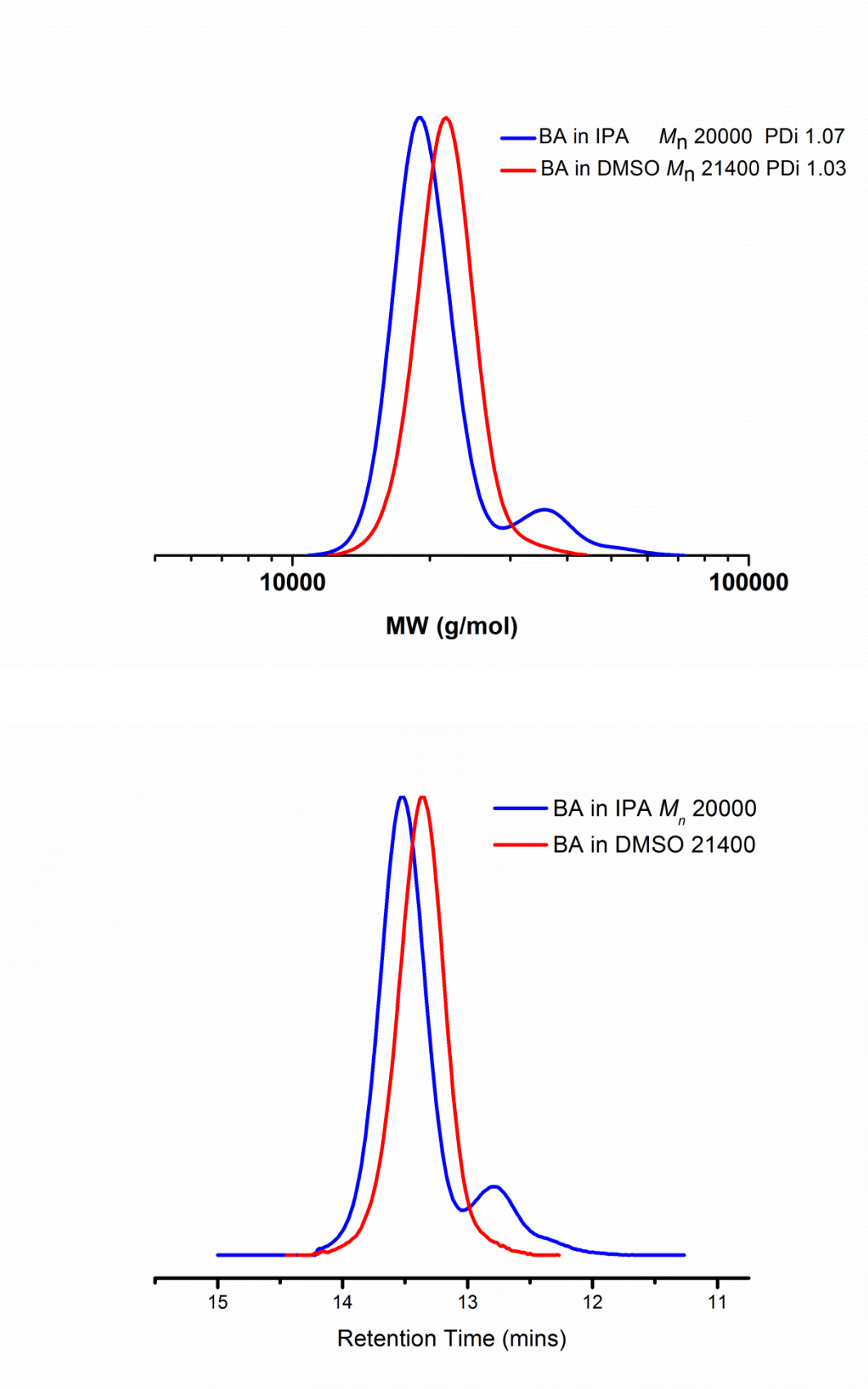


***Figure 3.9:*** *SEC comparison of poly(nBA) star polymers prepared in IPA and DMSO*

Clear bimodality is observed in the star polymer prepared in the homogeneous polymerization in IPA, whereas in DMSO a mono-modal distribution is observed as above, with a dispersity value lower than that of the IPA system. Some potential reasons for the apparently beneficial nature of the phase separation were given earlier, however these solvent-switching experiments may provide further insight; since DMSO is clearly not a 'good' solvent for poly(*n*-BA), we may assume that the polymer chains adopt a more densely coiled conformation due to the lack of solvation, compared with a theta solvent such as IPA. This may in turn result in the propagating chain ends being less sterically accessible to the other polymer chain, reducing the likelihood of termination events.

It is advisable that neither the MA/*n*-BA nor IPA/DMSO comparisons be considered in isolation when assessing the role of heterogeneity in suppressing star-star coupling, as some perturbations of the original *n*-BA/DMSO system are inevitably involved when monomer and/or solvent is changed. However, when viewed in tandem, these comparisons offer a robust assessment of the beneficial nature of phase separation in suppressing radical-radical coupling for these star polymers.

## 3.4 Expanding The Scope: Poly(lauryl acrylate) Stars

To extend the scope of these investigations into the preparation of high molecular weight lipophilic star polymers and further the understanding of the role of heterogeneity in reducing star-star coupling, the polymerization of lauryl acrylate (LA) monomer was chosen for study. In a similar fashion to poly(nBA), poly(LA) also phase separates during the polymerization in certain higher polarity solvents, such as IPA. Notably, LA monomer is insoluble in DMSO, hence the need for the less polar solvent for this highly lipophilic monomer.

Polymerization of LA in IPA ($DP_{target}$ = 100) from the octa-functional lactose initiator yielded poly(LA) stars in a clear, colourless layer at the bottom of the reaction vessel whilst a green colour indicated the vast majority of the catalyst resided in a top solvent-rich layer (same $Cu^{(0)}$-mediated RDRP conditions as *n*-BA/DMSO). The observed separation is similar to that previously noted for poly(n-BA) in DMSO, however, owing to the differences in density between the components of both systems, the polymer-rich layer resides on the bottom in the case of the poly(LA)/IPA system. The polymerization of LA proceeded relatively quickly in IPA, with 90% monomer conversion attained within 4 hours (Figure 3.8; > 99% within 7 hours). SEC analysis revealed mono-modal peaks which shift clearly to higher molecular weight with increasing conversion (**Figure 3.10**).

The star polymerization of LA in IPA fulfils the criteria of a controlled/living polymerization (**3.11**). Specifically, the polymerization exhibited a linear evolution of $M_n$ with conversion whilst a plot of $\ln[M_t]/[M_0]$ also increased linearly with time for conversions up to ~90%. $Đ_M$ values decreased from 1.17 (at 4% monomer conversion) to 1.03 for the final polymer at quantitative conversion (>99%) (Figures 5 and 6). Similar to the poly(*n*BA) stars, the SEC derived molecular weights for the poly(LA) stars deviated somewhat from theoretical values (15 000 instead of 24 000 for $DP_{target}$=100), an observation again attributed to the inherent hydrodynamic differences of the linear SEC calibrants and the star polymer analytes. Attempts to utilize $^1$H-NMR as a comparative molecular weight determinant proved unsuccessful due to broad polymeric peaks obscuring those of the initiator.

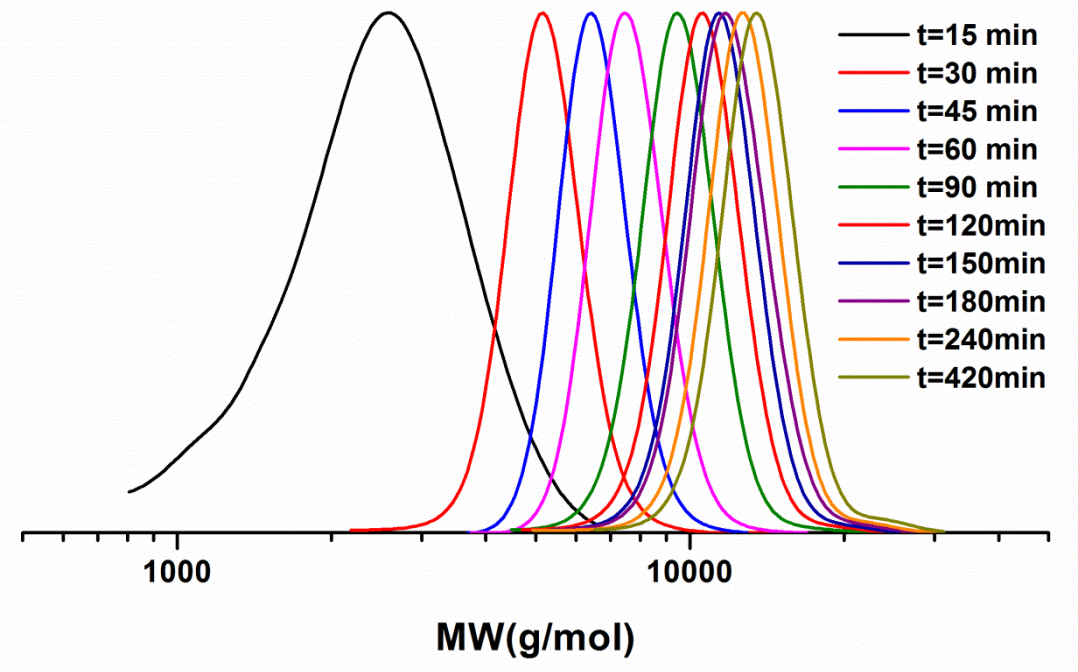


***Figure 3.10*** *SEC chromatograms over time for the $Cu^{(0)}$-mediated RDRP of lauryl acrylate in IPA from octa-functional lactose initiator (see Figure 3.11 for kinetic data). ([-Br]:[$Me_6$TREN]:[$Cu^{(II)}Br_2$] = 1: 0.18: 0.05)*

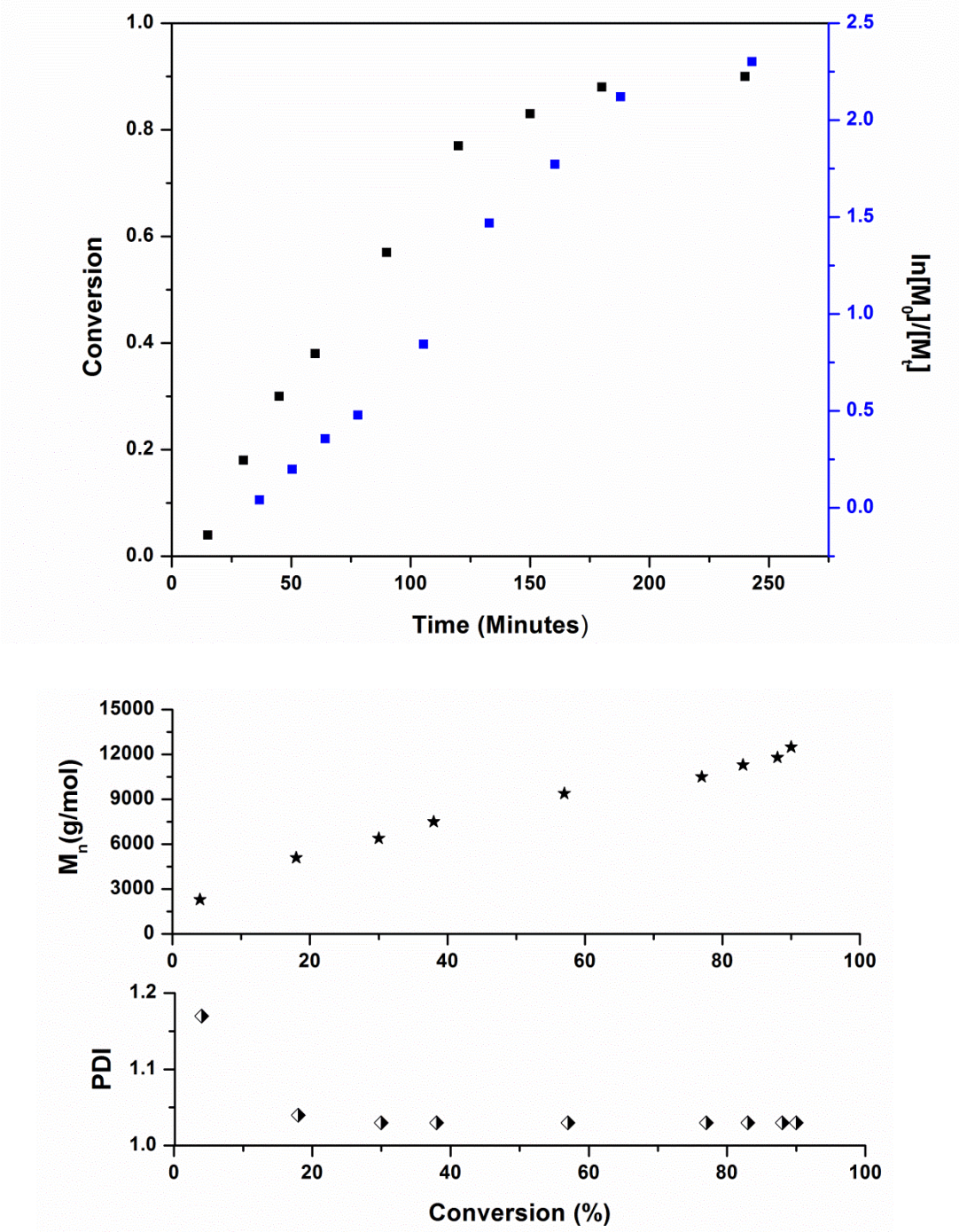


***Figure 3.11*** *Kinetic data (top) and $M_n$ and dispersity plotted as a function of conversion (bottom) for the $Cu^{(0)}$-mediated RDRP of lauryl acrylate in IPA from octa-functional lactose initiator (see Figure 3.10 for SEC chromatograms). (DP target = 100 [-Br]:[$Me_6$TREN]:[$Cu^{(II)}Br_2$] = 1: 0.18: 0.05)*

To further illustrate the scope of the LA polymerization a range of higher molecular weight experiments was also conducted to target DPs in the range of 200 to 800. Similarly to the DP 100 experiment, low dispersity star polymers were produced in each case (Table 3.3) with largely mono-modal molecular weight distributions in all cases (there is perhaps some evidence of limited star-star coupling in high molecular weight region). The polymerization targeting an overall DP of 800 (100 monomer units per arm) reached 70% conversion before stopping, thus illustrating the upper limitations in terms of molecular weight/conversion. This upper limit was not unexpected, with the steric nature of the monomer/polymer and high molecular weight expected to combine in preventing access of monomer to the active chain ends at higher conversions.

| DP $_{(target)}$ (per star) | $M_{n\ (theory)}$ (g mol$^{-1}$) | Conversion (%) | $M_{n\ (SEC)}$ (g mol$^{-1}$) | $Đ_M$ |
|---|---|---|---|---|
| **100** | 24 000 | 99 | 13 500 | 1.05 |
| **200** | 48 000 | 94 | 26 000 | 1.05 |
| **400** | 96 000 | 89 | 36 000 | 1.05 |
| **800** | 192 000 | 70 | 56 000 | 1.08 |

***Table 3.3*** *SEC data for the polymerization of 8-arm star poly(lauryl acrylate) in IPA. ([-Br]:[$Me_6$TREN]:[$Cu^{(II)}Br_2$] = 1: 0.18: 0.05)*

The polymerization of LA was also performed in a good solvent for the polymer as a comparison with the heterogeneous system. Toluene is capable of solubilizing poly(LA), however it is not expected to favour the disproportionation of $Cu^{(I)}$ (as required for SET-LRP). Hence, a binary mixture of toluene and methanol (1:4 *v*/*v*) was chosen to promote both solubility and disproportionation for the homogeneous polymerization of LA star polymers. Again, a range of DPs were targeted from 100

to 800 with low dispersities (**Table 3.4**) and mono-modal molecular weight distributions obtained in all cases. In a similar fashion to the LA/IPA system, polymerizations stopped earlier as higher DPs were targeted.

| DP (target) (per star) | $M_{n\ (theory)}$ g mol$^{-1}$ | Conversion (%) | $M_{n\ (SEC)}$ g mol$^{-1}$ | $Đ_M$ |
|---|---|---|---|---|
| **100** | 24 000 | 99 | 16 000 | 1.03 |
| **200** | 48 000 | 98 | 24 000 | 1.04 |
| **400** | 96 000 | 83 | 40 000 | 1.04 |
| **800** | 192 000 | 60 | 55 000 | 1.03 |

***Table 3.4*** *SEC data for the polymerization of 8-arm star poly(lauryl acrylate) in Toluene/Methanol (1:4 v/v). ([-Br]:[$Me_6$TREN]:[$Cu^{(II)}Br_2$] = 1: 0.18: 0.05)*

Despite limited levels of bimolecular termination, the star polymeriszation of LA in toluene/MeOH fulfils all the characteristics required for a controlled/living radical polymerization (**Figure 3.12**; DP target = 100; $M_n$ grows linearly with conversion throughout with final dispersity values as low as 1.03). In fact, the kinetic profile of this heterogeneous experiment (**Figure 3.13**) is remarkably similar to that of its homogeneous analogue in IPA (**Figure 3.11**), illustrating little effect of solvent and/or phase separation on the catalytic process and associated polymerization steps (activation, deactivation, propagation *etc*.)

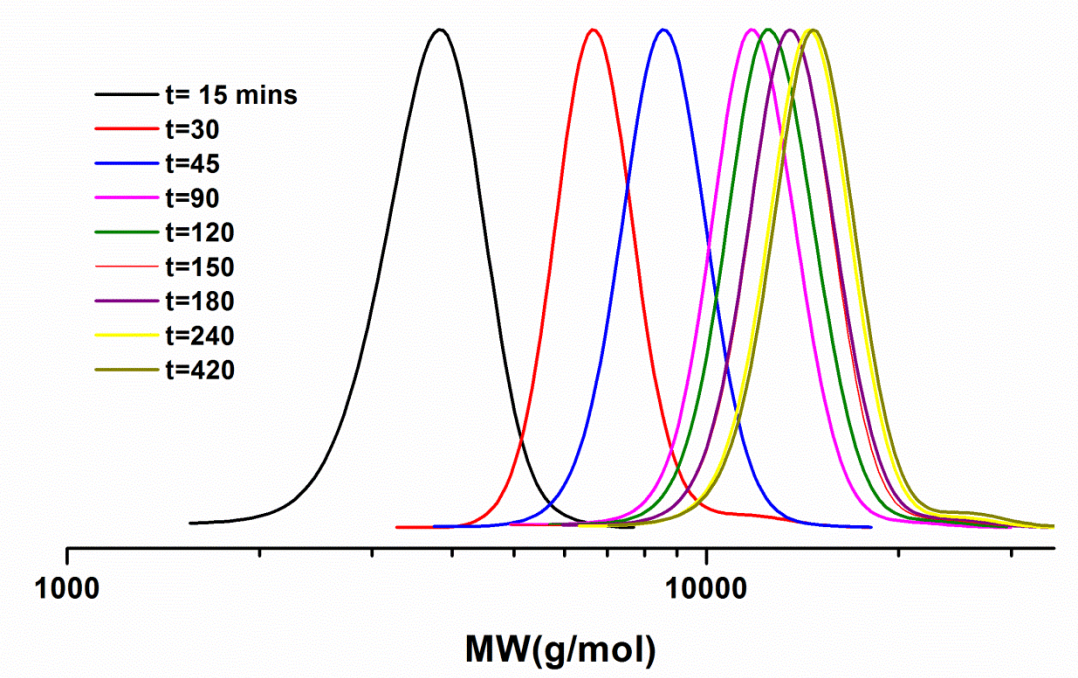


***Figure 3.12*** *SEC chromatograms over time for the $Cu^{(0)}$-mediated RDRP of LA in toluene/MeOH (1:4 v/v) from octa-functional lactose initiator. ([-Br]:[$Me_6$TREN]:[$Cu^{(II)}Br_2$] = 1: 0.18: 0.05) (DP target = 100; see Figure 3.13 for kinetic data)*

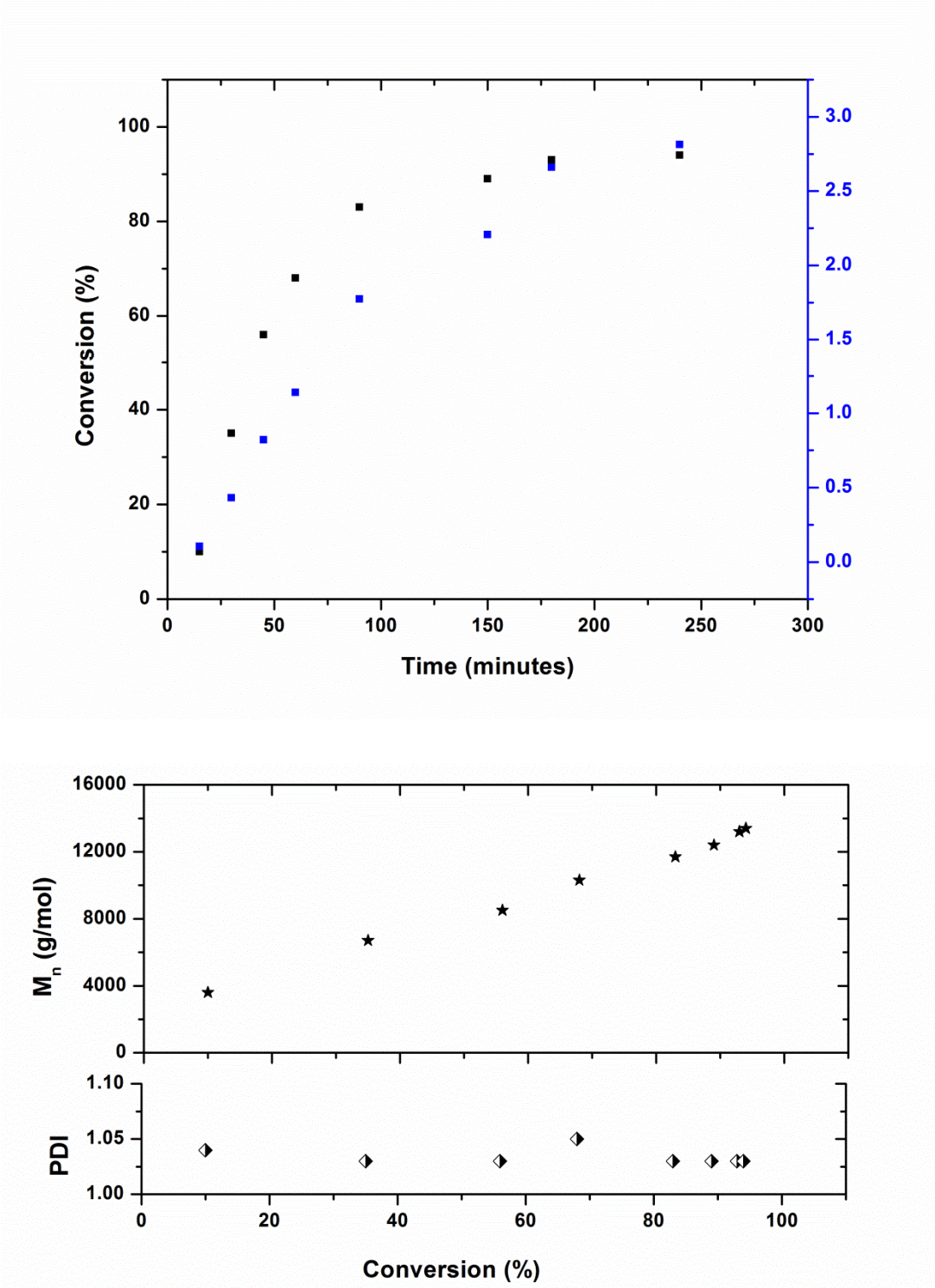


***Figure 3.13*** *Kinetic data (top) and $M_n$ and dispersity plotted as a function of conversion (bottom) for the $Cu^{(0)}$-mediated RDRP of LA in toluene/MeOH (1:4 v/v) from octa-functional lactose initiator. ([-Br]:[$Me_6$TREN]:[$Cu^{(II)}Br_2$] = 1: 0.18: 0.05) (DP target = 100; see Figure 3.9 for SEC chromatograms)*

## 3.5 Multi Detector SEC Analysis of Stars

As briefly discussed earlier, SEC analysis of star polymers can present a challenge when using 'conventional' techniques due to their different solution properties when compared with their linear equivalents. In this sub-chapter, the use of multi-detector SEC is investigated and the underlying theory discussed.

### 3.5.1 Conventional SEC

The basic purpose of SEC is to separate molecules according to their size and from this, their mass can be inferred. Polymer molecules are dissolved in an eluent to form spherical coils which are then passed through a column containing insoluble beads with well-defined pores. As they elute through the column, the polymer coils can diffuse in and out of the pores, with the smaller molecules being able to access more pores than the larger ones – the end result of this is that the largest molecules elute first, the smaller ones last[46, 47].

With conventional SEC, a concentration detector (usually a differential refractive index detector) is used to determine the amount of eluted material at a given retention time. This size separation information is then converted into a mass distribution by using a calibration curve generated by determining the retention times for a set of polymer standards of known narrow molecular weights. Since this is a comparative technique (as we are comparing the retention time of the sample to the retention time of a calibrant), accurate results depend on the chemistry and

architecture of the analyte and calibrant being similar. Ideally they should be the same material but often this is not possible.

### 3.5.2 SEC Using Viscometry Detection

A viscometer can be used to measure the solution viscosity of the sample as it elutes from the column and, when combined with the concentration information from the RI detector, a 'universal calibration'[48] can be obtained which allows for accurate molecular weight analysis without the need for the calibrant and polymer sample to have the same chemistry.

In such a detector the sample solution and a reference solvent are pushed through narrow capillaries and the pressure drop measured, which is then related to the viscosity using the Hagen–Poiseuille equation:

$$\Delta P = \frac{8\mu LQ}{\pi r^4}$$

***Equation 3.1*** *Hagen–Poiseuille's law, where ΔP is the pressure drop, L is the length of capillary, μ is the dynamic viscosity Q is the volumetric flow rate, r is the radius, and π is the mathematical constant*

A Universal Calibration is then derived from the fact that intrinsic viscosity and molecular weight are related to the hydrodynamic volume of the molecules in solution according to the following:

$$Hydrodynamic\ Volume = k \times MW \times [\eta]$$

***Equation 3.2*** *Where k is a constant, MW is the molecular weight and [η] is the intrinsic viscosity*

It follows from this that if a calibration curve is made by plotting log ([η] x MW) against retention time/elution volume for a set of known standards, that is equivalent to plotting log size vs. retention time. Since SEC separates according to hydrodynamic volume, the same calibration curve can be obtained regardless of the standards used, thus giving us a calibration which independent of chemistry or architecture (**Figure 3.14**).

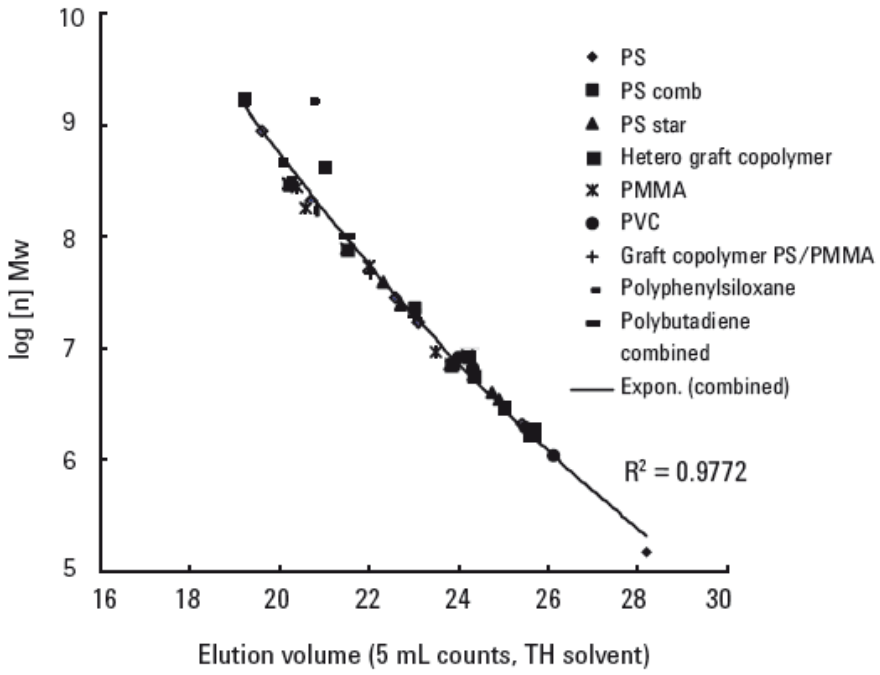


***Figure 3.14*** *log ([η] x MW) vs elution volume for various polymers, according to Grubisic et. al.(Reference 48)*

### 3.5.3 Kuhn-Mark-Houwink-Sakurada (KMHS) Plots

The use of viscometry SEC also allows for dynamic structural information about the polymer to be derived, by plotting the relationship between intrinsic viscosity and molecular weight according to the following equation:

$$[\eta] = KM^{\alpha}$$

$$\log[\eta] = \log K + \alpha Log M$$

***Equation 3.3*** *The Kuhn-Mark-Houwink-Sakurada equation in both normal and log forms*

Where M is the molecular weight and K , α are derived constants. A plot of the log-rearranged form of the equation gives a straight line with a slope of α and an intercept of logK (**Figure 3.15**).

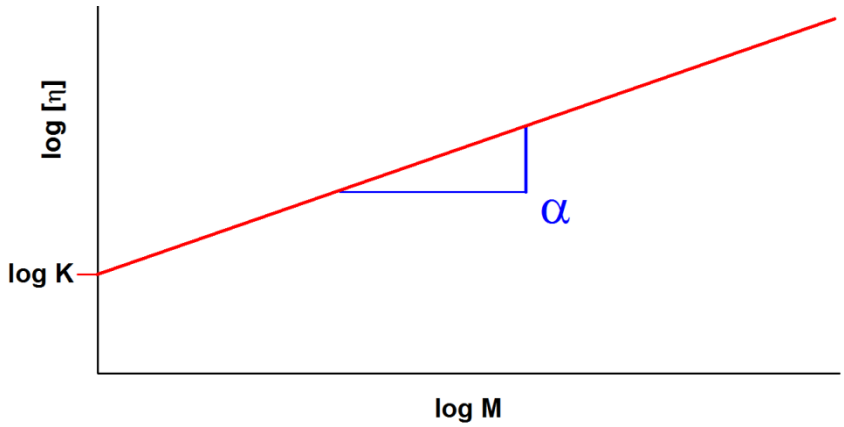


***Figure 3.15*** *Arbitrary KMHS plot*

The α exponent gives useful geometric information regarding the polymer in solution. For most polymers the value of α ranges between ~0.5 and 0.8, where lower values (>0.5) indicate that the polymer is a 'hard sphere'. Values of ~0.7-0.8 indicate a 'random' coil and those of ~2 indicate a larger, well solvated 'rigid rod' structure.

### 3.5.3.1 SEC Using Light Scattering Detection (LS) and, Triple Detection

The use of light scattering detection in SEC involves irradiating the eluting material from the columns with a laser and measuring the intensity of the resulting scattered light. The scattered light intensity, given as the Rayleigh ratio ($R_\theta$), is directly proportional to the molecular weight of the solvated material from which it has scattered according to the following **Equation 3.4**.

$$R_\theta = Mw\, K \left(\frac{dn}{dc}\right)^2 c$$

***Equation 3.4*** *The Rayleigh ratio $R_\theta$ , where Mw is the molecular weight, K is a constant, dn/dc is the refractive index increment and c is the concentration*

The use of the Rayleigh equation allows for the *absolute* molecular weight of the sample to be determined for a given slice of the chromatogram, independent of any column calibration. The radius of gyration ($R_g$) can also be determined using LS, although this requires the use of multi-angle detectors which are not always available[49]. The technique is not without drawbacks however, namely that since the detector response is directly proportional to the molecular weight, light-scattering is

generally unsuitable for analysing small, low molecular weight polymers. Additionally, since the scattering intensity is also proportional to the square of the dn/dc, this value should ideally be consistent across the sample meaning that this technique is generally unsuitable for analysing co-polymers. The analyte must be also very pure and free of any large particulate matter (eg. dust) which would otherwise cause noise in the signal.

All three detection methods discussed can be combined together; RI for determining the concentration, viscometry for structural analysis and LS to measure the molecular weight[50, 51]. This is known as Triple Detection and branching information is derived using theory developed by Zimm, Stockmayer and Kilb[52-54]. For a given branched polymer, the $R_g$ and IV will be lower than that for a linear polymer possessing the same chemistry, due to the branching points. The more branched the polymer is, the greater the reduction in $R_g$/IV is and this difference can be quantified in terms of either the radius of gyration contraction factor (g) or the intrinsic viscosity contraction factor (g'), depending on which detector is used (**Equations 3.6** and **3.7**). Typically g' is used due to the insensitivity of light scattering detection for low molecular weights and g' can be converted to g by the relationship $g = g'^{(1/\varepsilon)}$ where ε is a monomer-dependent structural factor.

$$g = \frac{(R_g)_{Branched}}{(R_g)_{Linear}} \qquad g' = \frac{[\eta]_{Branched}}{[\eta]_{Linear}}$$

***Equations 3.5 and 3.6*** *The radius of gyration ($R_g$) and intrinsic viscosity (IV) contraction factors*

These equations can give an indication (but not absolute measurements) of the branching extent by comparing a range of branched polymers against a linear analogue[50]. The value of g can be used, in conjunction with an appropriate statistical model, to estimate the number of branching points in the polymer or the number of arms if it is a star. Since we are concerned with the latter in this work, the 'Random Star Branched Model' (**Equation 3.8**) was used in the following study to derive the functionality (*f*) of the samples tested (which is the number of arms).

$$g = \frac{3f}{(f+1)^2}$$

***Equations 3.7*** *The random star branching model, where f is the number of arms and g is the radius of gyration contraction factor*

A series of poly(n-BA) stars were synthesized using the conditions used earlier in the chapter (8-arm initiator, [-Br]:[$Me_6$TREN]:[$Cu^{(II)}Br_2$] = 1: 0.18: 0.05, in DMSO) targeting molecular weights of 50, 100 and 150 Kg $mol^{-1}$, which should be sufficiently large enough for triple detection. In all cases, conversions above 90% were obtained and the samples first analysed using conventional SEC. As with the earlier stars tested, there appears to be a significant underestimation of the molecular weights, as shown in **Table 3.5**. The samples were then re-analysed using triple detection SEC, using a poly(*n*-BA) as a linear reference (MW ~200 kg $mol^{-1}$) and the Random Star Branching statistical model. The calculations for determining g, g' and *f* were performed using the Cirrus SEC software.

| DP (target, per star) | $M_n$ (Target) (g mol$^{-1}$) | *Conv. (%)* | $M_n$ (Conventional SEC) (g mol$^{-1}$) | $Đ_M$ *(conventional SEC)* | $M_n$ (Triple SEC) (g mol$^{-1}$) | *f (at $M_n$)* | *α* |
|---|---|---|---|---|---|---|---|
| **390** | 52000 | 95 | 44400 | 1.10 | 56300 | 5.06 | 0.77 |
| **780** | 101000 | 90 | 64600 | 1.13 | 84600 | 6.40 | 0.75 |
| **1170** | 151500 | 93 | 93500 | 1.17 | 143400 | 6.98 | 0.73 |
| **Linear Reference** | - | - | 191300 | 1.16 | - | - | 0.84 |

***Table 3.5*** *Conventional and triple detection SEC data for poly(n-BA) stars synthesized using an 8-arm initiator*

As shown in **Table 3.5**, it can be seen from the data that the triple detection SEC provides much more accurate mass determination than conventional, with the values obtained being far closer to that expected. The increasing discrepancy towards higher molecular weight is stark, with a difference of ~50 kg mol$^{-1}$ between the conventional and triple detection values for the polymer with a target $M_n$ of 150 kg mol$^{-1}$. The values of *f*, derived from the viscometric data and reported as the value at $M_n$, range from approximately 5-7 which is close to, but not precisely, the expected value of eight. There also appears to be an upward trend for *f* with molecular weight, which may be due to the generally higher sensitivity of the instrumentation towards larger molecular weights. The values of the α exponents also give an indication as to the extent of branching within the samples. For the linear reference, α = 0.84 which consistent with what would be expected for a linear polymer adopting a 'random coil' conformation in a good solvent. The values of α for the star polymers are in the range 0.77-0.73, which is lower than that of the linear reference, indicating contraction of the molecular structure and a branched architecture. The similarity of these values also indicate consistent branching

across the molecular weights of the samples, which is to be expected since the same multifunctional initiator was used for each sample (thus there should only be a singular branch point).

The difference between the expected and calculated values for *f* may be explained in two ways. Firstly, the possibility of termination/loss of chain end functionality during the polymerization cannot be disregarded as variations in the arm lengths could affect the perceived number of arms measured. Secondly, it should also be noted that these calculations are reliant on a number of polymer, solvent and machine related parameters, plus a statistical model. The underlying theory was also developed for high molecular weight, broad dispersity, industrial polyolefins and as such may not be completely applicable to the comparatively low molecular weight, narrow dispersity samples analysed here. However all things considered, including the chemistry used, the functionalities derived are reasonable and serve to demonstrate that the polymers synthesized are indeed multi-arm stars. The molecular weight distributions and associated MKHS plots are given below in **Figures 3.16**, **3.17** and **3.18**.

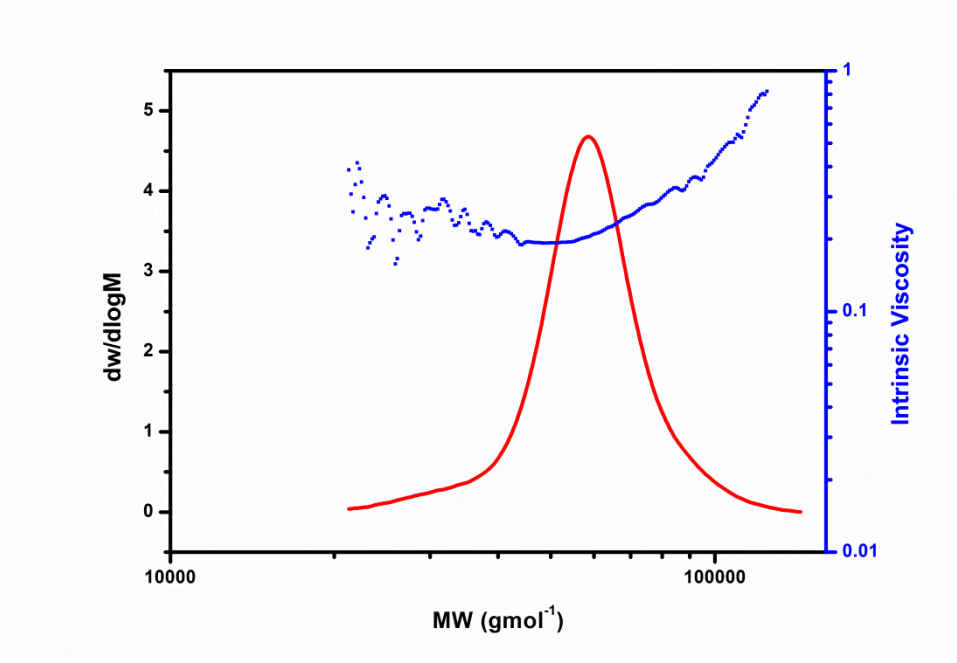


***Figure 3.16*** *Molecular weight distribution and MKHS plot for 8-arm poly(lauryl acrylate), target* $M_n$ *= 50 kg mol*$^{-1}$. α = 0.77

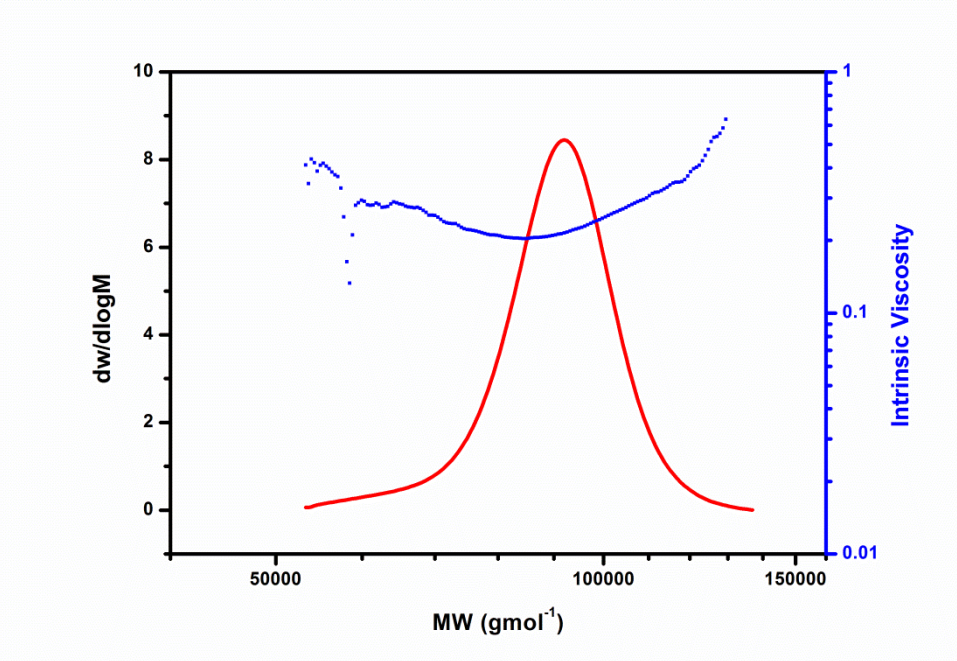


***Figure 3.17*** *Molecular weight distribution and MKHS plot for 8-arm poly(lauryl acrylate), target* $M_n$ *= 100 kg mol*$^{-1}$. α = 0.75

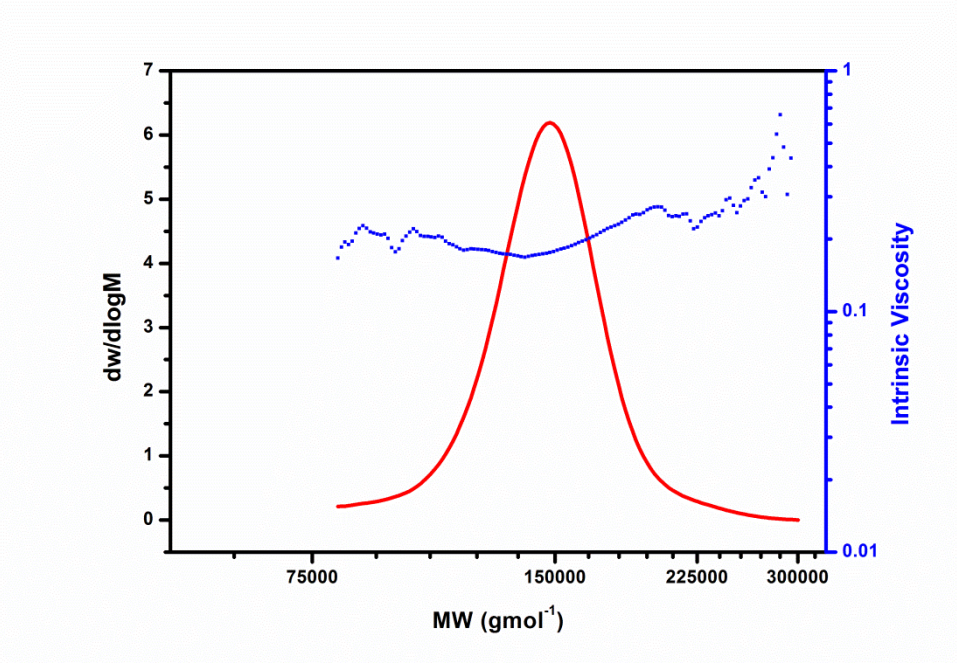


***Figure 3.18*** *Molecular weight distribution and MKHS plot for 8-arm poly(lauryl acrylate), target* $M_n$ *= 150 kg mol*$^{-1}$. α = 0.73

## 3.6 Large Scale Synthesis and Testing of Poly(lauryl acrylate) Stars Bearing Different Numbers of Arms

So far in this chapter, only the use of 8-arm initiators has been explored. In the following sub-chapter other multi-arm initiators are investigated as well as testing the large scale feasibility of these polymerizations, given the industrial backing of the project. The end goal was to synthesize a range of star poly(lauryl acrylates) with enough material produced to be able to carry out rheological/mechanical testing.

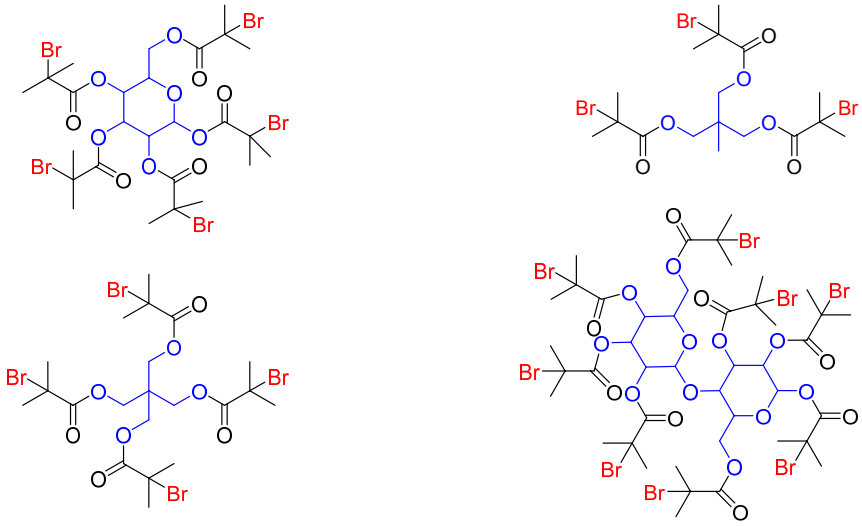

***Figure 3.19*** *The different initiators used in this study: 3 arm, 4 arm, 5 arm and 8 arm*

To begin, a previous reaction using the 8-arm lactose based initiator was scaled up using the same conditions as before ([-Br]:[$Me_6$TREN]:[$Cu^{(II)}Br_2$] = 1: 0.18: 0.05), with lauryl acrylate as the monomer and IPA as the solvent, targeting a molecular weight of 20 kg $mol^{-1}$. The polymerization was attempted on a 300 mL scale (50:50 monomer:solvent v/v) with the aim of producing ~130 g of product at complete conversion and was carried out in a Radley's double-jacketed reactor fitted with an overhead stirrer (**Figure 3.20**). 50 cm of acid-washed copper wire was wrapped

around the paddle and the reaction mixture degassed via nitrogen sparging for 30 minutes to account for the larger scale. Upon addition of the ligand, the reaction mixture was left to polymerize overnight.


***Figure 3.20*** *Photograph of the reactor setup post-reaction for the large scale polymerization of star poly (lauryl acrylate). The phase separation can clearly be seen*

This reaction performed in an analogous fashion to those carried out on a small scale with phase separation being observed when the stirrer was switched off. This feature has a particular advantage when using this reactor as due to the density of the polymer, the bottom tap can simply be opened and the bottom (polymer) layer then drained off, leaving the upper phase behind. A 95% conversion (determined by $^{1}$H NMR) was achieved in this case with the subsequent conventional SEC analysis confirming that the desired molecular weight had been reached and with excellent control over the polymerization ($M_n$ = 20500 g mol$^{-1}$ $Đ_M$ = 1.040). The product was then passed through an alumina column to remove any trace

metal/catalyst impurities, before being transferred into a jar for further testing. Analogous reactions using the same [I]:[M]:[L]:[$Cu^{II}$] were then carried out using the 3, 4 and 5 arm initiators illustrated in Figure 3.5.2 and in all cases high conversions were obtained (>90%), whilst reaching the target $M_n$ with exceptionally low dispersity. The characterization data for these reactions is given in **Table 3.6**.

| Number of Arms | $M_{n\,(SEC)}$ g $mol^{-1}$ | Conversion (%) | $Đ_M$ |
|---|---|---|---|
| **3** | 18 400 | 94 | 1.035 |
| **4** | 19 300 | 92 | 1.036 |
| **5** | 18 300 | 98 | 1.043 |
| **8** | 20 500 | 95 | 1.040 |

***Table 3.6*** *Characterization data for the polymerization of star poly(lauryl acrylate) bearing different numbers of arms in IPA ([-Br]:[$Me_6$TREN]:[$Cu^{(II)}Br_2$] = 1: 0.18: 0.05)*

The above polymers were then subjected to a series of tests in order to assess their suitability as VM's, in particular to see if the number of arms on the star polymer has any effect on the performance. These measurements represent some of standard test regimes used in the lubricant industry and were carried out during a visit to Lubrizol's R&D centre in Hazelwood, UK. To begin, each polymer was blended in a base oil, Yubase 4, to equal amounts by weight percentage (10%, known as blending to Equal Actives Content). The kinematic viscosities (KV) of each sample at 100°C were then measured, the values of which were then used to calculate the Thickening Efficiency of each polymer using **Equation 3.8**. These $KV_{100}$ values are also used in order to calculate the treat rates required to produce blends at equal viscosity, which will be discussed later.

$$TE = \left( log_{10} \left( \frac{KV_{100}oil + VM}{KV_{100}base\ oil} \right) \right) TR$$

***Equation 3.8*** *Calculation TE, where $KV_{100}$ oil+VM = the KV of the oil and VM blend at 100°C, $KV_{100}$ base oil = the KV of the base oil at 100°C and TR = Treatment Rate (%wt)*

| Sample | Treat Rate (%wt) | $KV_{100}$ (cSt) | T.E |
|---|---|---|---|
| **3-Arm Star in Y4** | 10 | 6.30 | 1.751 |
| **4-Arm Star in Y4** | 10 | 6.95 | 2.177 |
| **5-Arm Star in Y4** | 10 | 5.88 | 1.67 |
| **8-Arm Star in Y4** | 10 | 6.25 | 1.716 |

***Table 3.7*** *$KV_{100}$ values and derived Thickening Efficiencies for the poly(lauryl acrylate) star polymers tested*

As shown in **Table 3.7**, the TE's of each polymer are approximately in the same range, ~1.7-2, which is modest in comparison to current commercial products. There also appears to be little or no apparent trend regarding the number of arms. Using the $KV_{100}$ values obtained, the treat rates required to deliver a viscosity at 100°C of 12 cSt was then calculated and new blends produced accordingly. This is known as blending to Equal Viscosity and gives a more accurate measure as to the effect of the polymer in the system, which then allows for $KV_{40}$ and VI values to be calculated using **Equation 1.6**. The absolute viscosities (AV) at -40°C were also measured for these blends.

The data for these tests is given in **Table 3.8**. The viscosity index values calculated put these polymers in the 'Very High' VI category (VI >110) and are comparable to Lubrizol's Asteric commercial products which have VIs between 200 and 250, which is a promising result, although it should be noted that these are not the complete blends containing the other additives that would be present in the full commercial product. However, $AV_{-40}$ values could not be obtained due to the blends solidifying and being too viscous to measure (TVTM). This was rectified by the addition of a pour point depressant (PPD, 0.2 wt%), which are normally present in a full formulation and serves to prevent wax formation at low temperatures. The revised data is presented in **Table 3.9**.

| Sample | TR %wt | AV -40°C (cP) | $KV_{100}$ (cSt) | $KV_{40}$ (cSt) | VI |
|---|---|---|---|---|---|
| **3-Arm Star in Y4** | 25.99 | TVTM | 12.20 | 60.64 | 204.0 |
| **4-Arm Star in Y4** | 20.90 | TVTM | 11.45 | 55.03 | 208.0 |
| **5-Arm Star in Y4** | 31.82 | TVTM | 12.12 | 60.47 | 202.0 |
| **8-Arm Star in Y4** | 26.51 | TVTM | 12.20 | 60.57 | 204.0 |

***Table 3.8*** *$KV_{100}$ values and derived Thickening Efficiencies for the poly(lauryl acrylate) star polymers tested.*

| Sample | TR %wt | AV -40°C (cP) | $KV_{100}$ (cSt) | $KV_{40}$ (cSt) | VI |
|---|---|---|---|---|---|
| **3-Arm Star in Y4 +PPD** | 25.58 | >400 000 | 12.20 | 59.73 | 207.00 |
| **4-Arm Star in Y4 + PPD** | 21.88 | >400 000 | 11.16 | 53.35 | 208.00 |
| **8-Arm Star in Y4 + PPD** | 26.1 | >400 000 | 12.14 | 59.59 | 207.00 |

***Table 3.9*** *$KV_{100}$ values and derived Thickening Efficiencies for the poly(lauryl acrylate) star polymers tested*

The $AV_{-40}$ for the blends containing PPD were all above the maximum which can be measured by the rheometer, 400,000 cP. These values would typically be around 300,000 for the commercial products and so we would expect the values measured for these blends to be lower in the presence of the complete additives package. The presence of the PPD makes a negligible change to the VIs and once again, there is little, if any effect of the varying arm lengths on the rheological behaviour. It was intended that shear stability testing be conducted on these samples, however the large quantities of polymer needed, plus time constraints meant that this could not be completed. As mentioned in the introduction, shear stability is where we would expect to see any dependence on the number of arms and so this would be important for future investigations.

## 3.7 Conclusions

The findings of this investigation are two-fold. Firstly, a convenient route has been demonstrated to the synthesis of a range of lipophilic poly(acrylate) stars using $Cu^{(0)}$-mediated RDRP in a range of solvent systems, both heterogeneous and homogeneous. Using this method 8-armed acrylic stars have been synthesized to quite high molecular weights and conversions, whilst retaining excellent control over molecular weight distributions (dispersities as low as 1.03 and ≤ 1.10 in most cases). Secondly, it has been shown that phase separation of stars from the reaction medium is not only benign to the polymerization process, but in fact can reduce star-star coupling in certain cases, allowing for the synthesis of stars with unprecedented degrees of control relative to other controlled/living radical polymerization approaches. The *n*-BA/DMSO biphasic system exhibited clear advantages over analogous MA/DMSO and *n*-BA/IPA homogenous systems, with significantly reduced star-star coupling in the heterogeneous system. We have proposed that this could be due to the reduced mobility of the polymer stars upon phase separation or the compartmentalization of the active chain ends due to the lack of sufficient solvation. The star polymerization of LA proceeded equally well in both heterogeneous and homogeneous systems, with no distinct advantage exhibited by one protocol over the other.

A selection of 8-arm poly(butyl acrylates) were then analysed using multi-detector SEC to get a more accurate measurement of their molecular weights and to try and derive branching values which should indicate the number of arms. This was successful and functionalities between ~5-7 were obtained, which is reasonable given the chemistry and the number of assumptions which have to be made when performing the analysis.

This method of generating well-defined star polymers was scaled up and extended to the synthesis of stars bearing 3, 4, 5 and 8 arms on a 300 mL scale, which provided sufficient material to allow for rheological testing to be carried out, using techniques which are standard for the industry. These tests revealed that the materials tested had high VI's under the conditions used and that they function as VM's as per the definition by Selby[55]. However, no dependence on the number of arms was observed.

## 3.8 Experimental

### 3.8.1 Materials

*n*-Butyl acrylate (*n*-BA), methyl acrylate (MA), lauryl acrylate (LA), and $Cu^{II}Br_2$ were purchased from Sigma-Aldrich. Monomers were passed over a short alumina column to remove inhibitor prior to use. DMSO, isopropyl alcohol (IPA), toluene and methanol were purchased from Fischer Scientific and used as received. Tris-(2-(dimethylamino)ethyl)amine ($Me_6$-TREN)[56, 57] was synthesized according to previously reported literature, 8, 5, 4 and 3 arm initiators were previously synthesised by members of the Haddleton group. Cu(0) (gauge 0.25 mm) wire was purchased from Comax Engineered wires and purified by immersion in conc. HCl for 15 minutes, then rinsed with water and dried prior to use.

### 3.8.2 Characterization

NMR spectra were recorded on Bruker DPX-300 or DPX-400 spectrometers in $CDCl_3$. Chemical shifts are given in ppm downfield from the internal standard tetramethylsilane. Monomer conversions were determined via $^1H$ NMR spectroscopy by comparing the integrals of monomeric vinyl protons to polymer signals.

Size exclusion chromatography (SEC) measurements were conducted using an Agilent 1260 SEC-MDS fitted with a differential refractive index (DRI), Viscometry and light scattering detectors equipped with 2 × PLgel 5 mm mixed-D columns (300

× 7.5 mm), 1 × PLgel 5 mm guard column (50 × 7.5 mm) and autosampler. Narrow linear poly(methyl methacrylate) standards ranging from 200 to 1.0 × $10^6$ g·mol$^{-1}$ were used as calibrants. All samples were passed through a 0.45 μm PTFE filter prior to analysis. The mobile phase was chloroform with 2% triethylamine eluent at a flow rate of 1.0 mL/min. SEC data were analyzed using Cirrus v3.3 software.

### 3.8.3 Synthetic Methods

#### 3.8.3.1 A typical Cu(0) mediated polymerization using 8-arm initiator

*n*-Butyl acrylate (*n*-BA; 10 mL; 8.94 g; 0.069 mol; 70 eq. relative to initiator molecule), DMSO (10 mL), $Cu^{II}Br_2$ (89 mg; 3.98 x $10^{-4}$ mol; 0.05 eq relative to bromo functionality), *octa*-*O*-isobutyryl bromide lactose (8-arm initiator) (1.52 g; 9.96 x $10^{-4}$ mol) were charged to a Schlenk tube. Pre-activated Cu(0) wire (10 cm) wrapped around a stir bar was then added prior to sealing with a septum. The reaction mixture was degassed by $N_2$ sparging *via* a needle for 15 minutes. $Me_6$TREN (284 μL; 1.43 x $10^{-3}$ mol; 0.18 eq. relative to bromo functionality) was finally introduced *via* a degassed, airtight syringe to start the reaction, which was allowed to proceed overnight at ambient temperature. Samples were taken periodically for SEC and NMR analysis. NMR samples were diluted with $CDCl_3$ while SEC samples were diluted with chloroform and passed through a short alumina column to remove copper salts.

An analogous procedure was used for the polymerizations using the 3, 4 and 5 arm initiators.

## 3.9 References


1. Z. Li, E. Kesselman, Y. Talmon, M. A. Hillmyer and T. P. Lodge, *Science*, 2004, 306, 98-101.
2. G. Widawski, M. Rawiso and B. Francois, *Nature*, 1994, 369, 387-389.
3. J. T. Wiltshire and G. G. Qiao, *Aust. J. Chem.*, 2007, 60, 699.
4. K. Khanna, S. Varshney and A. Kakkar, *Polym. Chem.*, 2010, 1, 1171-1185.
5. D. J. A. Cameron and M. P. Shaver, *Chem. Soc. Rev.*, 2011, 40, 1761-1776.
6. A. Sulistio, A. Blencowe, A. Widjaya, X. Zhang and G. Qiao, *Polym. Chem.*, 2012, 3, 224-234.
7. Y. Deng, S. Zhang, G. Lu and X. Huang, *Polym. Chem.*, 2013, 4, 1289-1299.
8. H. Y. Cho, S. E. Averick, E. Paredes, K. Wegner, A. Averick, S. Jurga, S. R. Das and K. Matyjaszewski, *Biomacromolecules*, 2013, 14, 1262-1267.
9. T. Ooya, J. Lee and K. Park, *J. Controlled Release*, 2003, 93, 121-127.
10. C. T. Adkins, J. N. Dobish, C. S. Brown, B. Mayrsohn, S. K. Hamilton, F. Udoji, K. Radford, T. E. Yankeelov, J. C. Gore and E. Harth, *Polym. Chem.*, 2012, 3, 390-398.
11. Y. Li, M. Beija, S. Laurent, L. v. Elst, R. N. Muller, H. T. T. Duong, A. B. Lowe, T. P. Davis and C. Boyer, *Macromolecules*, 2012, 45, 4196-4204.
12. B. Helms, S. J. Guillaudeu, Y. Xie, M. McMurdo, C. J. Hawker and J. M. J. Fréchet, *Angew. Chem., Int. Ed.*, 2005, 44, 6384-6387.
13. Y. Chi, S. T. Scroggins and J. M. J. Fréchet, *J. Am. Chem. Soc.*, 2008, 130, 6322-6323.
14. T. Terashima, M. Kamigaito, K.-Y. Baek, T. Ando and M. Sawamoto, *J. Am. Chem. Soc.*, 2003, 125, 5288-5289.

15. S. Kanaoka, N. Yagi, Y. Fukuyama, S. Aoshima, H. Tsunoyama, T. Tsukuda and H. Sakurai, *J. Am. Chem. Soc.*, 2007, 129, 12060-12061.

16. K. Nomura, K. Tanaka and S. Fujita, *Organometallics*, 2012, 31, 5074-5080.

17. L. J. Fetters, A. D. Kiss, D. S. Pearson, G. F. Quack and F. J. Vitus, *Macromolecules*, 1993, 26, 647-654.

18. M. Morell, D. Foix, A. Lederer, X. Ramis, B. Voit and À. Serra, *J. Polym. Sci. A Polym. Chem.y*, 2011, 49, 4639-4649.

19. H. Gao and K. Matyjaszewski, *Macromolecules*, 2006, 39, 3154-3160.

20. A. W. Bosman, A. Heumann, G. Klaerner, D. Benoit, J. M. J. Fréchet and C. J. Hawker, *J. Am. Chem. Soc.*, 2001, 123, 6461-6462.

21. K.-Y. Baek, M. Kamigaito and M. Sawamoto, *Macromolecules*, 2000, 34, 215-221.

22. H. Gao and K. Matyjaszewski, *J. Am. Chem. Soc.*, 2007, 129, 11828-11834.

23. J. Liu, A. O. Burts, Y. Li, A. V. Zhukhovitskiy, M. F. Ottaviani, N. J. Turro and J. A. Johnson, *J. Am. Chem. Soc.*, 2012, 134, 16337-16344.

24. R. Knischka, P. J. Lutz, A. Sunder, R. Mülhaupt and H. Frey, *Macromolecules*, 1999, 33, 315-320.

25. S. Jacob, I. Majoros and J. P. Kennedy, *Macromolecules*, 1996, 29, 8631-8641.

26. K. Ohno, B. Wong and D. M. Haddleton, *J. Polym. Sci., A Polym. Chem.*, 2001, 39, 2206-2214.

27. Q. Zhang, G.-Z. Li, C. R. Becer and D. M. Haddleton, *Chem. Commun.*, 2012, 48, 8063-8065.

28. C. Zhang, M. Miao, X. Cao and Z. An, *Polym. Chem.*, 2012, 3, 2656-2664.

29. J. Ferreira, J. Syrett, M. Whittaker, D. Haddleton, T. P. Davis and C. Boyer, *Polym. Chem.*, 2011, 2, 1671-1677.

30. H. Gao, S. Ohno and K. Matyjaszewski, *J. Am. Chem. Soc.*, 2006, 128, 15111-15113.

31. T. Higashihara, R. Faust, K. Inoue and A. Hirao, *Macromolecules*, 2008, 41, 5616-5625.

32. J. Feldthusen, B. Iván and A. H. E. Müller, *Macromolecules*, 1998, 31, 578-585.

33. C. Barner-Kowollik, T. P. Davis and M. H. Stenzel, *Aust. J. Chem.*, 2006, 59, 719.

34. F. Cheng, E. M. Bonder, A. Doshi and F. Jakle, *Polym. Chem.*, 2012, 3, 596-600.

35. H. A. Zayas, N. P. Truong, D. Valade, Z. Jia and M. J. Monteiro, *Polym. Chem.*, 2013, 4, 592-599.

36. M. H. Stenzel-Rosenbaum, T. P. Davis, A. G. Fane and V. Chen, *Angew. Chem., Int. Ed.*, 2001, 40, 3428-3432.

37. S. Paillet, A. Roncin, G. Clisson, G. Pembouong, L. Billon, C. Derail and M. Save, *J. Polym. Sci., A Polym. Chem.*, 2012, 50, 2967-2979.

38. W. Ding, C. Lv, Y. Sun, H. Luan, T. Yu and G. Qu, *Polym. Bull.*, 2011, 67, 1499-1505.

39. M. R. Whittaker, C. N. Urbani and M. J. Monteiro, *J. Polym. Sci., A Polym. Chem.*, 2008, 46, 6346-6357.

40. C. Boyer, A. Derveaux, P. B. Zetterlund and M. R. Whittaker, *Polym. Chem.*, 2012, 3, 117-123.

41. Lubrizol, The Science Behind Lubrizol's Asteric™ Viscosity Modifiers, Accessed 2014.

42. P. Wright, PhD Thesis, The University of Warwick, 2008.

43. A. J. Limer, A. K. Rullay, V. S. Miguel, C. Peinado, S. Keely, E. Fitzpatrick, S. D. Carrington, D. Brayden and D. M. Haddleton, *Reactive and Functional Polymers*, 2006, 66, 51-64.

44. T. Kato, T. Hashimoto, T. Fujimoto and M. Nagasawa, *Journal of Polymer Science: Polymer Physics Edition*, 1975, 13, 1849-1854.

45. S. R. Samanta, M. E. Levere and V. Percec, *Polym. Chem.*, 2013, 4, 3212-3224.

46. P. C. Hiemenz and T. P. Lodge, *Polymer Chemistry, Second Edition*, Taylor & Francis, 2007.

47. A. Striegel, W. W. Yau, J. J. Kirkland and D. D. Bly, *Modern size-exclusion liquid chromatography: practice of gel permeation and gel filtration chromatography*, John Wiley & Sons, 2009.

48. Z. Grubisic, P. Rempp and H. Benoit, *Journal of Polymer Science Part B: Polymer Letters*, 1967, 5, 753-759.

49. S. Podzimek, T. Vlcek and C. Johann, *J. Appl. Polym. Sci.*, 2001, 81, 1588-1594.

50. G. Saunders, P. A. G. Cormack, S. Graham and D. C. Sherrington, *Macromolecules*, 2005, 38, 6418-6422.

51. S. T. Balke, T. H. Mourey, D. R. Robello, T. A. Davis, A. Kraus and K. Skonieczny, *J. Appl. Polym. Sci.*, 2002, 85, 552-570.

52. B. H. Zimm and R. W. Kilb, *Journal of Polymer Science*, 1959, 37, 19-42.

53. B. H. Zimm and W. H. Stockmayer, *The Journal of Chemical Physics*, 1949, 17, 1301-1314.

54. W. H. Stockmayer, *The Journal of Chemical Physics*, 1943, 11, 45-55.

55. T. W. Selby, *A S L E Transactions*, 1958, 1, 68-81.

56. M. Ciampolini and N. Nardi, *Inorg. Chem.*, 1966, 5, 41-44.

57. J. Queffelec, S. G. Gaynor and K. Matyjaszewski, *Macromolecules*, 2000, 33, 8629-8639.

# Chapter 4: Synthesis and Rheological Testing of Lipophilic Poly(alkyl acrylates) Bearing Quadrupolar Hydrogen Bonding Functionality

In this chapter, methods to synthesize lipophilic poly(alkyl acrylates) containing multiple-hydrogen bonding functionality is reported. The incorporation of the 2-ureido-4[1H]pyrimidinone (UPy) moiety was targeted due to its previously established utility in the literature as a means of conferring interesting material properties through the self-complimentary dimerization of the UPy units. As per the rest of this thesis, $Cu^{(0)}$-mediated RDRP was chosen as the polymerization technique, with pre- and post-polymerization strategies investigated to furnish the polymers with singular and multiple UPy units using isocyanate chemistry. Several of these materials then underwent rheological testing.

## 4.1 Ureidopyrimidinone Functionalized Polymers – A Brief Review

Over the past decade, the field of supramolecular polymer chemistry has developed rapidly[1, 2] as a multi-disciplinary field bridging the gap between the fields of 'classical' polymer science and supramolecular chemistry[3-6]. The development of these 'supramolecular' materials seeks to combine the classical properties of polymers with highly-directional and dynamic non-covalent secondary interactions, such as hydrogen bonds[7], host-guest interactions[8], Van Der Waals forces[9] and metal coordination sites[10]. These dynamic interactions allow for new properties which can be often reversibly tuned using external stimuli[11-13].

Hydrogen bonds can be described[14] as interactions between two molecules, one of which contains covalent bonds between hydrogen and a electronegative atom (e.g. O-H, N-H), called donors (D) and the other possessing an electronegative atom with lone electron pairs (e.g. O, N, F), called acceptors. The polarization of the X-H bond leads to a highly electropositive hydrogen atom which results in a strong dipole-dipole attraction with the electronegative acceptor atoms (**Figure 4.1**), forming the hydrogen 'bond'.

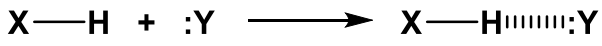


***Figure 4.1*** *Representation of hydrogen bonding, where X-H is the donor and Y the acceptor*

The H-bond prefers to adopt a linear geometry, with the position of the H atom residing along the line which connects the two heteroatoms, which gives rise to its directionality. However, the interaction is generally quite weak, with a binding strength often approximately one-tenth of that of a covalent bond[15].

The concept of supramolecular polymers utilising H-bonding is not new[16, 17], however, since single hydrogen bonding pairs are relatively weak compared to covalent and ionic bonds, there has been a drive to develop moieties containing multiple H-bonded arrays. The power of such groups is perhaps most strikingly demonstrated in nature by the multiple H-bonding units within the Watson-Crick base pairs, whose specific and powerful complementarity allows for the assembly of genetic material[18]. Work by Meijer and co-workers in the late 1990s[19, 20] revealed a new, synthetically-accessible quadrupolar hydrogen bonding motif, 2-ureido-4[1H]pyrimidinone (shortened to UPy, **Figure 4.2**), which subsequently lead to a range of applications and further research which continues today.

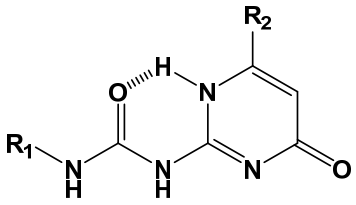


***Figure 4.2*** *Structure of 2-ureido-4[1H]pyrimidinone (UPy)*

The UPy unit contains two H-bond donor and two H-bond acceptor groups in a DDAA configuration, which allows it to dimerize self-complimentarily to another UPy unit, as illustrated in **Figure 4.3**. This dimerization is extremely strong, with a dimerization equilibrium constant ($K_{dim}$) of $6 \times 10^7$ $M^{-1}$ being measured in chloroform[21], the nature of the bonding also means that the dimerization is also

subject to changes in temperature, pH and shear which leads to stimuli-responsive behaviour.

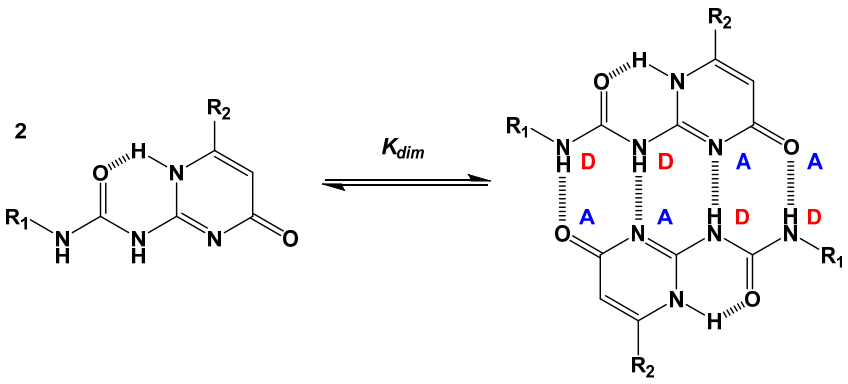


***Figure 4.3*** *Dimerization of two UPy units*

If one takes $R_1$ to be a polymer chain it can be seen how stimuli-responsive high molecular weight materials can be derived through the association of the UPy functionalities. The first example of this was by Meijer[22] who functionalized low molecular weight hydroxyl-telechelic poly(ethylene/butylene) using a UPy-containing isocyanate. In doing so a dramatic change in the physical properties was seen with the starting material changing from a viscous liquid to an elastic solid, with the bulk viscosity being highly temperature dependent (**Figure 4.4**).

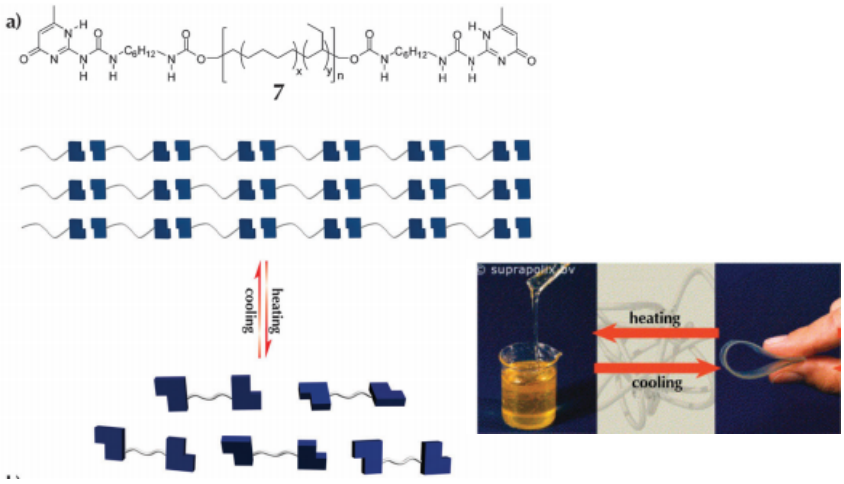


***Figure 4.4*** *Dimerization of telechelic UPy-poly(ethylene/butylene) units, reproduced from references 13 and 20*

The subsequent research into UPy-containing materials has been extensive and such functionalities have been incorporated into a wide range of polymers, including poly(siloxane)[23], poly(ethylene glycol)[24, 25], poly(ethylene glycol-*co*-propylene glycol)[26], poly(styrene)[27], poly(ethylene-*co*-propylene)[28], poly(ester)[29], poly(caprolactone)[30], poly(norbornene)[31] poly(lactide)[32], poly(alkyl (meth)acrylate) and (poly)acrylamide[33-40]. Many of the polymer synthesis techniques available have been utilized, including free-radical, step-growth, ATRP, RAFT, NMP and ROMP.

The telechelic poly(*n*-butyl acrylates) synthesized in Chapter 2, functionalized with polar end groups, were tested using viscometry to examine for any interesting or unique rheological properties – this screening showed that there was no effect of the different end groups on the solution viscosity of the materials tested. As a result of this, the focus of the project changed to the incorporation of UPy functionality into some oil-soluble poly(acrylates), hoping that doing so would confer them with interesting rheological characteristics, stimuli responsiveness, self-healing

properties *etc*. The methods attempted in order to achieve this are now discussed in the remainder of this chapter.

## 4.2 Results and Discussion

### 4.2.1 Incorporation of UPy Groups Using a Functional Monomer

The initial goal of this work was to synthesize lipophilic poly(acrylates) using the $Cu^{(0)}$-mediated RDRP techniques previously developed and to introduce multiple UPy motifs into their structure. The first approach attempted was to introduce UPy by using an acrylic monomer containing the UPy functionality and synthesising co-polymers with a hydrophobic acrylate. Potentially, this would allow for the one-pot synthesis of polymers with several H-bonding units without the need for any post-polymerization modification. The first step towards this was first to identify and synthesize an appropriate UPy containing synthon which can be used as a feedstock for the various reactions to come. 2-(6 Isocyanatohexylaminocarbonylamino)-6-methyl-4(1*H*)-pyrimidinone (which will now be referred to as UPy-hexyl-isocyanate), **Figure 4.5**, was chosen due its popularity in the literature. The isocyanate group is a good synthetic handle which can easily react with alcohols and amines to form the corresponding urethanes and ureas, providing a convenient method of attaching UPy groups to functional polymers. The UPy-hexyl-isocyanate can also be produced on a relatively large scale[41]. Recent studies[35, 42, 43] also showed that the extent of UPy-dimerization was dependent on the length of the aliphatic spacer, with a hexyl linkage being deemed optimal as lower numbers of carbon atoms in the chain resulted in a reduced $K_{dim}$ (up to 1000 times less) due to competitive intramolecular non-covalent interactions.

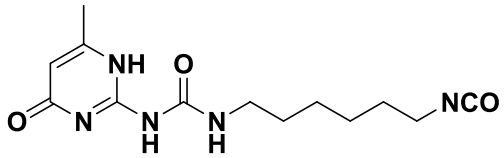


***Figure 4.5*** *UPy-hexyl-isocyanate*

UPy-hexyl-isocyanate was produced by refluxing 2-amino-4-hydroxy-6-methylpyrimidine in excess hexamethylene diisocyanate, which acts as both the solvent and reagent for this reaction (**Figure 4.6**). The large excess of it also ensures that only the monosubstituted adduct is formed. The $^{1}H$ NMR spectrum of the product is shown in **Figure 4.7**.

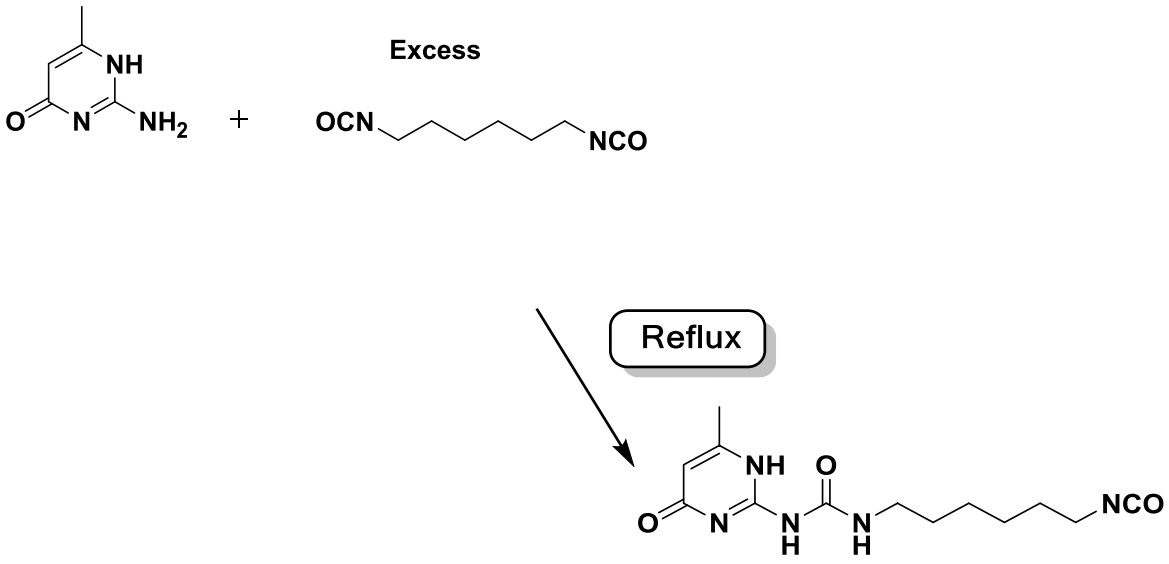


***Figure 4.6*** *Synthesis of UPy-hexyl-isocyanate*

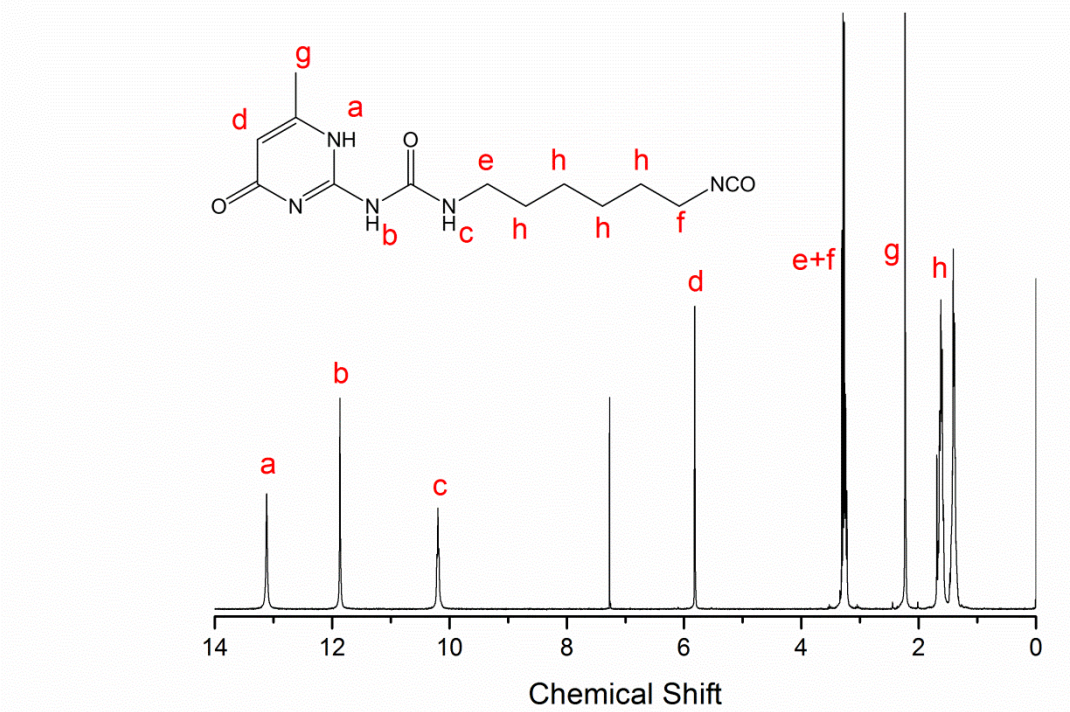


***Figure 4.7*** *$^{1}$H NMR (300 MHz, in $CDCl_3$) spectrum of UPy-hexyl-isocyanate*

Hydroxyethyl acrylate (HEA) provides a means of synthesizing a UPy-functionalized monomer as it contains a hydroxyl group which is capable of undergoing condensation with an isocyanate. Refluxing HEA in chloroform with UPy-hexyl-isocyanate in the presence of catalytic dibutyltin dilaurate (**Figure 4.8**) affords the desired UPy-acrylate in near-quantitative yield, which was then utilized as a co-monomer in the $Cu^{(0)}$-mediated RDRP of *n*-butyl acrylate using the methodology discussed in Chapter 2. Successful synthesis of the desired product was confirmed using $^{1}$H NMR spectroscopy (**Figure 4.9**).

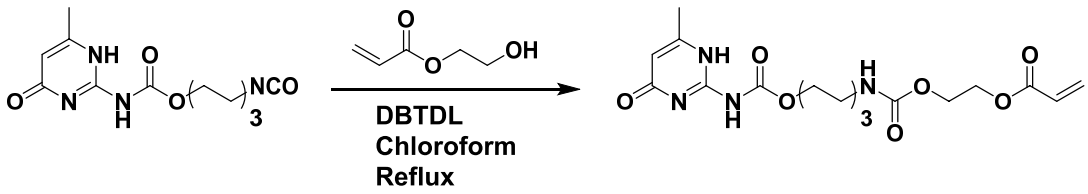


***Figure 4.8*** *Synthesis of UPy-acrylate monomer*

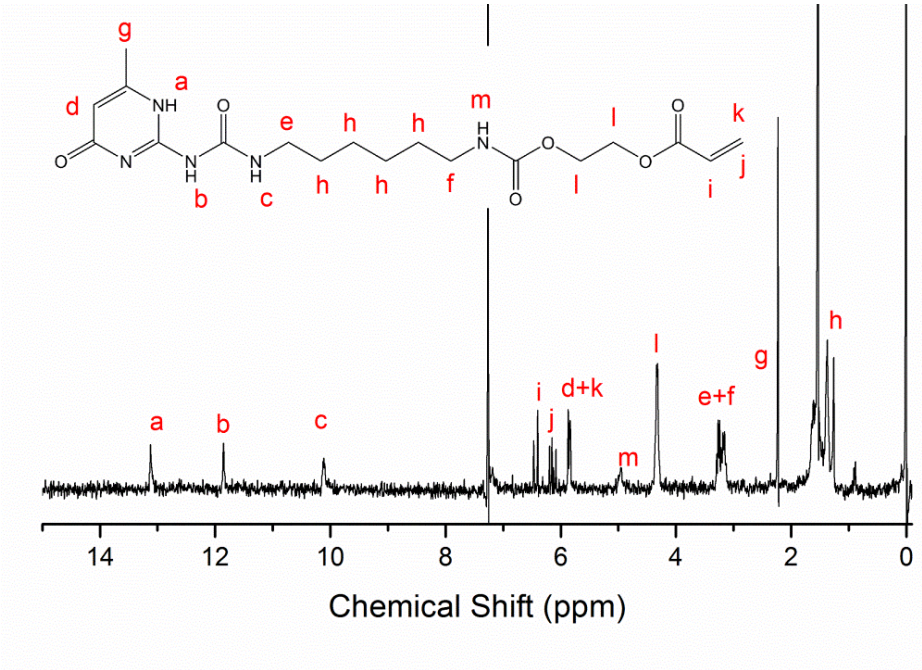


***Figure 4.9*** *$^{1}$H NMR (400 MHz, in $CDCl_3$) spectrum of UPy-acrylate monomer*

A telechelic poly(*n*-BA) was synthesized using the 2F-BiB initiator synthesized in Chapter 2, in DMSO with a target molecular weight of 4 kg mol$^{-1}$ ([-Br]:[$Me_6$TREN]:[$Cu^{(II)}Br_2$] = 1: 0.18: 0.05) and allowed to polymerize until >99% conversion was reached. Upon complete conversion of the *n*-BA, eight equivalents of degassed UPy-acrylate was added to the reaction mixture with the aim being to produce a telechelic n-BA polymer with four UPy functional units at both ends (essentially an A-B-A triblock polymer where A = UPy acrylate and B = *n*-BA, **Figure 4.10**). On being allowed to react overnight a strong thickening of the reaction medium was observed which initially seemed promising as it could be suggestive of a polymer network being formed. However, $^{1}$H NMR spectroscopy showed that the conversion of the UPy-acrylate was only approximately 1% meaning that it has not been incorporated into the poly(*n*-BA) to any great degree. This was the case for several repetitions of the experiment and it seems that when

dissolving the UPy-acrylate, the strong H-bonding between the molecules is enough in itself to increase the viscosity, or that even a small incorporation results in network formation. **Figure 4.10** (inset) shows the reactions mixtures prior and following the attempted chain extension using the UPy-monomer. On the left is the telechelic poly(*n*-BA) at 99%, which is present as a clear layer on top as discussed in Chapters 2 and 3. Upon addition of the UPy-acrylate, the reaction mixture could be turned upside down due to the thickening.

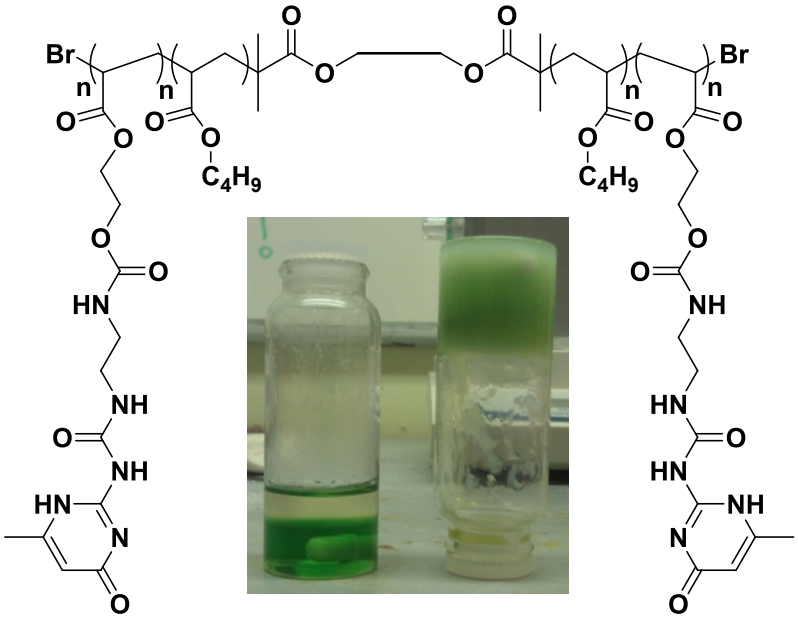


***Figure 4.10*** *Structure of targeted telechelic poly(n-butyl acrylate)-co-(UPy acrylate). Inset shows the reaction mixtures before and after chain extension with UPy-acrylate, left and right vials respectively*

### 4.2.2 Incorporation of Multiple UPy Groups Using Post-Polymerization Modification

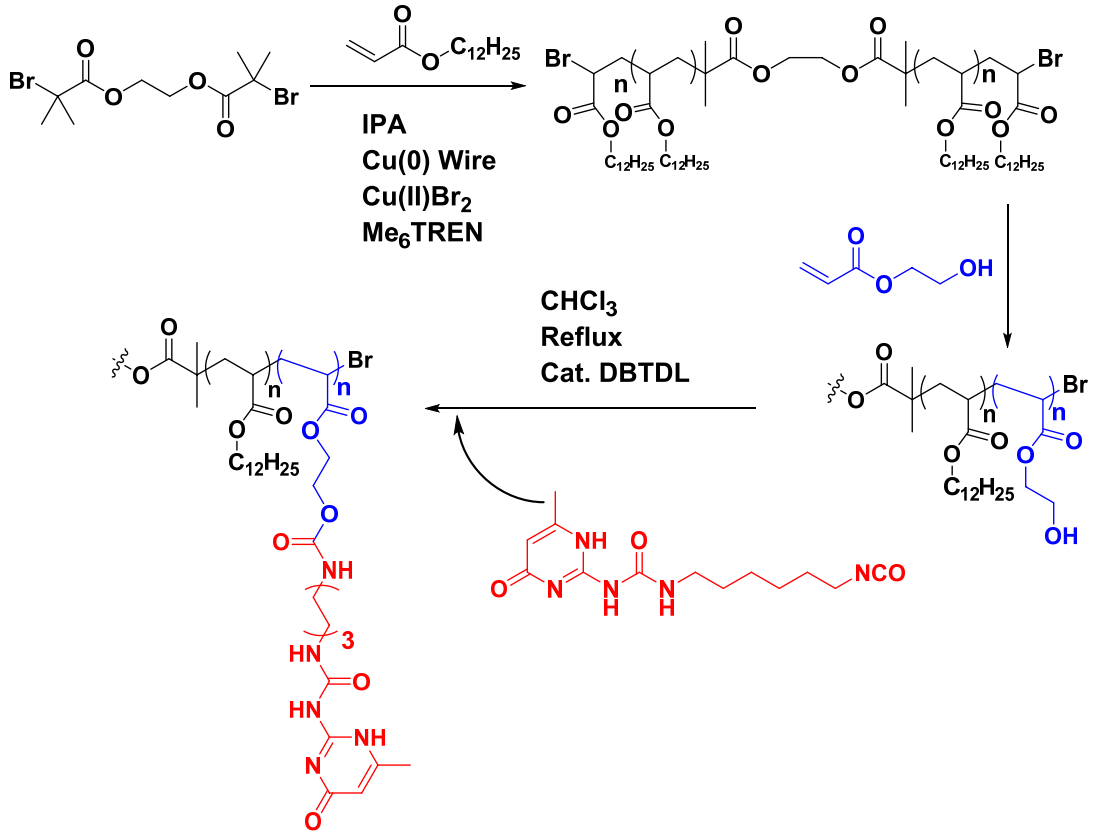


***Figure 4.11*** *Structure of targeted telechelic poly(lauryl acrylate)-co-(UPy acrylate)*

Due to the failure of the above attempts to utilize a UPy-monomer it was decided to adopt a post-polymerization approach to incorporate the H-bonding functionality to the polymers (**Figure 4.11**). Such approaches have been previously reported by Hawker and Meijer using ATRP and RAFT[36, 44] wherein amine and alcoholic co-monomers were employed as a means of reacting with UPy-isocyanates post-polymerization. However, these methods were complicated by the fact that the amine/alcohol groups of the monomers had to be masked using *n*-Boc/silyl protecting groups as it was found that they can have deleterious effect on the polymerization otherwise[45]. This adds several extra synthetic steps which ideally

could be avoided. Inspired by this work, the attempted synthesis of telechelic hydrophobic poly(acrylates) co-polymerized with hydroxyethyl acrylate (HEA) was conducted. In the same manner in which the UPy-monomer was synthesized, the alcohol group on the poly(HEA) can potentially be reacted with UPy-hexy-isocyanate post-polymerization. At this point it was also decided to utilize lauryl, rather than butyl acrylate as this has better oil solubility and is industrially available. In this study a number of products were made and below one such synthesis will be outlined in detail. Initially, telechelic poly(lauryl acrylate) was synthesized via $Cu^{(0)}$-mediated RDRP, again utilising the 2F-BiB bifunctional initiator. The polymerization was conducted in IPA in the presence of $Me_6$TREN ligand, $Cu^{(II)}Br_2$ and $Cu^{(0)}$ wire ([-Br]:[$Me_6$TREN]:[$Cu^{(II)}Br_2$] = 1: 0.18: 0.05), targeting a DP = ten ($M_{n\ (theo)}$ = 2700 g $mol^{-1}$). At approximately 80% conversion, 6 equivalents of degassed HEA monomer were subsequently added to the reaction, which should then form a statistical co-polymer with the remaining lauryl acrylate. This statistical, rather than block *co*-polymer approach was intended to keep termination low and to minimize any repulsive interactions between the UPy groups. As per the previous observations, phase separation of the polymer from the solvent/catalyst was seen throughout the polymerization. Samples of the reaction mixture were taken prior to and after the addition of HEA, with monomer conversions and estimates of the molecular weight, DP and dispersity made using SEC and $^1$H NMR spectroscopy. High monomer conversion was obtained in addition to precise control over the structure of the polymer with an average DP for the initial lauryl acrylate block of 7.55, **Table 4.1**, (*theo*. DP = 8 at 80% conversion) and a final DP of approximately 9.2 (*theo*. DP = 10). A DP of 6 HEA units per chain was targeted, with the analysis showing that this was largely successful with an average of DP 5.1 being measured. The controlled nature of the polymerization is also illustrated by the very low dispersity of 1.07.

| | Target $M_n$ | $M_n$ (SEC) | $M_n$ (NMR) | $Đ_M$ | DP LA | DP HEA | Conv.% |
|---|---|---|---|---|---|---|---|
| **LA Block** | 2800 | 2400 | 2300 | 1.06 | 7.55 | - | 78 |
| **LA+HEA** | 3500 | 3100 | 3000 | 1.07 | 9.21 | 5.1 | >99% |

***Table 4.1*** *Characterization data for the synthesis of poly(lauryl acrylate)-co-(hydroxyethyl acrylate) using $Cu^{(0)}$-mediated RDRP in IPA ([-Br]:[$Me_6$TREN]:[$Cu^{(II)}Br_2$] = 1: 0.18: 0.05)*

The poly(lauryl acrylate)-*co*-(hydroxyethyl acrylate) product was isolated, a process simplified by the phase separation, and volatiles removed under vacuum to remove traces of IPA which would otherwise cause unwanted side reactions in the next step of the synthetic procedure. The polymer was then re-dissolved in chloroform and six equivalents of the previously-synthesized UPy-Isocyanate plus a few drops of dibutyltin dilaurate added and the mixture heated under reflux. The extent of this urethane-forming reaction was monitored using FT-IR spectroscopy due to the characteristic and easily identifiable isocyanate and urethane absorbances in the reactants and product. An FT-IR spectrum of the reaction mixture at T = 0 is given in **Figure 4.12**, which clearly shows the urea, aryl carbonyl and isocyanate functionalities at 1660, 1698 and 2250 $cm^{-1}$ respectively. After three hours the reaction mixture was filtered to remove any undissolved UPy-NCO reactant before silica was added and the reaction left to reflux for a further one hour. This step is to remove any free isocyanate present in the mixture which has not reacted with the polymer, crucial for the subsequent determination of UPy incorporation using $^1H$ NMR spectroscopy. The free isocyanate in solution bonds to the silica which was then simply removed from the reaction mixture via filtration. **Figure 4.13** shows the FT-IR spectrum of the reaction mixture once the silica has been removed, which clearly shows that the characteristic isocyanate peak is no longer present.

Additionally, a peak at 1731 $cm^{-1}$ is now present due to the newly formed urethane bonds.

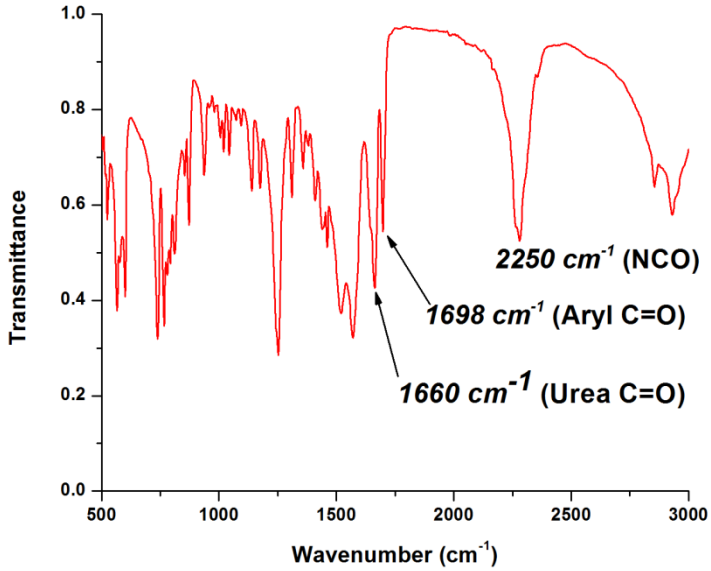


***Figure 4.12*** *FT-IR spectra for the reaction of poly(lauryl acrylate)-co-(hydroxyethyl acrylate) with UPy-Isocyanate at T = 0*

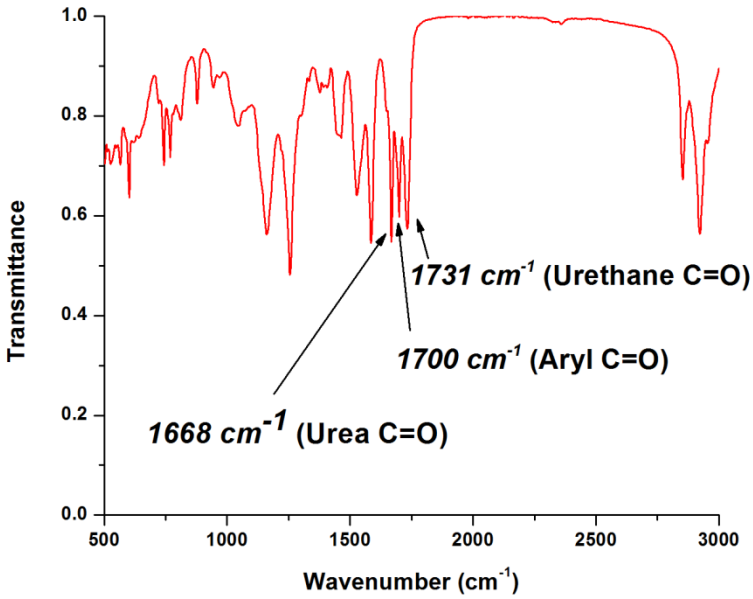


***Figure 4.13*** *FT-IR spectra for the reaction of poly(lauryl acrylate)-co-(hydroxyethyl acrylate) with UPy-Isocyanate after silica reflux*

With the free isocyanate removed from the reaction, the product was isolated by removing the volatiles under vacuum. It was then analysed using $^{1}$H NMR in order to determine the degree of UPy incorporation into the polymer backbone. This was calculated by integrating the twelve methyl protons ($H_a$) of the initiator against the C=C***H*** protons of the UPy groups ($H_b$), **Figure 4.14**.

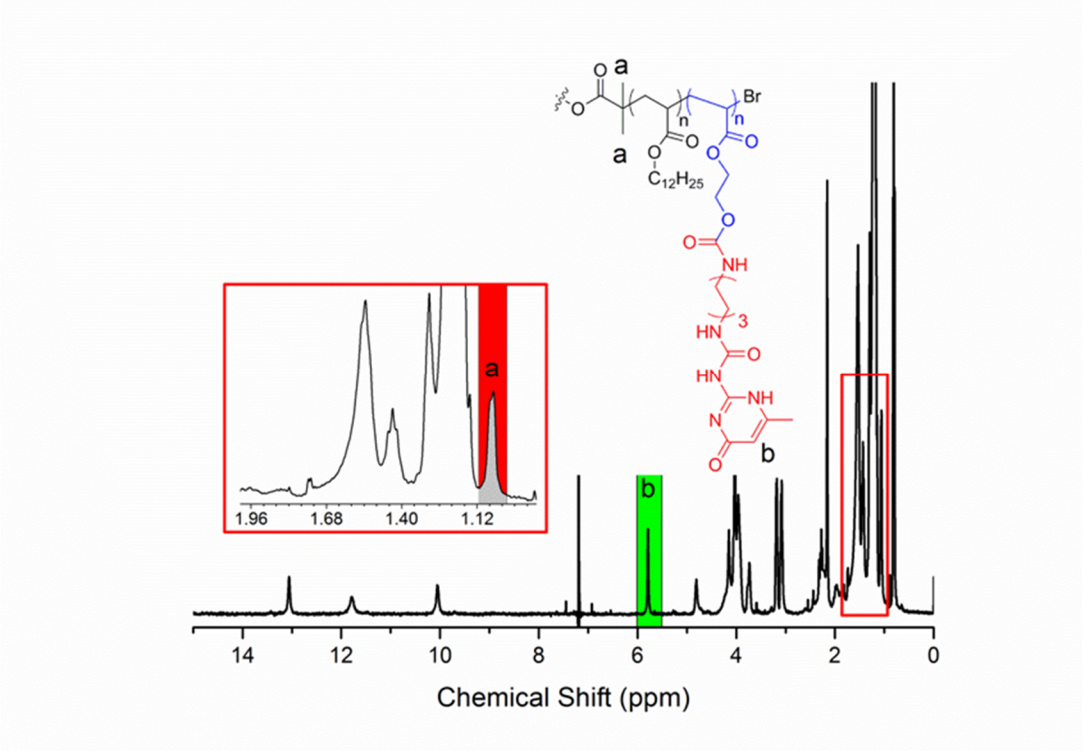


***Figure 4.14*** *$^{1}$H NMR spectra of poly(lauryl acrylate)-co-(UPy acrylate). Inset (red) is an expansion of the 1.1-1.2 ppm region to illustrate the protons, $H_a$ which were integrated relative to the protons $H_b$ (green region)*

In this instance the integral ratio = 3.9, suggesting that there are around 4 UPy units per polymer chain. Given that the previous analysis showed a HEA DP of ~5, it can be inferred that the reaction between the isocyanate and hydroxyl groups is approximately 80% efficient. Despite numerous attempts to improve this, quantitative conversion could not be obtained, which has been attributed to the

poor solubility of UPy-hexy-isocyanate. The appearance of this product, despite the low molecular weight, is of an opaque waxy solid (**Figure 4.15**), compared with the unfunctionalized polymer which is a free-flowing, transparent viscous liquid. This clear change in the physical properties is evidential of the quadrupolar hydrogen bonding units causing the polymer chains to dimerize together, forming a large network. This supramolecular crosslinking is further evidenced by the almost complete insolubility of the product in all solvents tested. (chloroform, DCM, acetone, THF, DMF, toluene, ethyl acetate and hexane)

***Figure 4.15*** *Physical appearance of some of the poly(lauryl acrylate)-co-(UPy acrylate) materials synthesized*

Due to the solubility issues, limited rheological testing could be carried out on the samples made, however they are currently being assessed for their mechanical properties instead.

### 4.2.3 Synthesis and Rheological Testing of Poly(lauryl acrylates) Bearing a Single UPy Moiety

Using the synthetic methods developed in in Section 4.2.2, the scope was then extended to the synthesis of poly(lauryl acrylates) with only contain a single UPy moiety, as it was hoped that these polymers would the retain stimuli-responsive nature of the H-bonding functionality whilst also being soluble in oil. This synthetic scheme, outlined in **Figure 4.16**, involves the polymerization of lauryl acrylate using $Cu^{(0)}$-mediated RDRP from a functional initiator (previously synthesized in the Haddleton group) bearing a terminal hydroxyl group. This end group was then reacted with UPy-Isocyanate in a manner entirely analogous to the procedure used to for the previous functionalization of poly(lauryl acrylate)-*co*-(UPy acrylate).

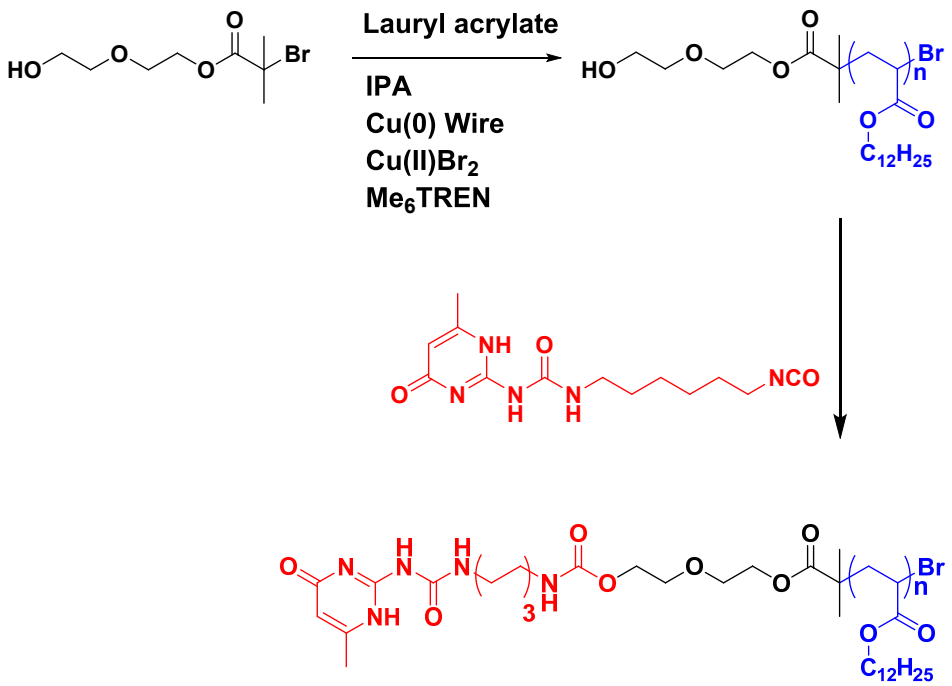


***Figure 4.16*** *Synthetic scheme for the synthesis of poly(lauryl acrylates) functionalized with a single UPy group*

The initial polymerizations were conducted using the standard conditions previously adopted; IPA solvent, $Me_6TREN$ ligand, $Cu^{(II)}Br_2$ and Cu(0) wire ([-Br]:[$Me_6TREN$]:[$Cu^{(II)}Br_2$] = 1: 0.18: 0.05) targeting molecular weights of 5, 10 and 15 kg $mol^{-1}$. In all cases near-quantitative monomer conversions, measured using $^1H$ NMR spectroscopy, were obtained in addition to dispersities of ≤1.15 (**Table 4.2**). The isolated polymers were then reacted with excess UPy-Isocyanate in the presence of DBTDL, following the same procedure and work-up that was utilized in section 4.2.2. $^1H$ NMR spectroscopy was conducted on the final products, with the UPy incorporation being determined by measuring the integral ratios between protons $H_a$ on the initiator against protons $H_b$ and $H_c$ from the hexyl linker on the UPy group. The signals of other protons corresponding to the UPy group were found to be too weak to obtain a satisfactory integral. An example $^1H$ NMR spectra is given in **Figure 4.17** and in this case the functionality was found to be 87%.

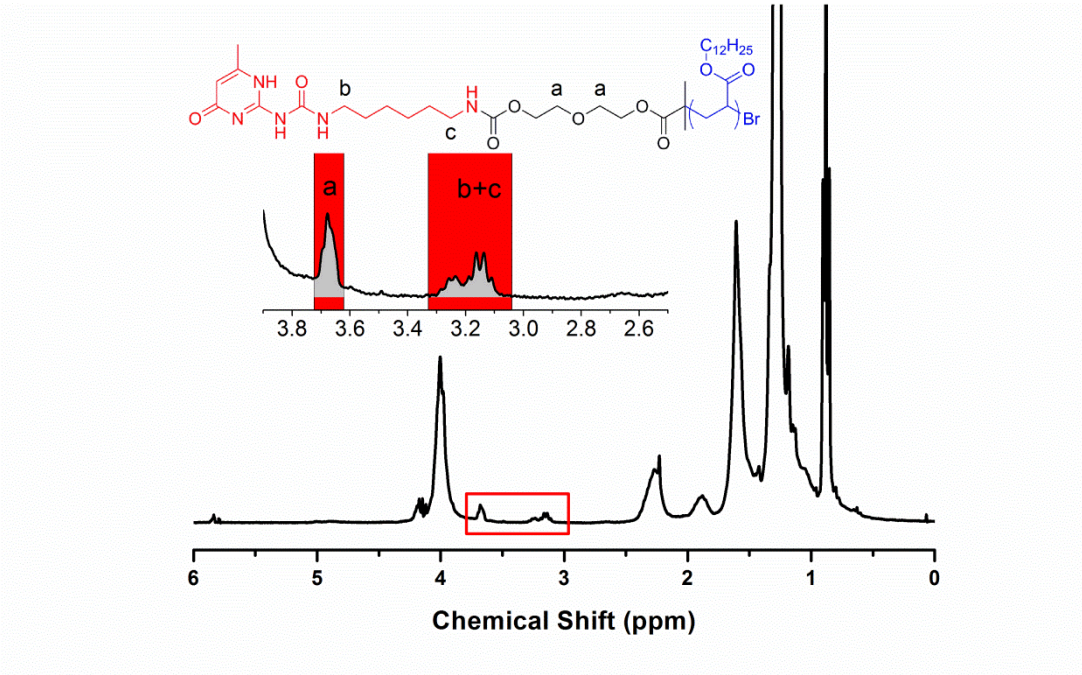


***Figure 4.17*** *$^1H$ NMR spectrum of poly(lauryl acrylate) functionalized with a UPy group. Where the UPy functionality is given by ∫($H_b$+$H_c$)/4 relative to ∫$H_a$*

| Sample | $M_n$ | $M_w$ | $Đ_M$ | Conversion (%) | UPy incorporation (%) |
|---|---|---|---|---|---|
| **CW4.A** | 4000 | 4300 | 1.08 | 96 | 83 |
| **CW4.B** | 7700 | 8700 | 1.13 | 90 | 87 |
| **CW4.C** | 12600 | 14600 | 1.15 | 92 | 80 |

***Table 4.2*** *Characterization data for the synthesis of OH-poly(lauryl acrylate)) using $Cu^{(0)}$-mediated RDRP in IPA ([-Br]:[Me6TREN]:[$Cu^{(II)}$Br2] = 1: 0.18: 0.05) and subsequent urethane formation with UPy-hexyl-isocyanate*

Physically, all of the samples made were present as soft, transparent gels in contrast to the multiple UPy-containing materials synthesized previously (**Figure 4.19**). This suggests that in these cases, a large H-bonded network has not been formed but instead the polymer chains form supramolecular dimers. Additionally it is known from the literature that UPy dimers bearing urethane/urea linkers are also able to form lateral H-bonding interactions[46, 47], which may produce the higher order structures responsible for the gel-like properties (**Figure 4.18**).

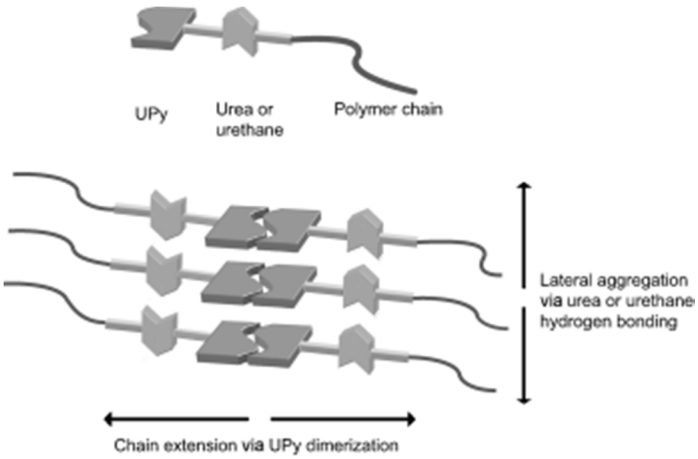


***Figure 4.18*** *Aggregation of UPy-urea/dimers into 1 dimensional stacks, reproduced from reference 47*

Also contrary to the multiple-UPy containing polymers, these monofunctional materials were soluble in a range of common lab solvents and, crucially, in mineral oil which allowed rheological testing to be performed in an environment relevant to the proposed use as an automotive lubricant. Two samples underwent testing at Lubrizol's testing engineers at Hazelwood, UK, the results of which will be discussed next.

***Figure 4.19*** *Representative example of low MW poly(lauryl acrylate) monofunctionalized with a UPy group*

Samples **CW4.A** and **CW4.C** (**Table 4.2**) and controls of poly(lauryl acrylate) of comparable molecular weight but without UPy functionality were blended in a base oil, S20617 at a treat rate of 10% to give optically clear solutions. The samples were loaded into a Discovery HR2 rheometer equipped with 30 mm, 2° steel geometry, before undergoing a conditioning procedure whereby the samples were sheared at a stress of 3 Pa for 30 seconds at 25°C and subsequently left to equilibrate for two minutes. Following this equilibration step, the samples were subjected to two different test regimes; the first involved investigating the effect of temperature on the viscosity of the samples, the second looked at the effect of shear rate on the viscosity. In the first test, the temperature was ramped from 25°C

to 100°C at a rate of 1°C $min^{-1}$ at a constant shear rate of 100 $s^{-1}$ before being ramped down from 100°C to 25°C at the same ramp rate. At all times the viscosity of the samples was recorded. The first blend tested was that containing polymer **CW4.A**, which has a molecular weight of approximately 4 kg $mol^{-1}$. From the viscosity/temperature graph, **Figure 4.20**, it can be seen that the control polymer has a profile parallel to that of the base fluid, showing that the polymer gives a proportional increase/decrease in viscosity across the entire temperature range. For the **CW4.A** blend, the initial viscosity at 25°C is higher than that of the control sample, however they both have the same viscosity at 100°C. This higher initial viscosity is consistent with the H-bond associations expected from the UPy group as any supramolecular polymer chains formed will have a higher molecular weight than the individual chains and the increased temperature dependence seen for the UPy-containing blend may be due to the disruption of such interactions with temperature. Both the control and UPy polymer blends have near-identical viscosities at 100°C, suggesting an absence of H-bonding effects at this temperature and furthermore, when extending the temperature ramp up to 120°C (not shown), the viscosity profiles for both remained flat.

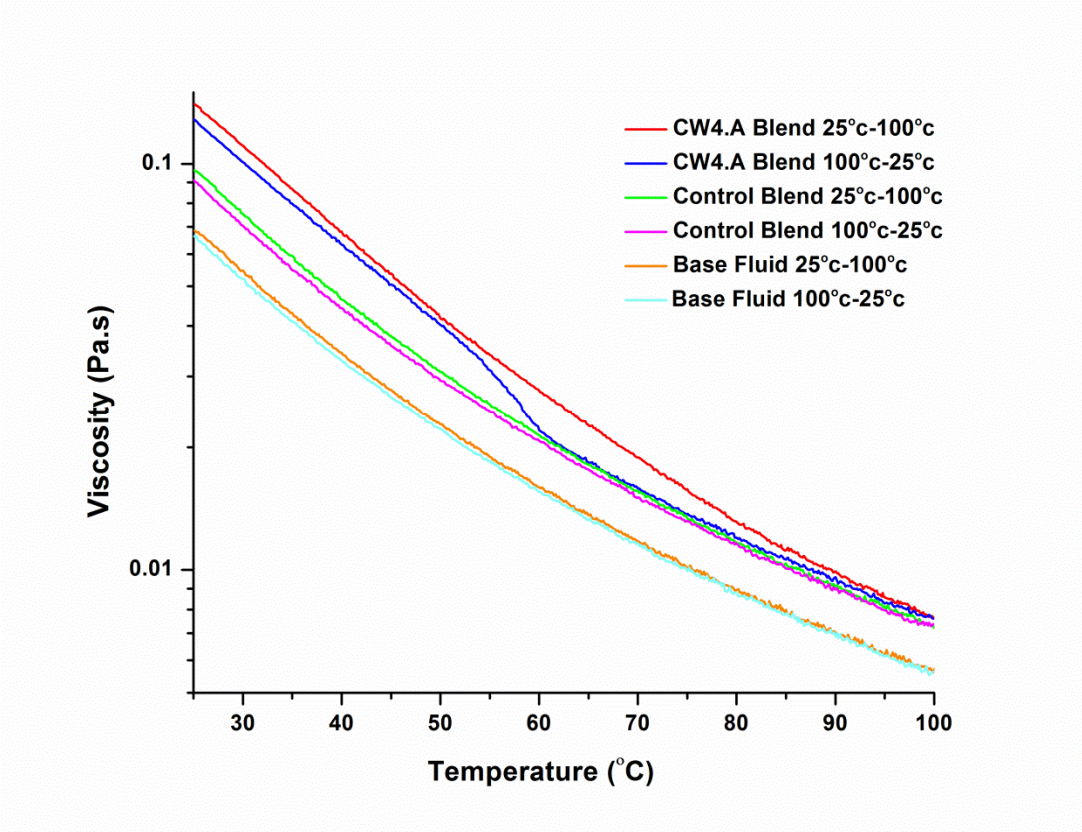


***Figure 4.20*** *Viscosity vs. temperature profiles for blends containing* ***CW4.A****, a control polymer and the base fluid*

With the UPy-containing polymer, the most interesting feature is the that the viscosity profile for the temperature decrease does not match that of the prior increase. Instead, the viscosity remains at the level of the control until a sharp increase occurs at approximately 60°C after which it meets the same viscosity profile as per the temperature increase at 50°C. The viscosity then returns to its initial value. To investigate this further, a plot of specific viscosity ($\eta_{sp}$) vs. temperature was constructed (**Figure 4.21**). The specific viscosity, calculated using **Equation 4.1**, gives a better idea as to the effect of the polymer in the system as it removes the viscosity contributed by the base fluid.

$$\eta_{sp} = \frac{\eta - \eta_0}{\eta_0}$$

***Equation 4.1*** *Equation for the calculation of specific viscosity where, $\eta_o$ is the viscosity of the solvent and $\eta$ is the viscosity of the polymer solution*

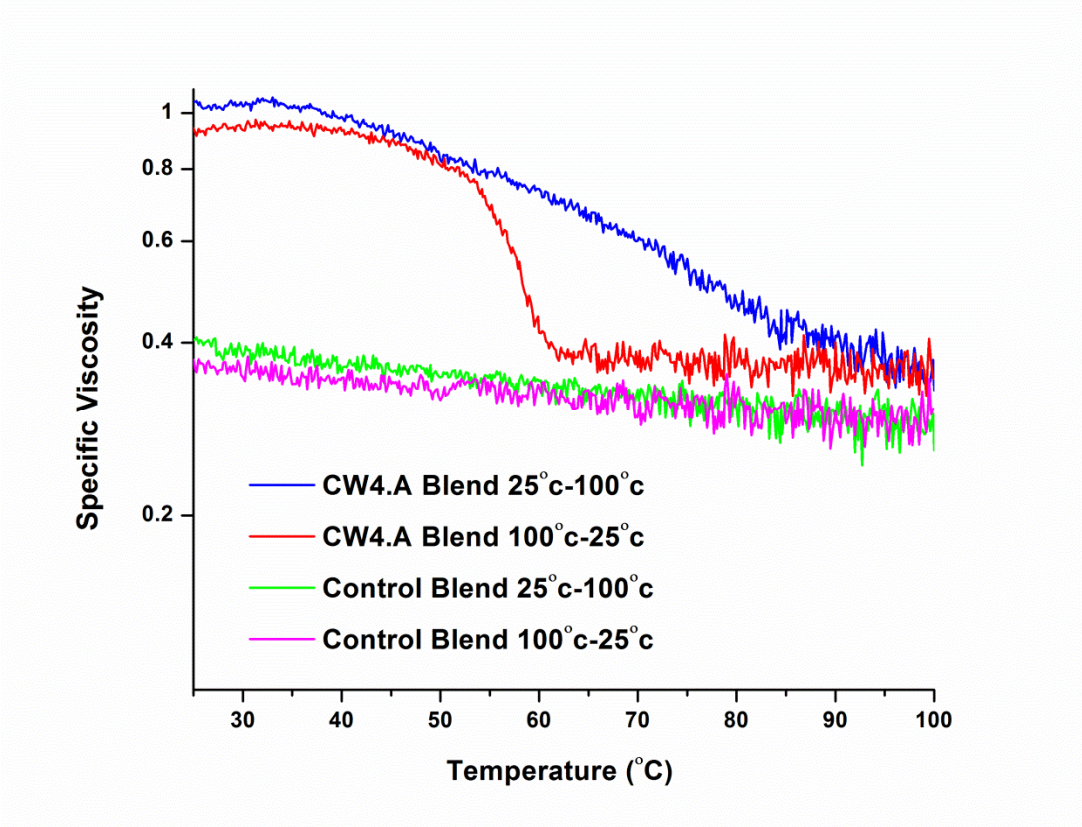


***Figure 4.21*** *Specific viscosity vs. temperature plot for blends* ***CW4.A*** *and the control polymer*

As illustrated in **Figure 4.21**, the control polymer has a practically flat specific viscosity across the whole temperature range, which is typical of the polymers used in the automotive industry as VM's. The UPy-containing polymer shows strong temperature dependence upon heating across the entire range, with a large drop in the specific viscosity which flattens at around 90°C. Upon cooling, the specific

viscosity remains generally flat from 100-60°C whereupon the previously seen sharp transition is observed, only much more apparent in this plot. The specific viscosity suddenly rebounds back to roughly its starting value between 60 and 50°C and then remains flat. Evidently there is thermo-responsive behaviour here, and given that they are the differentiating factor between the two samples, it is reasonable to attribute this to the UPy groups. We propose that this high temperature dependence is due to the dissociation of the UPy groups, the lateral H-bonding interactions, or both.

Previous studies by Long and co-workers[27, 33] demonstrated that poly(alkyl acrylates) containing UPy functionality undergo complete dissociation of the UPy groups upon heating to 80°C in toluene as determined by thermal and rheological tests. Additionally, variable-temperature $^{1}$H NMR studies by Hillmyer[32] also demonstrated that heating UPy-functionalized poly(lactides) to 95°C in toluene results in dissociation of the UPy groups. This was attributed to the tautomerization of 4[1*H*]-pyrimidinone to pyrimidin-4-ol, evidenced by the characteristic UPy N-H resonances becoming broader and shifting upfield as the temperature increased (**Figure 4.22**). Although the pyrimidin-4-ol tautomer can also undergo self-complimentary dimerization, the DADA configuration causes repulsive secondary interactions which lead to a greatly reduced $K_{dim}$ [48], up to 5 orders of magnitude lower[49, 50].

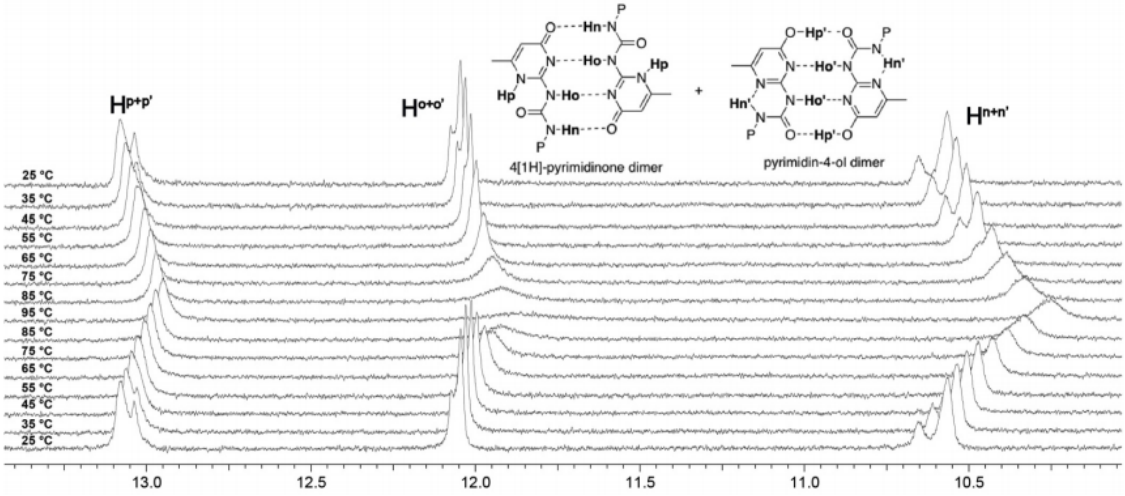


***Figure 4.22*** *Temperature dependent $^{1}H$ NMR experiments for UPy-functionalized poly(lactides), as reported by Hillmyer et. al.*[32]

A sample of **CW4.A** was subjected to analogous variable $^{1}H$ NMR experiments, in an effort to correlate the viscosity/temperature profile with any physical changes observed in the NMR spectra. , The N-H proton resonances 13.2 12.2 and 10.8 ppm all shift upfield and broaden with increasing temperature, in a manner identical to that reported by Hillmeyer and co-workers, **Figure 4.23**.

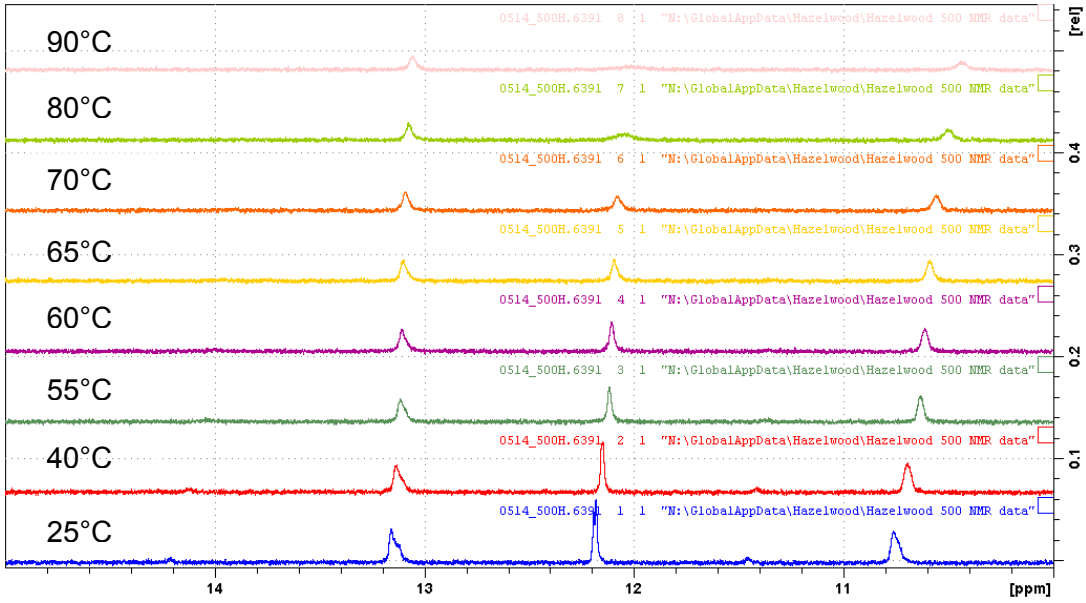


***Figure 4.23*** *Temperature dependent $^{1}H$ NMR experiments in the region 10-15 ppm for* ***CW4.A*** *in deuterated toluene. Temperature was varied between 25 and 90°C*

Based on this data, and that already reported, it is clear that the temperature-dependence of the viscosity profile is due to the gradual dissociation of the UPy groups, with full dissociation being apparent when the temperature reaches ~90°C. We can offer no explanation for the sudden recovery of the viscosity upon cooling, and clearly there is more work to be done regarding this.

Next, the effect of shear rate on the viscosity at a constant temperature was investigated (**Figure 4.24**). For these tests, the temperature was set at 25°C and the shear rate was ramped continuously from 10 $s^{-1}$ to 1000 $s^{-1}$ over 20 minutes, with samples being taken every 10s. The shear rate was then reduced step-wise from 1000 $s^{-1}$ to 10 $s^{-1}$ with 60 sample points being taken at 10 s intervals. This step-wise down ramp was necessary due to issues with the sample being retained within the rheometer geometry. In all of the samples, the viscosity was seen to decrease with increasing shear, however this effect was more pronounced for the blend containing **CW4.A**. This loss of viscosity also appears to be reversible due to

the similar shear rate ramp decrease. As with the temperature studies, this increased shear rate dependence could be due to the disruption of the H-bonding interactions present, however, it may simply be due to the increased effective molecular weight of the H-bonding polymer.

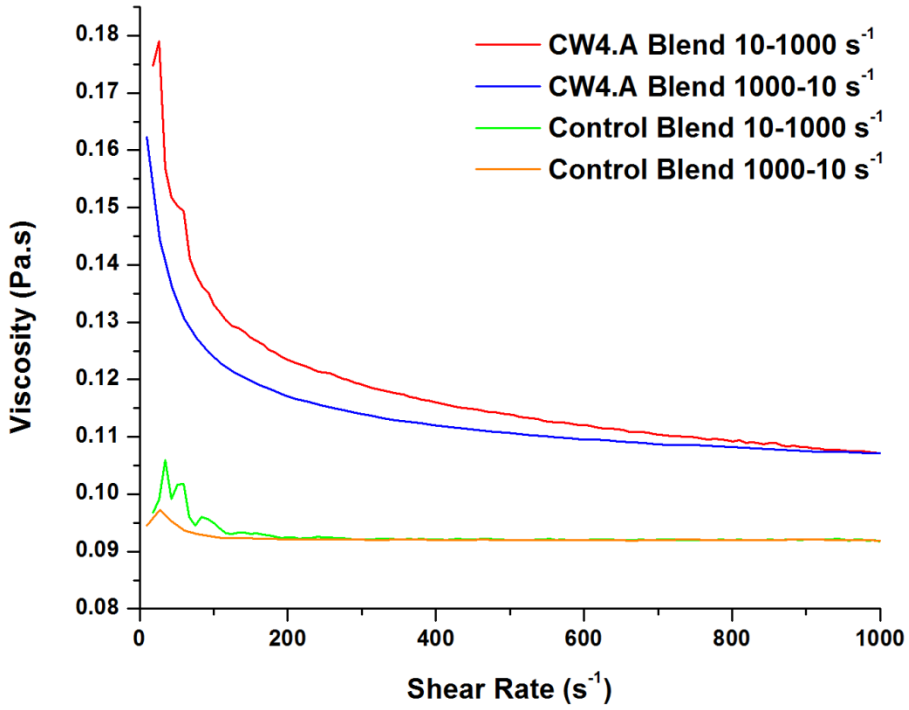


***Figure 4.24*** *Viscosity vs. shear plot for blends CW4.A and the control polymer*

Analogous rheological testing was then performed using the polymer **CW4.C**, which has a molecular weight of approximately 13 kg $mol^{-1}$ and a practically identical UPy incorporation. This was again blended in S20617 mineral oil at a treat rate of 10 wt% and the testing conducted as per the previous sample. Viscosity/temperature, specific viscosity/temperature and viscosity/shear profiles are given in **Figures 4.25**, **4.26** and **4.27**. The temperature/viscosity profiles behave in a similar fashion compared to the low molecular weight blend, with clear temperature-dependant

behaviour seen. In specific viscosity plot, the viscosity reaches its minima at ~65°C as opposed to ~90°C for **CW3.A** and the sharp transition seen upon cooling for the low molecular weight blend is not really seen here as it resembles more of a hysteresis. Furthermore the viscosity does not appear to completely recover which may indicate that either there has not been enough time for any H-bond interactions to re-form or that something is impeding this. This also appears to be the case when examining the shear/viscosity profile.

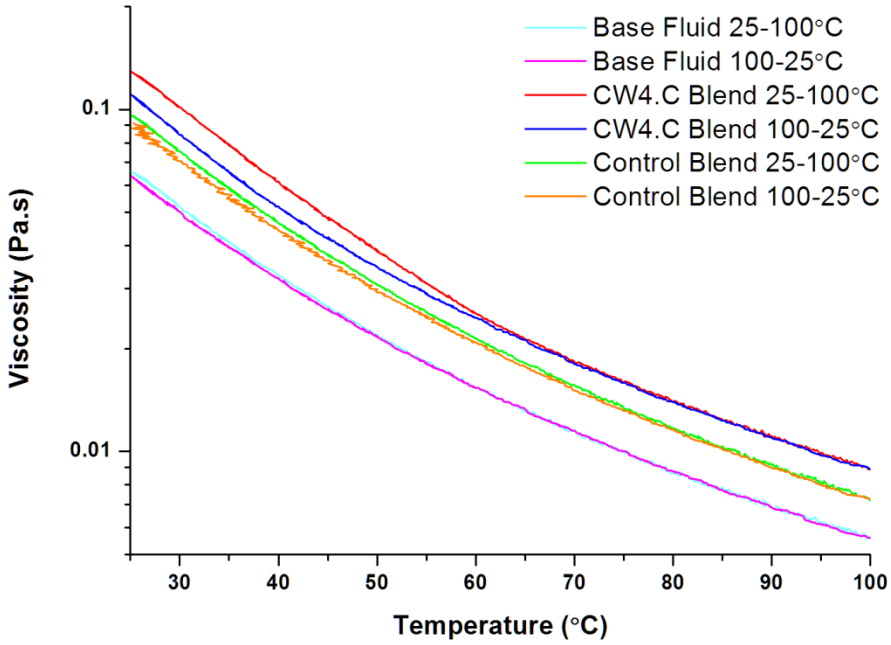


***Figure 4.25*** *Viscosity vs. temperature plot for blends CW4.C and the control polymer*

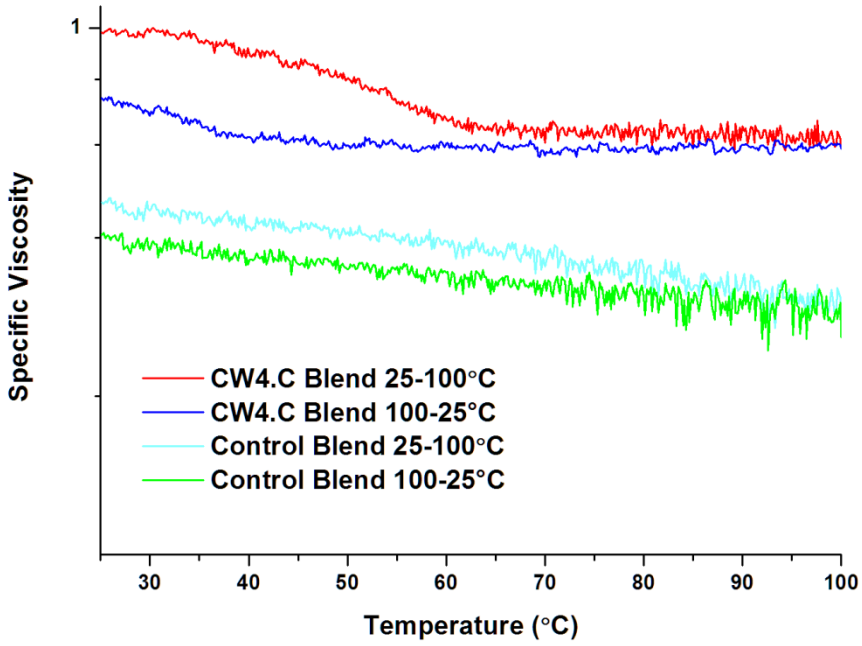


***Figure 4.6*** *Specific viscosity vs. temperature plot for blends CW4.A and the control polymer*

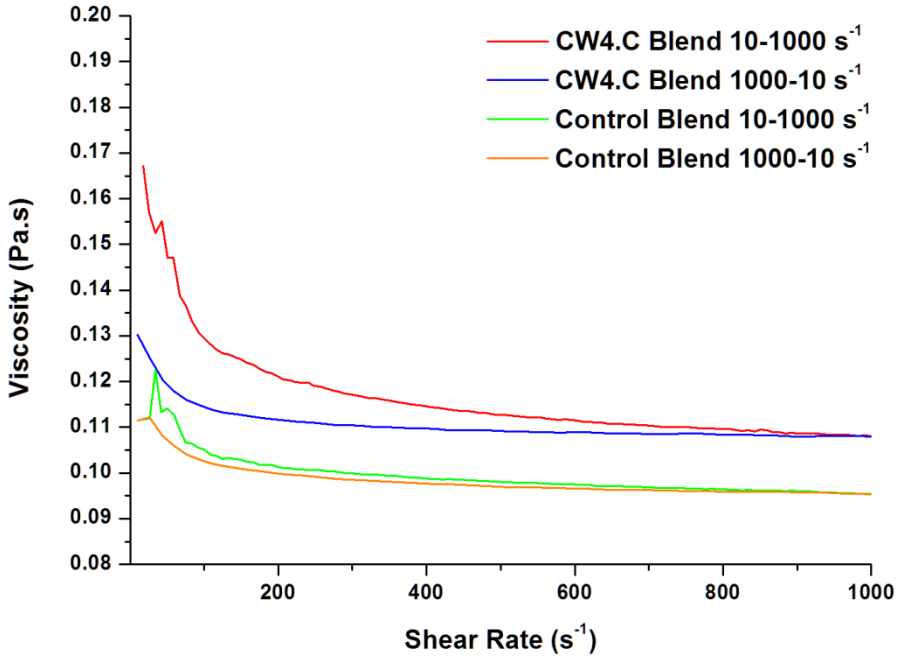


***Figure 4.27*** *Viscosity vs. shear plots for blends CW4.A and the control polymer*

## 4.3 Conclusions

In this chapter, methods to incorporate self-complimentary H-bonding functionality into oil soluble acrylic polymers were explored. This was achieved by combining the popular ureido-pyrimidinone motif with the $Cu^{(0)}$-mediated RDRP techniques discussed earlier in this thesis.

To begin, the incorporation of multiple UPy moieties at the polymerization stage was investigated by the use of a UPy-containing acrylate co-polymerized with butyl acrylate, however, this was unsuccessful due to the poor solubility of the monomer which led to very low conversions. A post-polymerization approach was then successfully attempted by co-polymerizing HEA/lauryl acrylate and then condensing the hydroxyl groups with an isocyanate containing the UPy functionality. This drastically changed the material properties of the starting polymers, changing them from viscous liquids to sticky, solid materials. Their insolubility rendered them unsuitable for rheological testing; however, they are now being assessed for their mechanical properties instead.

Due to the effect of the multiple UPy groups being too strong, the synthesis of monofunctional UPy poly(lauryl acrylates) was then targeted using an initiator bearing the UPy group. A selection of such materials was successfully made which were also found to be completely oil soluble; as such they then underwent rheological testing, which revealed strong shear dependent rheology in addition to thermo-responsive behaviour which could be related to the tautomerization of the UPy groups, evidenced by variable temperature NMR experiments. Further rheological testing was planned however, could not be completed due to time

constraints. Additionally, these samples underwent Small Angle Neutron Scattering (SANS) experiments to get a better understanding of the physical changes to the polymer structure that occur with temperature, which has yet to be carried out on any UPy containing materials in the literature. Unfortunately at the time of writing, this data is still being processed.

## 4.4 Experimental

### 4.4.1 Materials

Tris(2-(dimethylamino)ethyl)amine ($Me_6$TREN) was synthesized as previously described and stored under a nitrogen atmosphere prior to use. Lauryl acrylate (90%), Copper$^{(II)}$ bromide ($CuBr_2$, 98%), 2-amino-4-hydroxy-6-methylpyridine (98%), dibutyltin dilaurate (95%) and hexamethylene diisocyanate (98%) were purchased from Sigma-Aldrich and used as received. 2-(2-hydroxyethoxy)ethyl 2-bromo-2-methylpropanoate was previously synthesized within the group.

### 4.4.2 Analytical Techniques

$^1$H NMR spectra were recorded using a Bruker DPX-400 MHz spectrometer with deuterated chloroform being used as the sample solvent. Variable-temperature $^1$H NMR spectra were acquired on a Bruker AVIII 500 MHz Spectrometer equipped with a 5 mm BBFO probe with deuterated toluene being used as the sample solvent. Chemical shifts are cited as parts per million (ppm) and the following abbreviations are used to abbreviate multiplicities; s = singlet, d = doublet, t = triplet, q = quartet, m = multiplet.

FT-Infrared absorption spectra were recorded on a Bruker VECTOR-22 FTIR spectrometer using a Golden Gate diamond attenuated total reflection cell and the data analysed using the OPUS software.

Size Exclusion Chromatography (SEC) was conducted on an Agilent 390-LC system in $CHCl_3$ at ambient temperature, equipped with refractive index and viscometry detectors, 2 × PLgel 5 µm mixed-D columns (300 × 7.5 mm), 1 × PLgel 5 µm guard column (50 × 7.5 mm) and autosampler. The mobile phase was $CHCl_3$ with 2% triethylamine in order to prevent samples sticking to the columns. A calibration curve was generated with commercial linear poly(methyl methacrylate) standards ranging from 500 to $10^6$ g $mol^{-1}$.

Rheological testing was conducted using a Discovery HR2 rheometer from TA instruments using a 40 mm, 2° steel geometry (Part No. 993464).

### 4.4.3 Synthetic Procedures

#### 4.4.3.1 Synthesis of 2-(6 Isocyanatohexylaminocarbonylamino)-6-methyl-4(1*H*)-pyrimidinone (UPy-hexyl-isocyanate)

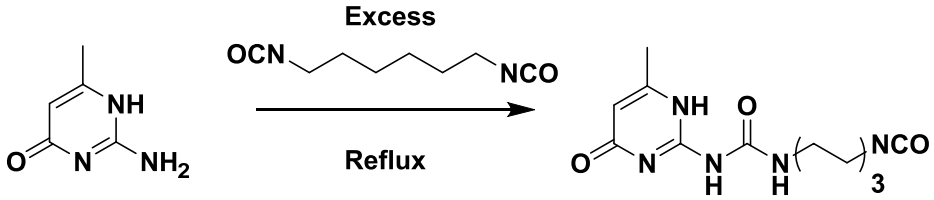


A solution of 2-amino-4-hydroxy-6-methylpyrimidine (10 g; 0.08 mol) in hexamethylene diisocyanate (80 mL; 0.5 mol) was heated under reflux at 100°C for 20 h. Pentane (40 mL) was then added and the resulting precipitate was filtered and washed with cold pentane. The white powder was then dried at 60°C *in vacuo*.

Yield: 18 g, 81%. $^{1}$H NMR (400 MHz, $CDCl_3$): δ 13.12 (s, 1H, $CH_3CN\boldsymbol{H}$), 11.85 (s, 1H,$CH_2NH(C=O)N\boldsymbol{H}$), 10.11 (s, 1H, $CH_2N\boldsymbol{H}(C=O)NH$), 5.83 (s, 1H, $C\boldsymbol{H}=CCH_3$), 3.24 (m, 4H, $NH(C=O)NHC\boldsymbol{H_2}$ + $C\boldsymbol{H_2}NCO$), 2.22 (s, 3H, $C\boldsymbol{H_3}C=CH$), 1.55-1.37 (m, 8H, $CH_2CH_2C\boldsymbol{H_2}CH_2CH_2$).

$^{13}$C NMR (100 MHz, $CDCl_3$): δ 172.82, 156.34, 154.45, 148.10, 121.62, 106.47, 42.68, 39.59, 30.92, 29.11, 26.01, 25.92, 18.74.

FT-IR: v ($cm^{-1}$) 2931, 2856 (NH(C=O)NH), 2281 (NCO), 1698 (aryl C=O), 1660 (urea C=O).

The characterization data is consistent with literature values[22].

### 4.4.3.2 Synthesis of 2-(((6-(3-(6-methyl-4-oxo-1,4-dihydropyrimidin-2-yl)ureido)hexyl)carbamoyl)oxy)ethyl acrylate (UPy Acrylate)

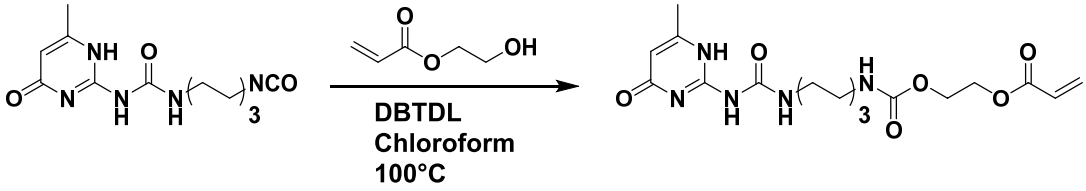


A solution of 2-hydroxyethyl acrylate (HEA, 0.58 g; 5 mmol), UPy-hexyl-isocyanate (1.73 g; 6 mmol) and DBTDL (2 drops) in chloroform (75 mL) was heated at 100°C for 20 h. The mixture was then filtered to remove any solids, returned to the flask and silica (1 g) plus one drop of DBTDL were added before refluxing for a further one hour. The solution was filtered, removing the silica and the volatiles removed *in vacuo* to give the product as a white powder.

Yield: 1.8 g, 88%. $^{1}$H NMR (400 MHz, $CDCl_3$): δ (ppm) 13.12 (s, 1H, $CH_3CN\boldsymbol{H}$), 11.85 (s, 1H, $CH_2NH(C=O)N\boldsymbol{H}$), 10.11 (s, 1H, $CH_2N\boldsymbol{H}(C=O)NH$), 6.40 (m 1H $C\boldsymbol{H}_2$=CH), 6.15 (m 1H $C\boldsymbol{H}_2$=CH), 5.87 (m 1H $CH_2$=C$\boldsymbol{H}$) 5.83 (m, 1H, C$\boldsymbol{H}$=$CCH_3$), 4.94 (s, 1H, N$\boldsymbol{H}$C(C=O), 4.32 (s, 4H, O$C\boldsymbol{H}_2C\boldsymbol{H}_2$O), 3.62 (m, 2H, NH(C=O)NHC$\boldsymbol{H_2}$) 3.15 (m, 2H, C(C=O)NHC$\boldsymbol{H_2}$), 2.23 (s, 3H, $C\boldsymbol{H_3}$C=CH), 1.4-1.20 (m, 8H, $CH_2C\boldsymbol{H_2}CH_2CH_2$).

FT-IR: ν ($cm^{-1}$) 2921, 2854 (NH(C=O)NH), 1731 (urethane C=O), 1700 (aryl C=O), 1668 (urea C=O).

The characterization data is consistent with literature values[51].

#### 4.4.3.3 Synthesis of poly(n-lauryl acrylate)-co-(hydroxyethyl acrylate)

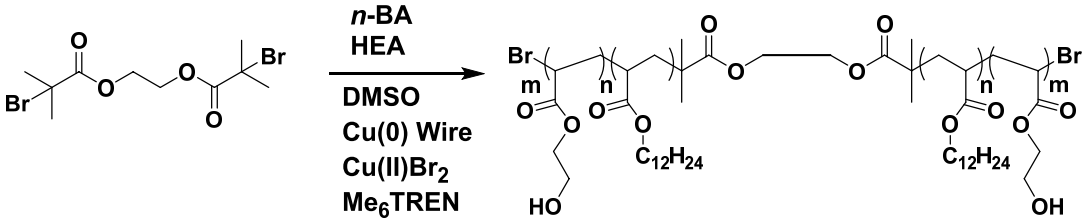


For a target $M_w$ of 5 kg mol$^{-1}$: Lauryl acrylate (LA; 10 mL; 8.84 g; 36 mmol; 10 eq. relative to initiator), IPA (10 mL), $Cu^{II}Br_2$ (80 mg; 0.2 mmol; 0.05 eq.), 2F-BiB (1.29 g; 3.36 mmol; 1 eq.) were charged to a Schlenk tube. Pre-activated Cu(0) wire (10 cm) wrapped around a stirrer bar was then added prior to sealing with a septum. The reaction mixture was degassed by $N_2$ sparging *via* a needle for 15 minutes. $Me_6$TREN (344 µL; 0.64 mmol; 0.18 eq.) was then introduced *via* a degassed, airtight syringe to start the reaction. Samples were taken periodically for SEC and NMR analysis and upon reaching 80% conversion, degassed HEA (3.3 mL; 3.34 g; 28 mmol; 6 eq. relative to initiator) was added using an airtight syringe and the reaction left overnight. The resulting polymer phase was then decanted, dissolved in chloroform and passed through alumina to remove any remaining catalyst before removing the volatiles *in vacuo*.

$^1$H NMR (400 MHz, $CDCl_3$): δ (ppm) 4.23 (s, 2H, (C=O)OC***H***$_2$), 4.04 (s, 2H, OC***H***$_2$$CH_2CH_2$), 3.81 (s, 2H, $CH_2$C***H***$_2$OH), 1.92-2.36 (polymer backbone), 1.62 (s, 4H $OCH_2$(C***H***$_2$)2, 1.27 (m, 18H, $CH_2$(C***H***$_2$)$_8$$CH_3$, 1.15 (s, 12H, C(C***H***$_3$)$_4$, 0.89 (t, 3H, $CH_2(CH_2)_8$C***H***$_3$)

### 4.4.3.4 Typical Procedure For The Synthesis of Poly(lauryl acrylate) Using OH-functional Initiator

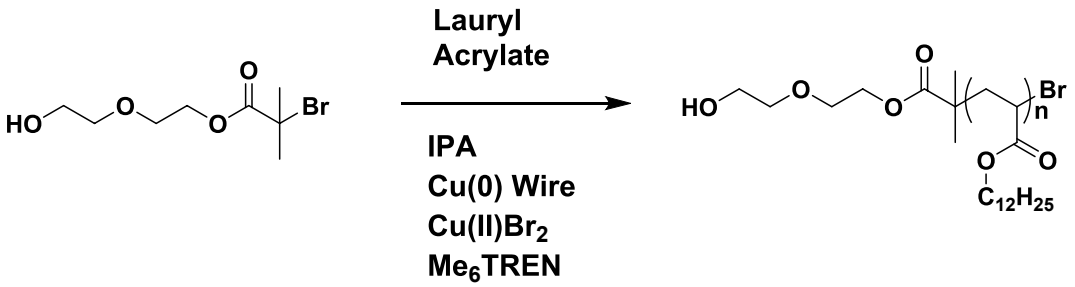


For a target $M_w$ of 5 kg mol$^{-1}$: Lauryl acrylate (LA; 10 mL; 8.84 g; 0.036 mol; 20 eq. relative to initiator), IPA (10 mL), $Cu^{II}Br_2$ (20 mg; 0.1 mmol; 0.05 eq.), 2-(2-hydroxyethoxy)ethyl 2-bromo-2-methylpropanoate (0.46 g; 1.18 mmol; 1 eq.) were charged to a Schlenk tube. Pre-activated Cu(0) wire (10 cm) wrapped around a stirrer bar was then added prior to sealing with a septum. The reaction mixture was degassed by $N_2$ sparging *via* a needle for 15 minutes. $Me_6$TREN (86 µL; 0.32 mmol; 0.18 eq.) was then introduced *via* a degassed, airtight syringe to start the reaction, which was allowed to proceed overnight at ambient temperature. Samples were taken periodically for SEC and NMR analysis. NMR samples were diluted with $CDCl_3$ while SEC samples were diluted with chloroform and passed through a short alumina column to remove copper salts.

$^1$H NMR (400 MHz, $CDCl_3$): δ 4.22 (ppm) (s, 2H, (C=O)OC***H***$_2$), 4.02 (s, 2H, OC***H***$_2$CH$_2$CH$_2$), 3.70 (s, 2H, C***H***$_2$OH), 3.61 (s, 4H, C***H***$_2$OC***H***2), 1.92-2.36 (polymer backbone), 1.62 (s, 4H OCH$_2$(C***H***$_2$)$_2$, 1.27 (m, 18H, CH$_2$(C***H***$_2$)$_8$CH$_3$, 1.17 (s, 12H, C(C***H***$_3$)$_4$, 0.9 (t, 3H, CH$_2$(CH$_2$)$_8$C***H***$_3$)

#### 4.4.3.5 Typical Procedure for the Post-Polymerization of Poly(lauryl acrylates) Using an –OH Functional Initiator

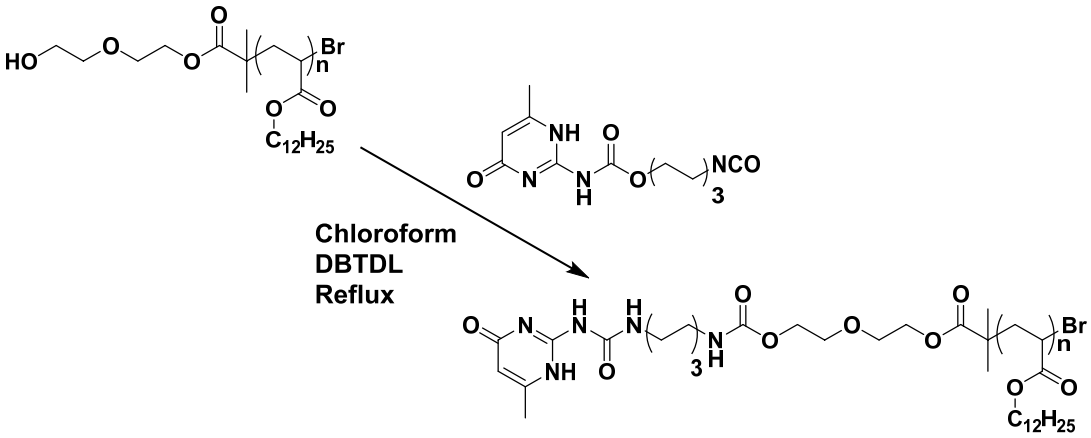


Poly(lauryl acrylate) (5 g), synthesized as per procedure 4.4.3.3 was added to a 500 mL round-bottom flask and dissolved in chloroform (250 mL). UPy-hexy-isocyanate was then added (2 eq) and the solution heated under reflux in the presence of three drops of DBTDL for 20 hours. The mixture was then filtered, returned to the flask and silica (2 g) plus one drop of DBTDL were added before refluxing for a further one hour. The solution was filtered to remove the silica and the chloroform removed under vacuum to yield the product, which was a sticky gel-like solid.

$^1$H NMR (400 MHz, $CDCl_3$): δ (ppm) 13.12 (s, 1H, $CH_3CN\boldsymbol{H}$), 11.85 (s, 1H, $CH_2NH(C=O)N\boldsymbol{H}$), 10.11 (s, 1H, $CH_2N\boldsymbol{H}(C=O)NH$), 6.40 (m 1H $C\boldsymbol{H}_2$=CH), 6.15 (m 1H $C\boldsymbol{H}_2$=CH), 5.87 (m 1H $CH_2$=$C\boldsymbol{H}$), 5.83 (m, 1H, $C\boldsymbol{H}$=$CCH_3$), 4.94 (s, 1H, $N\boldsymbol{H}C(C=O)$, 4.22 (s, 2H, $(C=O)OC\boldsymbol{H}_2$), 3.70 (s, 2H, $C\boldsymbol{H}_2OH$), 3.63 (s, 4H, $C\boldsymbol{H}_2OC\boldsymbol{H}$2), 3.1-3.3 (m, 4H, $NH(C=O)NHC\boldsymbol{H}_2$ + $C\boldsymbol{H}_2NH(C=O)O$) 1.9-2.4 (polymer backbone), 1.62 (s, 4H $OCH_2(C\boldsymbol{H}_2)_2$, 1.55-1.4 (m, 8H, $CH_2CH_2C\boldsymbol{H}_2CH_2CH_2$), 1.27 (m, 18H, $CH_2(C\boldsymbol{H}_2)_8CH_3$), 0.9 (t, 3H, $CH_2(CH_2)_8C\boldsymbol{H}_3$)

## 4.5 References


1. T. Aida, E. W. Meijer and S. I. Stupp, *Science*, 2012, 335, 813-817.
2. A. Bertrand, F. Lortie and J. Bernard, *Macromol. Rapid Commun.*, 2012, 33, 2062-2091.
3. D. J. Cram and J. M. Cram, *Science*, 1974, 183, 803-809.
4. C. J. Pedersen, *J. Am. Chem. Soc.*, 1967, 89, 7017-7036.
5. C. J. Pedersen, *Angew. Chem., Int. Ed.*, 1988, 27, 1021-1027.
6. J.-M. Lehn, *Makromol. Chem-M. Symp.*, 1993, 69, 1-17.
7. G. Armstrong and M. Buggy, *J. Mater. Sci.*, 2005, 40, 547-559.
8. H. Yang, B. Yuan, X. Zhang and O. A. Scherman, *Acc. Chem. Res.*, 2014, 47, 2106-2115.
9. Z. Zhang, G. Yu, C. Han, J. Liu, X. Ding, Y. Yu and F. Huang, *Org. Lett.*, 2011, 13, 4818-4821.
10. J. B. Beck and S. J. Rowan, *J. Am. Chem. Soc.*, 2003, 125, 13922-13923.
11. L. Brunsveld, B. J. B. Folmer, E. W. Meijer and R. P. Sijbesma, *Chem. Revs.*, 2001, 101, 4071-4098.
12. T. F. A. De Greef, M. M. J. Smulders, M. Wolffs, A. P. H. J. Schenning, R. P. Sijbesma and E. W. Meijer, *Chem. Revs.*, 2009, 109, 5687-5754.
13. X. Yan, F. Wang, B. Zheng and F. Huang, *Chem. Soc. Rev.*, 2012, 41, 6042-6065.
14. E. Arunan, R. Desiraju Gautam, A. Klein Roger, J. Sadlej, S. Scheiner, I. Alkorta, C. Clary David, H. Crabtree Robert, J. Dannenberg Joseph, P. Hobza, G. Kjaergaard Henrik, C. Legon Anthony, B. Mennucci and J. Nesbitt David, in *Pure Appl. Chem.*, 2011, vol. 83, p. 1619.
15. G. A. Jeffrey and G. A. Jeffrey, *An Introduction to Hydrogen Bonding*, Oxford university press New York, 1997.

16. L. L. De Lucca Freitas and R. Stadler, *Macromolecules*, 1987, 20, 2478-2485.

17. C. Hilger, M. Draeger and R. Stadler, *Macromolecules*, 1992, 25, 2498-2501.

18. J. D. Watson and F. H. C. Crick, *Nature*, 1953, 171, 737-738.

19. R. P. Sijbesma, F. H. Beijer, L. Brunsveld, B. J. B. Folmer, J. H. K. K. Hirschberg, R. F. M. Lange, J. K. L. Lowe and E. W. Meijer, *Science*, 1997, 278, 1601-1604.

20. F. H. Beijer, R. P. Sijbesma, H. Kooijman, A. L. Spek and E. W. Meijer, *J. Am. Chem. Soc.*, 1998, 120, 6761-6769.

21. S. H. M. Söntjens, R. P. Sijbesma, M. H. P. van Genderen and E. W. Meijer, *J. Am. Chem. Soc.*, 2000, 122, 7487-7493.

22. B. J. B. Folmer, R. P. Sijbesma, R. M. Versteegen, J. A. J. Van Der Rijt and E. W. Meijer, *Adv. Mater.*, 2000, 12, 874-878.

23. J. H. K. K. Hirschberg, F. H. Beijer, H. A. van Aert, P. C. M. M. Magusin, R. P. Sijbesma and E. W. Meijer, *Macromolecules*, 1999, 32, 2696-2705.

24. R. E. Kieltyka, A. C. H. Pape, L. Albertazzi, Y. Nakano, M. M. C. Bastings, I. K. Voets, P. Y. W. Dankers and E. W. Meijer, *J. Am. Chem. Soc.*, 2013, 135, 11159-11164.

25. T. Terashima, T. Mes, T. F. A. De Greef, M. A. J. Gillissen, P. Besenius, A. R. A. Palmans and E. W. Meijer, *J. Am. Chem. Soc.*, 2011, 133, 4742-4745.

26. R. F. M. Lange, M. Van Gurp and E. W. Meijer, *J. Polym. Sci., A Polym. Chem.*, 1999, 37, 3657-3670.

27. K. Yamauchi, J. R. Lizotte, D. M. Hercules, M. J. Vergne and T. E. Long, *J. Am. Chem. Soc.*, 2002, 124, 8599-8604.

28. C. L. Elkins, K. Viswanathan and T. E. Long, *Macromolecules*, 2006, 39, 3132-3139.

29. K. Yamauchi, A. Kanomata, T. Inoue and T. E. Long, *Macromolecules*, 2004, 37, 3519-3522.

30. H. Hofmeier, R. Hoogenboom, M. E. Wouters and U. S. Schubert, *J. Am. Chem. Soc.*, 2005, 127, 2913-2921.

31. E. J. Foster, E. B. Berda and E. W. Meijer, *J. Am. Chem. Soc.*, 2009, 131, 6964-6966.

32. P. A. Delgado and M. A. Hillmyer, *RSC Advances*, 2014, 4, 13266-13273.

33. K. Yamauchi, J. R. Lizotte and T. E. Long, *Macromolecules*, 2003, 36, 1083-1088.

34. M. G. McKee, C. L. Elkins and T. E. Long, *Polymer*, 2004, 45, 8705-8715.

35. T. F. A. De Greef, M. J. Kade, K. E. Feldman, E. J. Kramer, C. J. Hawker and E. W. Meijer, *J. Polym. Sci., A Polym. Chem.*, 2011, 49, 4253-4260.

36. K. E. Feldman, M. J. Kade, E. W. Meijer, C. J. Hawker and E. J. Kramer, *Macromolecules*, 2009, 42, 9072-9081.

37. M. H. Wrue, A. C. McUmber and M. Anthamatten, *Macromolecules*, 2009, 42, 9255-9262.

38. A. D. Celiz and O. A. Scherman, *J. Polym. Sci., A Polym. Chem.*, 2010, 48, 5833-5841.

39. C. L. Lewis and M. Anthamatten, *Soft Matter*, 2013, 9, 4058-4066.

40. E. B. Berda, E. J. Foster and E. W. Meijer, *Macromolecules*, 2010, 43, 1430-1437.

41. H. M. Keizer, R. van Kessel, R. P. Sijbesma and E. W. Meijer, *Polymer*, 2003, 44, 5505-5511.

42. T. F. A. de Greef, M. M. L. Nieuwenhuizen, R. P. Sijbesma and E. W. Meijer, *J. Org. Chem.*, 2010, 75, 598-610.

43. T. F. A. de Greef, M. M. L. Nieuwenhuizen, P. J. M. Stals, C. F. C. Fitie, A. R. A. Palmans, R. P. Sijbesma and E. W. Meijer, *Chem. Commun.*, 2008, 4306-4308.

44. P. J. M. Stals, M. A. J. Gillissen, R. Nicolay, A. R. A. Palmans and E. W. Meijer, *Polym. Chem.*, 2013, 4, 2584-2597.

45. P. J. M. Stals, T. N. T. Phan, D. Gigmes, T. F. E. Paffen, E. W. Meijer and A. R. A. Palmans, *J. Polym. Sci., A Polym. Chem.*, 2012, 50, 780-791.

46. H. Kautz, D. J. M. van Beek, R. P. Sijbesma and E. W. Meijer, *Macromolecules*, 2006, 39, 4265-4267.

47. M. M. L. Nieuwenhuizen, T. F. A. de Greef, R. L. J. van der Bruggen, J. M. J. Paulusse, W. P. J. Appel, M. M. J. Smulders, R. P. Sijbesma and E. W. Meijer, *Chem. Eur. J.*, 2010, 16, 1601-1612.

48. A.-M. Alexander, M. Bria, G. Brunklaus, S. Caldwell, G. Cooke, J. F. Garety, S. G. Hewage, Y. Hocquel, N. McDonald, G. Rabani, G. Rosair, B. O. Smith, H. W. Spiess, V. M. Rotello and P. Woisel, *Chem. Commun.*, 2007, 2246-2248.

49. R. P. Sijbesma and E. W. Meijer, *Chem. Commun.*, 2003, 5-16.

50. J. Sartorius and H.-J. Schneider, *Chem. Eur. J.*, 1996, 2, 1446-1452.

51. Y. Chen, N. Ballard, F. Gayet and S. A. F. Bon, *Chem. Commun.*, 2012, 48, 1117-1119.

# Chapter 5: Grafting of Poly(NiPAM) Brushes from Poly(sulfone) Ultrafiltration Membranes Using Aqueous $Cu^{(0)}$-Mediated RDRP

This final chapter explored the possibility of conducting surface initiated polymerization from poly(sulfone) desalination membranes provided by our collaborators at the King Abdullah University of Science and Technology, Saudi Arabia. The aqueous $Cu^{(0)}$-mediated polymerization technique recently developed by the Haddleton group was utilized in order to attempt to graft poly(NiPAM) brushes from the membranes, with the ultimate goal of changing their surface properties. Due to the nature of these reactions, the characterization techniques used earlier in the thesis (NMR, SEC, MS) were generally unsuitable for these materials, hence a range of surface characterization techniques were employed, including FT-IR, XPS and SEM.

## 5.1 Introduction

Poly(sulfone) has wide use as a material in the field of membrane separation technology with applications including filters for water desalination, kidney dialysis and gas separation[1-4]. Poly(sulfone) (**Figure 5.1**) is well suited for these purposes due to several desirable properties; their ability to easily form membranes[5], mechanical strength, chemical and oxidative inertness, hydrolytic resistance and thermal stability[6]. However, their principle drawback when used in aqueous media is their inherent hydrophobic nature[7, 8] which causes fouling (the surface adsorption of proteins and other solutes), leading to loss of performance. Due to this efforts have been made[5] to develop strategies for the introduction of hydrophilic functionality into the poly(sulfone), either by incorporation of such functionality into the backbone[9-12] during polymerization or by post-polymerization modification of the membranes themselves[7, 13-15].

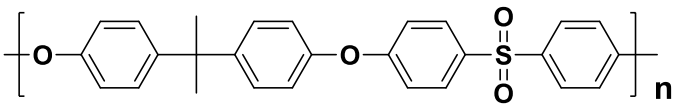


***Figure 5.1*** *The structure of poly(sulfone)*

In a recent publication[16] the Nunes group at KAUST reported the hydrophilic modification of commercial poly(sulfone) using the azide-alkyne click methodology popularized by Sharpless *et. al.*[17] They were able to introduce OH-functional triazaoles onto the poly(sulfone) before preparing it into ultrafiltration membranes. This functionalization procedure was carried out in three steps, **Figure 5.2**. The first was chloromethylation using the method described by Avram *et. al.*[18] followed by

azidification and finally copper-catalysed azide-alkyne Huisgen cycloaddition (also known as azide-alkyne 'click' or CuAAc) with propargyl alcohol.

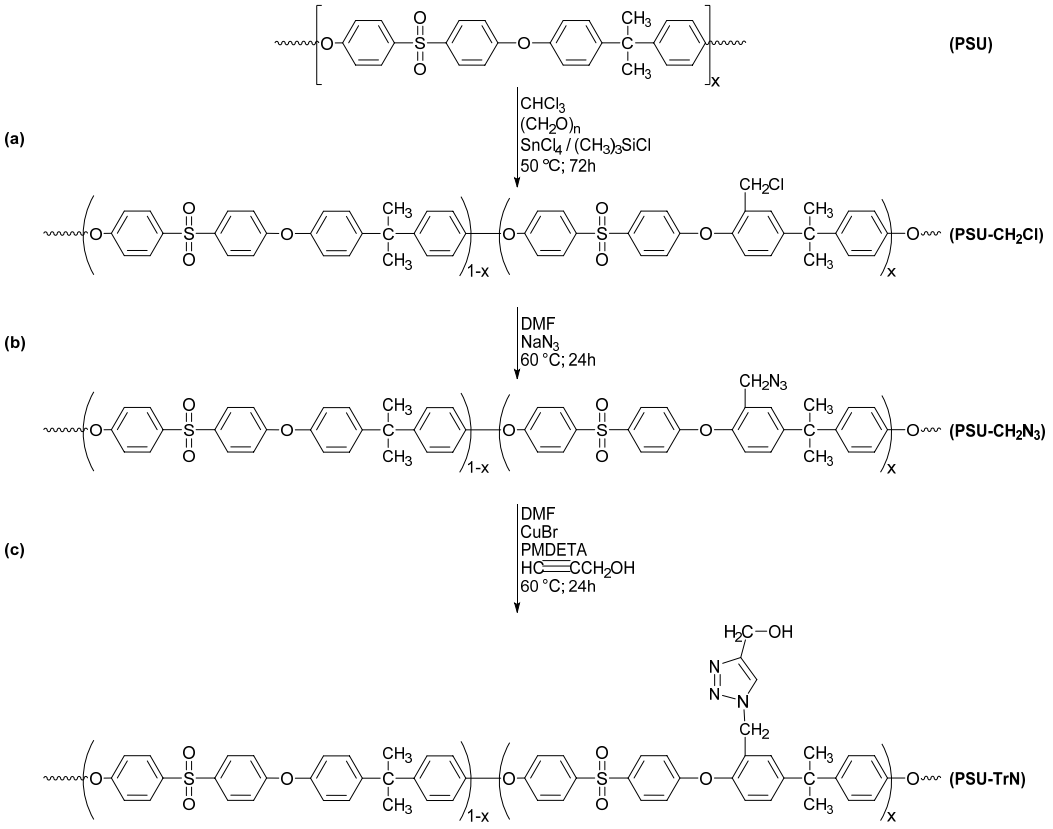


***Figure 5.2*** *Procedure for the –OH functionalization of poly(sulfone)*

Upon functionalization with –OH groups, the poly(sulfone) was then cast into porous membranes using non-solvent induced phase separation (NIPS) methodology[19, 20]. Testing on these new membranes showed that they exhibited up to a 23-fold increase in water permeability in addition to reduced susceptibility to fouling. Due to these promising results it was desired that the hydrophilicity of the membranes be increased even further and one potential method of doing this is to graft water-soluble polymer brushes to the surface. Based on the recent work[21-25]

on aqueous SET-LRP/$Cu^{(0)}$-mediated RDRP in the Haddleton group, a collaboration was initiated in order to investigate this.

This method (**Figure 5.3**) involves the in situ disproportionation of [$Cu^{I}$($Me_6$-TREN)Br] in water to form highly active $Cu^{(0)}$ and [$Cu^{II}$($Me_6$-Tren)$Br_2$], prior to addition of the initiator and monomer. This prior disproportionation step is the key feature of this protocol as it exploits the inherent thermodynamic instability of $Cu^{I}$ complexes in water which results in quantitative disproportionation to ensure that the reaction proceeds via the SET-LRP mechanism. The extent of disproportionation was determined by UV-VIS spectroscopy which showed that no detectable quantities of $Cu^{I}$ were present.

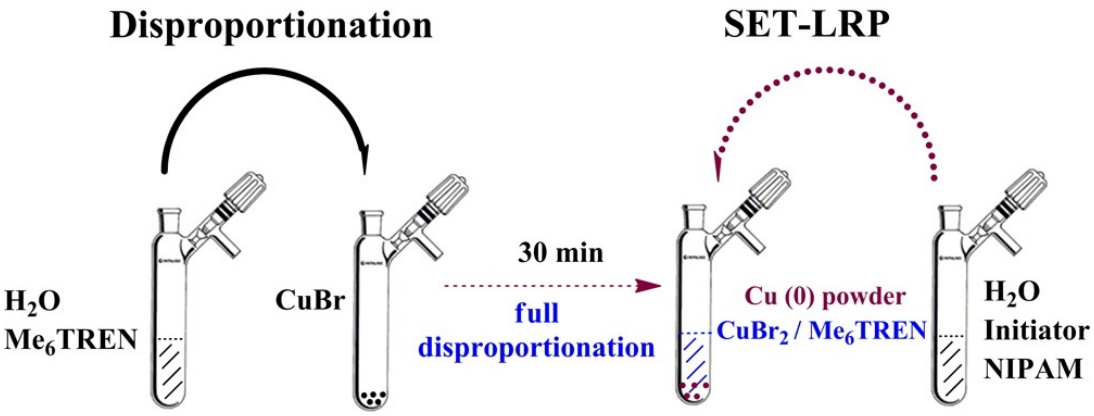


***Figure 5.3*** *General scheme for the aqueous SET-LRP protocol, as described by Zhang et. al.(Reference 21)*

This allowed for the polymerization of various water-soluble vinyl monomers including NiPAM, PEG acrylate, glyco-acrylamides and *N*-acrylomorpholine with unprecedented levels of control over the molecular weight and dispersity to high conversions at ambient temperature or below. Additionally the polymers were found

to possess excellent end-group fidelity allowing for iterative chain extension and the synthesis of multiblock co-polymers. The remarkable robustness of this technique was further demonstrated by the successful employment of aqueous solvents containing a multitude of chemical impurities, including blood serum and a range of international alcoholic beverages.

In this study the feasibility of conducting surface-initiated SET-LRP from poly(sulfone) membranes was investigated. The membranes had been previously modified with hydroxyl functionality, as described earlier, and so the strategy (**Figure 5.4**) was to convert these groups into initiator moieties and then to polymerize from them using aqueous SET-LRP forming poly(NiPAM) brushes from the surface. NiPAM was chosen as the monomer in this study due to the previously reported success when used in the aqueous SET-LRP protocol, and also due to the LCST phenomenon of poly(NiPAM) which gives the potential for the introduction of thermo-responsive behaviour to the polymer-functionalized membranes.

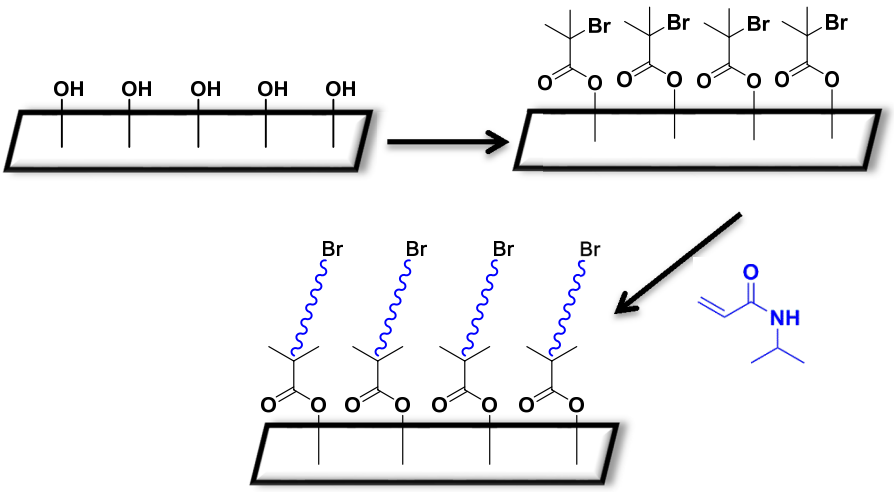


***Figure 5.4*** *General scheme for the attachment of initiator groups on the membrane surface and subsequent grafting of polymer brushes using surface SET-LRP*

## 5.2 Results and Discussion

### 5.2.1 Synthesis of Initiator-Modified Poly(sulfone) Membranes

In order to conduct SET-LRP of polymer brushes from the poly(sulfone) membranes it is first required that initiating groups are immobilized on their surface. The initial step in this project was to utilize the hydroxyl functionality on the membranes in order to introduce alkyl halide initiator moieties on the surface, this was achieved by reacting the membranes with α-bromoisobutyryl bromide in the presence of TEA to form the corresponding esters. One would normally conduct such reactions in a polar aprotic solvent, however, the membranes were found to be completely soluble in all such solvents tested (DMSO, DMF, MeCN, Acetone, THF) and in addition they were also soluble in halogenated solvents such as chloroform and DCM. As a result of this, the reactions were conducted in the non-polar hydrocarbon solvent, hexane. A range of poly(sulfone) membranes with varying levels of OH-functionality were provided by the Nunes group at KAUST, but to ensure consistency in testing, a single membrane with a degree of -OH functionalization of 0.44 was used throughout this study (**Figure 5.5**).

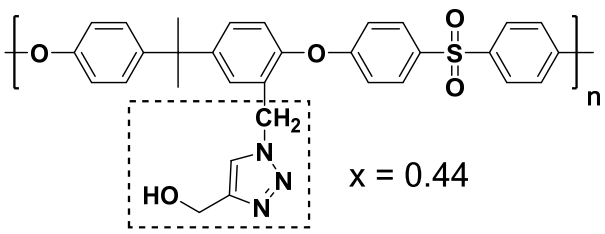


***Figure 5.5*** *Structure of the OH-poly(sulfone) membrane used in this study*

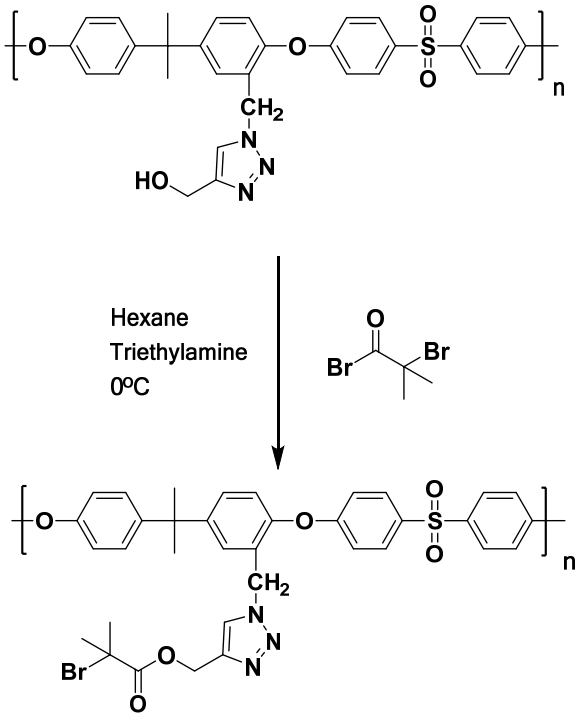


***Figure 5.6*** *Reaction scheme for the attachment of initiator groups on the membrane surface*

A 1 $cm^2$ piece of poly(sulfone) membrane was cut and added to a solution of TEA in hexane and an excess of α-bromoisobutyryl bromide was slowly added via syringe. The mixture was then left overnight with the membrane then removed and stirred in water for 48 hours in order to remove any free initiator/acid halide before any characterization took place.

The membranes were initially characterized using $^1H$ NMR spectroscopy, however, the signals corresponding to the initiator groups were obscured by that of the poly(sulfone) rendering this analysis unsuitable for assessing if the reaction was successful. The dried poly(sulfone) membranes were then analysed using infra-red spectroscopy and, as can be seen in the spectra, the disappearance of the –OH band at ~3300 $cm^{-1}$ and appearance of an ester peak at 1738 $cm^{-1}$ is highly

suggestive of the hydroxyl groups being esterified to the desired alkyl halide product (**Figure 5.7**).

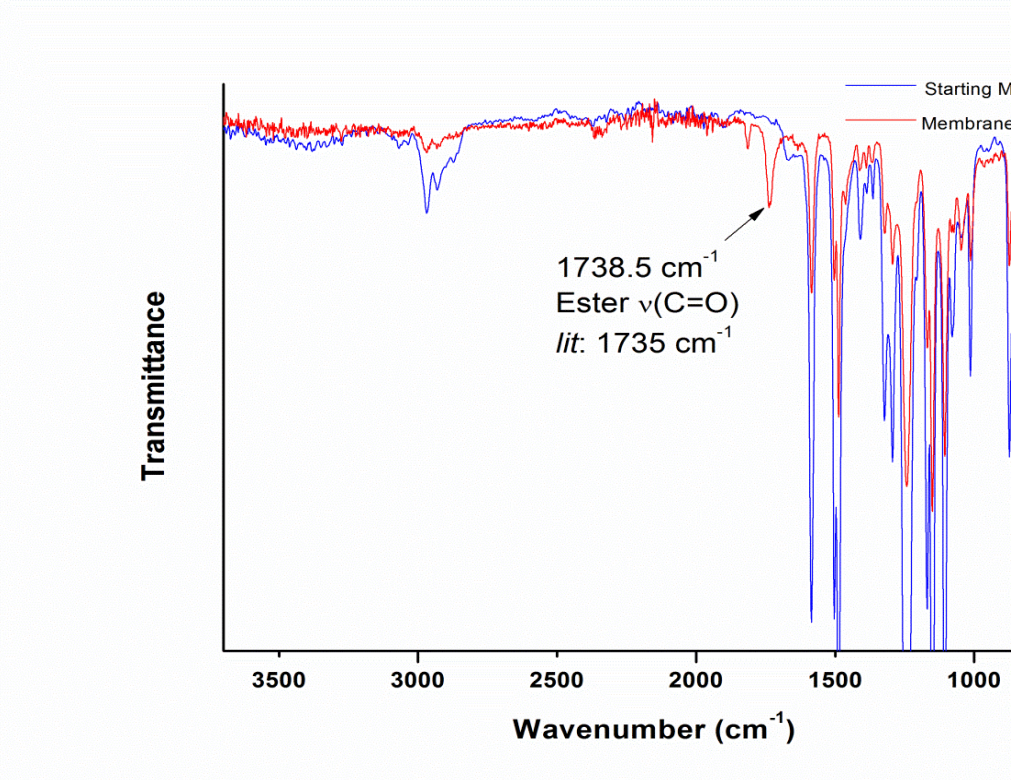


***Figure 5.7*** *FT-IR spectrum of poly(sulfone) membrane, pre and post esterification reaction*

It should be expected that functionalising surfaces with alkyl halide initiator groups will confer them with hydrophobicity and so contact angle measurements were carried out on the esterified membranes to test this. An increase in the water contact angle would be further proof of there being initiator groups attached on the surface and verifying the success of the esterification reaction.

The esterified and starting OH-membranes were analysed using a Krüss drop shape analyser with water static contact angles measured on the surfaces using the sessile drop method. The unfunctionalized membranes were found to have an average contact angle of 65°, which is consistent with their already hydrophobic

nature[26], and post-reaction the hydrophobicity of the surface was observed to increase with the average contact angle of 82° indicating increased hydrophobicity and that initiating groups have been successfully attached to the surface (**Figure 5.8**).

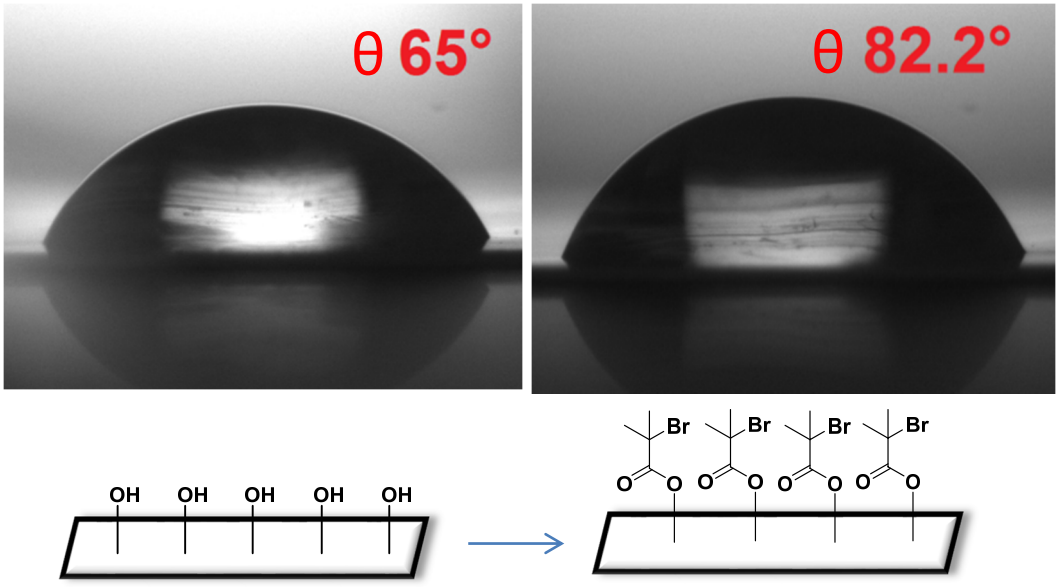


***Figure 5.8*** *Static water contact angle measurements of both poly(sulfone) membranes pre- and post-esterification with α-bromoisobutyryl bromide*

In order to further examine their surface chemistries, the samples were also analysed using X-ray photoelectron spectroscopy (XPS) which can be used to determine both the surface elemental stoichiometries of the samples as well as which chemical functionalities are present. As such, this analysis should be able to accurately determine the presence of the desired initiator functionality, complementing the previous IR and contact angle measurements made. To begin, the starting hydroxylated poly(sulfone) membranes were analysed to provide a 'baseline' for the subsequent measurements. **Figure 5.9** shows the respective XPS wide scan spectrum displaying four large peaks at binding energies of (BEs) 284.6,

531.40, 167.00 and 399.10 eV which correspond[27] to C 1s, O 1s, S 2p and N 1s. The sensitivity-factor corrected spectral area ratios of each peak are given in **Table 5.1** and are consistent with the structure of the OH-poly(sulfone).

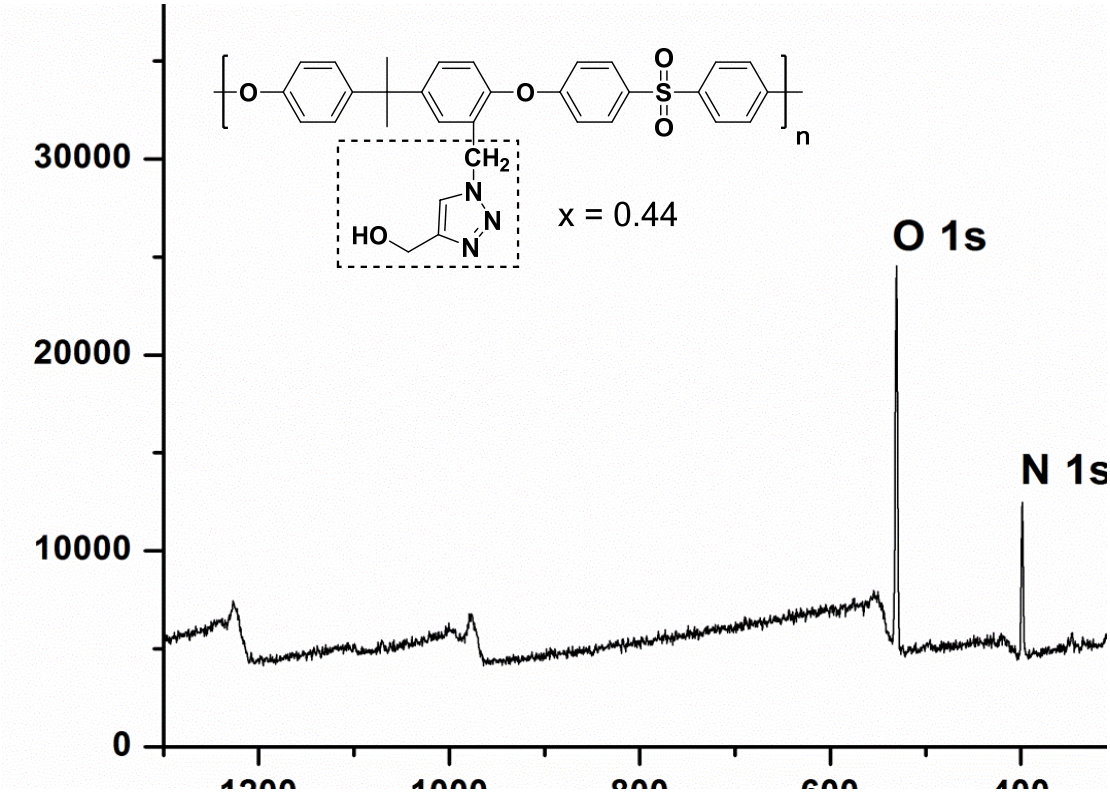


***Figure 5.9*** *Wide-scan XPS spectrum of OH-poly(sulfone) membrane. Binding energies and atomic percentages are given in Table 5.1*

| Sample | Peak | Binding Energy (eV) | Atom % | Theo. At. % |
|---|---|---|---|---|
| **Starting Membrane** | C 1s | 284.65 | 75.21 | 75.67 |
| | O 1s | 531.40 | 18.50 | 13.50 |
| | S 2p | 167.00 | 2.69 | 2.70 |
| | N 1s | 399.10 | 3.60 | 8.1 |

***Table 5.1*** *Binding energies, peak assignments and atomic percentages derived from the wide-scan XPS spectrum of OH-poly(sulfone) membrane*

A core-level spectrum of the C 1s peak was then obtained which was deconvoluted and curve-fitted (**Figure 5.10**) into four peak components at 284.59, 285.14, 286.33 and 287.96 eV, attributable to C-C/C-H, C-S/C-N, C-O and C=C-N species respectively.[28-30] In addition a small perturbance was observed at approximately 288 eV which corresponds to π- π* transitions caused by the aromatic groups in the poly(sulfone) backbone[31]. All of the above features are in agreement with the chemical composition of the membrane.

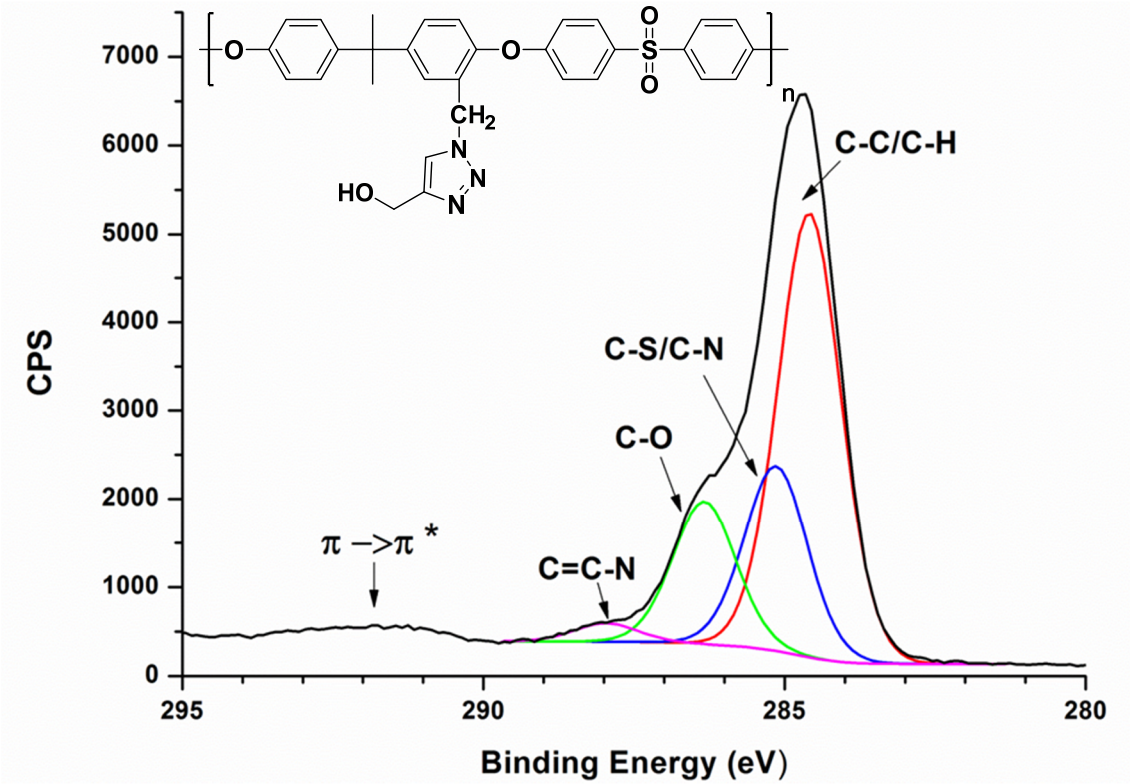


***Figure 5.10*** *C 1s core-level XPS spectra of OH-poly(sulfone) along with curve-fitted peak components. Binding energies and peak areas are given in Table 5.2*

| Sample | Peak | Binding Energy (eV) | Fitted Peak Area (%) | Assignment |
|---|---|---|---|---|
| **Starting Membrane** | C 1s | 284.59 | 56.27 | C-C/C-H |
| | | 285.14 | 23.38 | C-S/C-N |
| | | 286.33 | 18.03 | C-O |
| | | 287.96 | 2.32 | C=C-N |
| | | 291.71 | - | π- π* |

***Table 5.2*** *Binding energies, peak assignments and area ratios derived from the C 1s core-level XPS spectrum of OH-poly(sulfone) membrane*

An analogous XPS analysis was then carried out on the membrane which had been reacted with α-bromoisobutyryl bromide followed by extensive washing and drying. The wide scan spectrum is shown in **Figure 5.11** which displays five major peaks at BE's of 284.75, 531.30, 167.00 and 399.00 and 67.0 eV which correspond to C 1s, O 1s, S 2p, N 1s and Br 3d. The presence of the new peak, due to bromine, is a strong indication itself of the presence of initiator functionality, also the atomic percentages derived from the spectral areas of each peak closely agree with that of theory (**Table 5.3**). The peak-fitted C 1s core-level spectrum (**Figure 5.12**) contained five peak components at 284.59, 286.25, 285.18, 287.59 and 288.51, corresponding to C-C/C-H, C-S/C-N, C-O, C=C-N and O-C=O. As with the presence of bromine in the wide scan spectrum, the new component in the C 1s peak corresponding to ester groups is diagnostic of the initiator functionalization reaction being successful.

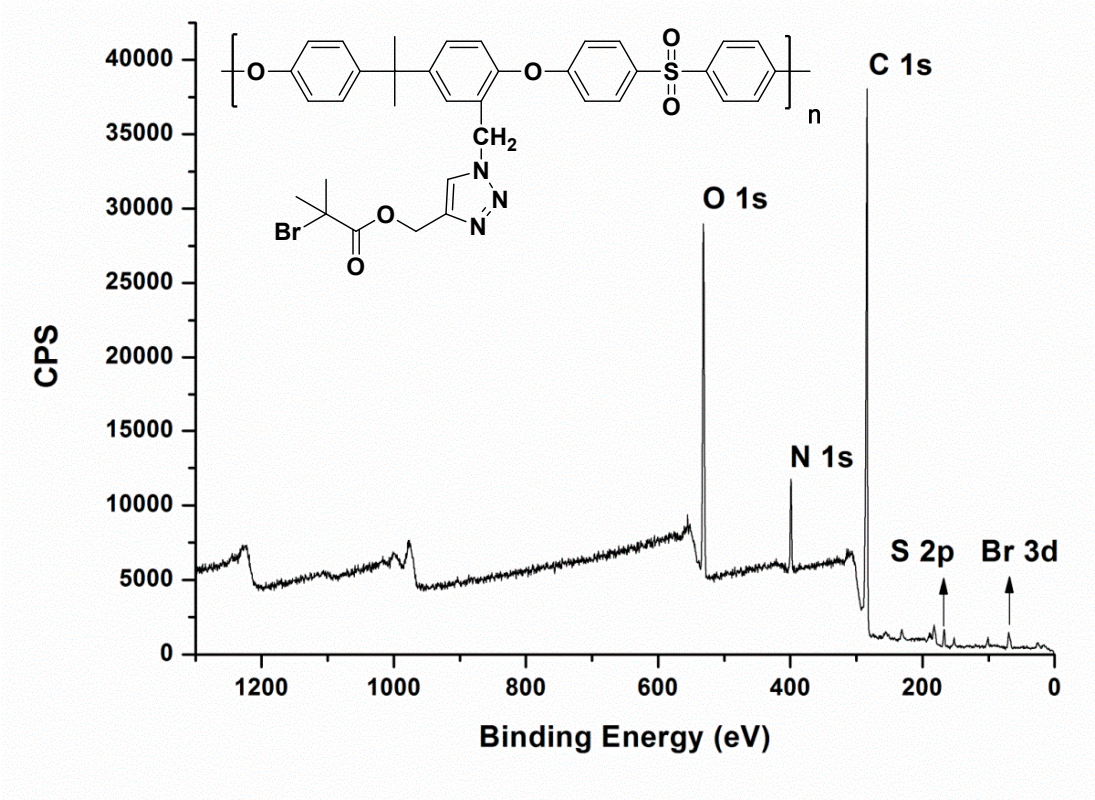


***Figure 5.11*** *Wide-scan XPS spectrum of initiator-poly(sulfone) membrane. Binding energies and atomic percentages are given in Table 5.3*

| Sample | Peak | Binding Energy (eV) | Atom % | Theo. At. % |
|---|---|---|---|---|
| **Membrane + Initiator** | C 1s | 284.75 | 75.56 | 76.59 |
| | O 1s | 531.30 | 18.90 | 16.21 |
| | S 2p | 167.00 | 1.48 | 2.12 |
| | N 1s | 399.00 | 6.19 | 4.05 |
| | Br 3d | 67.00 | 0.86 | 1.06 |

***Table 5.3*** *Binding energies, peak assignments and atomic percentages derived from the wide-scan XPS spectrum of initiator-poly(sulfone) membrane*

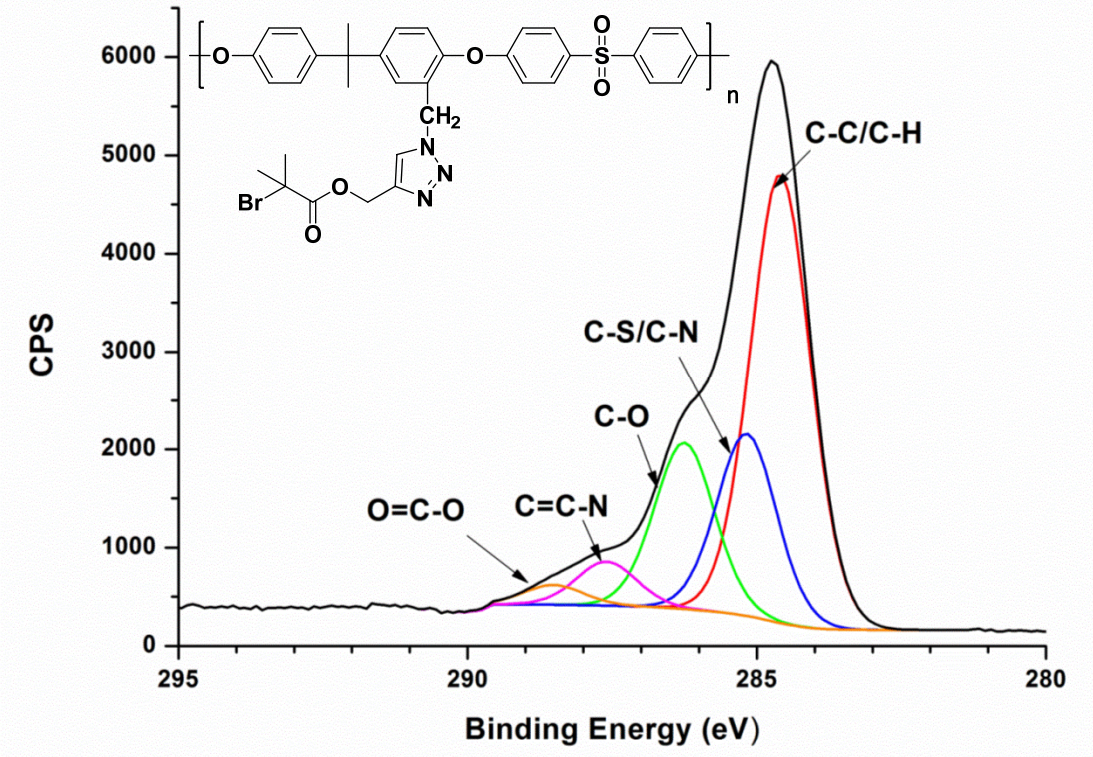


***Figure 5.12*** *C 1s core-level XPS spectra of initiator-poly(sulfone) along with curve-fitted peak components. Binding energies and peak areas are given in Table 5.4*

| Sample | Peak | Binding Energy (eV) | Fitted Peak Area (%) | Assignment |
|---|---|---|---|---|
| **Membrane + Initiator** | C 1s | 284.59 | 52.17 | C-C/C-H |
| | | 286.25 | 19.30 | C-O/C-Br |
| | | 285.18 | 21.13 | C-S/C-N |
| | | 287.59 | 5.10 | C=C-N |
| | | 288.51 | 2.29 | O-C=O |

***Table 5.4*** *Binding energies, peak assignments and area ratios derived from the C 1s core-level XPS spectrum of initiator-poly(sulfone) membrane*

### 5.2.2 Surface Initiated aqueous $Cu^{(0)}$-Mediated RDRP from Poly(sulfone) Membranes

With the above analysis confirming that the hydroxylated poly(sulfone) membrane has successfully been decorated with alkyl halide initiator functionality, the next step was to attempt to perform surface-initiated SET-LRP from them. For this purpose our previously reported aqueous SET-LRP methodology, featuring the key pre-disproportionation step, was adapted and the water soluble initiator replaced with the previously characterized initiator-membrane.

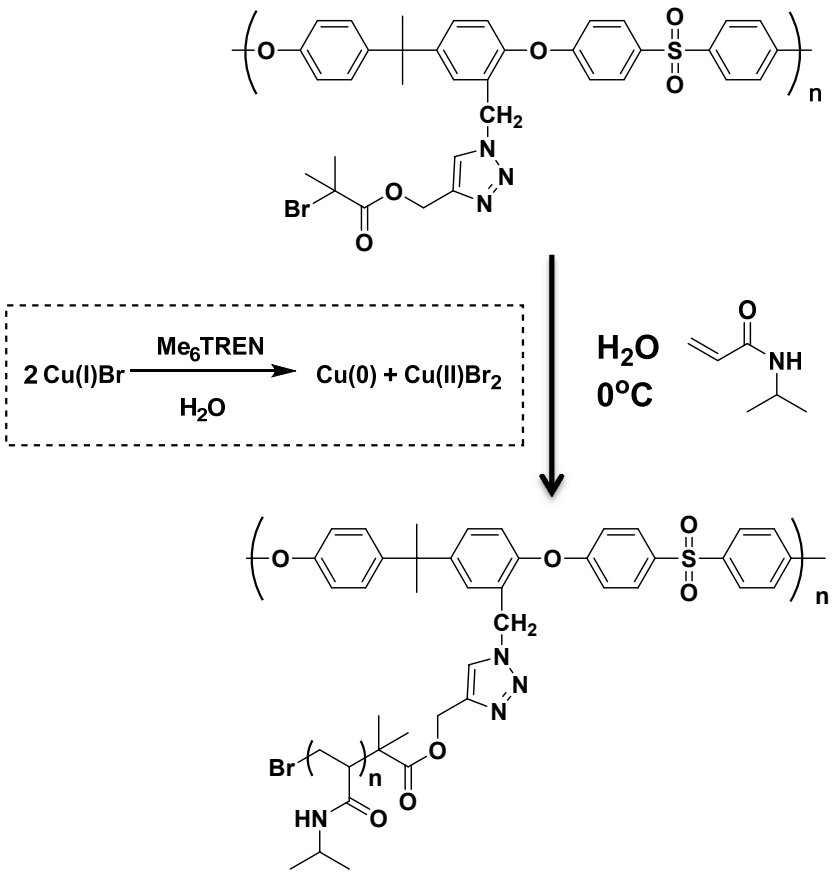


***Figure 5.13*** *General scheme for the surface initiated aqueous SET-LRP of NiPAM from initiator-functionalized poly(sulfone) membrane*

In this reaction the attempted polymerization of NiPAM was conducted in the presence of $Cu^{(0)}$ and $Cu^{(II)}Br_2$ obtained via the prior in situ disproportionation of CuBr and $Me_6TREN$ (in a 1:1 molar ratio, 14.3 mg and 27 µL respectively) in water. A 1 $cm^2$ piece of the functionalized poly(sulfone) membrane was employed as the initiator and the mixture allowed to react overnight. The membrane was subsequently removed from the polymerization mixture and washed in distilled water for 7 days in order to fully remove any free NiPAM and poly(NiPAM) which may be present. After this thorough washing step, the membranes were then dried

subjected to $^{1}$H NMR, FT-IR, XPS, SEM and contact angle analysis in an analogous fashion to that carried out previously in order to determine if poly(NiPAM) had been successfully grafted from the surface.

A sample of the dried membrane was first analysed using $^{1}$H NMR (possible due to their solubility in chloroform) which revealed new peaks characteristic of poly(NiPAM) at 4.00 and 1.14 ppm corresponding to C***H***-$(CH_3)_2$ and CH-$(C\boldsymbol{H}_3)_2$ respectively. Integration of these peaks, relative to the peak at 5.43ppm corresponding to the N-C$\boldsymbol{H}_2$ linkage, produces a ratio of approximately 7.6:1, implying a degree of polymerization of ~8. Representative $^{1}$H NMR spectra of the membranes pre- and post-polymerization are given in **Figure 5.14**.

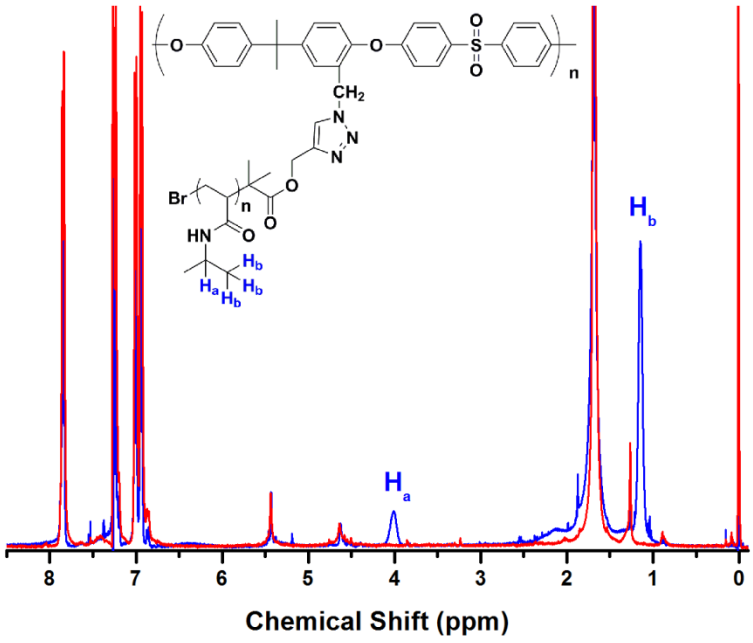


***Figure 5.14*** *$^{1}$H NMR spectra of poly(sulfone) membranes pre- and post- aqueous $Cu^{(0)}$-mediated RDRP with NiPAM*

The membrane was also analysed using FT-IR. By comparison with the spectra of the sample pre-polymerization, new absorbances at 1544 at 1646 $cm^{-1}$ can be observed corresponding to amide C=O stretching modes. In addition, absorbances at 3065 and 3300 $cm^{-1}$ corresponding to amide bending and amine stretching modes are also seen (**Figure 5.15**). All of the above features are evidence for poly(NiPAM) bonded to the surface and are consistent with the literature values[32].

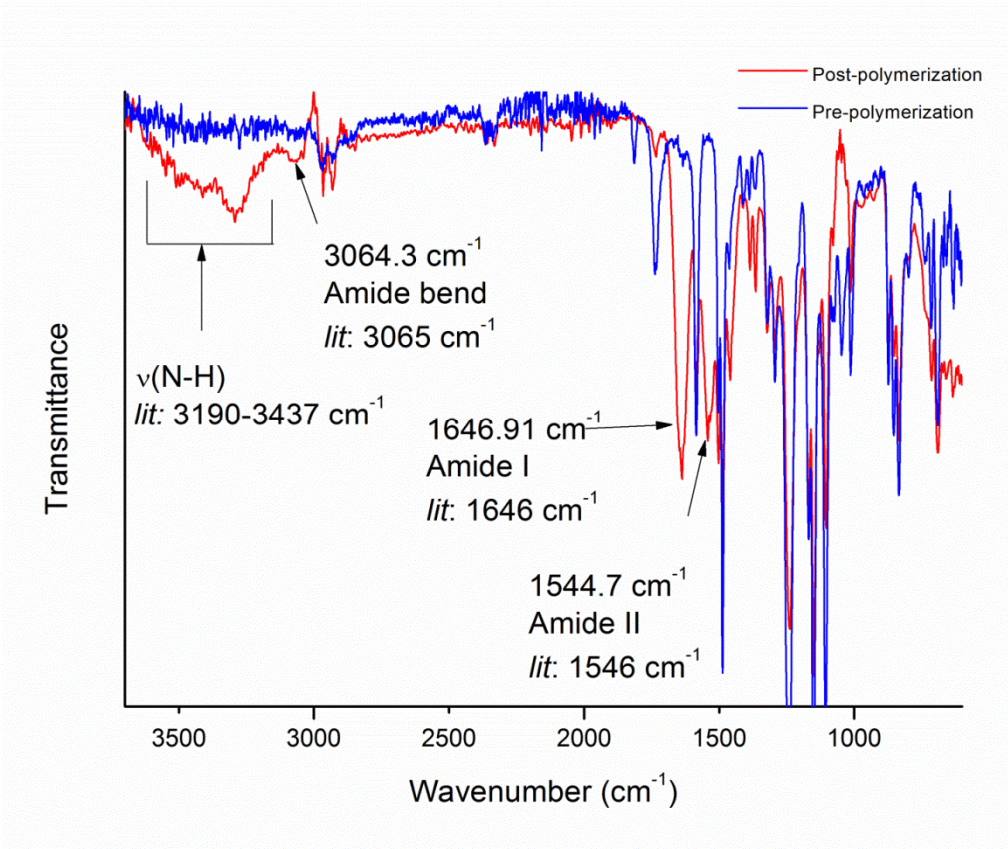


***Figure 5.15*** *FT-IR spectrum of poly(sulfone) membrane, pre and post esterification reaction*

Static contact angle of measurements of pure water on the surface were also undertaken, with reference to those obtained earlier from the initiator-modified membrane (**Figure 5.16**). Post-polymerization it can be seen that the membrane is now quite hydrophilic with the contact angle of the water droplet lowered from 82.2° to 33° and, on further observation, within approximately one minute the water

droplet had then flattened and wetted the surface completely. Such behaviour is to be expected of a surface with poly(NiPAM) brushes[33] and so this is continued evidence of the polymerization being accomplished and that the surface now contains the desired increased hydrophilicity.

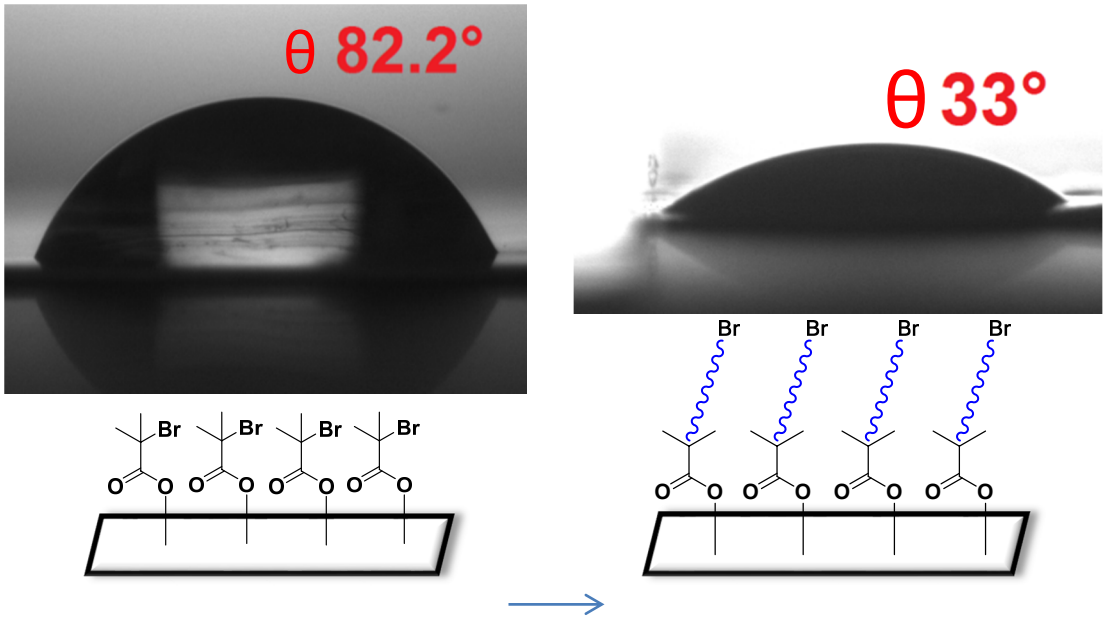


***Figure 5.16*** *Static water contact angle measurements of both initiator-poly(sulfone) and poly(sulfone) membranes containing poly(NiPAM) brushes obtained via aqueous SET-LRP*

Following the contact angle analysis the membrane was then subjected to XPS measurements beginning with the acquisition of a wide-scan spectrum. This reveals three peaks with binding energies of 284.70, 530.60 and 398.70 eV corresponding to C 1s, O 1s and N 1s. Interestingly the previously seen peak corresponding to sulfur has been almost completely attenuated (a very slight peak can be observed with an intensity of ~50 CPS, within the baseline noise and several orders of magnitude smaller than the other peaks being analysed) implying

that the layer of poly(NiPAM) on the surface is thicker than the sampling depth of the XPS technique, which is approximately 5 nm. If the x-ray beam is unable to penetrate fully through the polymer layer then it follows that the signals corresponding to the poly(sulfone) membrane will no longer be seen, hence the disappearance of the sulfur peak.

Additionally, the Br 3d peak is also absent from this spectrum indicating that bromine has been lost at some point during or after the polymerization. Prior work on aqueous polymerization of acrylamides using alkyl halide initiators has demonstrated that the terminal secondary bromides of the polymer are susceptible to hydrolysis in situ on the polymerization timescale[34, 35]. Given the lengthy washing that the membrane has undergone post-polymerization, it is thus assumed that extensive hydrolysis has occurred resulting in poly(NiPAM) chains furnished with terminal –OH functionality, corroborated by the absence of bromine in this elemental analysis. The wide-scan spectrum and derived atomic percentages are given in **Figure 5.17** and **Table 5.5**.

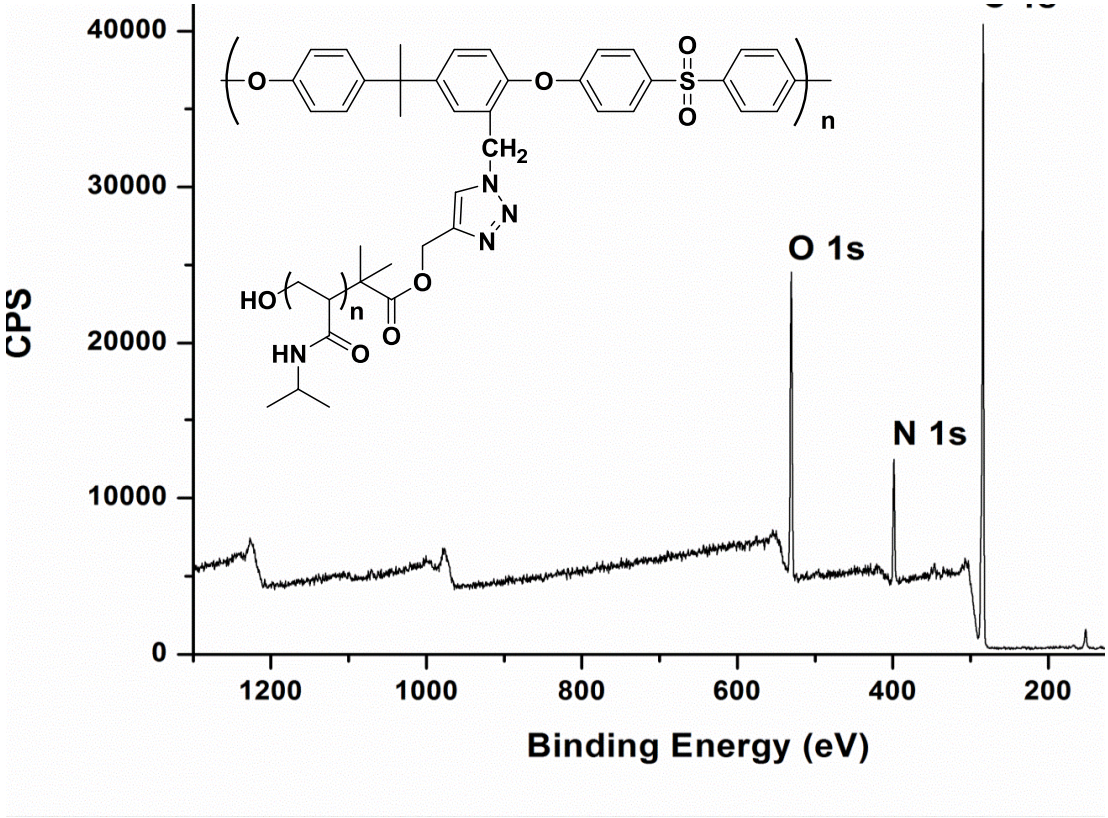


***Figure 5.17*** *Wide-scan XPS spectrum of poly(sulfone) membrane functionalized with poly(NiPAM) brushes. Binding energies and atomic percentages are given in Table 5.5*

| Sample | Peak | Binding Energy (eV) | Atom % | Mass % |
|---|---|---|---|---|
| **Membrane + Poly(NiPAM)** | C 1s | 284.70 | 77.99 | 71.42 |
| | O 1s | 530.60 | 14.50 | 21.43 |
| | N 1s | 398.70 | 7.51 | 7.14 |

***Table 5.5*** *Binding energies, peak assignments and atomic percentages derived from the wide-scan XPS spectrum of initiator-poly(sulfone) membrane*

As per the previous XPS analysis carried out, following the wide-scan analysis a core-level spectrum of the C 1s was then obtained and peak-fitted in order to determine the chemical functionalities present (**Figure 5.18**). Since the wide-scan spectra illustrated that the poly(NiPAM) layer essentially 'blocks' the membrane surface it could be expected that the C 1s core-level peak also reflects this. This is indeed the case as the peak could be fitted into four components with BE's of 284.71, 285.88, 287.54 and 288.63 eV corresponding to C-C/C-H, C-N/C-O, O=C-N, O-C=O which is indicative of poly(amide) functionality. The approximate 1:1 ratio of C-N:O=C-N is consistent with the repeat unit of poly(NiPAM) and furthermore an estimate of the degree of polymerization can be made by determining the ratio of amide bonds to ester bonds on the initiator moiety. In this case the ratio is 8:1 (10.89/1.36), suggesting a DP of 8 which agrees well with the DP was determined by $^{1}$H NMR.

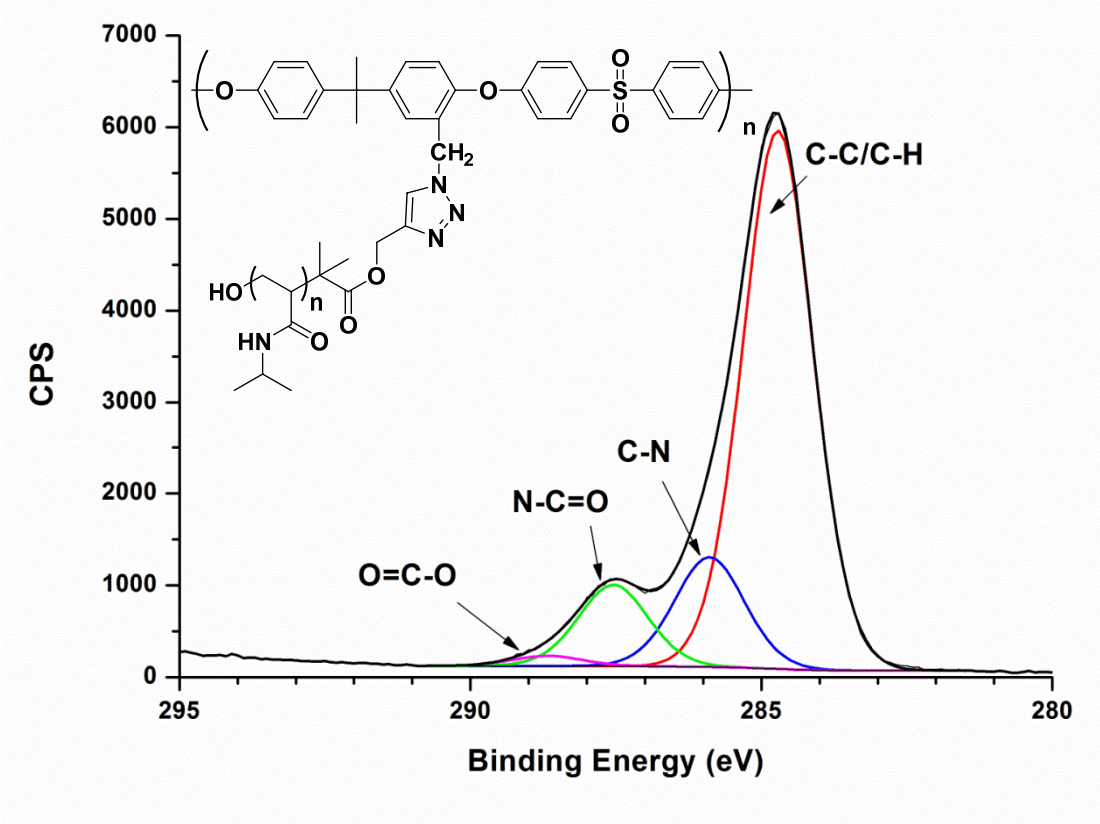


***Figure 5.18*** *C 1s core-level XPS spectra of poly(sulfone) membrane functionalized with poly(NiPAM) brushes, along with curve-fitted peak components. Binding energies and peak areas are given in Table 5.6*

| Sample | Peak | Binding Energy (eV) | Fitted Peak Area (%) | Assignment |
|---|---|---|---|---|
| **Membrane + Poly(NiPAM)** | C 1s | 284.71 | 72.85 | C-C/C-H |
| | | 285.88 | 14.89 | C-N/C-O |
| | | 287.54 | 10.89 | O=C-N |
| | | 288.63 | 1.36 | O-C=O |

***Table 5.6*** *Binding energies, peak assignments and area ratios derived from the C 1s core-level XPS spectrum of poly(sulfone) membrane functionalized with poly(NiPAM)*

Images were taken of the membranes using Scanning Electron Microscopy (SEM) to investigate any changes in the surface morphology pre- and post-polymerization. **Figure 5.19** shows the SEM image of OH-poly(sulfone) of which the fine surface details can be seen including the pores which are approximately 500 nm in diameter.

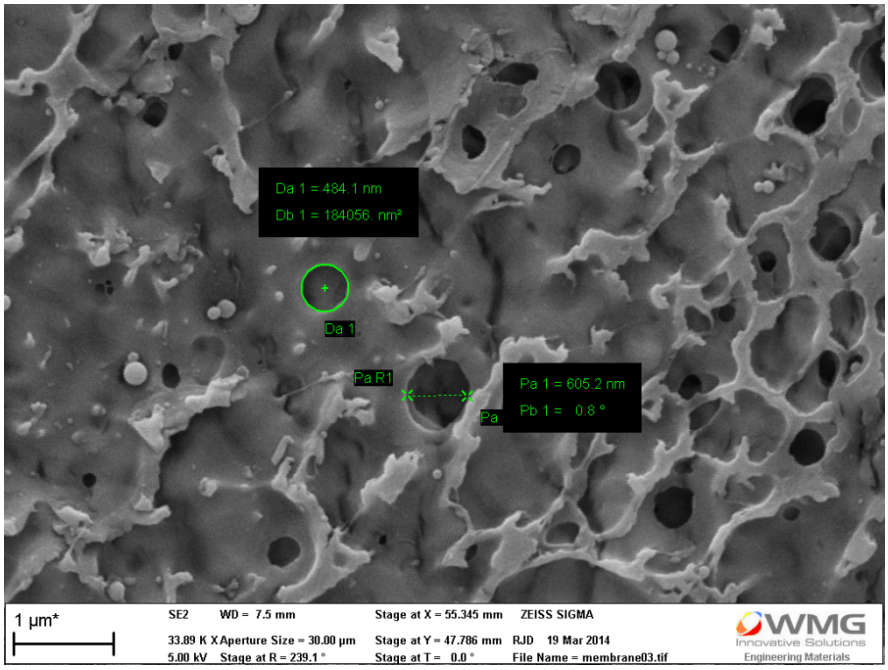


***Figure 5.19*** *SEM micrograph of OH-poly(sulfone) membrane, prior to surface polymerization*

Post-polymerization it can be seen (**Figure 5.20**) that there is a now a layer of material coating the surface which, given the previous characterization carried out, is likely to be grafted poly(NiPAM) further confirming that the SET-LRP reaction was successful. This also corroborates well with the XPS data which showed that the underlying poly(sulfone) membrane could no longer be detected. The observed loss of fine detail, including the pore structures, may indicate that the polymer layer is too thick or that the grafting density is too high (too many initiating groups),

however the effect of this would have to be further investigated by assessing their water permeability. In addition, carrying out the microscopy in water using Cryo-SEM would allow the membranes to be studied in their 'native' environment giving a better representation of how the surface behaves.

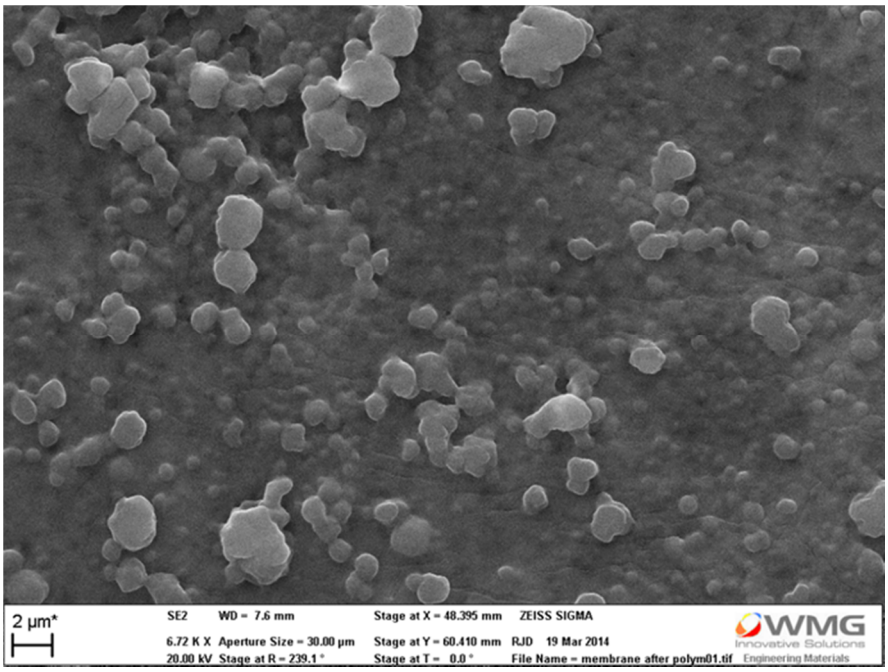


***Figure 5.20*** *SEM micrograph of poly(sulfone) membrane, post- surface SET-LRP with NiPAM*

## 5.3 Conclusions

In this chapter the feasibility of grafting poly(NiPAM) brushes from poly(sulfone) membranes was investigated. This process was developed in two steps, the first was to introduce initiator functionality via esterification of the surface hydroxyl groups, the success of which was confirmed by FT-IR, contact angle and XPS measurements. Surface aqueous SET-LRP of NiPAM was carried out and the subsequent material analysed using the same techniques as above in addition to $^{1}$H NMR spectroscopy and SEM. This analysis demonstrated that poly(NiPAM) had successfully been grown from the surface of the membrane and an estimate of the degree of polymerization could be made. In addition, complete loss of the terminal bromides on the polymer chains was observed using XPS, which has been ascribed to hydrolysis in agreement with results obtained within our group and elsewhere.

With the ability to conduct aqueous SET-LRP from these membrane surfaces confirmed, there is a large scope for further work - other water-soluble monomers could be screened with different brush lengths and grafting densities targeted. Ultimately this will allow for a large library of hydrophillically modified membranes to be produced and assessed for any enhanced water permeability and anti-fouling properties.

## 5.4 Experimental

### 5.4.1 Materials

Tris(2-(dimethylamino)ethyl)amine ($Me_6$TREN) was synthesized as previously described and stored under a nitrogen atmosphere prior to use. Copper(I) bromide (CuBr, 98%, Sigma-Aldrich) was purified by sequential washing with acetic acid and ethanol and then dried under vacuum to give a white solid. *N*-Isopropylacrylamide (NiPAM, 97%) and α-bromoisobutyryl bromide (98%) was obtained from Sigma-Aldrich and used without further purification. Reagent grade hexane and HPLC grade water (VWR International) were used for the esterification and polymerization reactions.

### 5.4.2 Analytical Techniques

XPS data were collected at the Science City Photoemission Facility in the Department of Physics at the University of Warwick. An Omicron XM1000 monochromated Al Kα X-ray source was used to illuminate the sample, with photoelectrons collected in an Omicron SPHERA analyser at a take-off angle of 90 degrees using an estimated sampling radius of 1.1 mm. An Omicron CN10 charge neutralizer was used to eliminate surface charging effects arising from the insulating nature of the samples. All data were analysed using the CasaXPS package, with compositional analysis facilitated via determination of the analyser transmission function, previously calculated using polycrystalline Ag, Au and Cu

foils. Binding energies throughout were charge-referenced to the C-C component of the C 1s region at 284.7 eV.

$^{1}$H NMR spectra were recorded using a Bruker DPX-400 MHz spectrometer with deuterated chloroform being used as the sample solvent.

Scanning electron microscopy (SEM) micrographs were obtained using a Carl Zeiss FE-SEM Σigma. The samples were gold coated under 0.1 mbar argon in an Agar Auto Sputter Coater.

Infrared absorption spectra were recorded on a Bruker VECTOR-22 FTIR spectrometer using a Golden Gate diamond attenuated total reflection cell and the data analysed using the OPUS software.

Contact angle measurements were obtained using a Krüss DSA 100 drop shape analyser using the sessile drop method and distilled water. Reported values are averages obtained by recording the angles at five different spots on the surface.

### 5.4.3 Synthetic Procedures

#### 5.4.3.1 Immobilization of Initiator Functionality to OH-poly(sulfone) Membranes

OH-Poly(sulfone) membrane ( 1 cm$^2$ piece, OH functionality = 0.44) was added to vial containing a solution of triethylamine (550 µL,4 mmol) in hexane (10 mL) and a stirrer bar. The solution was cooled to 0°C using an ice bath and, with constant

stirring, α-bromoisobutyryl bromide (500 μL, 4 mmol) was added drop-wise using a syringe. The mixture was left to react overnight before the membrane was removed and copiously rinsed with water. It was then left to stir in 100 mL of water for 48 hours, with the water being changed after the first 24 hours. The membrane was then dried in a vacuum oven prior to characterization.

#### 5.4.3.2 Surface $Cu^{(0)}$-mediated RDRP of NiPAM from initiator-modified poly(sulfone) membrane

CuBr (14.3 mg) and $Me_6$TREN (27 μL) were added to 5 mL of water in a 10 mL vial equipped with a stirrer bar and sealed with a rubber septum. Rapid disproportionation was observed, producing metallic Cu(0) particles on the sides of the vial and a deep blue colour to the solution. Nitrogen gas was then sparged through the solution for 15 minutes before NiPAM (0.563 g) was added to the vial under a blanket of nitrogen. The solution was left to stir/degas for a further 10 minutes before adding the initiator-functionalized poly(sulfone) membrane, taking care to minimize exposure to oxygen. The mixture was left under nitrogen and allowed to react overnight before removing the membrane which was washed with distilled water and further stirred in distilled water (100 mL) for 7 days, replacing the water every 24 hours to ensure total removal of any free or adsorbed polymer. The membrane was then isolated by removal of volatiles under vacuum and subjected to the analytical procedures outlined above.

## 5.5 References


1. H. Susanto, N. Stahra and M. Ulbricht, *J. Membr. Sci.*, 2009, 342, 153-164.
2. Z. Tang, C. Qiu, J. R. McCutcheon, K. Yoon, H. Ma, D. Fang, E. Lee, C. Kopp, B. S. Hsiao and B. Chu, *J. Polym. Sci., B Polym. Phys.*, 2009, 47, 2288-2300.
3. B. Zornoza, S. Irusta, C. Teì llez and J. n. Coronas, *Langmuir*, 2009, 25, 5903-5909.
4. Y. Yang and P. Wang, *Polymer*, 2006, 47, 2683-2688.
5. C. Dizman, M. A. Tasdelen and Y. Yagci, *Polym. Int.*, 2013, 62, 991-1007.
6. J. B. Rose, *Polymer*, 1974, 15, 456-465.
7. D. Rana and T. Matsuura, *Chem. Rev.*, 2010, 110, 2448-2471.
8. B. C. Johnson, I. Yilgor, C. Tran, M. Iqbal, J. P. Wightman, D. R. Lloyd and J. E. McGrath, *J. Polym. Sci., A Polym. Chem.*, 1984, 22, 721-737.
9. G. Yilmaz, H. Toiserkani, D. O. Demirkol, S. Sakarya, S. Timur, L. Torun and Y. Yagci, *Mater. Sci. Eng., C*, 2011, 31, 1091-1097.
10. Y. H. Cho, H. W. Kim, S. Y. Nam and H. B. Park, *J. Membr. Sci.*, 2011, 379, 296-306.
11. C. Zhao, J. Xue, F. Ran and S. Sun, *Prog. Mat. Sci.*, 2013, 58, 76-150.
12. Z. Yi, L.-P. Zhu, Y.-F. Zhao, B.-K. Zhu and Y.-Y. Xu, *J. Membr. Sci.*, 2012, 390-391, 48-57.
13. M. Ulbricht and G. Belfort, *J. Membr. Sci.*, 1996, 111, 193-215.
14. W.-W. Yue, H.-J. Li, T. Xiang, H. Qin, S.-D. Sun and C.-S. Zhao, *J. Membr. Sci.*, 2013, 446, 79-91.
15. Y.-F. Zhao, L.-P. Zhu, Z. Yi, B.-K. Zhu and Y.-Y. Xu, *J. Membr. Sci.*, 2013, 440, 40-47.

16. Y. Xie, R. Tayouo and S. P. Nunes, *J. Appl. Polym. Sci.*, 2014, DOI: 10.1002/app.41549.

17. H. C. Kolb, M. G. Finn and K. B. Sharpless, *Angew. Chem.*, 2001, 40, 2004-2021.

18. E. Avram, E. Butuc, C. Luca and I. Druta, *J. Macromol. Sci. Chem.*, 1997, 34, 1701-1714.

19. K.-V. Peinemann, V. Abetz and P. F. W. Simon, *Nat. Mater.*, 2007, 6, 992-996.

20. L. F. Hancock, *J. Appl. Polym. Sci.*, 1997, 66, 1353-1358.

21. Q. Zhang, Z. Li, P. Wilson and D. M. Haddleton, *Chem. Commun.*, 2013, 49, 6608-6610.

22. Q. Zhang, P. Wilson, Z. Li, R. McHale, J. Godfrey, A. Anastasaki, C. Waldron and D. M. Haddleton, *J. Am. Chem. Soc.*, 2013, 135, 7355-7363.

23. Q. Zhang, P. Wilson, A. Anastasaki, R. McHale and D. M. Haddleton, *ACS Macro Lett.*, 2014, 3, 491-495.

24. C. Waldron, Q. Zhang, Z. Li, V. Nikolaou, G. Nurumbetov, J. Godfrey, R. McHale, G. Yilmaz, R. K. Randev, M. Girault, K. McEwan, D. M. Haddleton, M. Droesbeke, A. J. Haddleton, P. Wilson, A. Simula, J. Collins, D. J. Lloyd, J. A. Burns, C. Summers, C. Houben, A. Anastasaki, M. Li, C. R. Becer, J. K. Kiviaho and N. Risangud, *Polym. Chem.*, 2014, 5, 57-61.

25. A. Anastasaki, A. J. Haddleton, Q. Zhang, A. Simula, M. Droesbeke, P. Wilson and D. M. Haddleton, *Macromol. Rapid Commun.*, 2014, 35, 965-970.

26. W. Zhang, M. Wahlgren and B. Sivik, *Desalination*, 1989, 72, 263-273.

27. http://srdata.nist.gov/xps/, Accessed 2014.

28. P. Louette, F. Bodino and J.-J. Pireaux, *Surf. Sci. Spec.*, 2005, 12, 100-105.

29. J. F. Moulder, W. F. Stickle, P. E. Sobol and K. D. Bomben, *Handbook of X-ray Photoelectron Spectroscopy*, Perkin Elmer Eden Prairie, MN, 1992.

30. W. Zhu, W. Li, C. Wang, J. Cui, H. Yang, Y. Jiang and G. Li, *Chem. Sci.*, 2013, 4, 3583-3590.

31. M. Temtem, D. Pompeu, T. Barroso, J. Fernandes, P. C. Simoes, T. Casimiro, A. M. Botelho do Rego and A. Aguiar-Ricardo, *Green Chem.*, 2009, 11, 638-645.

32. G. Socrates, *Infrared and Raman characteristic group frequencies: tables and charts*, John Wiley & Sons, 2004.

33. N. Yamada, T. Okano, H. Sakai, F. Karikusa, Y. Sawasaki and Y. Sakurai, *Makromol. Chem. Rapid. Comm.*, 1990, 11, 571-576.

34. J. T. Rademacher, M. Baum, M. E. Pallack, W. J. Brittain and W. J. Simonsick, *Macromolecules*, 1999, 33, 284-288.

35. M. Teodorescu and K. Matyjaszewski, *Macromolecules*, 1999, 32, 4826-4831.

# Chapter 6: Conclusions and Future Outlook

The goal of this thesis was to develop novel polymers which can be utilized as viscosity modifiers for automotive lubrication applications. A particular emphasis was put on building towards the delivery of stimuli-responsive behaviour, as there are currently no VMs which are able to do this. Overall, this aim has been achieved; a range of materials have been produced that have undergone some initial testing and additionally some interesting methodologies have been explored along the way. Aspects of this work are now being continued by other members of the group.

As a starting point, the synthesis of telechelic lipophilic polymers containing polar end groups was targeted, with the hope that the polymer chains could aggregate through the polar functionality, resulting in associative thickening. $Cu^{(0)}$-mediated RDRP was chosen as the polymerization technique due to the expertise within the Haddleton group, and also because this method produces polymers with terminal bromide functionality, which can then be utilized for post-polymerization functionalization.

Telechelic butyl acrylate polymers were successfully synthesized and, in in doing so, a novel biphasic reaction mechanism was observed and underwent further investigation. When polymerizing *n*-BA in DMSO, the resultant polymer phase separated resulting in almost complete separation of the polymer from the copper species *in situ* as demonstrated by ICP-MS. This phase separation event occurred with no apparent loss of control over the reaction, and the polymers could subsequently be chain extended iteratively within the biphasic system. Thus it is not the case that the polymer comes out of solution at some critical molecular weight, and then stops polymerizing. The isomers of BA could also be polymerized; however the attempted polymerization of DMSO-insoluble monomers, such as lauryl acrylate, resulted in gel formation indicating that monomer (but not polymer) solubility is critical for this system. It was found that conducting these reactions in mixed solvent systems or IPA, which solubilizes the monomer, offers a route to polymerizing these highly lipophilic monomers in an analogous fashion to BA, whilst retaining the biphasic nature.

The high end group fidelity of the telechelic poly(butyl acrylates) was then exploited by the successful thioetherification using a range of thiols, producing α,ω-functionalized polymers. In most cases, quantitative substitution was obtained, as measured using MALDI-TOF MS. These materials then underwent some viscometric screening, however it was found that there was no influence of the various end groups on the rheological behaviour. The industrial feasibility of this biphasic $Cu^{(0)}$-mediated RDRP technique was then assessed with some kilogram scale-up tests, which whilst not proceeding quite as well as the small scale reactions, still resulted in a well-controlled polymerization. One potential benefit of the reactors used for the large scale polymerizations is that the phase separation allows for the solvent/catalyst layer to be drained out from the bottom, to leave the polymer phase behind. This could allow for a one-pot functionalization strategy

wherein the desired solvent and thiol could simply be added to the reactor, eliminating the need for any intermediate purification steps.

This methodology was then extended to the synthesis of hydrophobic, multi-arm star poly(acrylates). 8-armed *n*-butyl and lauryl polymeric stars were synthesized to high molecular weights (up to 150 kg $mol^{-1}$) and conversions, whilst retaining excellent control over the molecular weight distributions ($Đ_M \leq 1.10$ in most cases). It was also shown that the phase separation of stars from the reaction medium can possibly result in greatly reduced star-star coupling in certain cases, allowing for the synthesis of stars with unprecedented degrees of control relative to other controlled/living radical polymerization approaches.

A selection of 8-arm poly(*n*-butyl acrylates) were then analysed using triple detection SEC to get a more accurate measurement of their molecular weights, as conventional SEC resulted in large underestimations. Furthermore, triple detection SEC can also be used to calculate branching values which give an estimate of the number of arms. This analysis revealed molecular weights which agreed significantly more with the theory and average functionalities between 5 and 7, which is consistent with the chemistry. The polymerization methodology used was then scaled up to produce poly(lauryl acrylate) stars containing different numbers of arms and these materials then underwent some rheological testing to assess their suitability as VMs in oil. These tests showed that the stars synthesized were able to function as high VI additives, although no dependence on the number of arms was seen. With regards to future work on the star polymers, it would be useful to synthesize a library of materials containing varying numbers of arms, across a large molecular weight range as the polymers tested in this thesis only really constitute a small selection of what could potentially be available. Shear stability testing is also crucial, which was planned but could not be completed due to time constraints.

Following on from the initial attempts to synthesize associative thickeners, the incorporation of the UPy quadrupolar hydrogen bonding motif into lipophilic poly(acrylates) was targeted, again utilizing $Cu^{(0)}$-mediated RDRP. It was hoped that by incorporating these groups, we would be able to form stimuli-responsive supramolecular networks, which can dissolve in oil and give deliver novel rheological properties. The first approach was to incorporate multiple UPy groups *via* a co-monomer containing the UPy functionality, polymerized with butyl acrylate; however this was unsuccessful due to the poor solubility of the monomer. This was alleviated by using HEA as the co-monomer and then reacting the –OH groups with UPy-hexy-isocyanate, post-polymerization. The resultant materials were found to be almost completely insoluble in all solvents tested due to the high number of UPy units, which is perhaps not surprising given the reports in the literature. These experiments did serve to demonstrate the powerful nature of the UPy moiety, however. The focus was then shifted to the synthesis of poly(lauryl acrylates) containing a single UPy group, which was achieved by using an initiator bearing a terminal –OH group which was condensed with UPy-isocyanate in an analogous fashion to the HEA polymers. These polymers were soluble in oil and so underwent some dynamic rheological testing, which revealed some interesting thermo-responsive behaviour which could partly be attributed to tautomerization.

It should be emphasized that this rheological testing was only preliminary in nature and served to give some initial indications as to the behaviour of these materials. Clearly there is much work that could be done in the future, such as increasing the molecular weights of the materials or examining the effect of pH on the system, which is a further stimulus that the UPy functionality is susceptible to. Additionally the effect, if any, on the presence of unfunctionalized polymer needs to be examined as the materials made were around 80% UPy functional. As mentioned in the conclusion part of Chapter 4, some of these UPy-poly(lauryl acrylate)

samples were submitted for SANS experiments, in an effort to correlate the rheological changes with temperature with any physical changes that can be seen by SANS. The data processing required for this is extensive however and unfortunately had not been completed in time for inclusion in this thesis.

The final chapter in this thesis was a short side project which deviated from the industrial work, but still involved $Cu^{(0)}$-mediated RDRP. This study examined the feasibility of grafting poly(NiPAM) brushes from poly(sulfone) ultrafiltration membranes and was a collaborative effort involving researchers from KAUST, Saudi Arabia, who provided the membranes. Initiator groups were first immobilized on the membrane surface and the recent aqueous 'SET-LRP' protocol developed by the Haddleton group was adapted to attempt surface-initiated polymerizations. These reactions were found to be successful, as evidenced by the numerous characterization techniques used, including NMR, FT-IR, XPS, SEM and contact angle measurements. There are many ways in which this investigation could be expanded in the future, from screening other water soluble monomers, to varying the molecular weights, grafting densities and even the membranes themselves – doing so would constitute a large project in itself. The ultimate aim would be to perform some actual filtration testing on the functionalized membranes and to see the effect of the polymer brushes.